JAERI-M
86-189

PROCEEDINGS OF THE JAPAN-US WORKSHOP ON TRITIUM TECHNOLOGY

(P89 IN THE JAPAN-US FUSION COOPERATION PROGRAM)

January 1987

Tritium Engineering Laboratory

日本原子力研究所
Japan Atomic Energy Research Institute

JAERI-Mレポートは，日本原子力研究所が不定期に公刊している研究報告書です。
入手の問合わせは，日本原子力研究所技術情報部情報資料課（〒319-11茨城県那珂郡東海村）あて，お申しこしください。なお，このほかに財団法人原子力弘済会資料センター（〒319-11 茨城県那珂郡東海村日本原子力研究所内）で複写による実費頒布をおこなっております。

JAERI-M reports are issued irregularly.
Inquiries about availability of the reports should be addressed to Information Division Department of Technical Information, Japan Atomic Energy Research Institute, Tokai-mura, Naka-gun, Ibaraki-ken 319-11, Japan.

編集兼発行　日本原子力研究所
印　　刷　いばらき印刷㈱

JAERI-M 86-189

Proceedings of the Japan-US Workshop on Tritium Technology P89 in the Japan/US Fusion Cooperation Program, 22-23 Oct., 1986

Tritium Engineering Laboratory
Department of Thermonuclear Fusion Research,
Naka Fusion Research Establishment
Japan Atomic Energy Research Institute
Naka-machi, Naka-gun, Ibaraki-ken

(Received December 15, 1986)

This report includes 25 papers presented in the Japan-US Workshop on Tritium Technology held at Tokyo Headquaters, JAERI, 22-23 October, 1986 under the auspices of Scientific and Technology Agency.

Keywords: Fusion Reactor, Tritium Technology, Fuel Cleanup, Isotope Separation, Waste Disposal, Safety Control, Blanket Technology, Tritium Recovery, Plasma-Materials Interaction, Plasma-Driven Permeation

JAERI－M 86－189

トリチウム技術に関する日米ワークショップ論文集

（日米核融合協力計画のP 89，10月22－23日，1986年）

日本原子力研究所那珂研究所核融合研究部
トリチウム技術研究室

（1986年12月15日受理）

本報告書は，科学技術庁主催により1986年10月22－23日に東京本部で開催された，「トリチウム技術に関する日米ワークショップ」における発表論文を集録したものである。

那珂研究所：〒311－02茨城県那珂郡那珂町大字向山801－1

Foreword

The Tritium Technology Workshop was based on the Japan-US Fusion Cooperation Program agreed at the Japan-US Fusion Coordinating Committee on May, 1986. This workshop was sponsored by Science and Technology Agency and held at the Tokyo Headquaters of Japan Atomic Energy Research Institute, 22 - 23 October, 1986. This report compiles the papers presented in the workshop.

We would like to express our thanks to all the participants for their active and constructive contribution to the workshop and to administration staff of STA and JAERI for their successfull collaboration in carring out the workshop. We would also like to acknowledge the substantial efforts by Mr. G.R. Nardella of DOE, Dr. J.L. Anderson of LANL and Prof. K. Kawamura of Tokyo Institute of Technology for framing the workshop.

December, 1986

Y. NARUSE

H.YOSHIDA

Opening Remark

Thank you Mr. Chairman and Gentlemen, I feel it a great honor to be able to have the Japan-US Workshop on Tritium Technology and to make an opening remark today. I give a hearty welcome to all participants of Japan and the United States of America.

As the beginning of my speech, I would like to introduce the brief history of this meeting. The workshop related to the fusion tritium technology has been held every three years in the framework of the Japan-US cooperation in the nuclear fusion R & D program. The first workshop was held at Tokyo on 13-15 October, 1980, and the second was at Los Alamos in New Mexico on 21-24 March, 1983. The third workshop, this meeting, was fixed by the 8th Meeting of the Japan-US Coordinating Committee on Fusion Energy on 8-9 May, 1986 in Tokyo, Japan.

During these few years of the cooperation, we could obtain the following excellent results:

(i) More than twenty peoples have mutually visited to national laboratories and universities in Japan and the USA,

(ii) Beneficial information has been exchanged both in the scientific and technological fields of the fusion fuel handling,

(iii) The first stage of tritium tests on a small scale for the development of TPL/TSTA process components such as palladium-diffuser and ceramic electrolysis cell have successfully been initiated,

(iv)Many joint papers of the cryogenic hydrogen isotope separation system, the liquid falling film helium separator, and the fuel cleanup system have been published by JAERI-TSTA scientists.

Meanwhile, particular striking progress has been established in both national fusion programs. They are the dedication of the TFTR and the JT-60, successfull experiments on the multi-national LCT and on the plasma heating, safe operation of the TSTA with tritium of 10^8Ci and the construction of the JAERI's tritium processing laboratory (TPL), and so on.

As for the future program of Japan, a new investigations, which cover every technological and polytical subjects needed for the realization of a Japanese D-T burning experiment device, have been carried out under the leadership of the Nuclear Fusion Council and the Atomic Energy Commission in Japan. THe new national fusion program for the next ten to fifteen years will be established in 1987 as a part of the long term schedule of developments of Japanese atomic energy resorces.

I believe that the present productive Japan-US cooperation should be substantially expanded in the near future, in which effective investment and collaboration will become more and more important. I hope that this meeting provides good opportunity to find the ways of strengthening the future bilateral cooperation.

Finally, I would like to express our sincere gratitude to those who have made efforts preparing for this workshop, especially Mr. Nardella DOE officials,

Prof. Kawamura of Tokyo Institute of Technology, and JAERI people. And I hope that American friends of our workshop make yourself at home and would enjoy your stay in Japan. Thank you.

CONTENTS

目　　次

No.1 : Overview of the JAERI Tritium Research Program

Oct.22,1986

Yuji Naruse

(JAERI)

Important Issues Related to Tritium Technology

(1) Basic processing technology :
Unit operations such as purification, recovery, isotope separation, storage, decomposition, pumping, etc.

(2) System technology for integrating various processes.

(3) Tritium production technology for initial loading.

(4) Blanket materials and tritium recovery technology.

(5) Waste processing technology.

(6) Safe handling and monitoring.

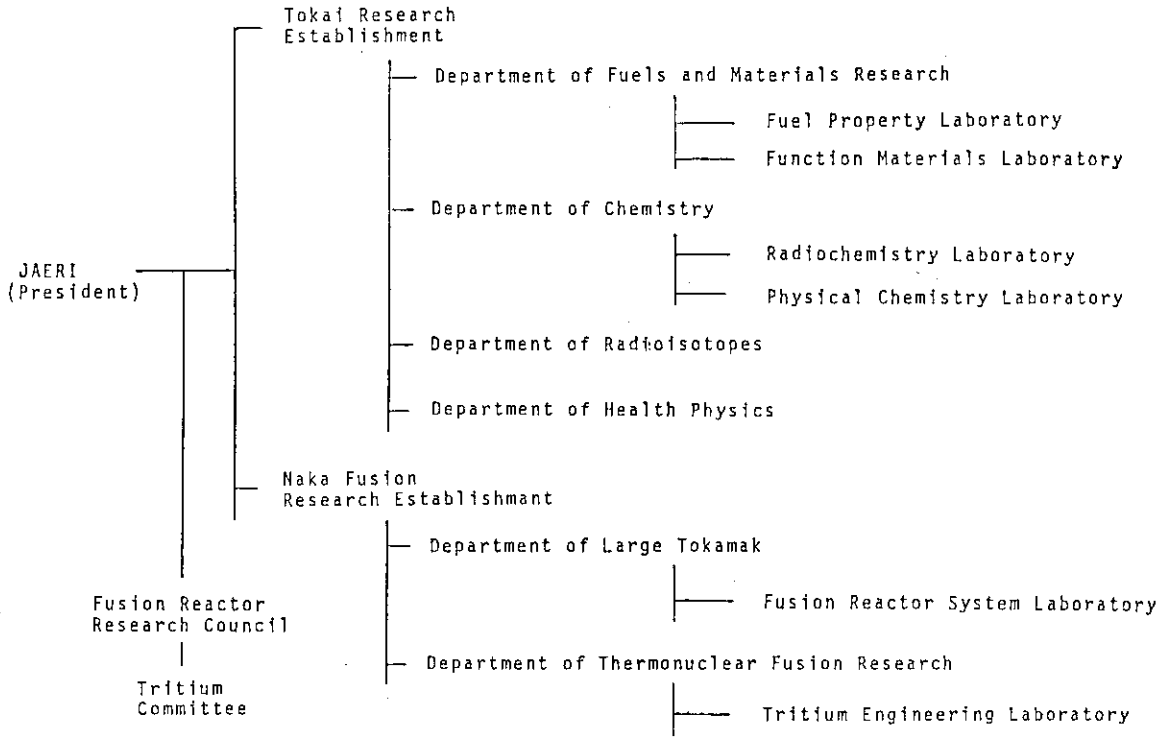

Organization Chart of Tritium Technology Development in JAERI

Main Activities for Breeding Materials

Fuel Property Laboratory

(1) Fabrication :
- *Li_2O, $LiAlO_2$ pellets
- *Li_2O single crystal

(2) Chemical properties :
- *Moisture absorption on Li_2O
- *Decomposition of LiOH

(3) Mechanical properties :
- *Compressive strength and creep on Li_2O single crystal

(4) Radiation damage :
- *Neutron and charged particle on single crystal and Li_2O pellet

(5) In-situ tritium recovery :
- *Tritium sweep gas capsule tests of Li_2O and $LiAlO_2$ pellets

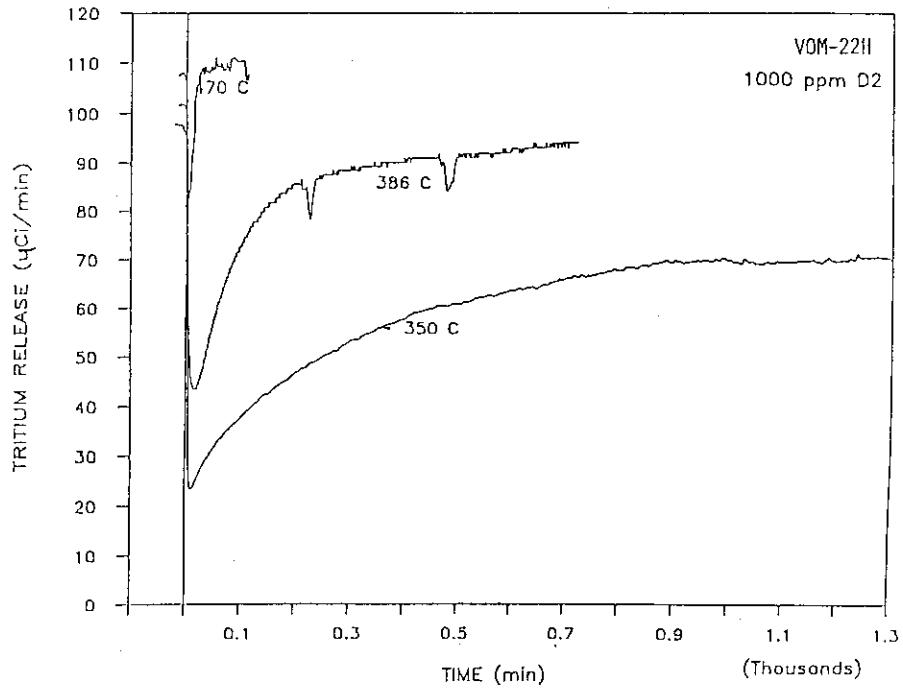

Tritium Release from Li2O

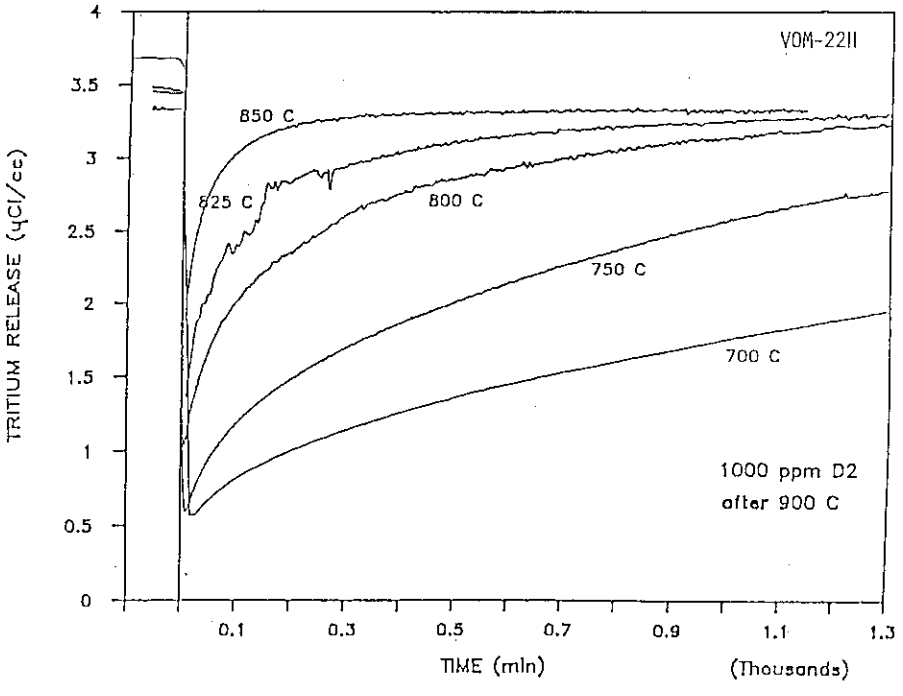

TRITIUM RELEASE FROM LiAlO2

Main Activities for Fusion Materials

Fuction Materials Laboratory

(1) Reversible tritium getter
- *Materials substituting for uranium metal
- *Fabrication of gettering materials (ZrCo etc.)
- *Measurement of "pressure - composition" isotherms

(2) Solid electrolyte for tritium recovery
- *Measurement of basic properties, ionic conductivity, thermal stability electrochemical stability
- *Development of new materials

(3) Plasma (Ion) driven permeation
- *How the permeation rate depends on parameters----ion flux, ion energy, temperature, etc.
- *What property determines the permeation rate
- *Why the permeation spike appears

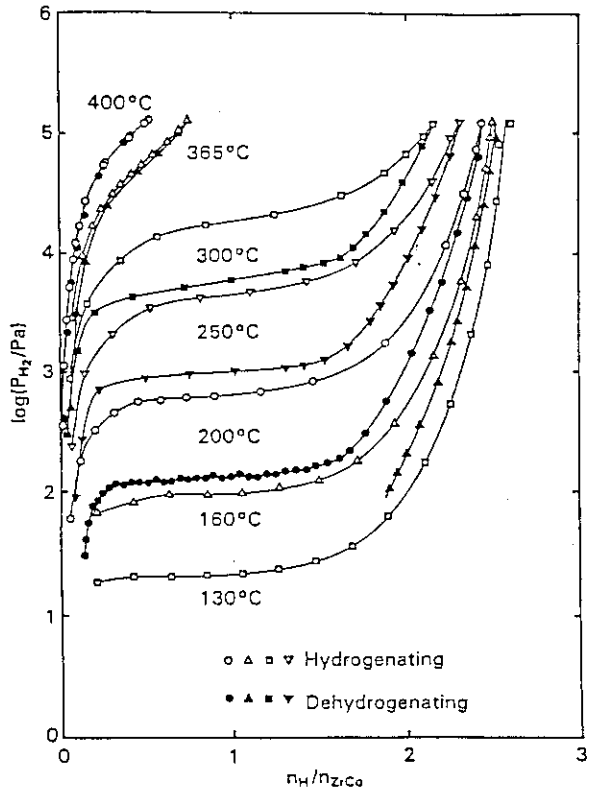

The pressure-composition isotherms for the ZrCo-H system.

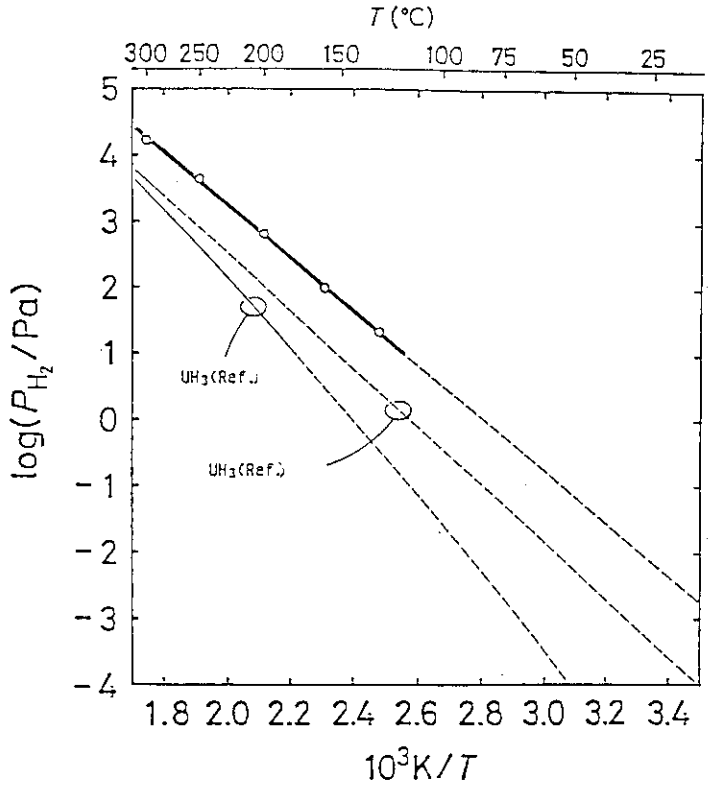

Comparison of hydrogen equilibrium pressure in ZrCo and U

Main Activities for Tritium Chemistry

Department of Chemistry

1. Sorption and desorption of tritium on various materials
2. Diffusivity of tritium in various materials
3. Removal of tritium by solid adsorbents
4. Removal of tritium from water by laser isotope separation method

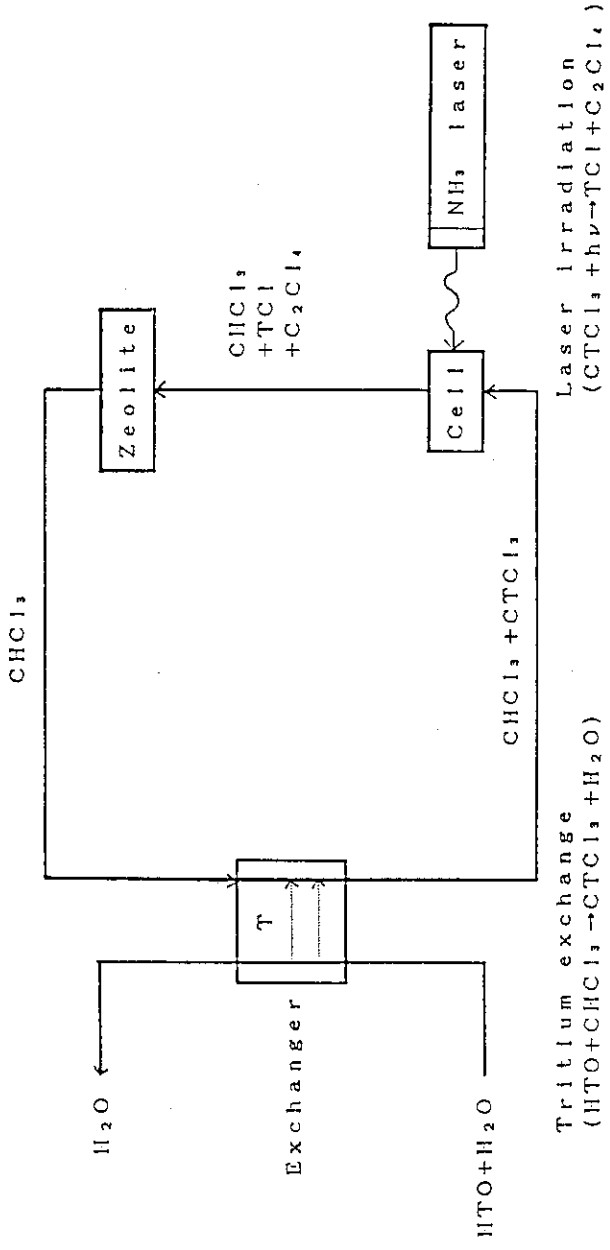

Tritium removal Process by Infrared Multiphoton Dissociation of Chloroform

Main Activities for Tritium Production

Department of Radioisotopes

(1) Facilities of tritium production

*Scale 1000Ci/batch

*Target Li-Al alloy

Li : 3wt%

(^{6}Li Enriched to 95.5%)

*Irradiation JMTR

($2\times10^{14}cm^{-2}s^{-1}$)

40～70 days

*Production process

Extraction from target

Recovery to U getter

(2) Results obtained

* Recovery yield ～100%

* Chemical purity > 99%

* Isotopic purity ～ 95%

* Tritium release from facilities

No observation

(3) Related R & D

*Development of caramic targets as alternatives

$LiAlO_2$, Li_2SiO_3

*Tritium inventry

Calorimetry

*Purification of product

Gas chromatography

*Studies of blanket materials

Chemical behavior of tritium produced in litium-containing materials

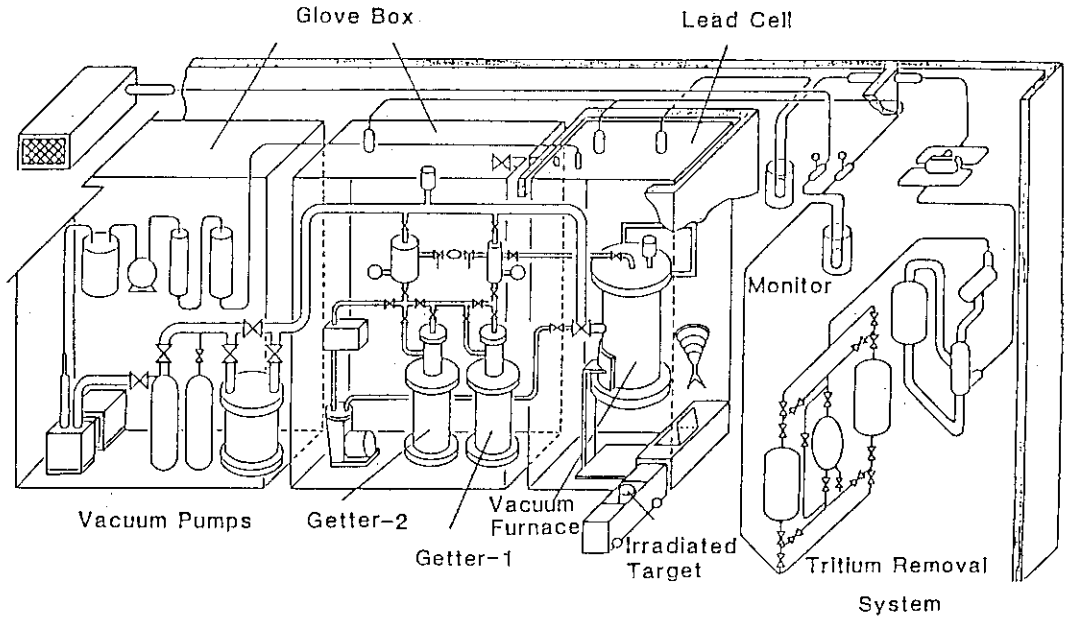

Production Facilities

DIFFUSION COEFFICIENT FOR TRITIUM DETERMINED FROM THERMAL RELEASE UNDER VACUUM

$D=D_0\exp(-Q/RT)$

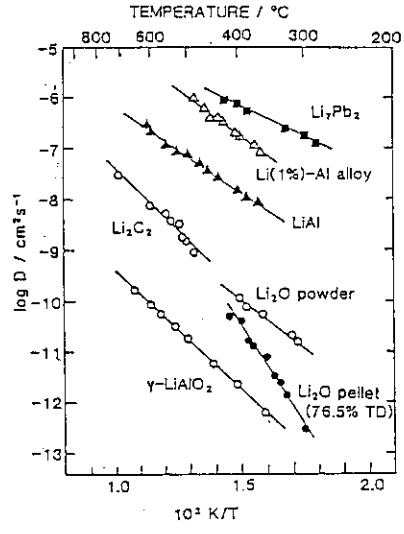

Material	Released species	log D_0 / cm^2s^{-1}	Q / kcal mol^{-1}	Temp. range / °C
Li_2O	HTO	-4.1±0.5	18.5±1.3	300-420
Li_2O pellet (76.5% TD)	HTO	1.8±0.7	36.9±2.1	300-410
$LiAlO_2$	HTO	-4.7±0.4	21.6±0.2	300-650
Li_2C_2	HT	-2.5±0.4	22.3±1.5	480-700
LiAl	HT	-0.8±0.5	22.5±1.7	350-650
Li(1%)-Al	HT	-1.3±0.6	16.7±2.3	360-520
Li_7Pb_2	HT	-2.7±0.1	10.8±0.4	280-450

Main Activities for Tritium Safety

Department of Health Physics

1. Permeability of tritiated water vapor through elastomeric and polymetic materials

2. Conversion of tritium gas to tritiated water vapor

3. Tritium concentration in concrete of JRR-3

4. Tritium monitoring for internal contamination

5. Monitoring of HTO and HT concentration in atmosphere

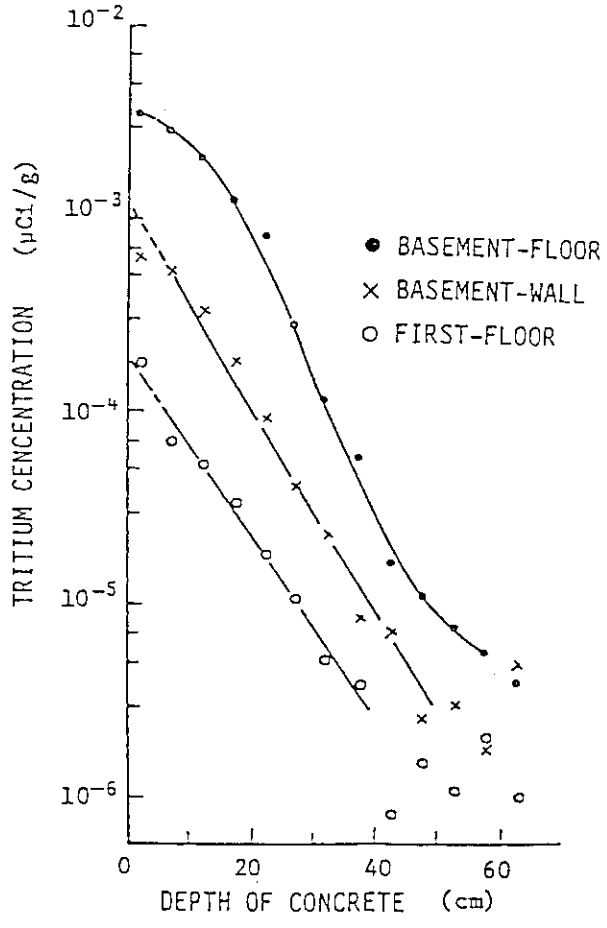

Typical profiles of tritium concentration in concrete

Main Activities for Tritium Technology

Tritium Engineering Laboratory

1. Construction of Tritium Process Laboratory (TPL)
   - *Building and utilities
   - *Safe handling systems
   - *Experimental apparatus

2. Basic experiments
   - *Components test of fuel cleanup system
   - *Measurement of separation characteristics on cryogenic distillation column. "N_2-Ar", "H_2-HD-D_2"system
   - *Others

3. Computer simulation studies
   - *Hydrogen isotope separation system by cryogenic distillation, chemical exchange and water distillation
   - *Blanket tritium recovery system
   - *Tritium-materials interaction (Permeation study)

4. Licensing procedures
   - *Handling of tritium and uranium
   - *High pressure gas regulations
   - *Tritium transport container

Tritium Process Laboratory

1. Objective
   Research and development of tritium processing and safe handling technology for fusion fuel cycle

2. R & D items
   (i) Fuel cleanup
      - *Pd-alloy membrane diffuser
      - *Catalytic oxidation bed
      - *Ceramic electrolysis cell
      - *Cryogenic falling liquid film He separator

   (ii) Hydrogen isotope separation
      - *Cryogenic distillation column
      - *Thermal diffusion column

   (iii) Tritium-materials interactions
      - *Permeation study
      - *Kinetic reaction study

   (iv) Tritium monitoring

   (v) Tritium containment and removal

   (vi) Waste processing

   (vii) Others

3. Facility

(1) Schedule

*Design : 1977 -

*Construction

Building and utilities : 1982 - 1984(May)

Safe handling systems : 1983 - 1985

Experimental apparatus : 1986 - 1987

(2) Specifications

(i) Building structure

*3 Floors (Ground area; 1400m², total floor area; 2300m²)

*Reinforced concrete (Withstand 300Gal seismic force)

*1st Floor : Glovebox room, detritiation systems room, semi-hot experiment room, utility room

*2nd Floor : Semi-hot experiment room

*Basement : Waste processing room, waste storage tank room

(ii) Tritium handling capacity

*Glovebox : 2 - 3g/Glovebox-block

*Storage : 10g

(iii) Uranium metal (Tritium gettering)

: 20kg

(v) Tritium containment system (Threefold containment)

*Primary containment : Experimental apparatus

*Secondary containment : Gloveboxes and detritiation systems

*Tertiary containment : Glovebox room and detritiation systems room

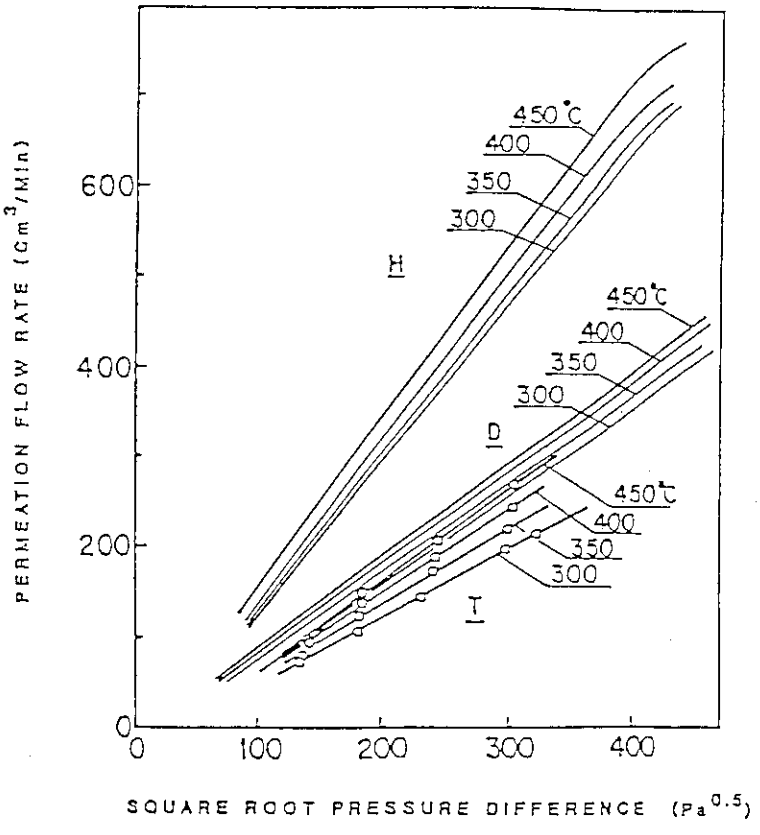

Permeation flow rates of 3 hydrogen isotopes through the JAERI diffuser.

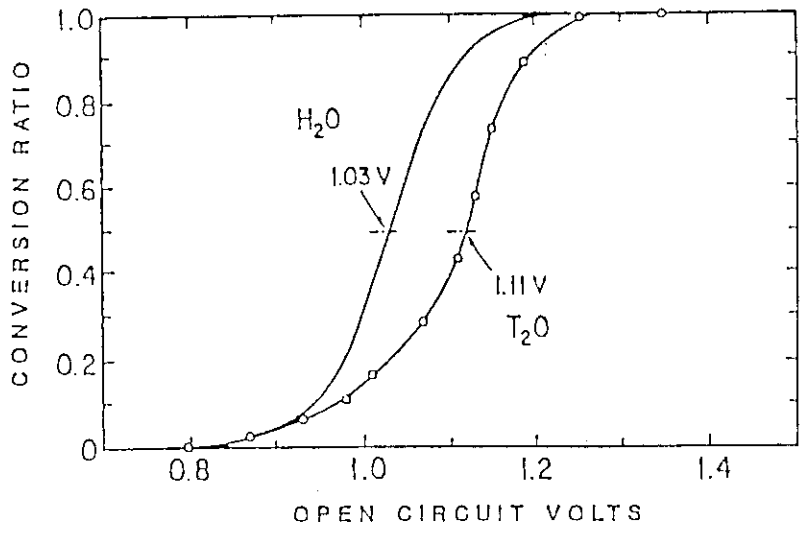

Isotopic difference between H_2O and T_2O in the electrolysis cell at 600°C.

No.2

Overview of the U.S. Magnetic Fusion Tritium Research Program

by
Gene R. Nardella
Division of Development and Technology
Office of Fusion Energy
U.S. Department of Energy

Tritium research within the U.S. has been going on in varying degrees and areas for approximately thirty years. Thus, there is a significant base of technology and information from which to build tritium systems for fusion applications. It is because of this solid base of information that the U.S. Magnetic Fusion Energy Program has had a significant start in conducting the necessary research to support the construction and operation of a large engineering test facility. However, to achieve on limited budgets a sufficient data base to build such a project in the suggested time frame (1990's) will take more successful collaboration as part of the ongoing U.S.-Japan fusion cooperation. Successful collaboration has already occurred in the tritium area with the integral neutronics experiments (Annex II) performed at the Fusion Neutron Source (FNS) facility in Japan and the small-scale tritium components (palladium diffuser and ceramic electrolysis cell) test performed at the Tritium Systems Test Assembly (TSTA) facility in the U.S. Additional collaboration in the tritium area is proceeding with the decision to pursue testing of larger versions of the same tritium components (process-ready) as Annex III and to pursue joint funding of TSTA for the purpose of sharing the information generated by the full operation of this facility as Annex IV.

In the U.S. Magnetic Fusion Energy Program today, tritium research is essentially being conducted in five general or generic areas: processing of plasma exhaust/blankets, safety, blanket development and breeding performance, material studies, and health and environmental effects.

The major purpose of the tritium processing program is to develop and demonstrate an effective technology for handling and processing deuterium and tritium fuel for use in fusion reactors. The cornerstone of the tritium processing program is the TSTA facility. TSTA, which is located at Los Alamos National Laboratory (LANL) and was completed in September 1982, consists of a large gas loop which can simulate a deuterium-tritium fuel cycle system. The first test with tritium (10 grams) occurred in June 1984 with the introduction of tritium into the Isotope Separation System (ISS).

During FY86, TSTA has been performing operational testing of various systems with tritium. Recent tests have included both the Fuel Cleanup System and the ISS and have utilized up to 50 grams of tritium. Present plans call for full operation of the gas loop by the end of 1987. In addition to demonstrating the

performance of an integrated fuel handling system, the facility will demonstrate the ability to control and contain tritium, test and qualify components for tritium service, demonstrate performance of safety systems and of monitoring and processing instrumentation and also conduct tritium property and cleanup experiments.

The major purpose of the tritium safety program is to understand and control tritium under different conditions especially with regard to reducing the magnitude of operational and accidental releases. At present there are two areas of research being conducted by the safety program at the Idaho National Engineering Laboratory (INEL). The first area is the continuing experiments on implantation driven permeation to determine the amount of tritium that permeates through and/or that is retained in first wall structural materials such as $V_{15}Cr_5Ti$ at reactor-like conditions. The second area is the continuing development of a tritium safety code entitled the Tritium Migration Analysis Program (TMAP) which will have the capability to determine the tritium loss from fusion systems during normal operation and accident conditions. Future plans call for the utilization of TSTA to do a variety of safety-oriented experiments and to conduct these experiments in close cooperation with INEL.

The major purpose of the tritium blanket development and breeding performance program is to determine the breeding capabilities, the engineering characteristics and requirements and the irradiation performance of different candidate blanket concepts. At present there are four major areas of research being conducted. The first area at Argonne National Laboratory (ANL) has the objective of developing an accurate data base of thermochemical, thermophysical, transport, and mechanical properties for candidate solid breeder materials. This data base would support both systems-design and blanket-processing activities. The lithium-containing ceramics Li_2O, $LiAlO_2$, Li_4SiO_4, and Li_2ZrO_3 are receiving greatest consideration. Development of an accurate data base of transport, thermochemical, and thermophysical properties for candidate solid breeder materials is continuing. Surface adsorption/desorption isotherms for H_2/H_2O on Li_2O will be investigated. Mechanical and elastic properties of Li_2O will be developed. Candidate solid breeder materials are prepared for other tasks and for near-term irradiation experiments including the BEATRIX matrix of the International Energy Agency (IEA) Materials Implementing Agreement. This task also continues to evaluate the implications of the current in-reactor experiments. The major planned accomplishment for FY87 is to characterize materials for the Fast Flux Test Facility/Materials Open Test Assembly (FFTF/MOTA) test as part of the IEA program.

The second area of research at Hanford Engineering Development Laboratory (HEDL) has the objective to evaluate the irradiation performance of potential candidate ceramic solid breeder

materials (1) for material selection and optimization and (2) for system design. The program has as an overall goal to evolve from simple isothermal capsule testing to more complex tests with large spatial temperature variations and flow through purge gas under the fast neutron spectrum which better approximate the fusion blanket environment. The scope of activities includes the FUBR1-B irradiation experiments in the EBR-II which will include lithium ceramics produced in Japan, England, France, Federal Republic of Germany, and Italy as a part of the BEATRIX-I program of IEA. Other materials fabricated in the U.S. have been and will be sent to The Netherlands and France for irradiation as part of the same program. Supporting activities continue to include the fabrication of new lithium ceramics, accumulation of thermal, mechanical and chemical properties, and post-irradiation measurement capabilities suitable for hygroscopic tritium bearing materials.

The third area of research is conducted at three places: ANL, Lawrence Livermore National Laboratory (LLNL) and University of California at Los Alamos (UCLA). The objective of their research efforts is the design and analysis of tritium producing blankets particularly for the Engineering Test Reactor (ETR).

A number of candidate blanket concepts for the ETR will be identified and evaluated against a set of criteria to determine the optimal blanket concept. The candidate blanket concepts will cover a broad range of options for materials combinations (structure/breeder/coolant/multiplier), geometrics and configurations. The evaluation criteria will address feasibility issues (e.g., can the blanket concept achieve adequate tritium breeding performance with required reliability of operation) and attractiveness issues (e.g., developmental costs). In FY 87 it is expected that a set of promising candidate blanket concepts would be selected and the process of evaluation to narrow down the choices would begin. The complete process leading to selection of a small set of leading blanket concepts will probably take several years.

The fourth area of research is a collaborative effort beginning in October 1984 between the U.S. and Japan in determining the tritium breeding performance of blankets from the neutronics aspects. Effort in this program is focused on evaluating the overall uncertainties (both analytical and experimental) in the tritium production rate (TPR) of candidate solid breeder materials. Integral neutronics experiments are performed at the Fusion Neutron Source (FNS) facility of the Japan Atomic Energy Research Institute and analytical predictions of the TPR are compared with experimentally measured values.

The program currently consists of two phases. Phase I experiments have been completed, while Phase II experiments were initiated in August 1986. Phase I concentrated on design-oriented engineering benchmark experiments to obtain experimental

data on blanket neutronics characteristics and compare it with calculated values. The experiments performed in this Phase I included neutron source characterization, TPR and spectrum measurements in a reference lithium oxide test assembly, first wall experiments with and without coolant simulation and beryllium neutron multiplier experiments in various configurations. The Phase I experiments were performed in an open geometry configuration where the neutron source target is located in the middle of a large room with the reference assembly embedded in a concrete wall. In Phase II, the fusion neutron spectra environment is more closely simulated with the reference assembly placed at one end of a rectangular enclosure made of lithium carbonate and the neutron source placed in the inner cavity.

Phase II experiments, which will be completed by the end of FY 87, will consist of four experimental periods. The first and second periods will aim at performing key experiments characteristic of Phase I, but with a closed geometry. The third and fourth periods will shift emphasis into engineering experiments, adding more structure and including basic penetration effects. Also during FY 87, plans for a Phase III will be considered and a decision will be made on whether or not to continue experiments.

The major purpose of the tritium-materials studies program is to understand and characterize the effects (e.g. permeation, adsorption, absorption, etc) that tritium has on different materials under different conditions. At present there are two programs in place to evaluate this area. The first program at ANL is studying tritium permeation through heat exchanger tubes which must be kept low in order to meet requirements for allowable tritium release from fusion reactors. Since this rate is sensitive to the amount of tritium present in the coolant as elemental tritium, the relative level of this species must be minimized. A method to do this is to oxidize the elemental tritium. Unfortunately, there is a poor understanding of the kinetics of tritium oxidation for the conditions expected in fusion reactors. As a consequence, the relative levels of elemental tritium and tritium oxide present in the coolant are uncertain. Therefore, there is a strong need to understand the kinetics of tritium oxidation so that effective tritium control systems can be designed and tested. The research at ANL is directed at performing experiments to determine the kinetic rate of tritium oxidation by examining the parameters that might enhance the rapid combination of tritium atoms and oxygen. In the first series of experiments, the parameters to be examined, using a 316 stainless steel surface, are temperature, tritium flux, oxygen potential, flow rate, time and excess hydrogen species. These and other experiments will be used to generate the kinetic rate expression for the surface oxidation of tritium atoms. This expression will be fitted against different mechanisms to determine a model which can explain the observed

oxidation behavior. In parallel with the experiments, an effort will be undertaken to produce a computer code that can be used to predict oxidation behavior in fusion systems.

In FY 85/86, the experimental system was assembled and shake-down testing was completed. The experimental system consists of a manifold, pumping systems, a loop with a tritium source, a loop with an analysis system, a calibration loop and the test cell where the surface reactions occur. A number of tests were completed at various temperature levels and test times.

During FY87, the experimental program will progress rapidly with rates of reaction measured in the range of 100 to 500 C. If only one rate is found in this temperature range, the oxygen potential will be varied in another set of experiments. Also, deuterium will be introduced in the analysis loop to ascertain its effect on the reaction rate and the completeness of oxidation reactions. If possible, a set of experiments will be conducted where the flow rate is varied to determine if the rate of removal of the reaction species affects the reaction rates. The program will most likely be completed by the end of FY 88.

The second program at Sandia National Laboratory at Livermore is studying the effects of tritium plasma on materials in the vacuum chamber. Of particular concern is the tritium uptake of different materials (e.g., first walls, coatings, limiters, etc.). In this program tritium inventories in materials are calculated for ongoing fusion experiments such as TFTR and for projected new facilities. This is done both theoretically and experimentally. In addition in FY 87 the first tritium permeation experiments on redeposited materials will be completed for stainless steel.

The major purpose of the tritium health and environmental effects program is to determine the effects of exposure to varying amounts and different forms of tritium as well as its transport and uptake in the environment. The results of this type of work are critical to the development of a safety design philosophy, safety analysis, dose models, etc. for fusion facilities.

At present there are three research projects being funded in this area by DOE. A summary of each project is described below.

1. Hazards of Radioactive Environmental Pollutants (Brookhaven National Laboratory)

   There is concern over the genetic and somatic effects of exposure to tritium. This project objective is to evaluate (in mice) the effects of various concentrations of tritium in drinking water as evidenced by (1) dominant lethal mutations (DLMs), (2) reduction in hematopoietic stem cells (CFU-S), (3) induction of cytogenetic (sister chromatid exchanges, SCEs) effects in bone marrow cells, and (4) induction of

micronuclei in their red blood cells. Early fertilized oocytes taken from animals maintained on HTO or exposed to external gamma or x rays will also be evaluated for changes in metaphase II. In order to evaluate possible carcinogenicity of HTO ingestion, animals receiving single injections or chronic ingestion of HTO will be evaluated for the possible induction of leukemia. These animals will be compared with dose-equivalent x-ray and gamma-exposed animals. The effects of nonnuclear pollutants will be compared in the same systems. It is desirable to know the amount of tritium incorporated into cellular components (e.g., RNA, DNA, and histones). Similarly, it is important to know the position at which tritium might be incorporated into the DNA since studies in some species indicated significant genetic effects depending upon where the tritium is incorporated. Standard biochemical procedures will be used. It is advantageous to know the effectiveness of liquid ingestion on enhanced tritium excretion in the event of accidental contamination of humans with HTO. This is being done by taking mice previously maintained on HTO solution and placing them on sweetened water solutions, which leads to enhanced water intake. The rate of tritium excretion is then evaluated.

2. Radiosensitivity of Oocytes and Other Mammalian Cells (Lawrence Livermore National Laboratory)

Hazards from low-level exposures to neutrons, gamma rays, and tritium are being carefully evaluated by measurement of damage to particularly vulnerable cells, especially female germ cells (oocytes) that are irreplaceable after birth. Studies are in mammals (mice and, for special purposes, monkeys) because of their relevance to man, and on neutrons, gamma rays, and tritium because of their importance in nuclear fission and fusion. Measured dose-effect relations provide data for critical comparisons at low exposures where hazard evaluations are most needed. Animals are exposed to carefully monitored doses, including chronic irradiation during highly sensitive developmental stages, then cell populations are evaluated by numbers of survivors, levels of function, and genetic effects. The studies have revealed severe oocyte loss from low-level tritium exposure in young mice and also in primates (squirrel, bonnet, and to a lesser extent, rhesus monkeys) exposed before birth. Making use of this high oocyte sensitivity, comparative radiation studies are providing a better understanding of mechanisms. Important results for genetics have come from combined neutron, gamma-ray, and tritium studies elucidating the nature of the extreme radiosensitivity of mouse oocytes. They clarify a key genetic controversy over applicability to women of data from female mice. Even more importantly, they identify, for the first time, special experimental conditions required for obtaining reliable genetic data from mice that

will be relevant to the human female. Quantification in mammals of radiation effects at very low exposures and provision of experimental data for estimating genetic risk in women is strengthening the scientific base from which human hazard evaluations must be drawn.

3. Mutagenic Effect of Radionuclides Incorporated into DNA of Drosophila Melanogaster (Louisiana State University)

Tritium decay can induce mutations by ionizing radiation and/or transmutation of ^{3}H to ^{3}He with associated energy of excitation and recoil. Ionizing radiation from tritium decay at the different incorporation positions in DNA is assumed to be equivalent throughout the nucleus; therefore, the differences in mutation frequency per tritium decay at different incorporation sites in DNA result from excitation, recoil, and transmutation of ^{3}H to ^{3}He. In previous work there has been detected local or site-specific effects of tritium decay by comparing the frequency of sex-linked recessive lethal (SLRL) mutations induced by tritium decay in specific DNA sites of Drosophila melanogaster sperm cells. There has been found a site-specific effect when tritium decay occurred at the 5 position of cytosine, 8 position of purine, or 6 position of pyrimidine. These differences in the site-specific mutagenesis can be described only as quantitative differences in induced mutation frequency because SLRL mutations can be induced by any known mechanisms of mutagenesis. Current focus is on detecting differences in mutational mechanism by analyzing mutant genes at the molecular level using labeled probes of the locus alcohol dehydrogenase (Adh) to determine molecular changes in DNA of the mutants. Comparing null mutants induced by x rays, the alkylating agent N-ethyl-N-nitrosourea (ENU), and decay of tritium incorporated into specific sites of DNA. Mutants induced by x rays have an unusually high frequency of multiple breaks in DNA in relatively short distances near the locus. Most of the x-ray-induced mutants were induced through a mechanism of multiple chain breaks in DNA.

No.3 Fusion Fuel Research Activities of Universities in Japan

Makoto Okamoto
Research Laboratory for Nuclear Reactors,
Tokyo Institute of Technology

Introduction

Tritium science and technology are being investigated mainly at universities and JAERI in Japan. Basic studies are carried on at universities and technology oriented studies at JAERI. The universities have only low level laboratories such as a few to 500 Ci for tritium, so there are limitations to carry out practical scale experiments.

There are many contributions, however, to be done by use of these low level laboratories, e.g. understanding phenomena, accumulation of quantitative basic data, confirmations of innovative ideas, education and training of young scientists, and so on.

There are more than 40 scientists who have been organized in the research project of tritium science and technology supported by the Grant-in-Aid for Scientific Research, Ministry of Education, Science and Culture (NBS) since 1980.

Table 1 shows the main institutions which are contributing to the R&D works at universities, and Table 2 indicates the handling capacity of tritium in several institutions.

Research Items in Japanese Universities

When the Grant-in-Aid scientific research program had been first organized in 1980, the research items on the tritium science and technology were widely spreading over whole subjects which seemed to concern to tritium issues.

This trend was gradually amended as Grant-in-Aid group brought up the general consensus on the fusion fuel cycle scheme. The out line of the consensus are as follows:

The tritium flow in fusion system is consisted of four sub-tritium flows; the primary tritium (fuel)flow, the secondary tritium (fuel) flow, permeation flow through the plasma facing materials, and leakage flow to the environment.

Along with the above four tritium flows, the research activities have been forcused on the following subjects from about 1983.

I. Breeding chemistry and technology

II. Tritium cleanup technology

III. Recovery and storage of tritium

IV. Diffusivity of hydrogen isotopes

V. Isotope separation

VI. Plasma driven permeation and hydrogen plasma chemistry

VII. Waste treatment

IIX. Others

Existing Experiments and Reseraches

The research and working institutions are as follows.

I. Breeding chemistry and technology

i) Fundamental investigation of tritium release behavior by means of post irradiation release,

Tokyo Institute of Technology: Li_2O(pellet), LiPb, $LiFPbF_2$

University of Tokyo : Li_2O(powder), LiC, LiN, etc.

ii) Fundamental investigation of tritium extraction by means of under irradiation release,

University of Tokyo (Tokai) : Li_2O(powder)

iii) Basic study of extraction of tritium from metalic lithium,

Osaka University

II. Tritium cleanup technology

Catalytic oxidation and absorption of tritium and tritium contained gaseous molecules,

Kyushu University, Toyama University, University of Tokyo, Nagoya University

III. Recovery and storage of tritium

Fundamental studies of recovery and storage of tritum by use of metalic getters,

Toyama University, Kyushu University

IV. Diffusivity of hydrogen isotopes in materials

Fundamental studies of diffusivity of tritium and deuterium in materials under various conditions including high magnetic field,

Nagoya University, Kyushu University

V. Isotope separation

i) Basic study of laser separation method for enrichment of tritium,

University of Tokyo

ii) Enrichment and separation of tritium by thermal diffusion column,

Toyama University, Tokyo Institute of Technology

VI. Plasma driven permeation and hydrogen plasma chemistry

i) Plasma driven permeation using RF-discharge of D_2,

Kyoto University

ii) Plasma driven permeation and chemical behavior of T and/or D plasma,

Tokyo Institute of Technology, Nagoya University

VII. Waste treatment

i) Solidification of tritiated water with cement,

Nagoya University

ii) Solidification and enrichment of tritiated water with beeswax,

Kyushu University

iii) Design concept of down stream in fusion fuel cycle,

Nagoya University

iv) Volume reduction and enrichment of tritiated water using electrolysis cell having hydrogen permeable cathode,

Kyushu University

IIX. Others

i) Tritium impact to CTR system safety,

Nagoya University

ii) CTR system safety assesment,

Tokyo Institute of Technology

iii) Lithium-6 enrichemnt,

Tokyo Institute of Technology

iv) Detection and analysis,

Musashi Institute of Technology, University of Tokyo, Yamaguchi University, Tohoku University, Toyama University, Osaka University

v) Breeder making,

Nagoya University

vi) Tritium fueling into pellet for ICF,

Osaka University

vii) Tritium behavior in metals,

Tohoku University, Tokyo Institute of Technology

and so on.

A Prospect on Research Trends in University of Japan

The trends, which can be seen in the itemization of research subjects, will be continued for a while. Besides, the intensive movement for the level up of tritium handling capacities will be grown up among the research groups. So, if there is any possibility to proceed and scale up the present work by handling high level tritium even in U.S., many researchers will be ambitious to catch the chances.

Table 1 Main Institutions

University of Tokyo (Tokyo, Tokai)

Tokyo Institute of Technology (Tokyo)

Toyama University (Toyama)

Nagoya University (Nagoya)

Kyoto University (Kyoto)

Osaka University (osaka)

Kyushu University (Fukuoka)

Table 2 Locations and Capacities for Tritium Handling of Main Tritium Laboratory

Nuclear Engineering Research Laboratory (Tokai),
University of Tokyo
100 Ci

Research Laboratory for Nuclear Reactors,
Tokyo Institute of Technology
30 and 3 Ci

Tritium Science Research Center,
Toyama University
500 Ci

Institute of Plasma Physics,
Nagoya University
10 Ci

Laser Engineering Research Center,
Osaka University
1000 Ci (special use for pellet making)

Faculty of Engineering,
Kyushu University
1 Ci

No.4 Tritium fueling for ICF pellet target

Takayoshi Norimatsu, Masaru Takagi, Sadao Nakai

and

Chiyoe Yamanaka

Institute of Laser Engineering
Osaka University
Yamada-oka, Suita, Osaka, 565
Japan

1. Introduction

In laser fusion research, glass[1] or plastic microballoon[2], filled with pressurized deuterium-tritium gas, is employed as a target. The DT gas is loaded into the microspheres by heating in high pressure DT gas to induce diffusion through the glass wall. For the high pressure DT loading, the following technical issues such as pumping of DT gas up to 30 MPa, reduction of tritium leak due to diffusion from fill system, process monitoring at the order of 1.3 Ci/cc STP, recovery of tritium from vacuum lines and non-destructive fuel assay in the plastic balloon are extensively investigated.

In this report, brief outline of DT fill process is presented in section II. Reduction of tritium leakage from fill vessel by Au plating[3] and process monitoring using β scintillation powder are described in section III and IV, respectively.

In order to reduce the permeation of tritium, a Be tube has been used as fill vessel[4]. However, the draw back of Be is its thermal expansion coefficient differing from that of adjoining tube materials. Also, the tensile strength reduces when it is heated. Tritium leakage through AIST Type 316 stainless steel was reduced to practically negligible level by Au plating applied to outside surface. Results and mechanism of diffusion reduction are presented.

The tritium concentration in fill system must be monitored in order to obtain equivalent deuterium-tritium mixture at

existence of isotope effect on dissociation of uranium hydride. The concentration of tritium in the low pressure line of the fill system is at the order of 1.3 Ci/cm^3 STP and the pressure varies up to 1 MPa.

Detection of such high level of tritium may be accomplished by ionization chamber techniques[5] or solid β scintillator[6]. However, ionization chamber encounters a obstacle in electron discharge when the pressure in line become low. The solid β scintillator has the problem of saturation resulting from β absorption by hydrogen itself when characteristic length of detection volume becomes larger than the range of β ray. Fluorescent powder was employed to avoid the saturation problem.

II. DT loading

The process to fabricate DT loaded targets is shown in Fig.1. Glass microballoons, whose diameters are 300 - 1500 μm and wall thicknesses are 1 - 10 μm, are put in an array of holes on a fill rod after strict characterization of sphericity and uniformity of the wall.

The experimental arrangement adopted for loading the glass microspheres with DT gas is shown in Fig. 2. The whole system is contained in a sealed glove box of 0.5 m^3 volume, filled with argon gas, and equipped with tritium recovery system. The high-pressure line enclosed by a dashed line in the figure consists of uranium bed (U)[7], cryopump (C), loading vessel (L) and high-pressure valves

(V_9-V_{12}) with small dead volume. The DT gas, previously mixed to equal amount, is stored in the uranium bed. The glass microspheres are placed in the loading vessel and the high pressure line is evacuated by vacuum pump. The uranium bed is heated up to transfer the DT gas to the loading vessel, in the course of which the gas is pressurized to 3 X 10^6-3 X 10^7 Pa by the cryopump, which also serves to rapidly evacuate the loading vessel. The vessel is heated up to 300-330 C and held for 10-48 hours to allow the pressurized DT gas to permeate into the glass microspheres. The buffer tank (B) installed between the high pressure and vacuum pumping lines protects the bellow valves (V_1-V_8) in the event of abrupt release of high pressure DT gas by any operational fault. The high pressure line itself is totally enclosed in a sealed inner box as indicated in the figure by dashed line, and provided with a 2nd tritium recovery system.

The loading vessel is stainless steel rod 6.3 mm diameter X 100 mm long, bored through its axis to form a hollow space 3 mm diameter X 96 mm long as shown in Fig. 3. After machining, the hollowed rod has been electrolytically etched to remove surface oxide layer, and a nickel base of 1 μm thick plated on, to serve as adhesive intermediate layer to receive the gold plating 20 μm thick. This nickel layer also prevents iron atoms from diffusing into the gold layer. The gold plating has been applied in concentrated cyanide solution, to cover not only the loading vessel, but also the

connecting swagelok joint, ferrules and 1/8-inch tube.

The copper jacket serves to ensure uniform temperature distribution throughout the loading vessel.

After the DT fill, the glass balloons are cleaned up and quantity of tritium in the each balloon is estimated from the characteristic X-ray of the glass wall which is stimulated by β rays from tritium decay[8].

The glass balloon is suspended by a plastic fiber of 7 μm in diameter for laser irradiation. Figure 4 shows a single shell target for stagnation-free-compression by shock multiplexing[9]. The fuel pellet is surrounded by outer shell to compose a cannon ball target[10].

III Reduction of Tritium leakage by Au plating

i) Tritium leakage

The experimental setup was similar to Fig.2, except the cryopump which was not used. Tritium leakage was estimated from the resulting tritium concentration measured in the glove box.

Through gold-plated wall the tritium permeation proved to be as reported in Fig. 5. The initial flat stretches, lying at levels of the order of 10^2 μCi/h, occurring before the rise of the measured curves, is attributable to tritium release into argon atmosphere from the inner surface of the glove box. The discontinuities seen on the same curves after the lapse of 6-8 hours derive from interruption of heating necessitated for renewing the argon atmosphere in

the glove box. At 420 C and above, detectable leakage from vessel is seen to have started upon lapse of around 3 hours after start of heating, and to progress at attenuating rate indicative of approach to saturation. The runs at 350 C are seen to have incurred practically no leakage.

Theoretical calculation based on permeation through pure gold[6] indicates that reduction of tritium leakage by gold plating is only 1/45 at 450 C. In contrast, the present experimental result for gold-plated vessel has indicated a suppression factor of $1/10^4$ in reference to the calculated value for unplated vessel during the first 2.5 hours. Moreover, the diffusivity of tritium through gold layer, estimated from the time lag elapsing before tritium detection outside the loading vessel, was 2×10^{-11} cm^2/sec, which is $1/10^5$ -$1/10^6$ of the value reported by the others[11),12)].

ii) Mechanism of tritum leakage suppression

In order to determine the cause of the disagreement seen above between the present experimental results and what would be expected from calculations based on published studies, the mechanism of tritium leakage suppression by the gold plating was examined through the following studies.

The layers that effectively trapped the tritium were sought by autoradiography, using Sakura MR-2 film. The results are illustrated in Fig. 6, which represents transverse cross section of loading vessels that had been exposed to β ray from tritium decay. The films were exposed

for 3 hours. The specimens were from vessels that had been used for DT loading at 350 C, in runs that lasted 54 hours, and which had registered no appreciable tritium leakage (Run 32 in Fig.5. In Fig.6, film grayness is seen to be greater on the side facing gold layer than on that facing stainless steel wall, despite 10^{-3} lower solubility shown by hydrogen in gold[13] than in 316 stainless steel[14].

This would indicate that tritium is consistently trapped by impurities or imperfections in the gold layer, or else that tritium permeation is obstructed by certain oxides at the grain boundaries of gold, formed by the base metal diffusion into the gold layer.

Upon treatment of higher temperatures, nickel and iron were observed to diffuse into the gold layer, but within the range covered of experimental conditions, the depth of nickel diffusion was found upon calculation to be less than 2 μm. For this reason, nickel and other oxides were excluded from consideration as possible significant sites for tritium trapping.

The impurities contained in the plated gold layer were determined by Auger electron analysis. Clear indications are observed of emissions from oxygen and carbon. The presence of carbon is attributed to dissociation of cyanide, and codeposition of the resulting carbon in the process of electro-plating.

The concentration of carbon in gold was measured by carbon analyzer (Horiba EMIA-110 and 3200), which

registered 30 ppm and 540 ppm by weight as values of carbon concentration in the gold layer and stainless steel wall, respectively.

Tritium concentration in the loading vessel was measured by slowly grinding a segment of the vessel in a sealed chamber connected to a gas-chromatograph equipped with thermal conduction detector (Shimazu GC-7A). Outputs from the tritium monitor connected to the gas-chromatograph are shown in Fig. 7. The peaks seen at 1 min and 1.8 min on the time scale correspond to tritium and tritiated methane, respectively. While the peak heights do not correspond exactly to the values of hydrogen and methane concentrations present in metal, these peaks clearly evidence a considerable amount of tritium absorbed as hydrogen in the stainless steel wall and as methane in the gold layer.

What is note worthy here is the much higher concentration of carbon in the stainless steel wall than in the gold layer, while no tritiated methane was detected from the wall. This means that the carbon contained in the wall steel does not serve as trapping site, being bound to metal atoms. The carbon contained in the gold layer, on the other hand, is apparently not bound by the gold atoms, and are consequently free to react easily with hydrogen and thus trap tritium under the influence of low energy electrons released from tritium decay [15),16)].

The total amount of carbon present in the gold layer of the loading vessel is 1.7×10^{-5}g. Assuming tritium to be

trapped in the carbon as CD_2T_2, the gold layer of the vessel is susceptible of accommodating 90 mCi of tritium at 470 C, at which the Run 26 in Fig. 5 was performed. This value is roughly equals the amount of tritium that would permeate through the same gold layer if devoid of trapping site during the 9 hours taken in Run 26 for the tritium leakage rate to reach calculated level. These results indicate that carbon deposited in the gold layer serves as main trapping site for the tritium, to impede its permeation through the gold plating.

IV Process monitoring by fluorescent powder detector

i) Experimental equipments

The tritium detector with fluorescent powder is shown in Fig. 8. The detector consists of swagelok joints, a glass filter and a quart rod. The cavity (2.4 mm i. d. and 6 mm length) inside the joint is filled with fluorescent powder (as received) which is optically coupled to a photon counter (modified National UD-505A) by the quart rod and optical fiber. A nylon ferrule was employed for a sealing between the joint and the quart rod. This detector was connected to DT fill system.

The tritium gas purchased from Dupon NEN was stored in the uranium bed in order to eliminate ^3He and CT_4.

Deuterium tritium mixture was prepared in a mixing chamber measuring pressure by a piezo electric transducer.

In order to measure the back ground level and its change due to repetitious use, the flourescent powder was repeatedly exposed to DT mixture of 0.26 MPa in pressure. The back ground noise was measured after evacuating to 10 Pa.

ii) Results and discutions

Luminance emitted from the powder exposed to DT mixture (T;40%) is shown in Fig.9 as a function of DT pressure. The luminance was in direct proportion to gas pressure. ZnS and Zn_2SiO_4:Mn gave sufficiently bright luminance to measure tritium in low pressure line of DT fill system. In following experiment, Zn_2SiO_4:Mn was chosen because of its short decay time of luminance and high signal to noise ratio.

Figure 10 shows dependence of luminance on tritium concentration and pressure of DT mixture. The luminance increased in good proportion to the tritium concentration and the total pressure of the DT mixture. These results indicate that fluorescent powder detector can directly measure partial pressure of tritium in DT mixture.

Increase of back ground noise of Zn_2SiO_4:Mn is shown in Fig,11. Initial noise of 0.06 (Arb.U.) is due to that of photon multiplier. Saturated noise after repetitious exposure was at the revel of 0.3 which can be calculated to the tritium partial pressure of $1.2X10^3$ Pa, which can be negligibly small for use in DT fill system.

Signal to noise ratio is shown in Fig.12, where the signal is defined as luminance obtained by exposure to equivalent DT mixture of 0.1 MPa in pressure and noise is defined as that obtained in 10 Pa. As far as the volume of powder is same, SN ratio becomes better when the powder diameter becomes smaller. This result may indicate that the back ground noise is not due to tritium absorbed on particle surface but due to that diffused into the powder particle.

V Summary

Various DT filled targets have been fabricated for implosion experiments by Gekko XII glass laser system, which achieved high neutron yield of $4X10^{12}$. Tritium fueling system and technical issues for tritium handling have been invesitgated and developed.

In order to reduce tritium leakage from the DT fill vessel, gold plating was applied to outside surface of the fill vessel. The leakage was suppressed to be 10^{-5}-10^{-6} times lower than what would be expected from the values reported for wrought gold. The effective suppression of tritium permeation is attributable to trapping of hydrogen by C contained in Au as impurity.

The tritium detection technique by means of fluorescent powder have been developed for monitoring the tritium in low pressure lines of DT fill system. Luminance emitted from Zn_2SiO_4 showed good linearity to partial pressure of tritium in DT mixture. Effect of impurity such as ^3He on luminance of fluorescent must be studied.

References

1) D.M.Nogami, J.Hayakawa, Y.Moriya ; J. Mater. Sci., 17, 2845, (1982).

2) U.Kubo et.al. ; ILE Osaka University annual report, ILE-APZ-79, 177, (1979).

3) T.Norimatsu, M.Takagi, Y.Izawa and C.Yamanak ; J. Nucl. Sci. and Technol., 23, 650, (1986).

4) E.H.Farnum, H.R.Maltrid ; Topical mtg. on inertial confinement fusion, Feb., 7-9, (1978), San Diego, CA..

5) C.Colmenares ; Lowrence Livermore National Laboratory Rept. UCRL-74680, (1973).

6) C.Colmenares, E.G.Shapiro, P.E.Barry and C.T.Prevo ; Nucl. Instr. and Meth., 114, 277, (1974).

7) D.H.W.Carstens ; Pro. 23rd Conf. Remote System Technol., 69, (1975).

8) R. J. Fries and E. H. Farnum ; Nucl. Instr. and Meth., 126, 285, (1975).

9) C.Yamanaka and S. Nakai ; Nature, 319,757, (1986).

10) C.Yamanaka et.al. ; 10th International Conf. on Plasma Phys. and Controlled Nucl. Fusion Research, IAEA-CN-44, London, UK, 12-19, Sept. (1984).

11) G.R.Gasky, G.R.Derrick ; Scripta Met., 10, 377, (1976).

12) Y.I.Zvezdin and Y.I.Belyyakov ; Diffusion Data, 2, 117, (1968).

13) R.B.Mclellan ; J. Phys. Chem. Solids, 34, 1137, (1973).

14) S.Imoto, Private communication.

15) C.I.H.Ashby ; J. Vac. Sci. Technol., A2(2), 639, (1984).

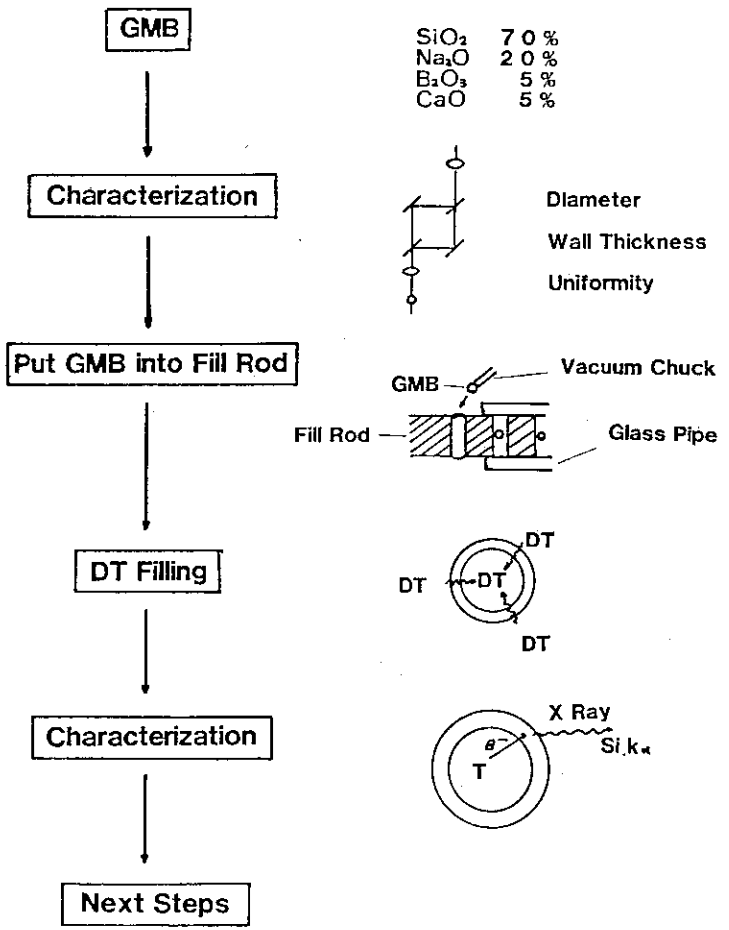

Fig. 1 Basic process to make DT filled glass microballoon target.

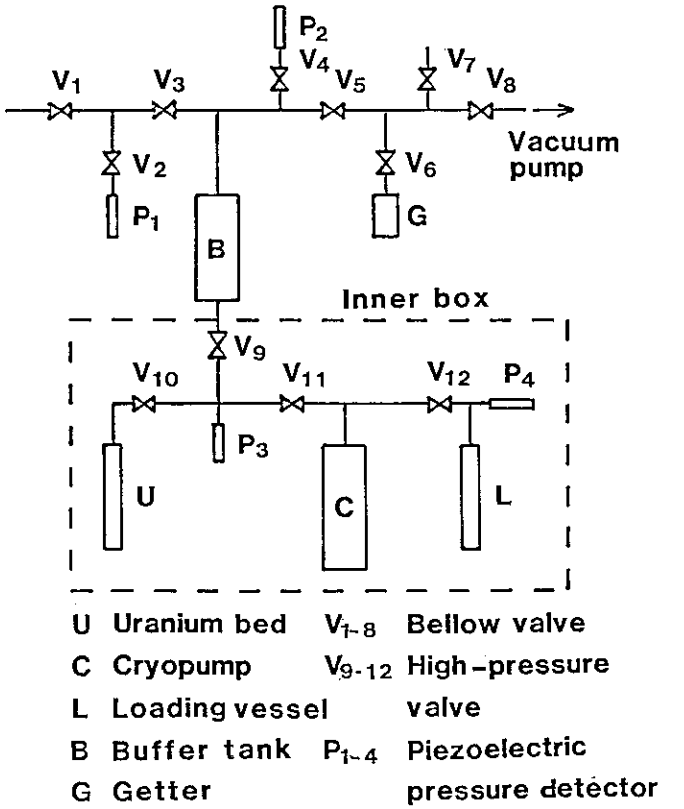

Fig. 2 DT fill system for ICF pellet target.

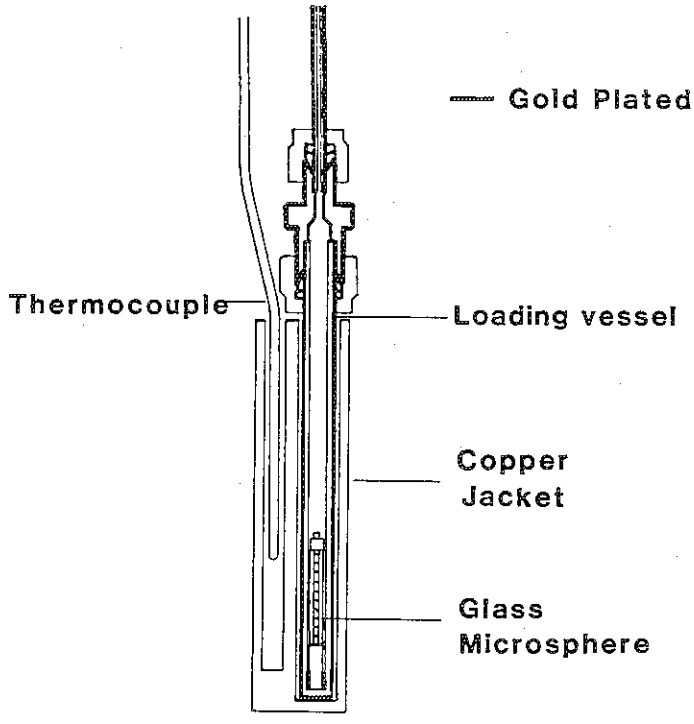

Fig. 3　Cross section of DT fill vessel. Walls applied exterior gold plating are indicated by bold lines.

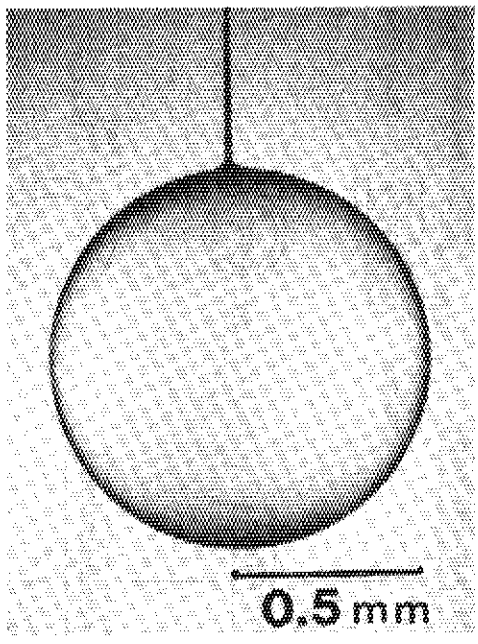

Fig. 4　Simple glass microballoon target.

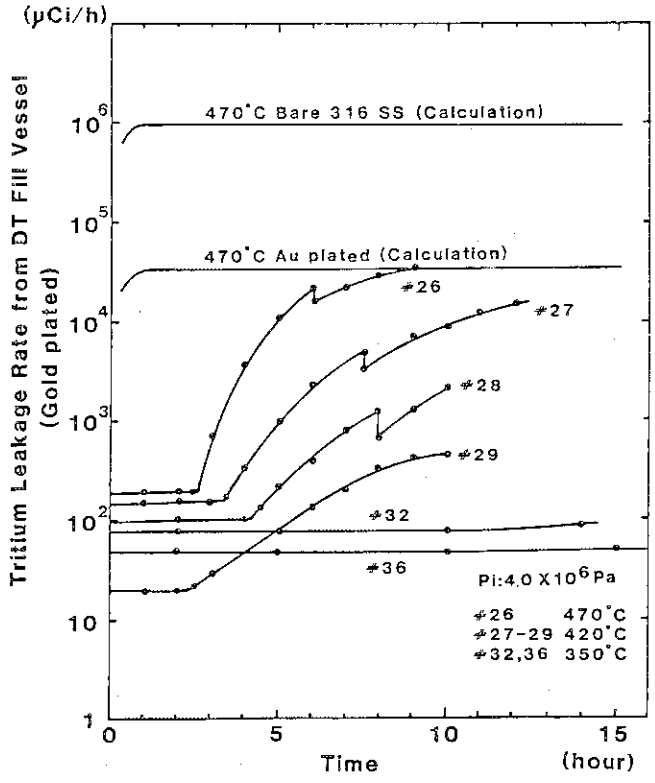

Fig. 5 Tritum leakage rate through Au plated SS vessel wall, derivered from tritium concentration in glove box.

Autoradiography of DT Absorbed Fill Tube

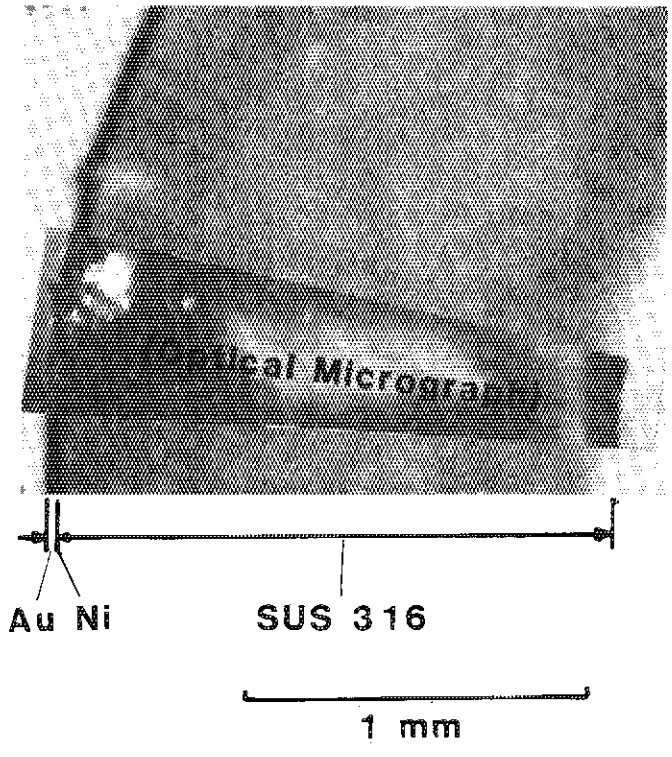

Fig. 6 Autoradiographs of fill vessel cross section after use.

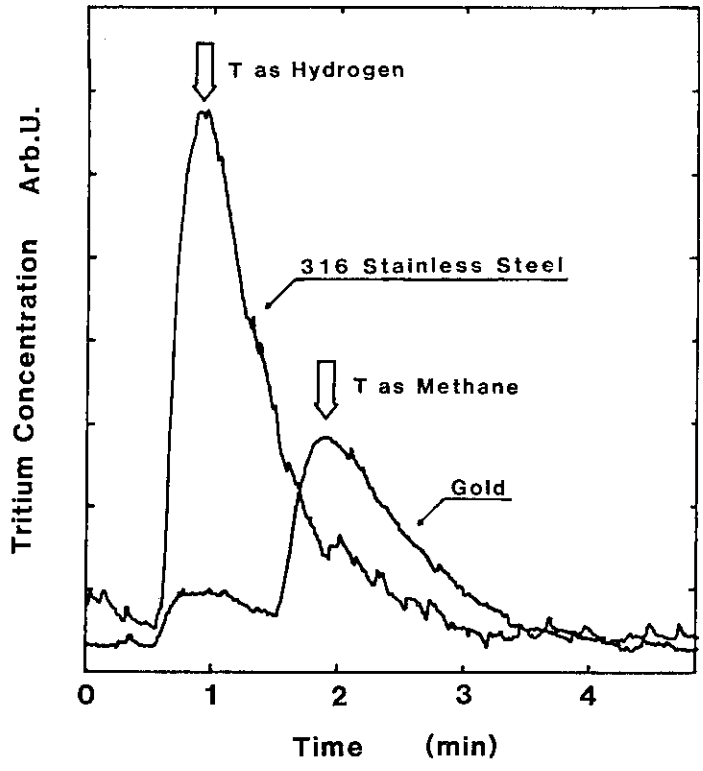

Fig. 7 Chromatograms of gases released from stainless wall and Au plating.

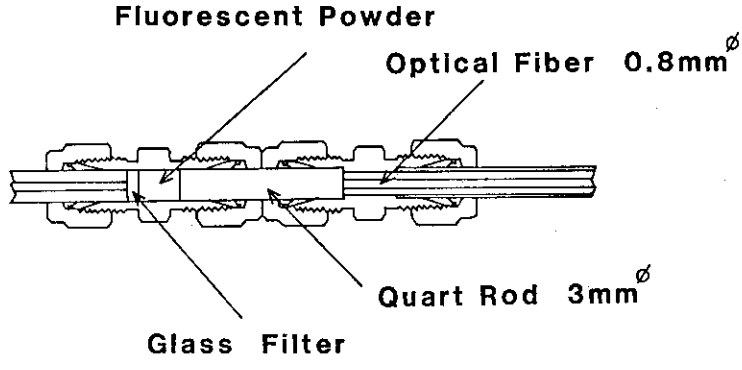

Fig. 8 Cross section of tritium detector by means of flourescent powder

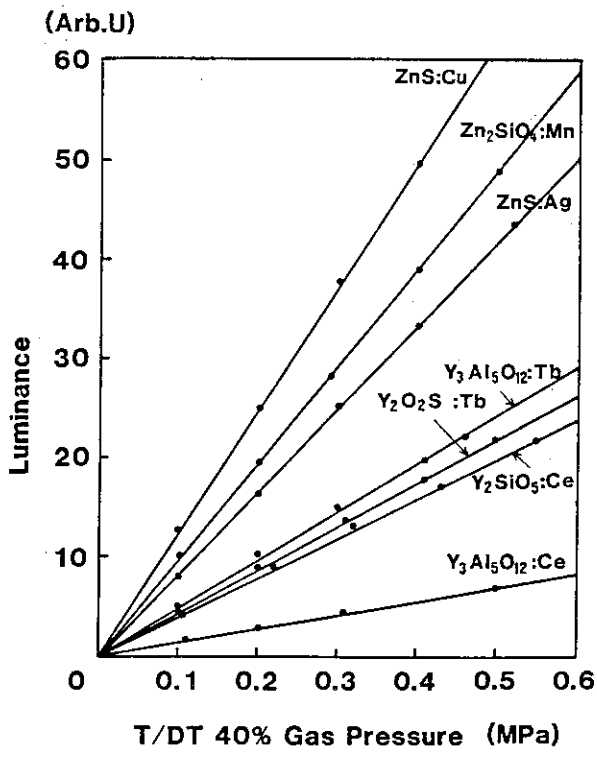

Fig. 9　Luminance emitted from fluorescent powders of 0.03

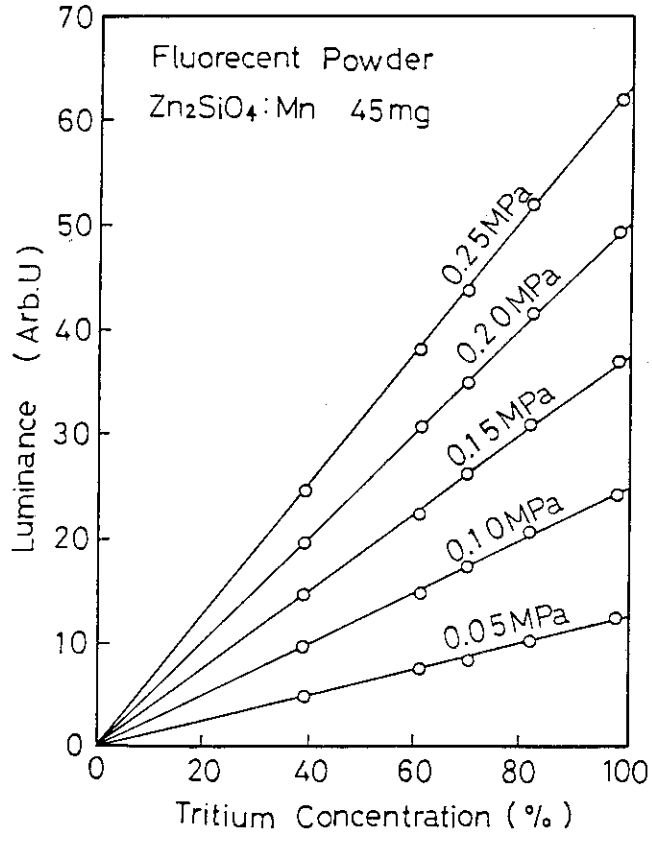

Fig.10　Dependence of luminance on tritium concentration and total pressure of DT mixture

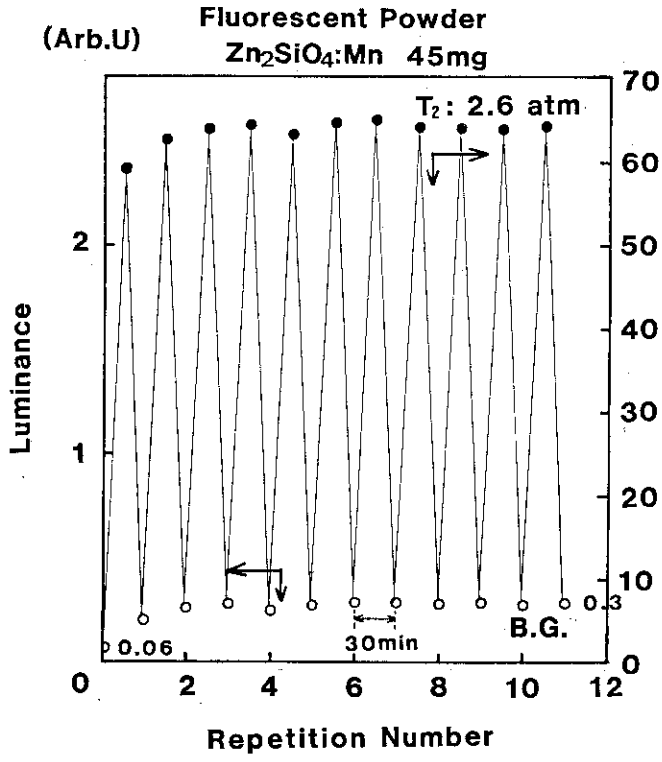

Fig.11 Back ground noise after repetitious exposure to DT gas

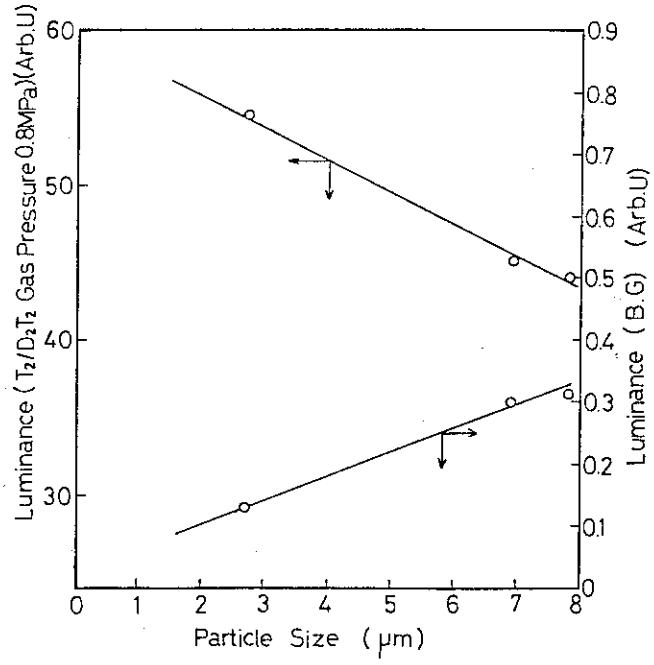

Fig.12 Dependence of SN ratio on particle diameter.

No.5 : Tritium Processing Technology Development at the Tritium Systems Test Assembly

by

James L. Anderson, Project Manager
Tritium Systems Test Assembly
Materials Science and Technology Division
Los Alamos National Laboratory
Los Alamos, New Mexico 87545, U.S.A.

ABSTRACT

The Tritium Systems Test Assembly (TSTA) at the Los Alamos National Laboratory has been operating with tritium since June 1984. Presently there are some 50 g of tritium in the main processing loop. This 50 g has been sufficient to do a number of experiments involving the cryogenic distillation isotope separation system and to integrate the fuel cleanup system into the main fuel processing loop. In January 1986 two major experiments were conducted. During these experiments the fuel cleanup system was integrated, through the transfer pumping system, with the isotope separation system, thus permitting testing on the integrated fuel processing loop. This integration of these systems leaves only the main vacuum system to be integrated into the TSTA fuel processing loop. In September 1986 another major tritium experiment was performed in which the integrated loop was operated, the tritium inventory increased to 50 g and additional measurements on the performance of the distillation system were taken. In the period June 1984 through September 1986 the TSTA system has processed well over 10^8 Ci of tritium. Total tritium emissions to the environment over this period have been less than 15 Ci. Personnel exposures during this period have totaled less than 100 person-mRem. To date, the development of tritium technology at TSTA has proceeded in progressive and orderly steps. In two years of operation with tritium, no major design flows have been uncovered.

INTRODUCTION

The Tritium Systems Test Assembly (TSTA) at Los Alamos is charged with developing the tritium technology required to fuel a fusion reactor. This technology includes vacuum systems for exhausting unburned D,T from the reactor; purification systems for removing chemical impurities from this exhaust gas; isotopic separation systems for separating HD, D_2, T_2, and DT; circulation and transfer pumps; and the evaluation, but not development, of tritium pellet injectors. A second major task at TSTA is the development and evaluation of safety and environmental systems associated with the tritium handling facilities at a fusion reactor. This includes development of new tritium monitors; room air detritiation systems; gaseous effluent detritiation systems; secondary and tertiary containment techniques; and techniques for performing routine and emergency maintenance on tritium contaminated systems.

Tritium experiments were initiated in June 1984 when 10 g of tritium was introduced into the cryogenic distillation isotope separation system. Since June 1984 the system has processed approximately 10^8 Ci of tritium.

The success of these operations is at least partially demonstrated by the fact that in the 19 month period from June 1984 through August 1986, tritium emissions to the environment have been less than 7 Ci as elemental tritium and less than 6 Ci as tritium oxide. This is a record unmatched by any other major tritium facility. Personnel exposures during this period have totaled less than 100 person-mRem. Experiments performed during this period include the tests on the isotope separation system,[1] tritium testing of a palladium alloy membrane diffuser,[2] evaluation of a ceramic electrolysis cell for decomposing tritiated water,[2] and tests to study the contamination and decontamination of surfaces exposed to elemental tritium and tritium oxide.[3]

RECENT OPERATIONS

In January 1986 two major experiments involving the isotope separation system were performed. The isotope separation system is a cryogenic, fractional distillation system.[4] This system takes 20-24 hours to cool from room temperature to liquid hydrogen temperature (20K), to liquify the hydrogen and to establish near equilibrium conditions in each of the four columns.

Also, when shutting down the system, it takes several hours to warm the columns, vaporize the hydrogen isotopes and transfer all of the hydrogen gas to the uranium beds for long-term storage as uranium hydrides. For this reason, a major experiment takes several days to conduct. During these periods, the TSTA must continuously be staffed by a minimum of two experienced, knowledgeable people. Within the limitations of our staffing level, as dictated by budget constraints, it is difficult to operate frequently for extended periods of time. Because we are thus limited in how frequently we can schedule these major runs, we must carefully plan the experiments to be performed during these periods.

The first run in January 1986 was the first major experiment since June 1984. Following the June 1984 run, several small, but significant modifications were made to the isotope separation system and to the associated plumbing. Because of this long down-time between experiments, it required even longer than the planned 24 hours to bring the distillation system on-line. Once on-line, several significant accomplishments were attained. During this run the tritium inventory in the isotope separation system was increased from ~10 g (10^5 Ci) to ~30 g (300,000 Ci). Hydrogen and deuterium gas was removed from the distillation system and replaced by tritium over a period of two days as the tritium inventory was increased to the 30 g level. This demonstrated the ability to replace and to change the gas mixture to the isotope separation system. During this experiment, the isotope separation system was operated in a recycle mode. In this mode, products from the four columns are mixed together and this mix fed as input to the first column.

At the end of this week, the isotope separation system was shut down and the new deuterium-tritium gas mixture was quantitatively transferred to the uranium storage beds. One week later a second major experiment was conducted, again involving the isotope separation system. This time we were able to bring the distillation system on-line quickly (less than 24 hours) and to re-establish the stable operating mode reached during the first week. Once this state was established, the chemical impurity removal system, (the fuel cleanup system) was interfaced with the isotope separation system. This integration of these two major systems plus the associated transfer pumping system was a major advance in the TSTA program. During this test the D,T gas mixture

was circulated through the fuel cleanup system, using the TSTA developed, all-metal transfer pumping system, into the cryogenic distillation system. The D,T gas used during this test was free of chemical impurities so the fuel cleanup system was not used to remove impurities. The major goal of this test was the integration of the fuel cleanup-transfer pump-isotope separation systems.

In addition to the integrated operation of this loop with a 30 g tritium inventory, several other technical goals were achieved in the January operations. Within the cryogenic distillation columns, the axial composition profiles of hydrogen isotopes were measured. We also began to accumulate a data base on how flow rates, pressure differential and hydrogen isotope ratios affect the interactions among the four columns.

In September 1986, a third major experimental campaign resulted in the increase of the tritium inventory in the loop to 50 g. In this experiment we again operated the integrated fuel cleanup, transfer pump, isotope separation system in the recycle mode. During this experiment the molecular sieve front-end portion of the fuel cleanup from the tritium which was added to the system to increase the inventory to the 50 g level. The impurities removed were primarily N_2 but some traces of other compounds of carbon, nitrogen and oxygen were successfully removed by the fuel cleanup system. Also during this experiment we prepared and collected approximately 5 g of high purity (>99%) tritium. Small quantities of tritium of purity greater than 99.9% were also collected.

The distillation system was designed for an equilibrium tritium inventory of about 90 g. Until we have introduced that complete inventory we will not be able to demonstrate completely the ultimate performance of this system for separating hydrogen isotopes. However, the total data collected through September 1986 definitely indicate that the distillation system will perform well within the design specifications. These specifications are to produce four hydrogen steams:

1) A HD stream free of tritium
2) A pure D_2 stream (>99.96% D_2)
3) A 1:1 mix DT stream (>99.99% DT)
4) A pure T_2 stream (>99% T_2)

while operating at the maximum flow rate of 360 g moles per day of a deuterium tritium gas mixture. This corresponds to a tritium flow of about 1 kg per day through the loop. This is essentially a full scale system for an INTOR-size fusion machine (1.5 GWe).

Other major accomplishments during the January experiment include the demonstration of easy start-up and rapid, safe shutdown of the system. Start-up for the first week of operation was admittedly slow, but the system had undergone significant modifications between June 1984 and January 1986. Start-up for the second experiment in January 1986 went very smoothly. At the conclusion of each of the runs in January the deuterium-tritium mixture was vaporized and the gas mixture transferred quickly to the uranium storage beds where the hydrogen isotopes are stored as solid uranium hydrides. These tests confirmed the reversible operation of our uranium storage beds.[5]

After the eight month shutdown between January and September, we were able to start up the system very quickly for the September experiments. This indicates that as the TSTA staff becomes more familiar with the system, the operations will become more routine.

MAINTENANCE TECHNIQUES DEMONSTRATED

A major accomplishment at TSTA since the start of tritium experiments in June 1984 has been the demonstration of techniques for doing maintenance and equipment change-out on tritium contaminated components. In the time between the June 1984 and the first run in January 1986, extensive modifications and maintenance were performed on these systems. Similarly, in the period between the two runs in January 1986 and immediately following the second run, extensive maintenance was performed on the system. This maintenance included replacement of some components, repair of a faulty weld joint, addition of new piping and components to the tritium contaminated system, and major modifications to the gloveboxes which provide secondary containment for these systems.

All of this maintenance and modification was performed without any major release of tritium to the facility or to the environment (<1 Ci total) and with no measurable exposure of operating personnel to tritium. This was accomplished by carefully purging and evacuating any line before starting the maintenance operation, by the use of gloveboxes as secondary containment, and by

extensive use of the flexible ventilation duct (elephant trunk) to control air flow around the contaminated components under maintenance, Fig. 1. Frequently a glovebox window had to be removed to provide adequate access to the component in question. In these cases the elephant trunk is used to provide adequate air flow by attaching the trunk to a glove port in a different area of the glovebox. This then pulls air in the box where the window is removed, across the work area, and out through the elephant trunk, thus converting the glovebox to a fume hood, Fig. 2. On very large components which might not be enclosed in a glovebox, a plastic tent or shroud can be erected around the components, again using the elephant trunk to provide an adequate air flow. The operating personnel may use self-contained breathing air units or in extreme cases, may be suited up in plastic suits with supplied breathing air.

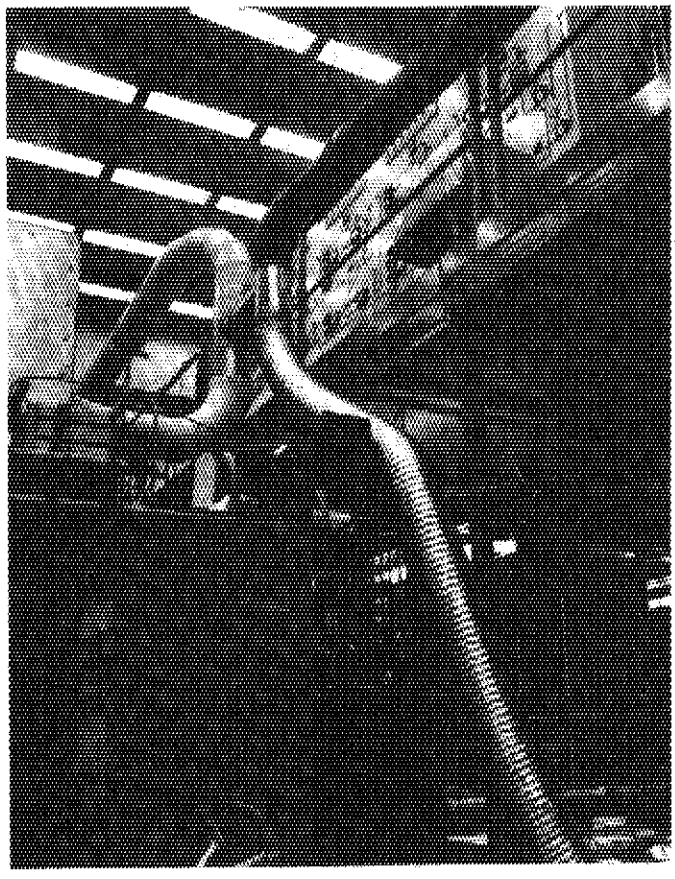

Fig. 1. The Flexible Ventilation duct (Elephant Trunk) at TSTA.

The experience at TSTA has demonstrated that these techniques are perfectly suitable for performing maintenance on tritium-contaminated equipment. The exhaust gas from the elephant trunk is continuously monitored during operation. In future fusion facilities, if high tritium levels are detected in the gas, the stream can be routed to an air detritiation system. If the tritium levels are low (as we have observed at TSTA), this exhaust gas can be released directly to the atmosphere through the facility stack. The practical experience at TSTA in 1986 has clearly demonstrated that these techniques can and will work.

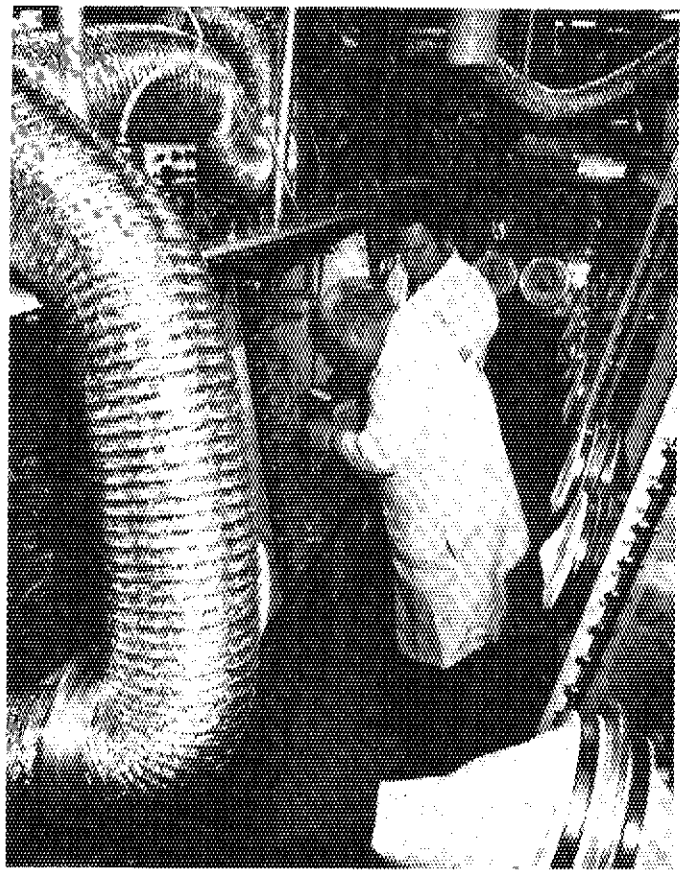

Fig. 2. The Elephant Trunk attached to a glovebox, thus converting the glovebox to a fume hood. Also shown is a Health Physics Technician providing monitoring help during a maintenance operation.

FUTURE PLANS AT TSTA

In the coming few months, a number of major experiments are anticipated at TSTA. We will continue to evaluate the efficiency of the fuel cleanup system for removing and decomposing impurities[7] in the D,T gas stream. These tests can be done using the transfer pumping and fuel cleanup system, but will not require the isotope separation system. At the completion of these tests, a series of major experiments using the integrated process loop will be performed. During these tests the tritium inventory in the loop will be increased to about 100 g and the performance of the distillation system will be thoroughly investigated. We will also begin to do integrated operation of the fuel clean-up transfer pump-isotope separation systems at the design flow rates and with impurity injection in the D,T gas feed to the fuel cleanup system. Once these series of tests have been completed, we will work to integrate the vacuum system into the process loop and proceed to evaluate the compound cryopumps with tritium. Ultimately we will plan to operate this integrated loop for long periods of time to build up a data base on system efficiency, component reliability and system availability. This data base will then be available to designers of future fusion machines such as the Compact Ignition Tokomak (CIT), the Fusion Engineering Reactor (FER) in Japan, and the Engineering Test Reactor (ETR) now being considered on the international front.

To date the development of tritium technology at TSTA has proceeded in progressive and orderly steps. In two years operations with tritium, no major design flaws have been uncovered. In addition to operating and evaluating the existing components at TSTA, we are continuing to work on the development of new and improved components. By maintaining close contact with other tritium technology projects within the US DOE (Sandia Laboratories, Mound Laboratory, Savannah River, other Los Alamos tritium projects, and the Tokamak Fusion Test Reactor, TFTR, at Princeton) and with the developing fusion tritium programs in Japan, Canada, and Europe, we have stayed at the forefront of tritium technology. As the only integrated loop testing facility in the fusion program we have an opportunity and an obligation to develop avenues for the exchange of data, ideas, and operating experience among these parties. This is a responsibility we consider to be among our most important assignments.

REFERENCES

1. J. R. BARTLIT and J. L. ANDERSON, "Current Operations and Experiments at the Tritium Systems Test Assembly," Proc. of 11th Symposium on Fusion Engineering, IEEE, Austin, TX, Nov. 18-22, 1985.

2. S. KONISHI, et. al, "Experiments on a Ceramic Electrolysis Cell and a Palladium Diffuser at the Tritium Systems Test Assembly." Fusion Tech; 8 #2, Part 2, 2042 (1985).

3. D. F. HOLLAND and R. A. JALBERT, "A Model for Tritium Concentration following Tritium Release into a Test Cell and Subsequent Operation of an Atmospheric Cleanup System," Proc. of 11th Symposim on Fusion Engineering, IEEE, Austin, TX, Nov. 18-25, 1985.

4. J. R. BARTLIT, W. H. DENTON, and R. H. SHERMAN, "Hydrogen Isotope Distillation for the Tritium Systems Test Assembly," Proc of 3rd Topical Meeting on Technology of Fusion Energy, Santa Fe, NM, May 9-11, 1978, p. 778.

5. C. R. WALTHERS, "Description and Performance of Uranium Beds used to Pump Tritium-Deuterium at the Tritium Systems Test Assembly," J. Vac. Sci. Technol., A2 (2), 722 (1984).

6. E. C. KERR, J. R. BARTLIT, and R. H. SHERMAN, "Fuel Cleanup System for the Tritium Systems Test Assembly: Design and Experiments," Proc. Tritium Technology in Fission, Fusion and Isotopic Applications, Dayton, OH, April 29-May 1, 1980, p. 115.

No.6 TRITIUM SCAVENGING FROM GAS STREAM UNDER VARIOUS CONDITIONS

Masabumi NISHIKAWA (Kyushu University)

It has been conceptualized to set up the multi-barrier containment system for tritium handling facilities and it has been also discussed to apply the catalytic treatment on tritium or tritiated water in both of atmospheres with and without the chemically active components. Four methods are thought to be available for scavenging tritium from gas streams, that is, oxidation of tritium and following adsorption of oxidized tritium, fixation of tritium as the crystal water by isotope exchange reaction, formation of the metal tritide and adsorption at cryogenic temperature.

Performances of various catalysts shown in Fig. 1 have been experimented and compared under various conditions as summarized in Fig. 2, and remarks obtained based on our experiencies are listed in Fig. 3. In this figure, such empty positions mean "no need of consideration", as the oxidation capacity of the precious metal catalysts without oxygen gas in the bulk stream, water adsorption characteristics of the metal oxide catalysts or hydrophobic catalysts, uptake capacity of tritium into metal oxide catalysts which have no crystal water.

Proper voidage in a packed bed can be obtained with almost

all catalysts except fibered catalysts such as Pt-asbestos. A porous silver substrate and CuO wire have only small effective surface area, which results that they are not useful to make the packed column.

Almost all metal oxide catalysts have the good oxidation capacity. Hopcalite catalysts are recommended to use at the higher temperature than 200 °C for oxidation of tritium in an inactive gas as glovebox atmosphere from the viewpoint of oxidation rate and performancies at reacivation. Mixing of precious metal catalysts with hopcalites is also recommended because some amount of oxygen is released from hopcalites. Effective surface area of spongy CuO decreases with repeated reactivation because of sintering. These metal oxide catalysts tested have almost no activity for the isotope exchange reaction and show almost no poisoning effect by water vapor because of high temperature to be used.

Oxidation rate of tritium with precious meatal catalysts are superior to that with metal oxide catalysts, though a fair amount of oxygen is needed. Rather rapid reduction of the catalytic activity occurs with the precious metal catalysts, thogh this poisoning effect of the adsorbed water can be neglected by setting the pre-adsorption bed at the upper course of the catalyst bed , by swamping of the hydrogen gas to obtain the heat of reaction or by heating the catalyst bed. It is noted, however, that the bed temperature of the hydrophobic catalyst should not rise higher than 150 - 200 °C, because the substrate burns. Overall mass transfer coefficient

of oxidation with Pt-MS 4A is almost same as that with Pt-alumina or Pt-MS 5A but gradually reduces with time. This may be caused by the water formed in the micro pores.

Isotope exchange reaction rate with precious metal catalysts are excellent.

The adsorption characteristics of hydrophilic catalysts are almost same as that of the substrate without precious metal particles though the adsorption capacity decreases a little. Accordingly, use of the catalyst bed at the ambient temperature may need no adsorption column in the lower course when the preadsorption bed is set in the upper course, though other catalysts should have the adsorption column in the lower course of the catalyst bed. Cooling of the stream from the catalyst bed is required, then.

The uptake capacity of tritium as the crystal water of the hydrophilic substrates are excellent and those values are not so much affected by temperature.

Oxidation of hydrocarbon can take place at higher temperature than 400 °C with precious metal catalysts, though the effective oxidation can not be expected with the metal oxide catalysts. It is also noted that uptake of tritium from tritiated hydrocarbon would occur by the isotope exchange reaction at the rather slow rate.

Chemical forms and places of tritium scavenged vary for any combination of catalyst beds and adsorption beds or any combination of chemical forms of tritium to be treated and swamping gases as shown in Figs. 4 - 7. In these figures,

upper bunches mean that O_2 , H_2O or H_2 is included in the bulk gas stream and lower bunches mean no existence. Figs. 5 - 7 give the chemical forms and places of scavenged tritium for T_2 , T_2O and CT_4 , respectively. The places where the scavenged tritium is dominantly held are indicated by solid underlines in these figures and tritium caught in the places shown by broken underlines can not be ignored in considering tritium balance.

Tritium in the form of adsorbed water can be easily released from catalyst or adsorbent by purging with dry gas at high temperature, though tritium held in the form of the crystal water of the substrate would not. It is needed for the recovery of tritium from the crystal water to apply the isotope exchange reactions. Tritium in molecular form can be recovered by introducing H_2 or D_2 gas into the purge gas to the catalyst bed with hydrophilic catalysts and tritiated water by H_2O.

Tritium may be recovered from inert gases by active metal getters or cryosorption bed. However, there are no better ways than the catalytic scavenging methods where oxygen, water or other chemically active species are present in the gas stream. Use of precious metal catalysts with hydrophilic substrate is recommended because they can oxidize tritium at moderate to ambient temperatures and the ability to operate at the ambient temperature without preheating and post cooling is a large advantage in the ease of the system operation. the catalyst bed with hydrophilic substrate

can also play the role of adsorption bed. It can also catch tritium from the inert gas by isotope exchange reaction.

Activity in the tritium oxidation of the precious metal catalysts is largely decreased, however, when the water vapor exists in the gas stream. The way to get the pre-adsorption bed bed in the upper course of the catalyst bed is recommended to preserve the oxidation ability of tritium at the ambient temperature.

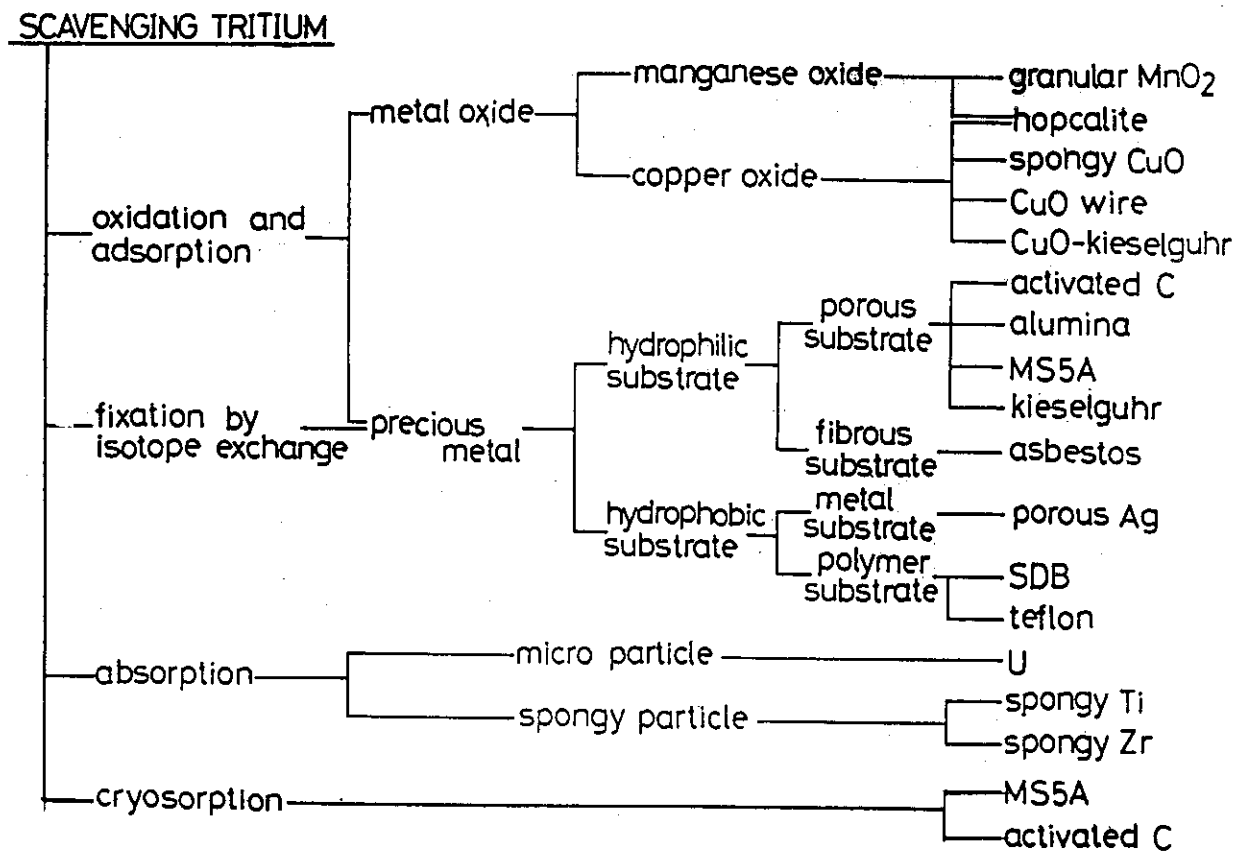

Fig. 1

Characteristics

1. Packing bed with proper voidage, α
2. Effective surface area, BET area
3. Oxidation capacity (in case no O_2 in stream)
4. Oxidation rate, K_F , k_r , k_g , k_s
   --- ambient temperature
   --- 100 - 200 C
   --- 200 - 400 C
   --- 400 C -
5. Oxidation rate in humid atomosphere
6. Reactivation performance
   (oxidation, drying, exchange reaction)
7. Rate of isotope exchange reaction
8. Adsorption of HTO
   --- cryo condition
   --- low temperature
   --- ambient temperature
   --- high temperature
9. Adsorption rate
10. Uptake capacity of tritium into packed pellet
    --- cryo condition
    --- ambient temperature
    --- 100 - 200 C
    --- 200 - 400 C
    --- 400 C -
11. Oxidation of hydrocarbon
12. Isotope exchange from hydrocarbon
13. Needs of adsorption bed

Fig. 2

Characteristics		Catalyst materials												
		(1)	(2)	(3)	(4)	(5)	(6)	(7)	(8)	(9)	(10)	(11)	(12)	(13)
(1)		ex	ex	g	p	ex	ex	ex	ex	ex	ng	ex	ex	ex
(2)		ex	ex	g	ng	ex	ex	ex	ex	ex	g	p	ex	ex
(3)		ex	ex	ex	g	ex								
(4)	i	ng	ng	ng	ng	ng	g	ex	ex	ex	ex	g	ex	g
	ii	p	p	ng	ng	ng	g	ex	ex	ex	g	g	ex	ex
	iii	g	ex	p	p	p	ng	ex	ex	ex	g	g	ng	ng
	iv	g	ex	g	g	g	ng	ex	ex	ex	g	g	ng	ng
(5)		g	g	g	g	g	p	p	p	p	p	p	p	p
(6)		ex	ex	p	p	g	ex	ex	ex	ex	g	g	g	ex
(7)		ng	ng	ng	ng	ng	ex	ex	ex	ex	ex	ex	ex	ex
(8)	i	g	g	g	p	g	g	g	g	g	g	p	p	p
	ii						g	ex	ex	p	ng	ng	ng	ng
	iii					p	p	ex	ex	p	ng			
	iv					ng	ng	ng	ng	ng	ng			
(9)						g	g	ex	ex	g	p			
(10)	i	p	p	p	ng	p	p	p	p	p	p	p	p	p
	ii					p	ng	ex	ex	p	ng	ng	p	ng
	iii					ng	ng	g	g	ng	ng	ng	p	ng
	iv					ng	ng	g	g	ng	ng	ng	ng	ng
	v					ng	ng	g	g	ng	ng	ng	ng	ng
(11)		ng	p	ng	ng	ng	ng	g	g	g	p	ng	ng	ng
(12)		ng	ng	ng	ng	ng	g	g	g	g	g	p	p	ng
(13)		need	need	need	need	need	need	not always	not always	need	need	need	need	need

remarks: ex---excellent, g---good, p---poor, ng---no good, ---no need of consideration

Fig. 3

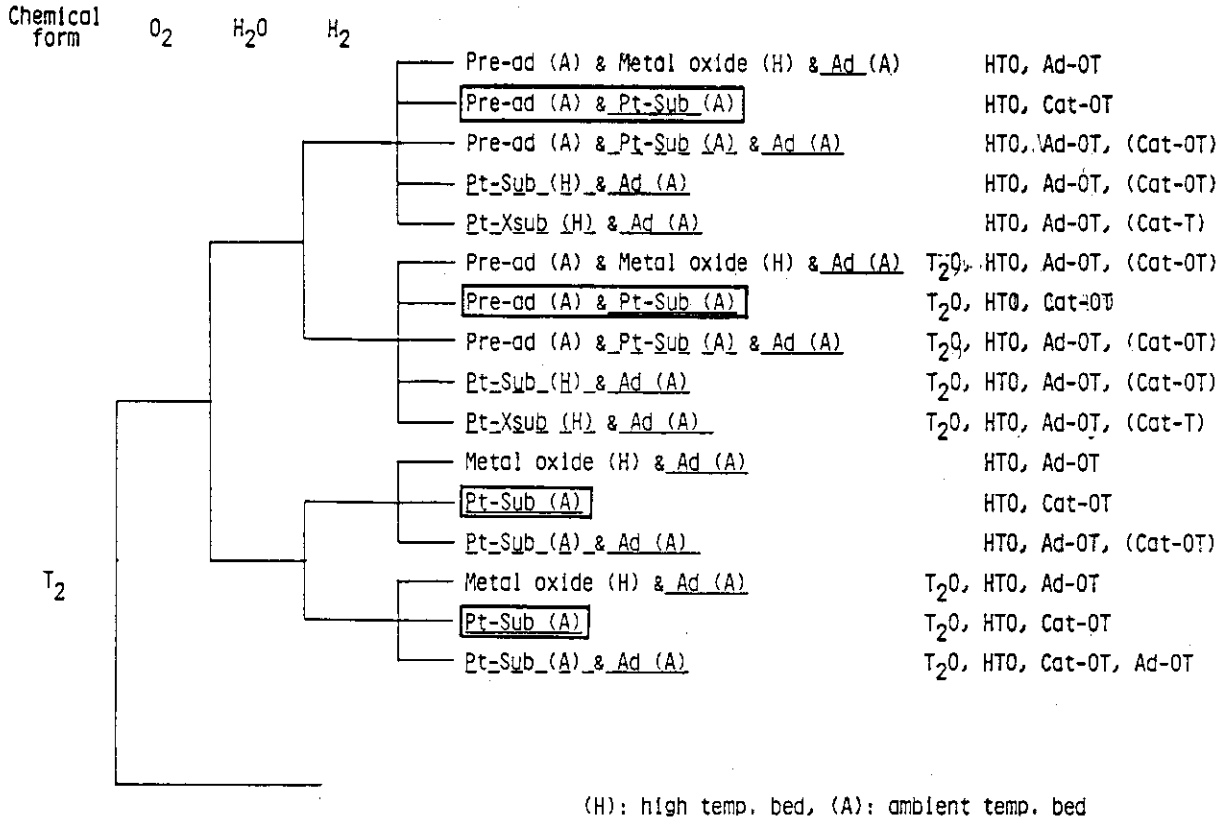

(H): high temp. bed, (A): ambient temp. bed
Ad: adsorption bed,
Pt-Sub: precious meatal catalyst with hydrophilic sub.
Pt-Xsub: with hydrophobic substrate

Fig. 4

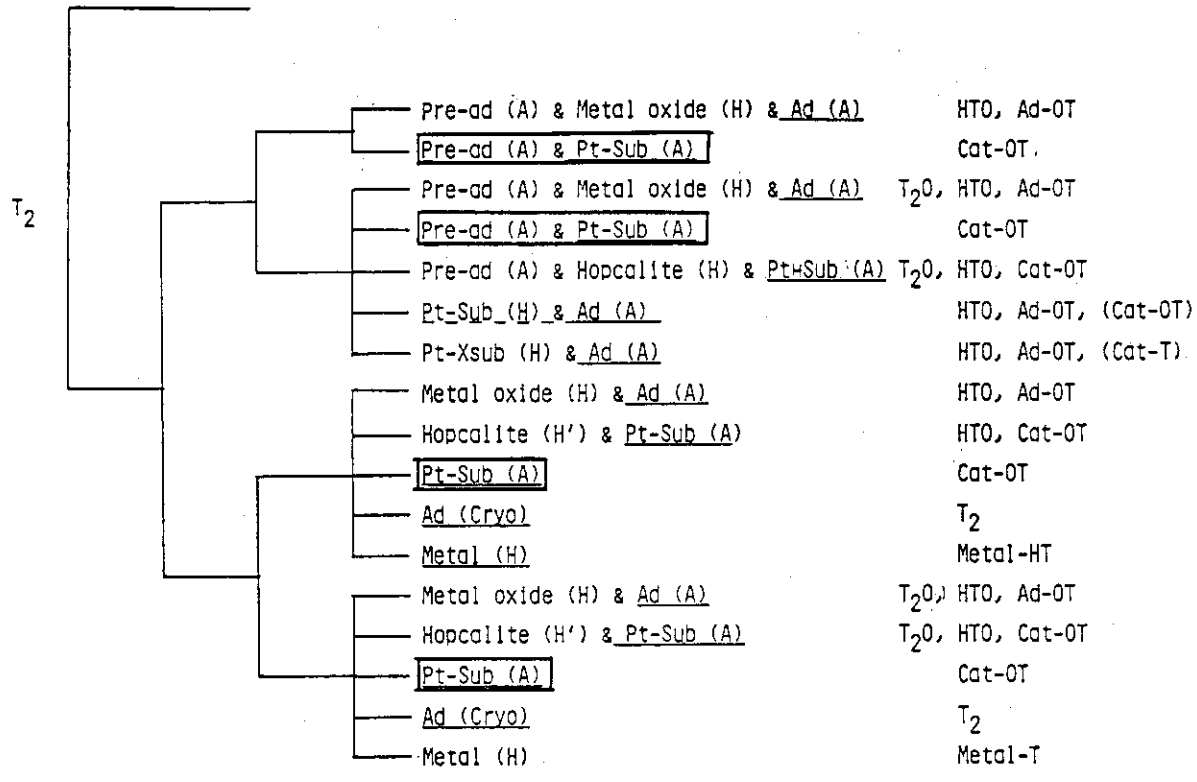

Fig. 5

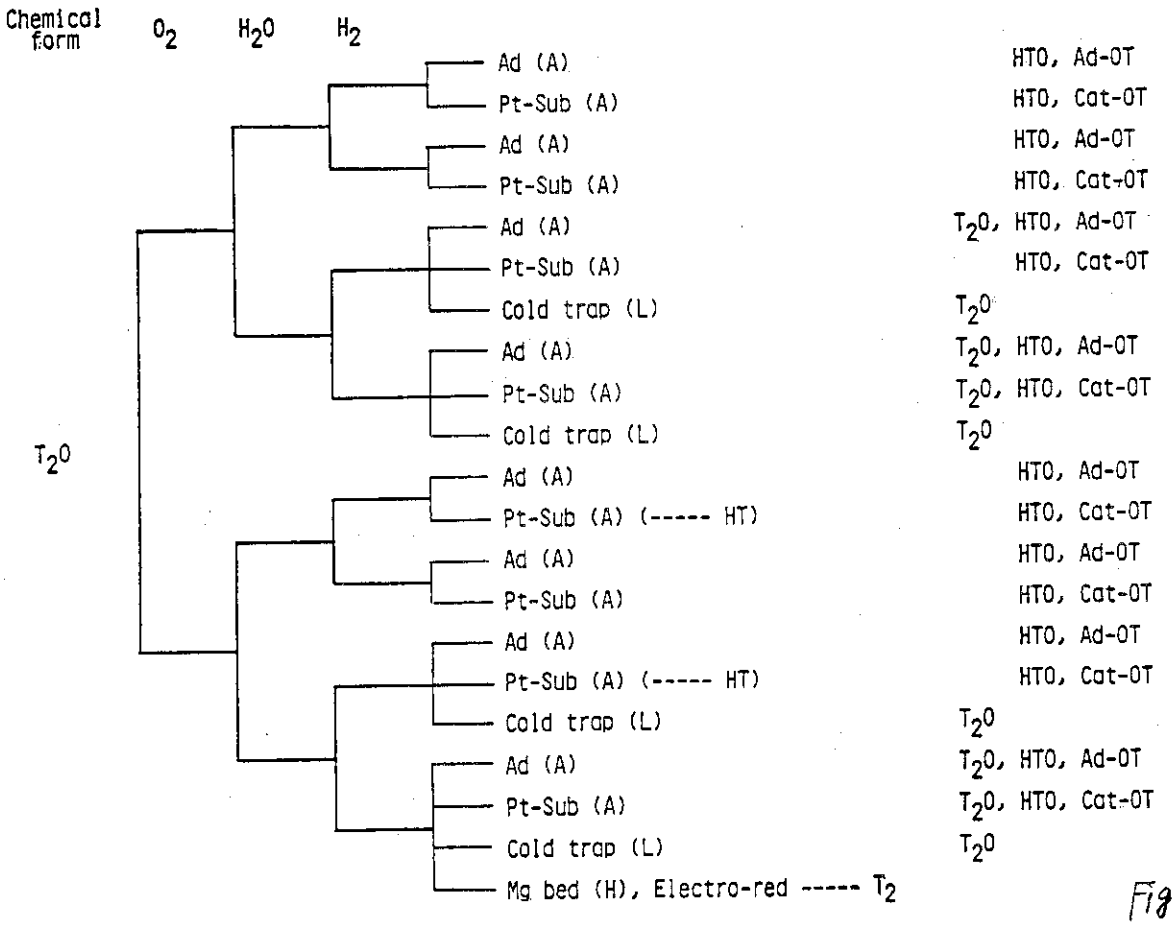
Chemical form
O_2
H_2O
H_2
T_2O
Ad (A) — HTO, Ad-OT
Pt-Sub (A) — HTO, Cat-OT
Ad (A) — HTO, Ad-OT
Pt-Sub (A) — HTO, Cat-OT
Ad (A) — T_2O, HTO, Ad-OT
Pt-Sub (A) — HTO, Cat-OT
Cold trap (L) — T_2O
Ad (A) — T_2O, HTO, Ad-OT
Pt-Sub (A) — T_2O, HTO, Cat-OT
Cold trap (L) — T_2O
Ad (A) — HTO, Ad-OT
Pt-Sub (A) (----- HT) — HTO, Cat-OT
Ad (A) — HTO, Ad-OT
Pt-Sub (A) — HTO, Cat-OT
Ad (A) — HTO, Ad-OT
Pt-Sub (A) (----- HT) — HTO, Cat-OT
Cold trap (L) — T_2O
Ad (A) — T_2O, HTO, Ad-OT
Pt-Sub (A) — T_2O, HTO, Cat-OT
Cold trap (L) — T_2O
Mg bed (H), Electro-red ----- T_2

Fig 6

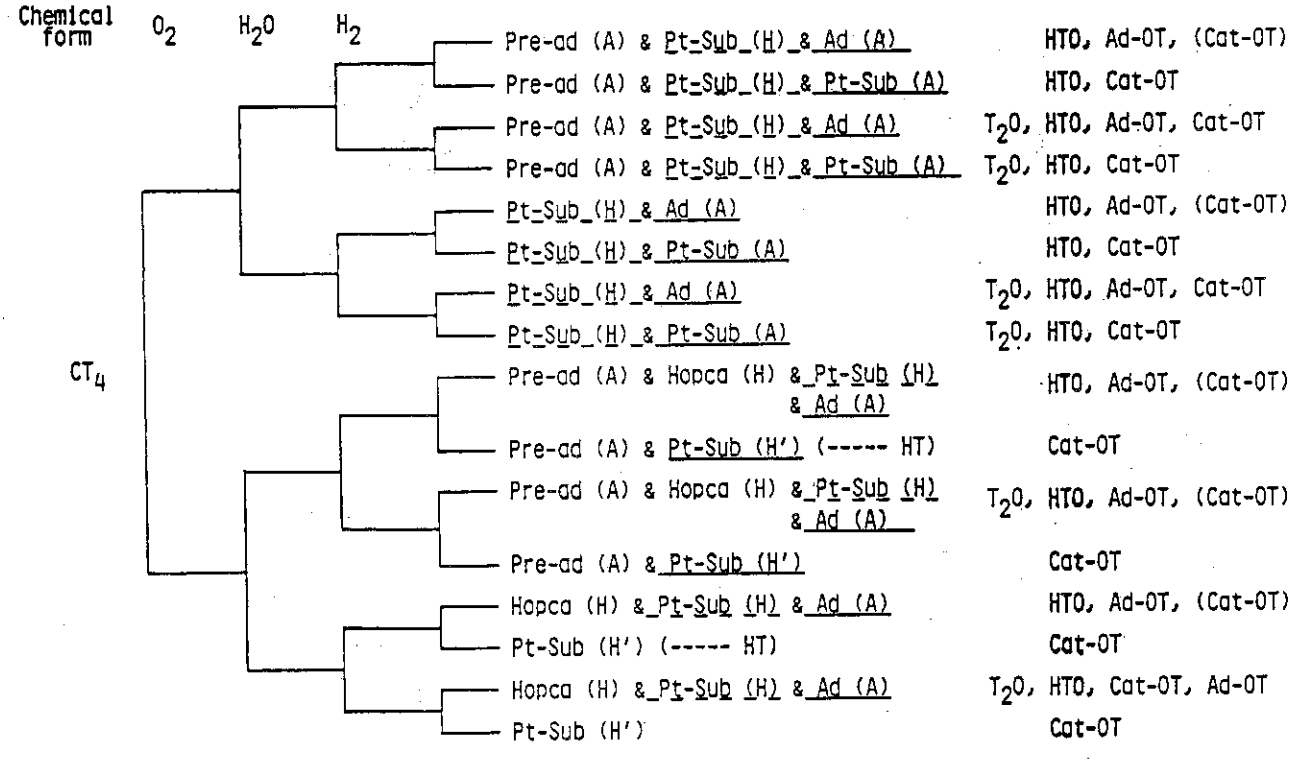
Chemical form
O_2
H_2O
H_2
CT_4
Pre-ad (A) & Pt-Sub (H) & Ad (A) — HTO, Ad-OT, (Cat-OT)
Pre-ad (A) & Pt-Sub (H) & Pt-Sub (A) — HTO, Cat-OT
Pre-ad (A) & Pt-Sub (H) & Ad (A) — T_2O, HTO, Ad-OT, Cat-OT
Pre-ad (A) & Pt-Sub (H) & Pt-Sub (A) — T_2O, HTO, Cat-OT
Pt-Sub (H) & Ad (A) — HTO, Ad-OT, (Cat-OT)
Pt-Sub (H) & Pt-Sub (A) — HTO, Cat-OT
Pt-Sub (H) & Ad (A) — T_2O, HTO, Ad-OT, Cat-OT
Pt-Sub (H) & Pt-Sub (A) — T_2O, HTO, Cat-OT
Pre-ad (A) & Hopca (H) & Pt-Sub (H) & Ad (A) — HTO, Ad-OT, (Cat-OT)
Pre-ad (A) & Pt-Sub (H') (----- HT) — Cat-OT
Pre-ad (A) & Hopca (H) & Pt-Sub (H) & Ad (A) — T_2O, HTO, Ad-OT, (Cat-OT)
Pre-ad (A) & Pt-Sub (H') — Cat-OT
Hopca (H) & Pt-Sub (H) & Ad (A) — HTO, Ad-OT, (Cat-OT)
Pt-Sub (H') (----- HT) — Cat-OT
Hopca (H) & Pt-Sub (H) & Ad (A) — T_2O, HTO, Cat-OT, Ad-OT
Pt-Sub (H') — Cat-OT

Fig. 7

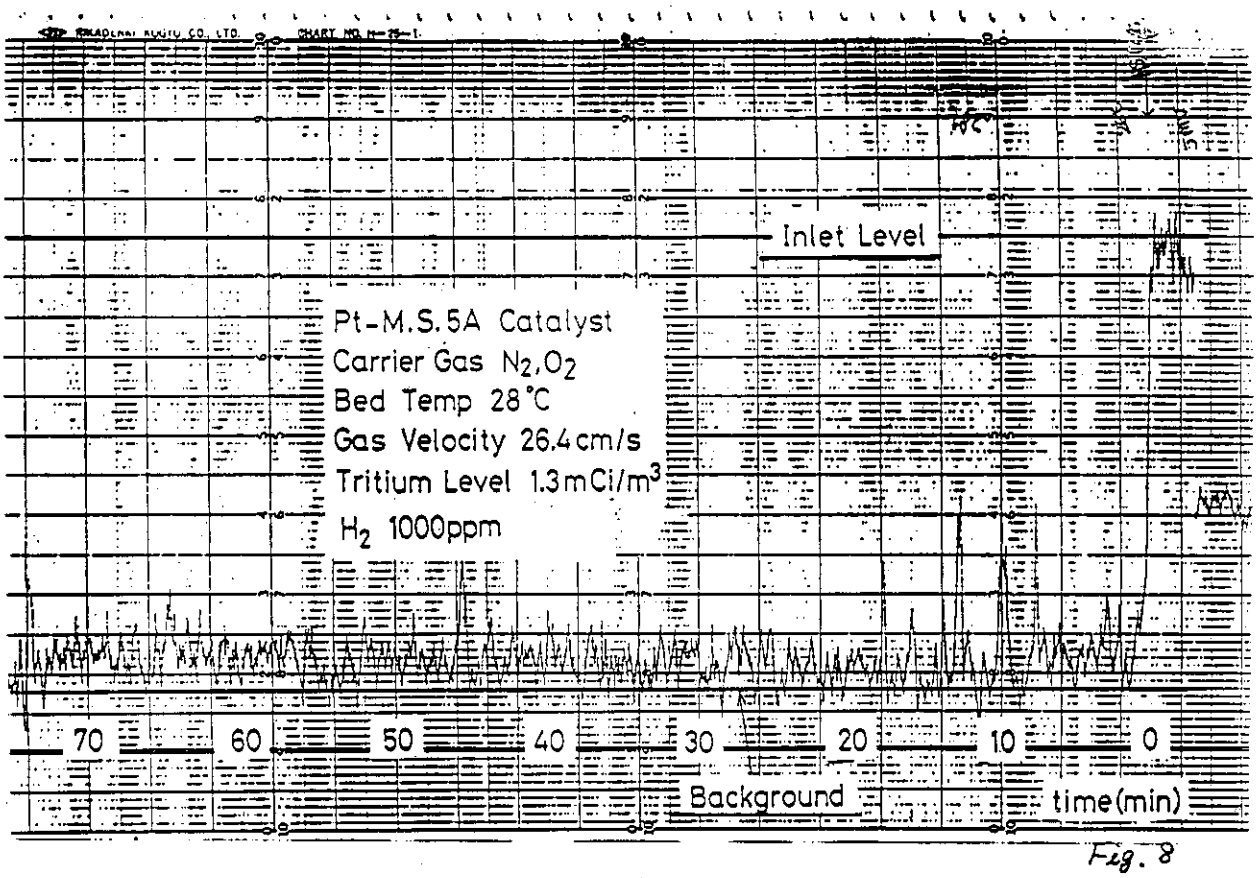
Inlet Level
Pt-M.S.5A Catalyst
Carrier Gas N_2,O_2
Bed Temp 28℃
Gas Velocity 26.4cm/s
Tritium Level 1.3mCi/m^3
H_2 1000ppm
70
60
50
40
30
20
10
0
Background
time(min)

Fig. 8

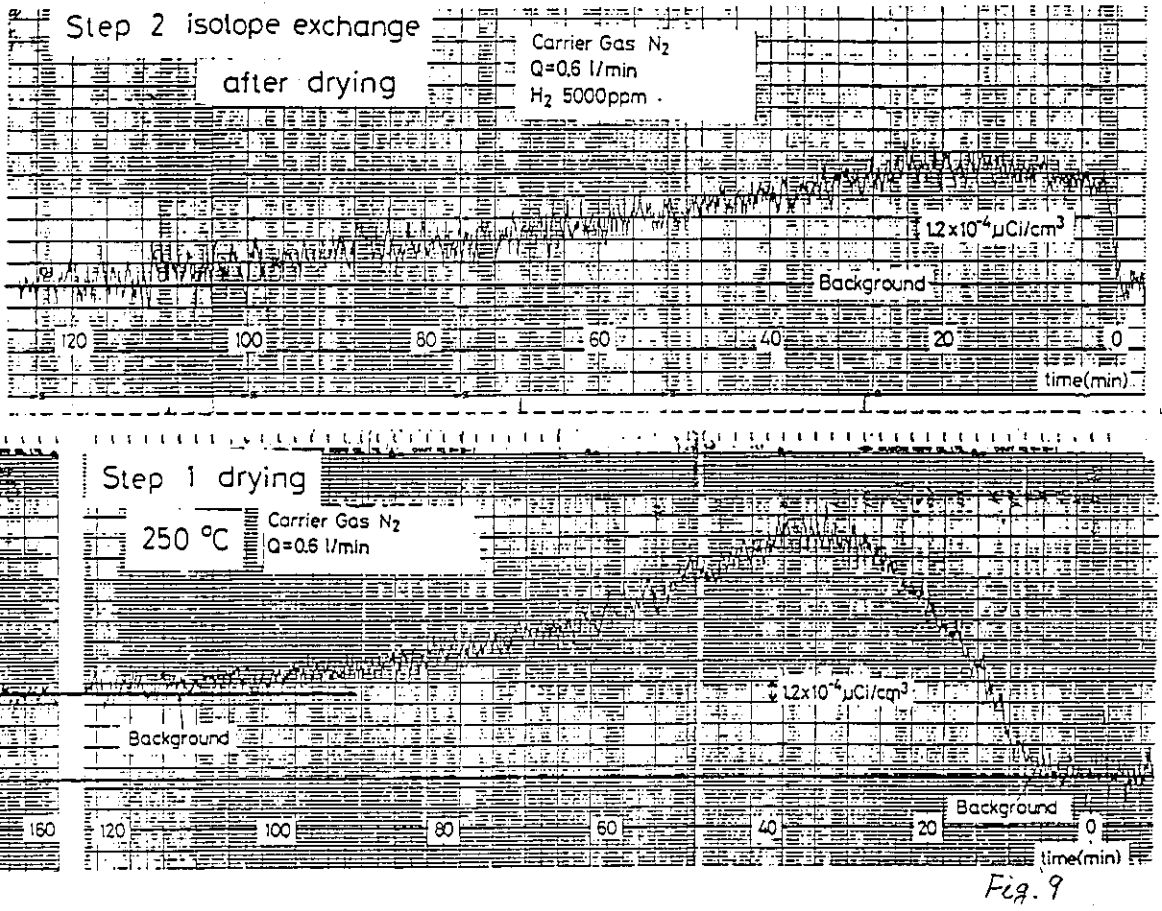
Step 2 isotope exchange
after drying
Carrier Gas N_2
Q=0.6 l/min
H_2 5000ppm
1.2x10^{-4}μCi/cm^3
Background
120
100
80
60
40
20
0
time(min)
Step 1 drying
250 ℃
Carrier Gas N_2
Q=0.6 l/min
1.2x10^{-4}μCi/cm^3
Background
160
120
100
80
60
40
20
Background
0
time(min)

Fig. 9

No.7 Test production of tritium in 1000 Ci level from ^{6}Li-Al alloy target

Tanase, M., Kato, M., Kurosawa, K., Motoishi, S.
Okane, S., Sugai, H., Fujie, M., Onoma, K.,
Yamabayashi, H.

Facilities for tritium production in a 1000 Ci level were constructed. Gaseous tritium was extracted from neutron-irradiated ^{6}Li-Al alloy targets by heating them at 700 °C under vacuum and collected in a uranium-getter. The tritium was recovered with a yield of about 100 % and the isotopic purity of the product was about 95 %. Through the production run, no leakage of tritium from the facilities was observed.

I. INTRODUCTION

In the Japan Atomic Energy Research Institute, tritium production technology has been developed [1-6] with the object of supplying tritium to nuclear fusion research and development, and also with the object of progressing safe handling of tritium. During last few years, tritium had been produced in 100 Ci level from neutron-irradiated ^{6}Li-Al alloy [3] and the related

technology such as modification of a tritium removal system had been developed [4,5]. From the results obtained in the production and development, facilities for producing tritium in 1000 Ci level was constructed. This paper describes the results of the production runs carried out in the facilities.

II. FACILITIES

The process for the production is shown in Fig. 1. Facilities, in which the processes from extraction to recovery are carried out, were shown in Fig. 2. The main components of the facilities were a tritium extraction system (TREX) and a tritium removal system (TRS). The TREX was installed in an airtight lead cell and glove boxes. The cell was equipped with lead wall for shielding γ-rays due to ^{60}Co induced by neutron activation of ^{59}Co impurity in targets. The TREX consisted of a vacuum furnace, two getter cartridges (Getter-1 and -2), a circulation pump (noted as M.P. in Fig. 2) and a set of vacuum pumps. The vacuum furnace and the getter cartridges were made of stainless steel (316-SS) and tripply walled. The vacuum furnace (2760 ml in volume) contained a molybdenum heater which was set in the most inner wall to heat the targets directly and then to suppress leakage of tritium through the inner wall by permeation. The getter cartridges were provided with stainless steel filters (5μm in mesh size) at the inlet

and outlet of uranium (U) containers. The whole system was designed to possess a very low leak rate which was found to be below 2×10^{-2} Pa $cm^3 s^{-1}$ by a He leak detector. On the other hand, leak rates of the cell and glove boxes were below 0.1 vol%/h.

The TRS, in which gaseous tritium leaked into the cell and glove boxes was oxidized and trapped, has a regeneration function of the dryer. The performance of the system had been tested with 1 to 10 Ci of tritium gas before practical use. The results showed that the decontamination factor of the TRS was higher than 10^4 at a flow rate from 1 to 7 $cm^7 h^{-1}$ in a once-through mode and that tritium water in the dryer could be released by heating it at 150 °C and collected in a small waste vessel through the cooler (Fig. 2).

III. Production Procedures

1. Target preparation

Lithium-aluminum (^{6}Li-Al) alloy, containing 3-4 w% of Li (^{6}Li enriched to 95.5 %), was prepared by dissolving Li in molten Al at 973 K. The alloy ingot was roll-spread to a plate and then clad with Al plates. The final sizes of the clad target plate and alloy meat were 100 mm^l x 20 mm^w x 2 mm^t and 80 mm^l x 2 mm^w x 0.5 mm^t, respectively.

2. Neutron Irradiation

The ^{6}Li-Al alloy targets enclosed in capsules were

irradiated with the Japan Material Testing Reactor in a neutron flux of 2×10^{14} $cm^{-2}s^{-1}$ for 40 to 70 days. The amount of tritium produced was estimated to be 1-3 TBq per target, and the burn-up of ^{6}Li was 20-60 %. After cooling for a few years, the targets were submitted to the following procedures.

3. Procedures in facilities

(1) Uranium (U) turnings of 9 g (Getter-1) and 22 g (Getter-2) were packed in each cartridge. The U of 9 g in the getter cartridge has a capacity of absorbing about 3900 Ci of tritium gas (T_2). The turnings were activated in the same way described in a previous paper [3].

(2) After the amounts of tritium involved in the neutron-irradiated ^{6}Li-Al alloy targets were determined by calorimetry [7], the targets were put in a stainless steel (316-SS) crucible which had been baked beforehand. The crucible was set in the vacuum furnace. The targets were heated at 120 °C for a few hours under vacuum to remove gaseous impurities such as H_2O from the surface of the targets. The temperature of the targets was raised until 700 °C at the rate of 5 °C/min to release tritium, while pressure in the vacuum furnace was observed.

(3) The tritium gas released with He was circulated through Getter-1 with a circulation pump in order to be

absorbed in U-getter kept at room temperature.

(4) After the amount of He in the residual gas was determined, the gas was evacuated by a set of pumps. The tritium collected in Getter-1 was transferred to Getter-2 by releasing from Getter-1 heated at about 400 °C.

(5) During the production procedures, the tritium gas in the system was analyzed by radiogas chromatography. A portion of the tritium gas was taken into a sampler (3.35 ml, STP) at various stages of the procedures. The tritium gas was carried by Ne flow (50 ml/min) into a radiogas chromatograph assembled as shown in Fig. 3. The chromatograph enabled us the determination of the chemical and isotopic purities of the tritium gas.

(6) Results

Recovery yields obtained in some production runs were summarized in Table 1. The amount of tritium treated in each run was estimated by calorimetry and by the amount of He involved in the run. The yields were about 100 % in every run, although some experimental error would be included.

In the extraction and trapping procedures of run 6, changes of the pressure in the vacuum furnace are shown in Fig. 4. The abrupt increase of the pressure, which was based on release of gas from the targets, was observed at nearly 350 °C. Gas chromatographic analysis

made clear that main species of the gas were found to be tritium gas and He. Sugai et al reported [8] that tritium gas was released at about 350℃ but that He was released at about 700℃ from the alloy containing 0.022 w% of ^{6}Li. The discrepancy, which appeared in He behavior, might be due to a quantity of He in the alloy: a large amount of He might exist as releasable bulk but a small amount of He can exist as stable cluster [8]. However, further study will be necessasry for confirming the mechanism.

The tritium released from the targets was easily trapped with Getter-1 by circulating a mixture of He and tritium gas. Completion of this process required about 1 h (Fig. 4).

The chemical and isotopic purities of the tritium gas released from Getter-1 was more than 99.9 % and about 95 %, respectively. As chemical impurities, methane and water were detected. Figure 2 shows a radiogas chromatogram of the tritium gas obtained in Run 5. The impurity of H would originate from the clad Al material or inner wall of the tritium extraction system. To obtain the tritium gas of the higher isotopic purity, the gas should be enriched. Some of authors have been trying to enrich the gas by means of gas chromatography [9,10].

Through the production run, no tritium was released from the facilities to the environment. Comparing with 100 Ci level production [3], tritium leakage from the inner wall of the vacuum furnace in 1000 Ci production

was greatly suppressed. The TRS was also confirmed to be very effective and the regeneration function of the dryer was very practical. As a next step, test production in levels of 10^4-10^5 Ci is scheduled, after further improvement of the facilities.

IV. CONCLUSION

Gaseous tritium was produced in 1000 Ci quantities from the neutron-irradiated ^{6}Li-Al alloy with the yield of about 100%. It was confirmed that the present production systems and procedures were adequate and that especially multi-enclosure system of the facilities was very useful for safe handling of a large amount of tritium.

Acknowledgement

The authors wish to express their thanks to Mr. T. Abe for his great encouragement during this work. The authors wish to express their thanks to Dr. E. Shikata and Dr. H. Kudo for valuable discussion in this work. Sincere appreciation is expressed to Mr. T. Genka and Mr. M. Ohkubo for measuring the amount of tritium by calorimetry and for help of tritium analyses. Many thanks are also due to the JMTR staff for irradiation of the targets in the reactor.

References

[1] Kudo, H.:J. Radioanal. Chem., **67**, 37(1981).

[2] Tanase, M., Yamaguchi, K., Tanaka, K.:Radioisotopes, **31**, 571(1982).

[3] Tanase, M., Kato, M., Motoishi, S., Onoma, K., Yamabayashi, H., Ishikawa, I., Nagame, Y., Kudo, H., Shikata, E., J. Nucl. Sci. Technol., **22**, 147(1985).

[4] Kato, M. et al, Fall Meet. At. Energy Soc. Japan, J28 (1983), (in Japanese).

[5] Motoishi, S. et al, Fall Meet. At. Energy Soc. Japan, H28 (1985), (in Japanese).

[6] Ishikawa, I., Tanase, M., Kato, M., Hoizumi, K., Shikata, E., Appl. Radiat. Isot., :**37**, 443 (1986).

[7] Genka, T. et al, Fall Meet. At. Energy Soc. Japan, F56 (1984), (in Japanese).

[8] Sugai, H., Kushita, K., Tanase, M., J. Nucl. Mater.,**139**, 248(1986).

[9] Tanase, M., Kato, M., Int. J. Appl. Radiat. Isot.,**34**, 687(1983).

[10] Fujie, M., Kato, M., Tanase, M., Annual Meet. At. Energy. Soc. Japan, G33, (1986), (in Japanese).

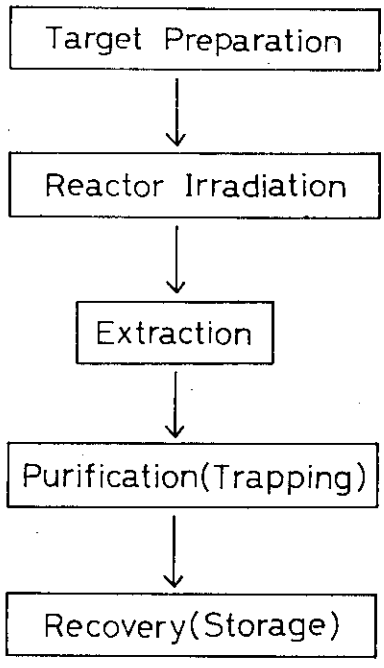

Fig. 1　　Tritium Productin Process

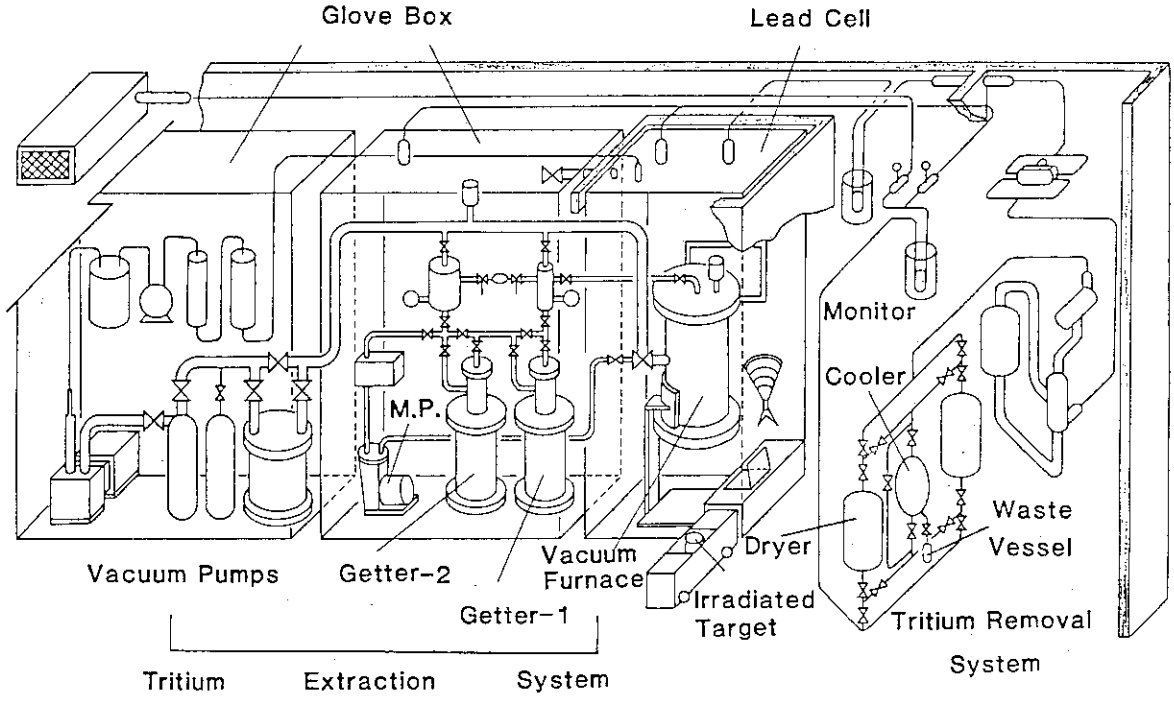

Fig. 2　　Tritium Production Facilities

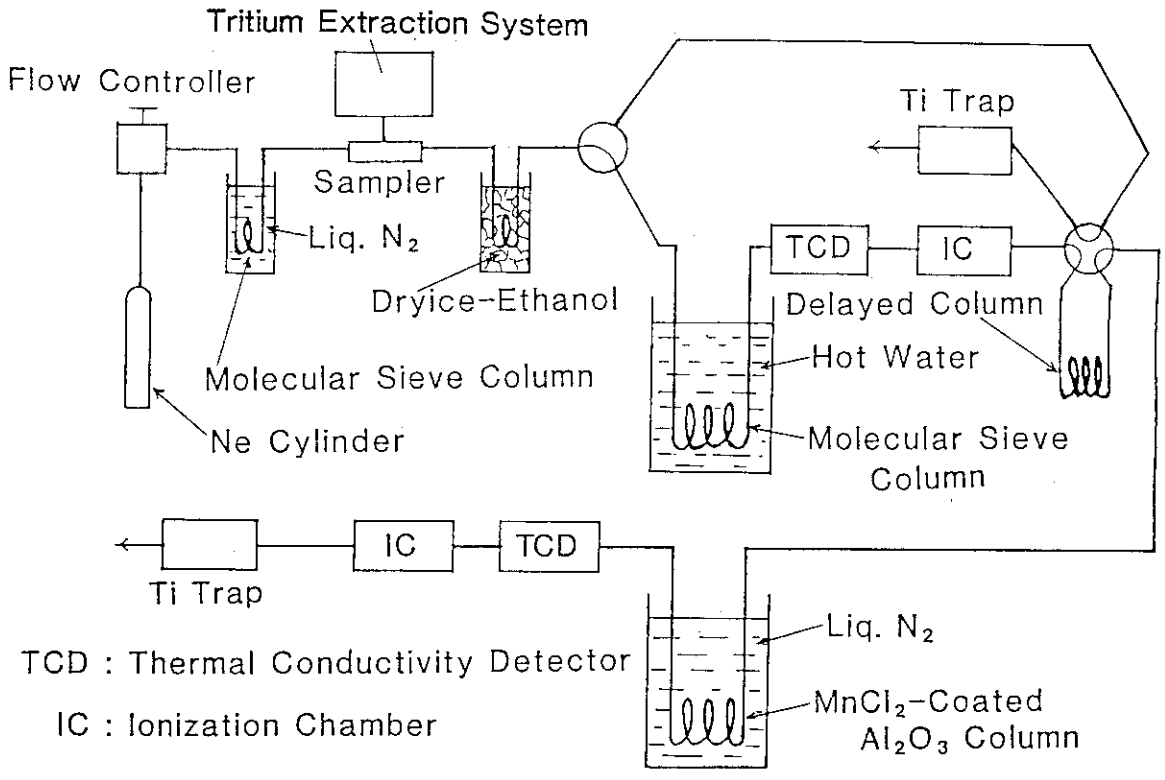

Fig. 3 Schematic Path of Radiogas Chromatograph

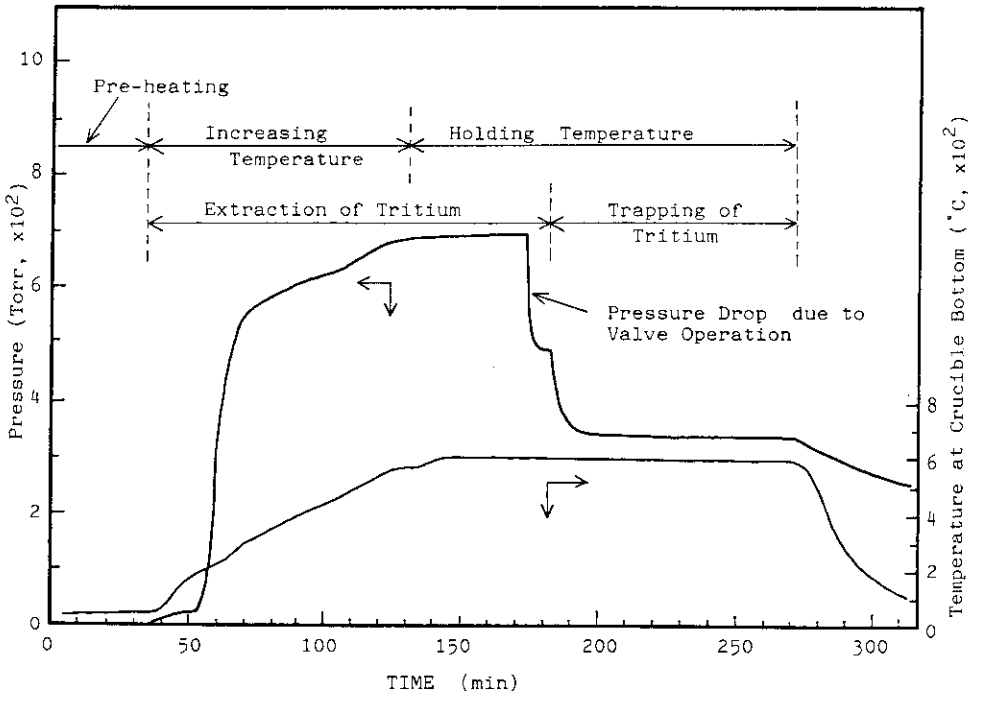

Fig. 4 Inner Pressure of Vacuum Furnace in Extraction and Trapping Process

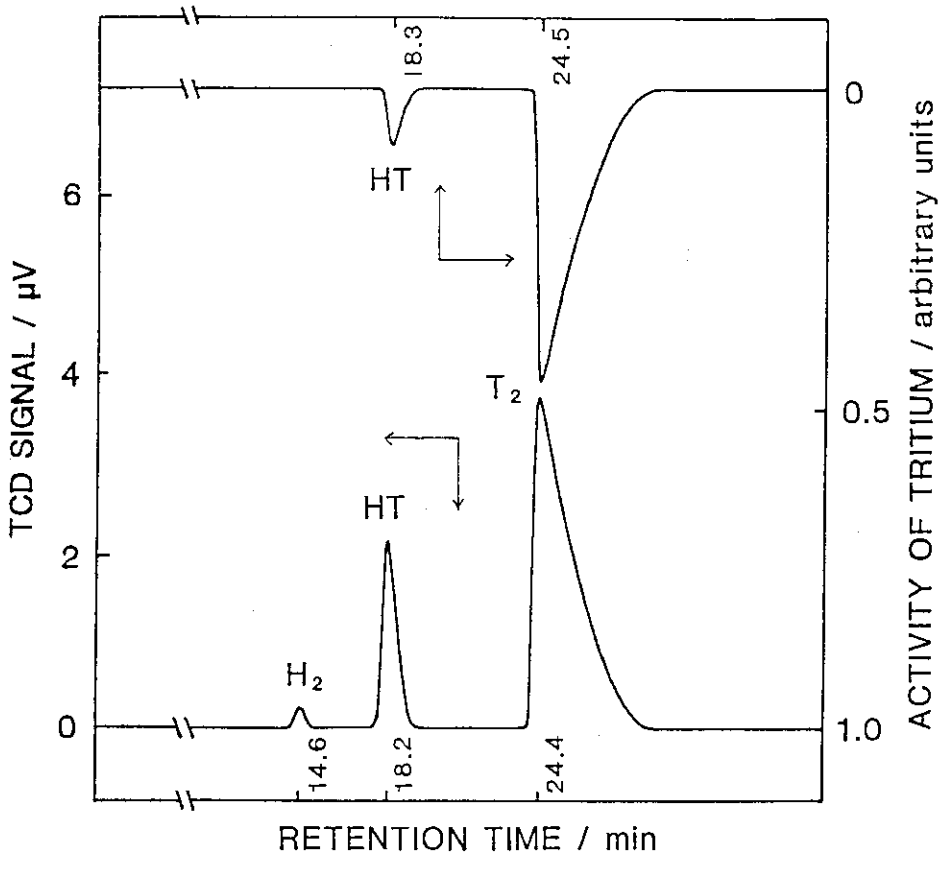

Fig. 5 A Radiogas Chromatogram of Tritium Gas Released from Getter-1

Table 1 Recovery Yields in Tritium Production

Run No.	Tritium Treated (Ci) (A) Calorimetry	(B) Amount of He	Tritium Recovered (Ci)	Recovery Yields (%) (A)	(B)
1	100	95	95	95	100
2	112	100	124	111	124
3	120	123	-	-	-
4	-	285	296	-	104
5	997	1080	1050	105	97
6	998	1060	1020	102	96

No.8 AN ASSESSMENT OF TRITIUM ISSUES AND DATA REQUIREMENTS FOR LIQUID BREEDERS*

Dai-Kai Sze, Argonne National Laboratory
9700 South Cass Avenue, FPP-205
Argonne, Illinois 60439-4837 USA
(312) 972-4838

ABSTRACT

Liquid breeding materials have received wide attention in the U.S. fusion reactor design studies over the past few years. There are major uncertainties of the tritium recovery system design over the constraints of tritium inventory, tritium containment, and recovery system costs. The key problems are identified, and the data required to resolve these issues are discussed.

I. INTRODUCTION

A number of large uncertainties exist in the behavior of liquid breeder blankets, leading to uncertainties in their feasibility and attractiveness. Generic issues have been defined to encompass the most promising blanket designs. These issues are listed in Table 1.[1] Issues relating to safety and/or transient effects are not listed separately, as they are considered an integral part of each issue.

Liquid breeder blankets encompass a variety of generic design variations and material combinations. Current designs include a number of self-cooled and separately cooled options with widely varying geometries. Table 2 indicates the effect of material choices on the dominant near-term issues. The existance and seriousness of the major issues depend not only on the particular blanket concept, but also on the operating conditions such as power density, magnetic field, surface heat flux, temperature, and duct length. The tritium recovery and containment is a critical issue associated with various blanket concepts.

The tritium recovery issues depend strongly on both the breeding material and on the particular recovery method chosen. Not only are the issues for Li

* Work supported by the U.S. Department of Energy, Office of Fusion Energy.

and 17Li-83Pb completely different, but the issues for molten salt recovery or gettering to recover tritium from lithium are also completely different. The testing needs for different recovery methods are, therefore, also completely different. To identify the critical issues and testing needs to resolve these issues, a particular recovery method must be identified.

The problems associated with tritium recovery from breeding materials are evolved around trade-offs among tritium inventory, tritium containment, and tritium recovery system cost. A typical range of the parameters is listed in Table 3. A significant relaxation of any one parameter will often completely change the characteristics of the problem. The testing needs will then need to identify a process which can be scaled to a fusion reactor that satisfies the three parameters simultaneously.

The testing needs are to determine a process which can recover tritium to an acceptable concentration and to reprocess it under an acceptable economic constraint. The tritium containment is dependent on structural material, operating temperature, and power conversion systems. The process identified must reduce the tritium partial pressure to a level consistent with the power system design.

II. TRITIUM ISSUES

There are four different liquid breeders being considered in the U.S. fusion community (i.e., lithium, 17Li-83Pb, Flibe, and lithium compounds-aqueous solution).[2] The key comparison of the four candidates are listed in Table 4. Lithium is by far the most promising choice, being the candidate of the breeding materials for major design studies.[3,4] 17Li-83Pb was chosen for the breeding material for Mini-MARS.[5] Flibe and aqueous solutions have some interesting applications since the pool reactor concept has been proposed in the U.S. to improve fusion safety.[6] Since the BCSS, approximately 90% of the U.S. design study has focused on liquid breeders, either self-cooled or separate-cooled. The aqueous solution is a new concept recently developed in the U.S.[2] The basic idea is to dissolve a lithium compound in water and use the water as both coolant and breeding material. The reactor will operate in PWR mode. The main advantage is using existing technology.

The key tritium problems of the four different liquid breeders are very

different. Table 5 lists some characteristics of the different breeding materials. The critical limiting factor for tritium recovery is tritium inventory for lithium, tritium containment for LiPb and Flibe, and recovery system cost as well as inventory for aqueous solution.

Since the issues and facilities required for a tritium recovery process are entirely different for different processes, it is necessary to identify the most promising process for each breeding material and develop a testing scenario for that process. To identify the feasibility and scenarios for all the processes proposed will be clearly beyond the scope of this paper. The process identified here is judged to be the most promising at this time. It does not suggest, however, that this is the only recovery process to be studied in the future. The status of tritium recovery process development is such that none of the methods have been positively identified as completely satisfactory.

A. Tritium Recovery from Lithium

The solubility of tritium in lithium is very high. The pressure concentration relationship is

$$C = K_S\sqrt{P}$$

where

C is concentration in wppm,
P is pressure in Pa, and
K_S is Sievert's constant in wppm/$\sqrt{Pa}$

K_S has been measured and is

$$K_S = 3.4\ e^{5220/T}$$

Current wisdom has defined C=1 wppm, which corresponds to approximately 1 kg tritium inventory in the breeding material for a self-cooled lithium blanket. At this concentration at 500°C, the equilibrium tritium partial pressure over lithium is 1.2×10^{-7} Pa. Most problems associated with tritium

recovery from lithium are caused by this very low pressure. Since the pressure is so low already, the tritium containment is usually not a serious problem.

Three tritium recovery methods have been experimentally studied. These are molten salt extractions,[7] permeation window,[8] and gettering.[9] The molten salt extraction system has been demonstrated to be capable of recovering tritium from lithium to a concentration relevant to fusion applications and is, therefore, chosen as the candidate method for Blanket Comparison and Selection Studies (BCSS).[10] The key problem is how to scale the system to reactor levels. The stability of the molten salt dissolved in lithium and its impact on the corrosion to the structural material is also yet to be answered. However, the critical issues are clearly identifiable, and developed programs can be outlined.

The key problem associated with the tritium recovery process by gettering and permeation window is caused by the low tritium partial pressure over lithium. To recover 500 g/d of tritium at 1.2×10^{-7} Pa, a purge gas flow rate or vacuum pumping rate of 5×10^{10} liter/sec must be processed. It is clearly beyond the capability from economic considerations to process such a high flow rate. For the gettering process, if gettering and regeneration occurs at the same temperature, the regenerating pressure must be equal to or less than the gettering pressure. To reduce the flow rate to a reasonable value ($\sim10^{6}$ liter/sec), the gettering must be at 200-250°C and regeneration at ~800°C. For such a system, the gettering area acts as the cold trap, and the effect of corrosion products deposit to the gettering may be large. For the permeation window process, the downstream pressure must be equal to or less than the upstream pressure (i.e., 1.2×10^{-7} Pa). To reduce the problem, it is suggested that a palladium layer be used to cover the downstream side of the permeation window. The palladium will act as a catalyst to oxidation for the tritium so that the downstream tritium will be in the form of T_2O instead of T_2. By doing so, the partial pressure of T_2O can be much higher than the upstream partial pressure of T_2. However, the oxide layer on the downstream side of the window may have a detrimental effect on the permeation rate. The potential problems associated with the gettering and permeation window processes have to be assessed further.

B. Tritium Recovery from LiPb

In constrast to the lithium system, for which tritium recovery processes have been verified experimentally, no experimental work has been carried out for tritium recovery process for LiPb. Whereas the key problem for tritium recovery from lithium is tritium inventory, and for LiPb, the key problem is tritium containment. The Sievert's constant for LiPb is about 1.7×10^{-3} wppm/$Pa^{1/2}$ compared to 3,000 wppm/$Pa^{1/2}$ for Li. Therefore, a very efficient tritium recovery system is required for LiPb to reduce the tritium partial pressure to an acceptable level.

Three different tritium recovery schemes from LiPb have been proposed. These are inert gas purging,[11] vacuum droplets degassing,[12] and multiple-stage counter current extraction.[13] All the processes try to take advantage of the high tritium partial pressure to recover tritium from gas phases. The key problem is caused by the required efficiency of the recovery system. Therefore, the recovery system must handle a large stream of LiPb (probably the entire coolant stream), and the fractional recovery must be high so that liquid phase diffusion becomes an important step. It is judged that the multiple-stage counter current extraction system is the most promising scheme due to its simplicity. A program has been developed to study the feasibility of using this process for tritium recovery.

C. Tritium Recovery from Flibe

The key problem of tritium recovery from Flibe is the same as LiPb (i.e., how to prevent tritium permeation). The very high tritium partial pressure may also cause enough tritium to be dissolved in the structural material to cause hydrogen embrittlement problems and/or helium embrittlement problems. As can be seen from Table 5, the tritium partial pressure gained per coolant passing through the blanket is high enough to cause great concern of material embrittlement problems. Therefore, the T_2 partial pressure must be reduced as the coolant is passed through the blanket.

Another interesting point needs to be discussed. The tritium generated in the fusion reactor blanket may behave very differently than hydrogen dissolved in the Flibe. Although there is no doubt that hydrogen dissolved in

Flibe obeys Henry's law, as hydrogen is dissolved in molecular form, the tritium generated in the blanket is in the atomic form and will not form T_2 at least until it can meet another tritium. Since the tritium concentration is perceived to be very low, the mean time between collision of the two tritium atoms can be very long. If the mean time between collision is much larger than the tritium residence time in Flibe, the thermodynamics behavior of tritium in Flibe must be completely restudied. For this discussion, we assume that thermodynamics equilibrium is reached.

Tritium can be recovered either in T_2 or TF form. To recover T_2 form, the tritium containment is a critical problem. Moir[14] suggested using multi-barrier to provide enough resistance for tritium permeation. The reliability of the barriers over long periods of time may be of concern. The potential hydrogen embrittlement problem cannot be resolved by this method. Johnson[15] suggested recovering tritium in TF form; however, TF will cause material compatibility problems unless materials like Mo and W are used.

A method recently proposed has the potential of resolving both the corrosion and tritium containment problems.[6] A process has been developed at ORNL that, by dissolving MoF_6 in Flibe, MoF_6 will react with structure containment materials and form a Mo coating on the structure, thus preventing further corrosion.[16] MoF_6 is also anticipated to react with tritium to form TF. Thus, tritium permeation will not be a problem since it is in TF form, and corrosion will not be a problem since the Flibe sees only Mo. The thermodynamic calculation indicated that the Flibe/MoF_6 will behave as discussed here. There is no experimental evidence to support this scheme.

As can be seen from this discussion, tritium forms a feasibility issue on the application of Flibe in the fusion system. Whether this issue can be resolved, consistent with other requirements of the blanket, is quite uncertain at this time.

D. Tritium from Aqueous Solution

Tritium recovery from water has been demonstrated by many different methods.[17] The problems are determining what is the allowable tritium concentration in water and how much the tritium recovery system will cost. INTOR suggested that the maximum allowable tritium concentration in water is 1

Ci/liter, and the tritium recovery system cost is

$$C\ (M\$) = 15\ [\frac{(L/D)}{1000}]^{.55}$$

in which L/D is the water process rate in liter/day. The cost of the tritium recovery system for 500 g/d will be 1.5 billion dollars which is clearly not acceptable.

It was recently suggested that the allowable tritium concentration could be increased to 10-50 Ci/liter. At the same time, a tritium recovery system is scaled from Darlington. The total cost of Darlington is 100-150 M$ (Cdn), out of which only 27 M$ (Cdn) is associated with Vapor Place Catalyst Exchange (VPCE) and cryogenic distillation system. To scale from Darlington to a typical 1000 MW(e) fusion plant, the direct cost estimate is 140 M$ (US) with the total capital cost of 280 M$ (US). The tritium concentration used is 10 Ci/liter.[18]

The cost of the tritium recovery system for water is undoubtedly very high. Whether this cost is acceptable must be resolved. The high tritium concentration will result in high tritium inventory of a few kgs. The high tritium concentration may also cause large tritium leakage from the high pressure water. The tritium concentration in CANDU coolant water is only ~1 Ci/liter, and the tritium loss to the ambient is ~150 Ci/day.[19]

E. Data Requirements

For tritium recovery from lithium, the molten salt recovery process has demonstrated its applicability for tritium recovery to the concentration relevant to fusion applications. The main unresolved issue is determining the effort of the tritium recovery system to the operation of the lithium loop. The salt used in the process will be partially dissolved in the lithium and carried back to the blanket. The major concern is the structural material corrosion caused by the salt-contaminated lithium. The behavior of the salt, such as decomposition rate under fusion environment, will be also of concern.

For 17Li-83Pb, a very efficient tritium recovery system will be required. Since the vapor pressure is very high, it is reasonable to assume that tritium will be recovered from the vapor phase. Therefore, tritium must

diffuse to the boundary of the liquid and be recombined and released to the vapor phase. The solubility and diffusivity of tritium in 17Li-83Pb, as well as the surface recombination constant, must be obtained. The diffusing of atoms in a liquid can easily be calculated if the diffusivity and surface recombination constant are known.

The tritium recovery system has not been defined for a Flibe system. The thermodynamics of the Flibe system must be established first. The tritium concentration pressure relationship must be established as a function of time as tritium is generated (not dissolved!). A small scale experiment will be set up at ANL to study the chemistry of a Flibe/MoF_6 system.

For the aqueous solution system, the basic process of the tritium recovery system has been established, and an industry scale facility is in operation. The major uncertainty is establishing cost scaling of the tritium recovery system.

Since tritium containment is such a critical problem, the study of permeation will also be critical. The classical permeation rate is pressure square root dependent. However, this relationship will change to linear dependency at lower tritium partial pressures. The change over pressure depends on many parameters (i.e., surface conditions, hydrogen, isotope concentration, etc.). The permeation mechanism must be understood so that a design goal of tritium partial pressure can be established.

The effect of a chemical form of tritium to permeation is also important. It has generally been assumed that tritium in oxide form will not permeate.[5] However, some experimental results indicated that tritium in oxide form will permeate as rapidly as tritium in elemental form.[20] The permeation rate of tritium in different chemical forms with different surface conditions must be established.

III. CONCLUSIONS

The issues and data requirements for tritium recovery from liquid breeders are summarized. There is reasonable confidence that tritium recovery from lithium breeders can be designed under the various constraints. The tritium inventory for 17Li-83Pb and Flibe blanket will be small; but significant engineering problems remain. The cost of a tritium recovery

system for water coolant may be so high that it will have a major impact on the reactor economics.

REFERENCES

1. M. Abdou, et al., "FINESSE Phase 1 Report," PPG-909, UCLA-Eng-85-39, Dec. 1985.

2. W. P. Duggan, et al., "Applications of the Integrated-Blanket Coil Concept to the Compact Reversed-Field Pinch Reactor," The Seventh Topical Meeting on the Technology of Fusion Energy, Reno, Nevada, June 15-19, 1986, to be published in a special issue of Fusion Technology.

3. C. C. Baker, et al., "Tokamak Power System Studies," ANL/FPP-85-2, Dec. 1985.

4. K. Schultz, et al., "TITAN RFP Reactor Design Studies Scoping Phase Report," to be published by UCLA.

5. I. N. Sviatoslavsky, et al., "Thin Blanket Design for Mini-MARS - A Compact Tandem Mirror Fusion Reactor," The Seventh Topical Meeting on the Technology of Fusion Energy, Reno, Nevada, June 15-19, 1986, to be published in a special issue of Fusion Technology.

6. D. K. Sze, "IPFR, Integrated Pool Fusion Reactor Concept," ibid.

7. V. A. Maroni, R. D. Wolson, and G. G. Staahl, "Some Preliminary Considerations of a Molten Salt Extraction Process to Remove Tritium from Liquid Fusion Reactor Blankets," Nucl. Technol. 25, 83 (1976).

8. R. E. Buxbaum, "The Use of Zirconium-Palladium Windows for the Separation of Tritium from the Liquid Metal Breeder Blanket of a Fusion Reactor," J. Separation Science and Technology, 18, 1251-73, (1983).

9. S. D. Clinton and J. S. Watson, "Tritium Removal from Liquid Metals by Absorption on Ytterium," Proceedings of the 7th Symposium on Engineering Problems of Fusion Research, Knoxville, TN, Oct. 25-28, 1977.

10. D. L. Smith, et al., "Blanket Comparison and Selection Study," ANL/FPP-84-1, Sept. 1984.

11. B. Badger, et al., "WITAMIR - A University of Wisconsin Tandem Mirror Reactor Design," UWFDM-400, 1980.

12. K. E. Plute, et al., "Tritium Recovery from Lithium-Lead by Vacuum Degassing," Nuclear Technology/Fusion, Volume 4, No. 2, Part 3 (1983).

13. D. K. Sze, "Counter-Current Extraction System for Tritium Recovery from 17Li-83Pb," Fusion Technology, Volume 8, No. 1, Part 2A (July 1985).

14. A. E. Sherwood, "Tritium Permeation and Recovery for the Helium-Cooled Molten Salt Fusion Breeder," Lawrence Livermore National Laboratory Report UCID-20141 (1984).

15. E. F. Johnson, "Fuel Handling in a Fusion Power Plant," R. G. Mills, ed., pp. 362-409.

16. J. DeVan, ORNL, Private communication, 1986.

17. M. Rogers, "Tritium Separation Methods," pp. 2-28 to 2-36, and "Appendix C: Cost and Technology Tradeoffs for Separating Tritium from Water," FED/INTOR Tritium and Safety Issues, FED-INTOR/TRIT/B2-4 (July 1982), C-1 - C-16.

18. P. Gierszewski, CFFTP, Private communication, 1986.

19. K. Y. Wong, "Permeation of Tritium Through Steam Generator Tubes at CANDU Stations," 10th Symposium on Fusion Engineering, Philadelphia, Dec. 5-9, 1983.

TABLE 1. Liquid Breeder Blanket Issues

Tritium self-sufficiency
Magnetohydrodynamic (MHD) effects
Fluid flow (including pressure drop)
Heat transfer
Material interactions (e.g., corrosion)
Structural response in the fusion environment
Irradiation effects on material properties
Response to complex loading conditions
Failure modes
Tritium recovery and control

TABLE 2. Effect of Coolant, Breeder, and Structural Material Choices on the Dominant Issues for Liquid Breeder Blankets

Liquid Metal Cooling	Li or 17Li-83Pb	MHD effects (including viability of insulators)
		corrosion (including viability of inhibitors)
Coolant or Breeder	Lithium	chemical reactivity
	17Li-83Pb	tritium containment
	Flibe	tritium containment
	Helium	tritium containment
	Aqueous solution	tritium recovery system cost
Structural Material	Vanadium alloys	bimetallic mass transfer
		DBTT[a]
	Ferritic steels	DBTT[a]

[a] Ductile-to-brittle transition temperature (changes due to impurities, radiation, H, and He)

TABLE 3. Parameter Ranges for Tritium Recovery Systems

Blanket tritium inventory	order of kg's
Tritium recovery system	order of 10×10^6 $ cost
Tritium leakage rate	order of 10 ci/d

TABLE 4. Different Liquid Breeder Comparisons

Key Advantages	Key Disadvantages
Li	
Good neutronics Established tritium technology High tritium solubility	Reactivity MHD
Li17-Pb83	
Relatively inert Good neutronics	Density Activation MHD Corrosion, T containment
Flibe	
Relatively inert Low pressure operation Semi-established technology No MHD	High melting temperature T containment/corrosion
Aqueous Solution*	
Inert Established technology High tritium solubility	Low temperature operation High pressure system Cost of tritium recovery

*Li compound dissolved in water.

TABLE 5. Comparisons of Key Tritium Issues of Three Liquid Breeders

	Concentration Pressure Relationship	Constant	ΔP/Pass, Pa	Tritium Concentration** at 10^{-6} Pa, g/cc
Li	$X = k_s/P^{1/2}$	K_s = 3,000 wppm/$Pa^{1/2}$	1.3×10^{-13}	1.5×10^{-6}
17Li-83Pb	$X = k_s/P^{1/2}$	$K_s = 1.7\times10^{-3}$ wppm/$Pa^{1/2}$	6×10^{-4}	1.8×10^{-13}
Flibe	$X = k_h/P$	$K_h = 2\times10^{-6}$ wppm/Pa	310	2×10^{-20}

*Recent measurement reported by F. Reiter $K_s = 1.7 \times 10^{-4}$ wppm/$Pa^{1/2}$.

**Tritium density for ideal gas at 500°C is 10^{-15} g/cc at 500°C and 15^6 Pa.

No.9 Studies on Steps Affecting Tritium Residence Time in Solid Blanket

Satoru Tanaka
Nuclear Engineering Research Laboratory
University of Tokyo
Tokai-mura, Ibaraki 319-11, Japan

1. Introduction

For self-sustaining of CTR fuel cycle, effective tritium recovery from blanket is essential. This means that not only tritium breeding ratio (CTR) must be greater than 1.0 but also high recovering speed is required for short tritium residence time in the blanket. Short residence time means that tritium inventory in the blanket is small. In this paper, tritium residence time and tritium inventory in the solid blanket is modeled by considering steps constituting tritium release. Some of these tritium migration processes are experimentally evaluated.

2. Modelling of Tritium Release in the Solid Blanket

Figure 1 shows tritium migration steps in the solid blanket, where sintered breeding material is used. These steps consist of diffusion in grain, desorption at the grain edge, diffusion and permeation through grain boundaries, desorption at the particle edge, diffusion and percolation through interconnected pores to purge stream and convective mass transfer to stream. Corresponding to these tritium migration steps, tritium inventories of various kinds can be considered such as diffusive,

soluble, adsorbed or trapped inventories and tritium in the gas phase as shown in Fig. 2.

Code named TTT was constructed to calculate these tritium inventories and tritium residence time. In this model, absorption in bulk material, diffusion in grain, diffusion and percolation through grain boundaries and through interconnected pores, adsorption at the surface of particle or grain are considered. However trapping at defects and mass transport phenomena at the surface are not taken into considerations though they are thought to be processes of very important.

An example of the calculation results is shown in Fig. 3. Tritium partial pressure at the outer surface of annular blanket is plotted against $K(=De/D_{AB}$, effective diffusivity factor) taking κ (permeability) as a parameter. The annular blanket module (inner rad. 1.5mm, outer rad. 7.5mm) is cooled at the outer surface and sweep gas flows through the central hole. Tritium production rate of $1.0\times10^{-10}g/cm^3.sec$ corresponds to that near first wall. And temperatures of 500°C (outer surface) and 800°C (inner surface) are supposed. This figure shows that effective diffusivity has a larger effect on tritium migration than permeabily. To keep soluble and adsorptive inventories in a low level it is necessary to suppress tritium partial pressure in the inner pore of the sintered material. This figure shows the limits of effective diffusion coefficient and permeability which are necessary for low tritium inventory.

Tritium inventories and residence time were calculated for REPUTER-1 blanket[1]. REPUTER-1 is a conceptual design of commercial reversed field pinch fusion reactor studied at the University of Tokyo. The blanket of REPUTER-1 is all ceramic type composed of Li_2O, BeO and SiC as shown in Fig. 4. Generated tritium in the Li_2O diffuses in the grain and particle of Li_2O, desorbs at the particle edge, migrates through interconnected pores to the surface of Li_2O pellet and migrates along the boundary between Li_2O and BeO pellets, and through porous SiC cladding material. In the calculation, apparent diffusion coefficient in the particle was assumed and tritium solubility of reported value was used.[2] As for adsorption, data by Yoshida[3] was used after correction of surface area. Calculated steady state tritium inventory is shown in Table 1. From this table it is understood that adsorptive inventory is a major part when small particle is used. This tendency is shown in Figs. 5 and 6. Tritium residence time of a certain region in the blanket is obtained from steady state tritium inventory and tritium generating rate in that region. Total tritium release rate can be calculated by summing up the release rate of each region over the total blanket. Results are shown in Fig. 7 and Table 2.

3. Experimental Studies on Tritium Migration Steps

In order to investigate unit process of the tritium transport in the solid breeding material, following experimental studies have been performed.

3-1. Tritium Release Experiment from Li_2O Powder under Neutron Irradiation at High Temperatures

In-situ tritium release experiments have been performed using research reactor YAYOI at the Nuclear Engineering Research Laboratory, University of Tokyo[4]. Block diagrams of the experimental apparatus are shown in Figs. 8 and 9. Irradiation section is shown in Fig. 10. Powder of Li_2O was used as a sample. Sweep gas of He, $He+O_2$, $He+H_2$ was used. Hydrogen-containing sweep gas can also be added at the outlet of irradiation section to study whether delay of tritium release occurs in the connecting tube or at the sample itself. Swept tritium was trapped by water bubblers to study chemical form of the released tritium and to study time dependence of release rate (Fig. 8). When fast tritium release behavior was studied, on-line tritium measurement by a proportional counter was used (Fig. 9). Comparison of in-situ tritium release experiments with others are shown in Table 3.

(1) Chemical form of the released tritium

When sweep gas of $He+4\%H_2$ was used, tritium release rate became steady state in a relatively short period after reactor start up (Fig. 11), and chemical form of the released tritium was found mainly hydrogen gas (HT) as shown in Table 4. When a sweep gas of $He+1\%O_2$ was used, dominant chemical form of tritium was found to be moisture (HTO).

On the other hand, when He sweep gas was used, chemical form was found to depend on extent of pre-dehumidification and kind of material used for containing Li_2O. Tables 5 and 6 summarize the experimental results. In these experiments, stainless steel tube and wool were used. Table 5 shows that when Li_2O sample was dehumidified more than 5 days at the temperature of 800°C dominant species is HT. However, when dried for three days it was HTO. It is interesting that chemical form of released tritium was mainly HT for no pre-dehumidification. Fraction of HT was found to decrease with irradiation time. It was considered that tritium just released from Li_2O sample was HTO form but then it was thought to be converted to HT form on the surface of containing tube of stainless steel or on packing wool of steel. Surface of these materials are considered to be oxidized by oxygen or moisture. And once oxide film are formed released HTO is considered not to be reduced to HT form, this corresponds to the experimental result for pre-dehumidification period of three days, in which case HTO form was dominant. Table 6 shows the experimental results where steel or nickel are used as a containing tube and packing material. When nickel was used, dominant tritium form was found to be HTO. This difference can be attributed to the redox characteristics of Ni and SUS.

As conclusion, released chemical form was found to be determined by oxygen activity in the place of sample.

(2) Tritium Release Rate

Time changes of release rate are plotted in Figs. 12 and 13. It took a relatively long period to reach steady state when He sweep gas was used. This is considered to be caused by the processes at the surface of Li_2O particle and/or containing tube. To study which portion has a larger effect on delaying tritium release rate, experiments using two patterns of H_2 adding to the sweep gas were conducted. One is H_2 addition to the main sweep gas which flows through Li_2O sample, the other is H_2 addition after He sweep gas left Li_2O sample. Experimental results are shown in Fig. 14, and no distinct difference was observed between He sweep gas and H_2 adding after Li_2O sample. This is considered to mean that delaying of tritium release by surface phenomena are mainly occuring at the sample.

For tritium migration steps in the sintered particle, diffusion along the grain boundaries as well as diffusion in the grain must be considered. In order to study these, we have performed in-situ tritium release experiments using Li_2O powder of different particle sizes. These powder was made by cracking large particle followed by sieving them into different mesh sizes. He + 1% H_2 was used as a sweep gas.

Steady state tritium inventory (I) are calculated as following by assuming two steps tritium diffusions in the grain and along the grain boundaries,

$$\frac{I}{S} = \frac{1}{15}\left(\frac{a_g^2}{D_g} + \frac{a_p^2}{D_{int}^2}\right),$$

where S is the tritium generating rate, a_g radius of grain, a_p radius of particle, D_g diffusivity in the grain and D_{int} diffusivity along the grain boundaries.

This equation expresses that when I/S is plotted against a_p^2, we can calculate D_{int} from the slope and D_g/a_g^2 from the intercept. The value of diffusion coefficient in the grain, D_g, then can be evaluated by the knowledge of grain size a_g.

Example of the tritium release rate after reactor start-up obtained by on-line measuring system, is shown in Fig. 15.

Experimental results are shown in Fig. 16. Tritium inventory becomes larger with the particle size, especially at low temperatures. This indicates that tritium diffusion along the grain boundaries must be taken into considerations. In small particles of 28-32 mesh and 32-48 mesh, tritium inventories were found to become larger. This was considered to be attributed to adsorption, trapping or surface phenomena at the surface of particle. Mechanism of it remains to be studied. Diffusion coefficient in the grain and along the grain boundaries are shown in Fig. 17. Value of a_g was determined from SEM observation as 20 μm. Our data of D_g are obtained from in-situ tritium release experiment while others from post irradiation release. It is interesting that values of D_g thus obtained is relatively close to the reported values of Guggi[5] and Tanifuji[6].

3-2. Hydrogen Diffusion and Percolation through Interconnected Pores of Sintered Materials

Tritium transport resistances in diffusion and percolation through interconnected pores of sintered materials are to be understood. When high density (e.g. well sintered) material is used, tritium partial pressure in the pore becomes high and tritium inventory of solution and/or adsorption may become larger.

In this experiment, LiF pellets of different sintered degree were used because of its easy handling. Experimental apparatus is shown in Fig. 18. Percolation experiment was conducted using Ar gas, while effective diffusivity was measured by diffusion of H_2 in Ar gas. Experimental results are shown in Fig. 19, which shows changes of permeability and effective diffusivity factor with sintering temperature. Relations of these values with porosity was studied as shown in Fig. 20. And linear relation between permeability and effective diffusivity factor ($k=D_e/D_{AB}$) was found (Fig. 21).

3-3. Water Vapor Adsorption on Li_2O Powder

As depicted in the tritium inventory calculation and the in-situ tritium release experiments, adsorptive inventory sometimes becomes dominant. However there has been little studies on the adsorption of gas and/or water vapor on Li_2O.

We have been performing water vapor adsorption study by breakthrough method using Li_2O powders of different particle sizes (Fig. 22). Before breakthrough experiment, the sample was

dried at 700°C under vapor pressure of less than 5 ppm. An example of the experimental results is shown in Fig. 23.

Amounts adsorbed for two particle sizes (Cerac/Pure) was found to coincide and they were almost similar to the values by Yoshida for pellet sample. This is thought to indicate that water vapor adsorbs on the grain surface.

4. Conclusion

Steps affecting tritium residence time was analyzed by model calculation and it was found that surface processes such as adsorption are important.

Some of the tritium migration processes such as diffusion in the grain, diffusion along the grain boundaries, diffusion along the interconnected pores and water vapor adsorption were experimentally studied and useful data base was obtained.

5. References

(1) S. Kondo et al., "REPUTER-1", UTNL-R-0189 (1986).

(2) J.H. Norman and G.R. Hightower, J. Nucl. Mater. **122&123** (1984) 913.

(3) H. Yoshida et al., J. Nucl. Mater. **122&123** (1984) 934.

(4) T. Terai et al., Fusion Technol., **8** (1985) 2143.

(5) D. Guggi et al., J. Nucl. Mater. **118** (1983) 100.

(6) T. Tanifuji et al., Trans. Atomic Energy Society of Japan, Fall Meeting J41 (1983).

Table 1. Tritium Inventory in the REPUTER-1 Blanket (Unit: kg)

K κ (cm^2) \ Rp (cm)		1E-4		1E-3		1E-2		1E-1	
3E-1 1E-9	SOL	8.57	E-2	8.57	E-2	8.57	E-2	8.57	E-2
	DIF	4.41	E-5	4.41	E-3	4.41	E-1	4.41	E+1
	GAS	2.99	E-6	2.99	E-6	2.99	E-6	2.99	E-6
	ADS	1.05	E+1	1.05	E+1	1.05	E-1	1.05	E-2
	TOTAL	1.06	E+1	1.14	E+0	6.30	E-1	4.42	E+1
3E-2 1E-10	SOL	2.41	E-1	2.41	E-1	2.41	E-1	2.41	E-1
	DIF	4.41	E-5	4.41	E-3	4.41	E-1	4.41	E+1
	GAS	2.99	E-5	2.99	E-5	2.99	E-5	2.99	E-5
	ADS	4.60	E+1	4.60	E+0	4.60	E-1	4.60	E-2
	TOTAL	4.62	E+1	4.85	E+0	1.14	E+0	4.42	E+1
3E-3 1E-11	SOL	7.86	E+1	7.86	E-1	7.86	E-1	7.86	E-1
	DIF	4.41	E-5	4.41	E-3	7.41	E-1	4.41	E+1
	GAS	2.99	E-4	2.99	E-4	2.99	E-4	2.99	E-4
	ADS	2.01	E+2	2.01	E+1	2.01	E+0	2.01	E-1
	TOTAL	2.02	E+2	2.09	E+1	3.23	E+0	4.51	E+1
3E-4 1E-12	SOL	3.77	E+0	3.77	E+0	3.77	E+0	3.77	E+0
	DIF	4.41	E-5	4.41	E-3	4.41	E-1	4.41	E+1
	GAS	2.99	E-3	2.99	E-3	2.99	E-3	2.99	E-3
	ADS	8.75	E+2	8.75	E+1	8.75	E+0	8.75	E-1
	TOTAL	8.79	E+2	9.13	E+1	1.30	E+1	4.87	E+1

Table 2. Delay of Tritium Release from REPUTER-1 Blanket

K κ (cm^2) \ R_p (cm)		1E-4	1E-3	1E-2	1E-1
3E-1 1E-9	50%	1.6 d	4.2 h	3.8 h	12 d
	90%	9.3 d	1.1 d	14 h	40 d
	99%	46 d	4.6 d	1.4 d	94 d
3E-2 1E-10	50%	8.1 d	19 h	6.1 h	12 d
	90%	46 d	3.7 d	1.0 d	40 d
	99%	170 d	23 d	2.9 d	94 d
3E-3 1E-11	50%	29 d	3.0 d	11 h	13 d
	90%	150 d	18 d	2.0 d	43 d
	99%	2.1 y	92 d	9.3 d	95 d
3E-4 1E-12	50%	130 d	12 d	2.3 d	14 d
	90%	3.2 y	93 d	10 d	46 d
	99%	10 y	350 d	41 d	97 d

Table 3. Parameters of In-Situ Experiments

	VOM-15/21H (JAERI)	TRIO-01 (ANL)	This work
Material	Li_2O:2.03-6.67g Sintered Pellet	$LiAlO_2$:42.9g Sintered Pellet	Li_2O:0.6g, ~6 g Powder
Neutron Flux (thermal)	$1x10^{14}n/cm^2.sec$	$4x10^{14}n/cm^2.sec$	$1x10^{7}$-$1x10^{8}n/cm^2.sec$
Irrad. Temp.	350-900°C	500-700°C	400-700°C
Irrad. Time	990-2655 hrs	2112 hrs	approx. 3 hrs x N tir
Burnup	0.24-0.85%	0.18%	approx. 10^{-11}
Sweep Gas	He, He-D_2, He-O_2	He-H_2, He, He-O_2	He, He-H_2, He-O_2

Table 4. Chemical Form of Released Tritium (Effect of sweep gas)

Run No.	Dehumid. Period (time)	Sweep gas	Temp.(°C)	W(%)	G(%)
7 - 1	3 (1)	He-4%H_2	609	5.5	94.5
- 2	3 (2)	He-4%H_2	706	3.7	96.3
- 3	3 (3)	He-4%H_2	510	2.3	97.7
- 4	3 (4)	He-4%H_2	411	11.6	88.4
3 - 1	3 (1)	He	604	79.0	21.0
4 - 1	3 (1)	He	604	90.8	9.2
12 - 1	1 (1)	He-1%O_2	604	98.7	1.3
12 - 2	1 (2)	He-1%O_2	604	99.7	0.3
12 - 3	1 (3)	He-1%O_2	604	99.9	0.1

Tube and packing materials: steel or stailess steel

Table 5. Chemical Form of Released Tritium
(Effect of pre-dehumidification)

Run No.	Dehumid. Period (day)	W(%)	G(%)
11 - 1	0*(1#)	5.2	94.8
- 2	0 (2)	21.6	78.4
- 3	0 (3)	18.7	81.3
- 4	0 (4)	30.0	70.0
3 - 1	3 (1)	79.0	21.0
4 - 1	3 (1)	90.8	9.2
10 - 1	5 (1)	5.4	94.6
- 2	5 (2)	2.8	97.2
- 3	5 (3)	2.5	97.5

Temp.: 604°C
Sweep gas: He 100 cc/min
Tube and packing materials: steel or stainless steel
*: pre-dehumidification
#: in reactor

Table 6. Chemical Form of Released Tritium
(Effect of tube and packing materials)

Run No.	Material	Dehumid. Period (day)	W(%)	G(%)
10 - 1	steel	5 (1)	5.4	94.6
- 2	steel	5 (2)	2.8	97.2
- 3	steel	5 (3)	2.5	97.5
15 - 1	Ni	5 (1)	91.8	8.2
- 2	Ni	5 (2)	98.5	1.5

Temp.: 596 - 604°C
Sweep gas: He 100 cc/min

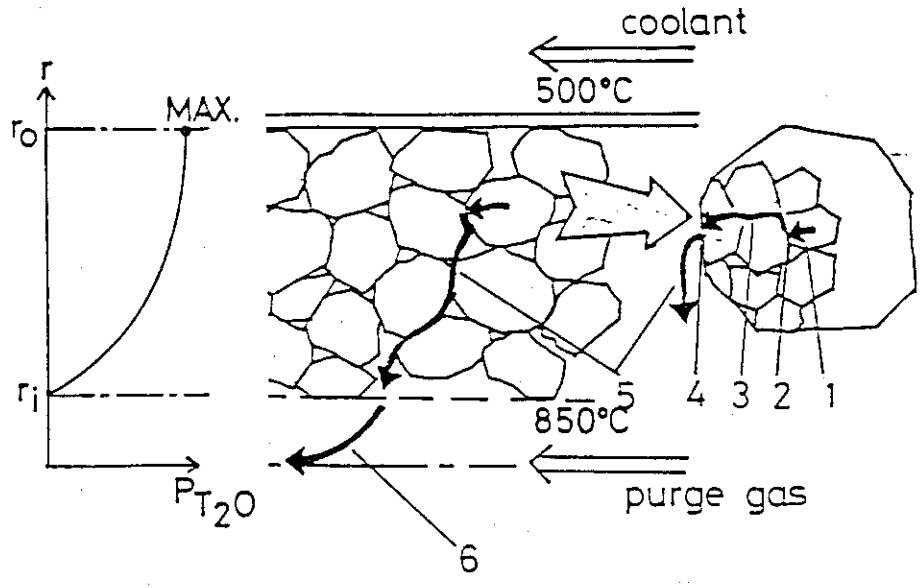

(1) Bulk diffusion in grains.
(2) Desorption of T_2O at grain edge.
(3) Diffusion along grain boundaries.
(4) Desorption at particle edge.
(5) Diffusion to purge stream.
Percolation to purge stream.
(6) Convective mass transfer to stream.

Fig. 1 Steps in Tritium Transport in CTR Solid Blanket System

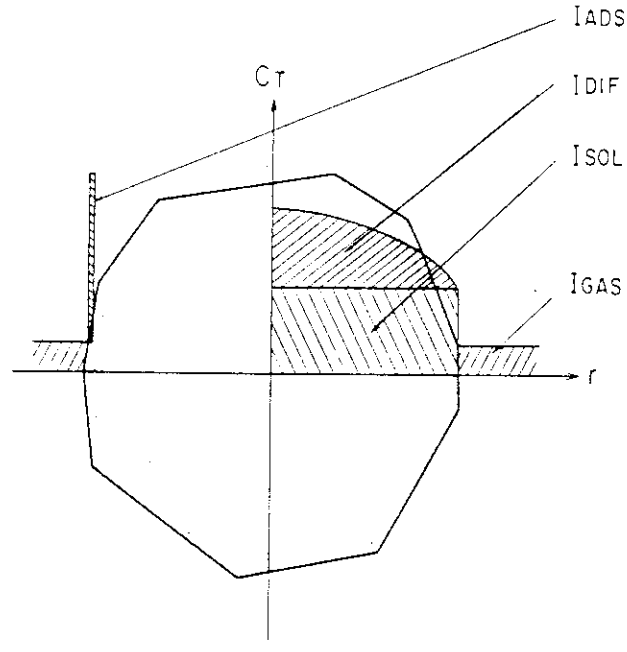

Fig. 2 Tritium Inventories on a Particle Constituting Sintered Breeding Material

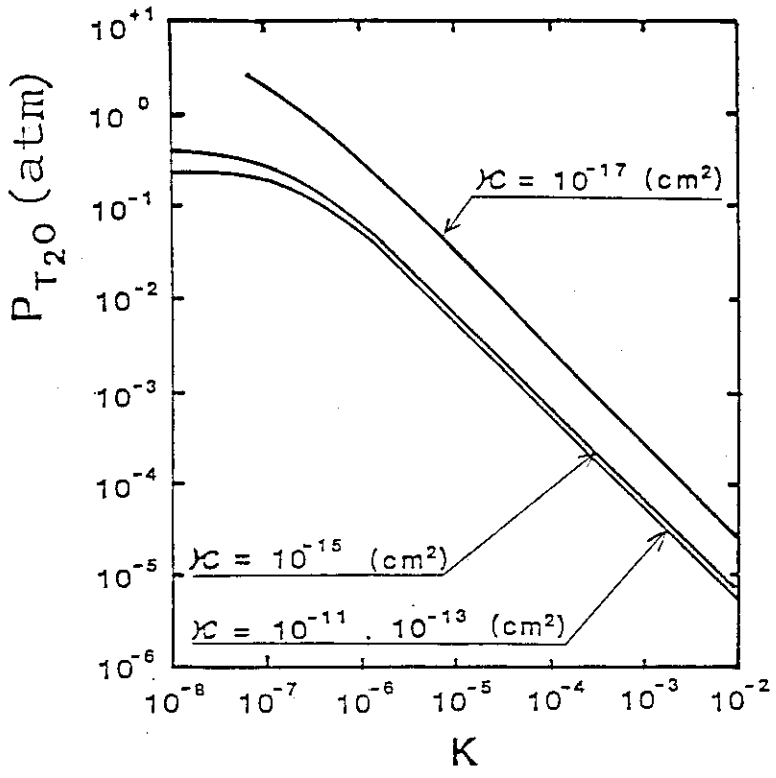

Fig. 3 Partial Pressure of T_2O at the Outer Boundary of Annular Pellet (tritium generation rate: 1×10^{-10} g/cm^3 sec, outer radius 7.5mm, inner radius 1.5mm, temperatures: 850°C (outer boundary), 500°C (inner boundary)).

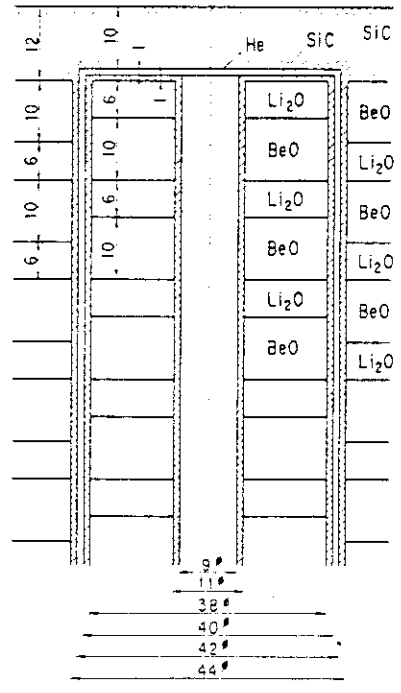

Fig. 4 Blanket of REPUTER-1

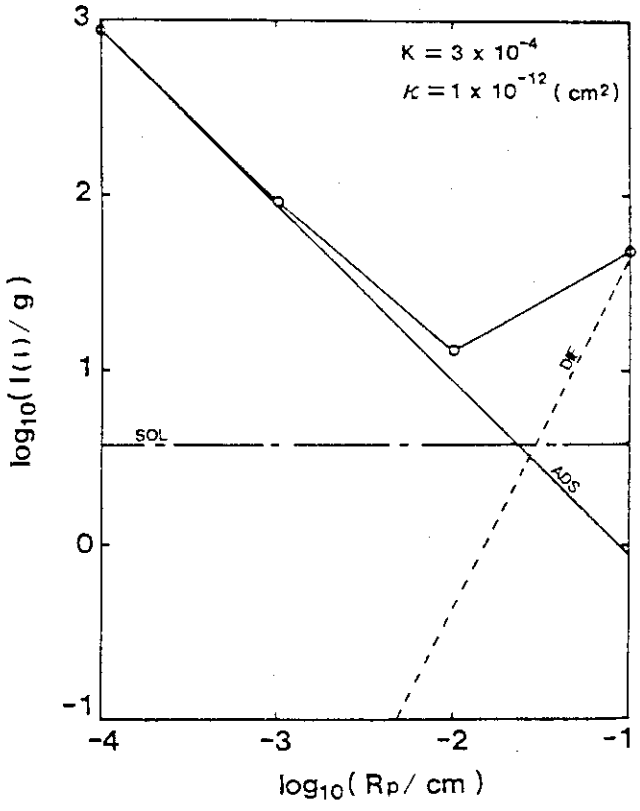

Fig. 5 Contribution of Each Process to Total Inventory

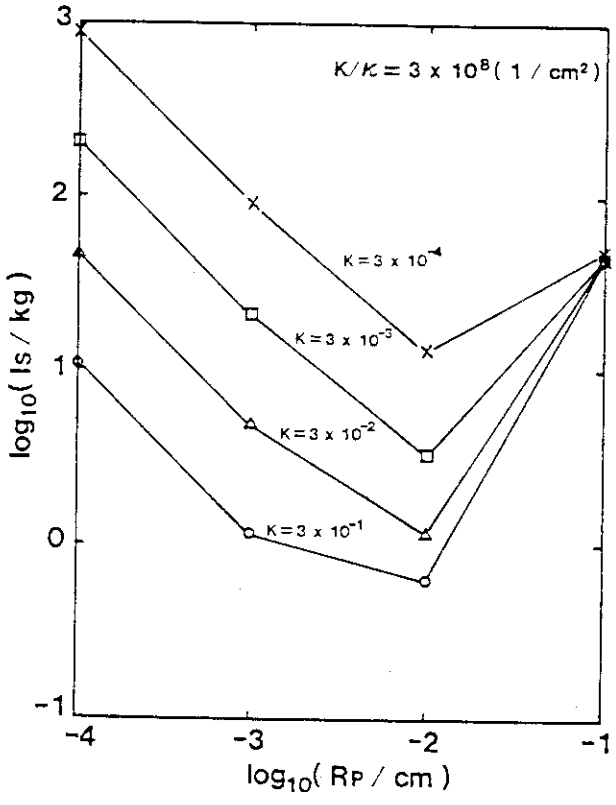

Fig. 6 Particle-Size Dependence of Tritium Inventory

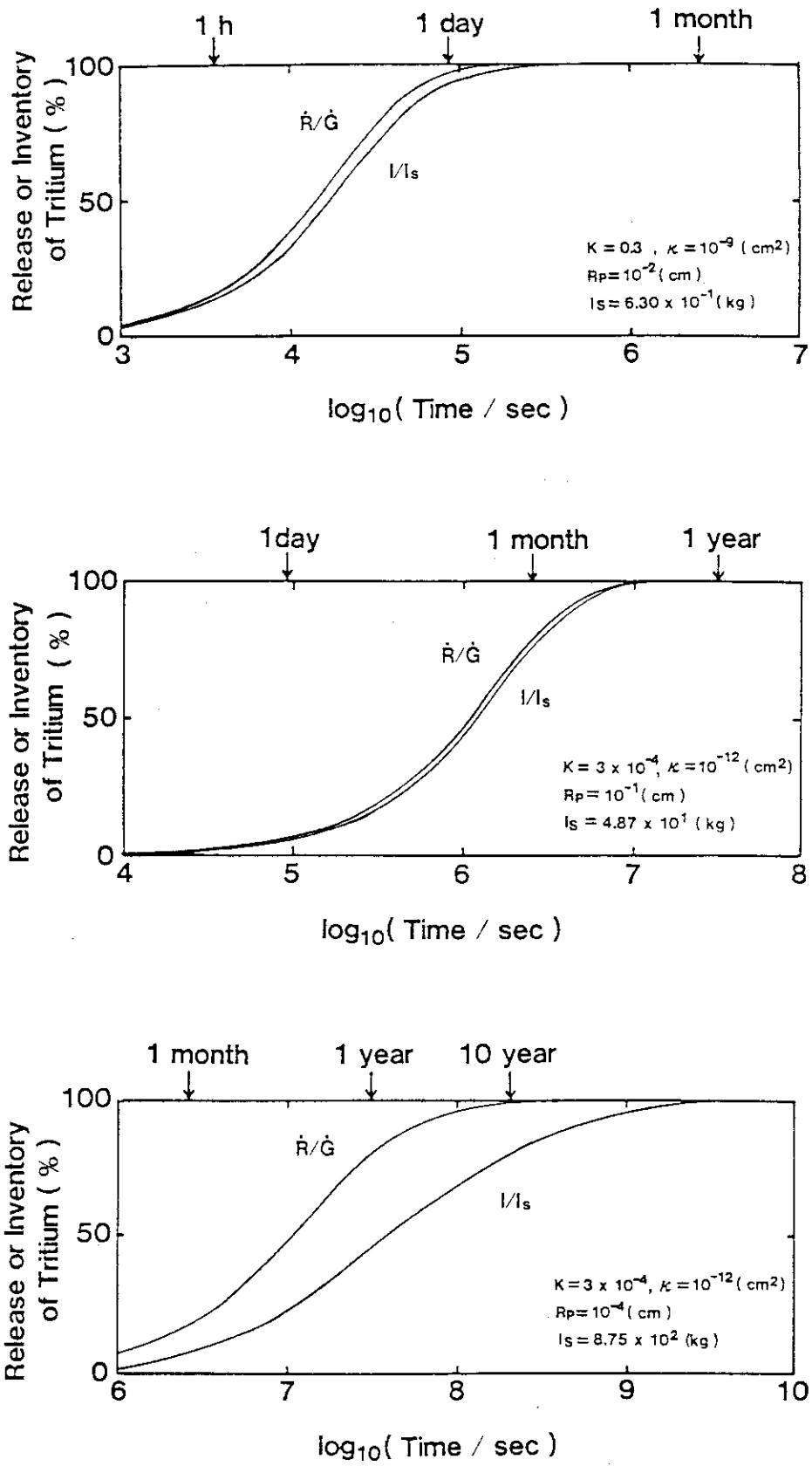

Fig. 7 Time Dependence of Release Rate and Inventory

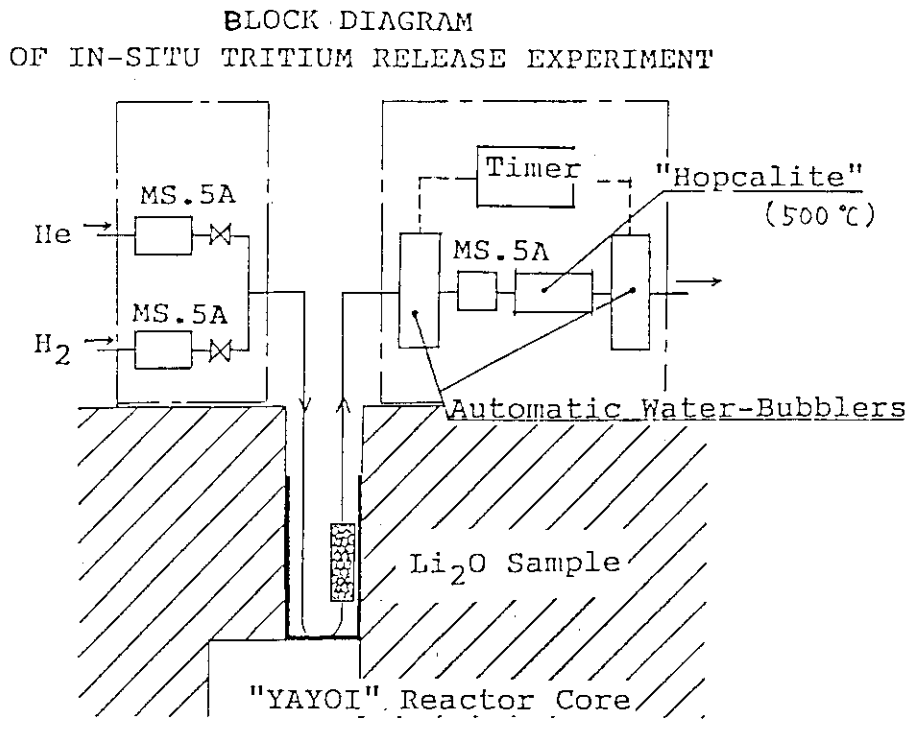

Fig. 8 Block Diagram of In-Situ Tritium Release Experiment
(tritium trapped by bubblers)

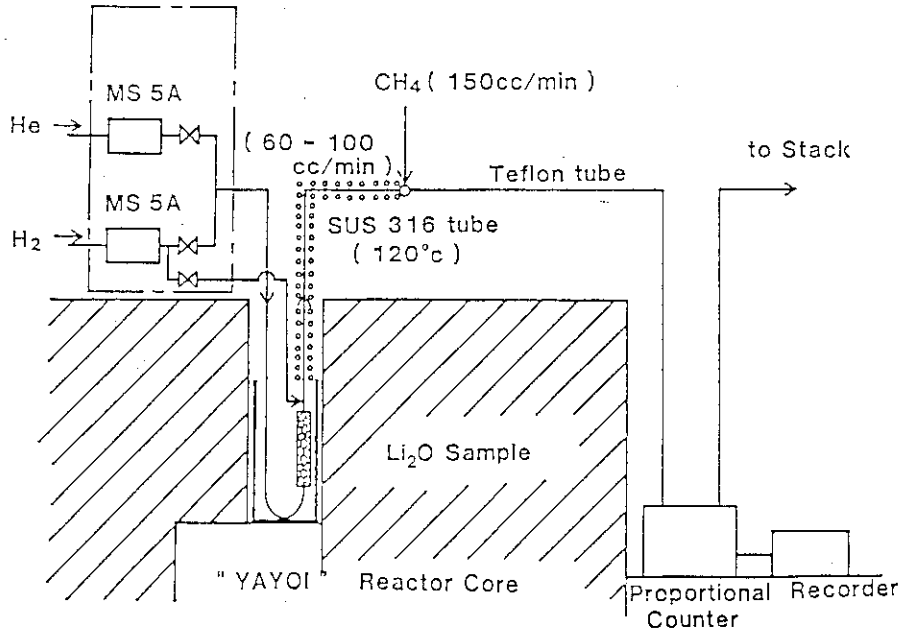

Fig. 9 Block Diagram of In-Situ Tritium Release Experiment
(on-line measurement)

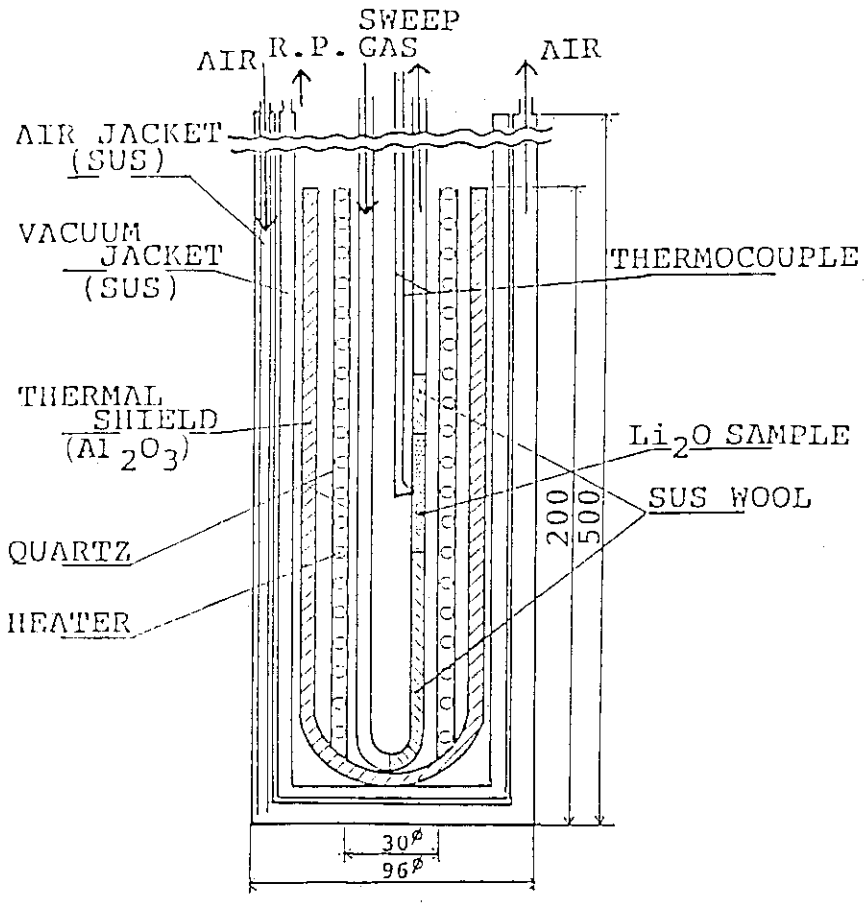

Fig. 10 Irradiation Apparatus

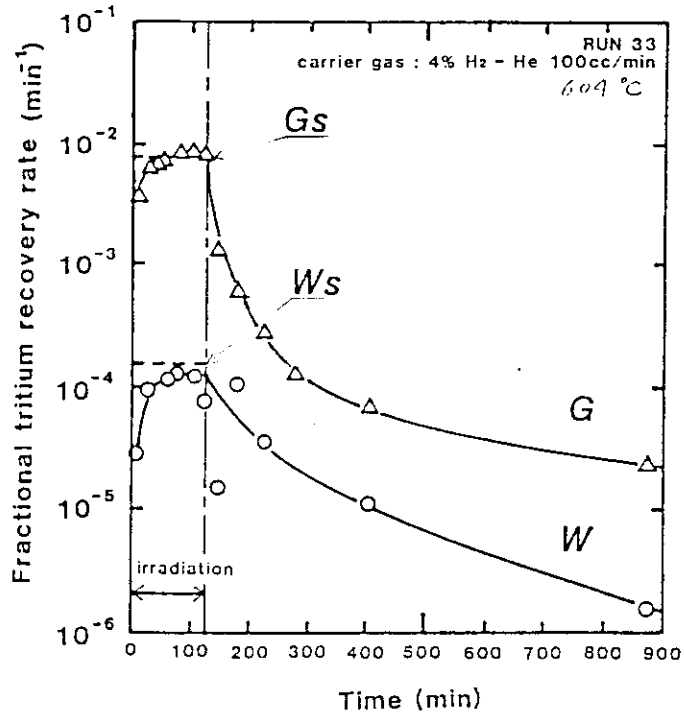

Fig. 11 Time Dependence of Tritium Recovery Rate
(carrier gas: He+4%H_2, 100 cc/min,
W: water-soluble component
G: water-insoluble component)

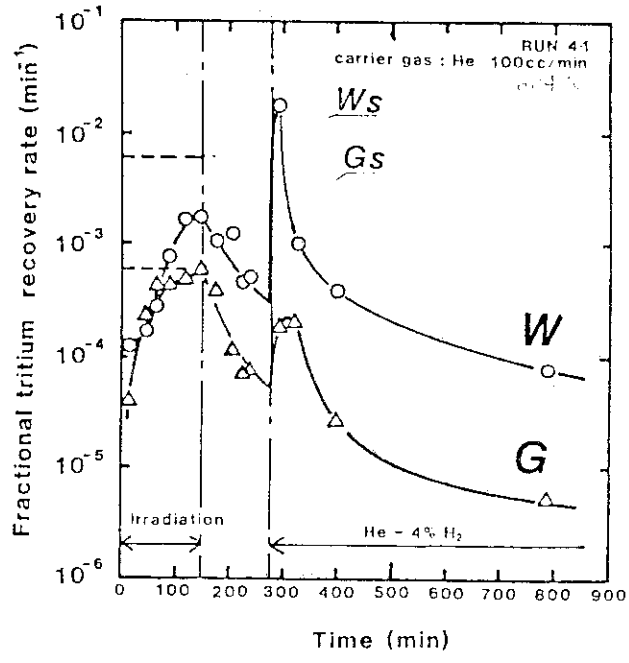

Fig. 12 Time dependence of Tritium Recovery Rate
(carrier gas: He+4%H_2, 100cc/min,
W: water-soluble component
G: water-insoluble component
pre-dehumidified for three days)

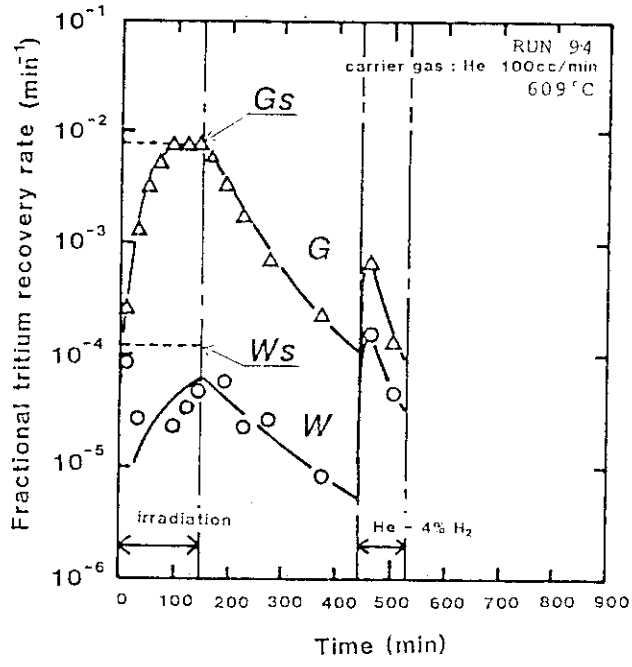

Fig. 13 Time Dependence of Tritium Recovery Rate
(carrier gas: He 100 cc/min,
W: water-soluble component
G: water-insoluble component,
pre-dehumidified for five days)

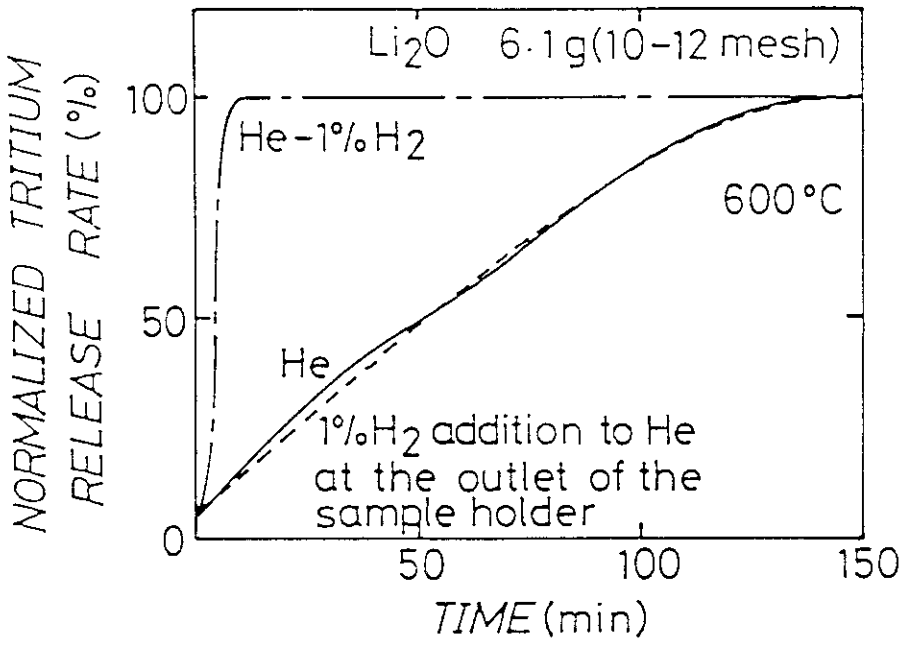

Fig. 14 Time Dependence of Tritium Release Rate (effect of H_2 addition)

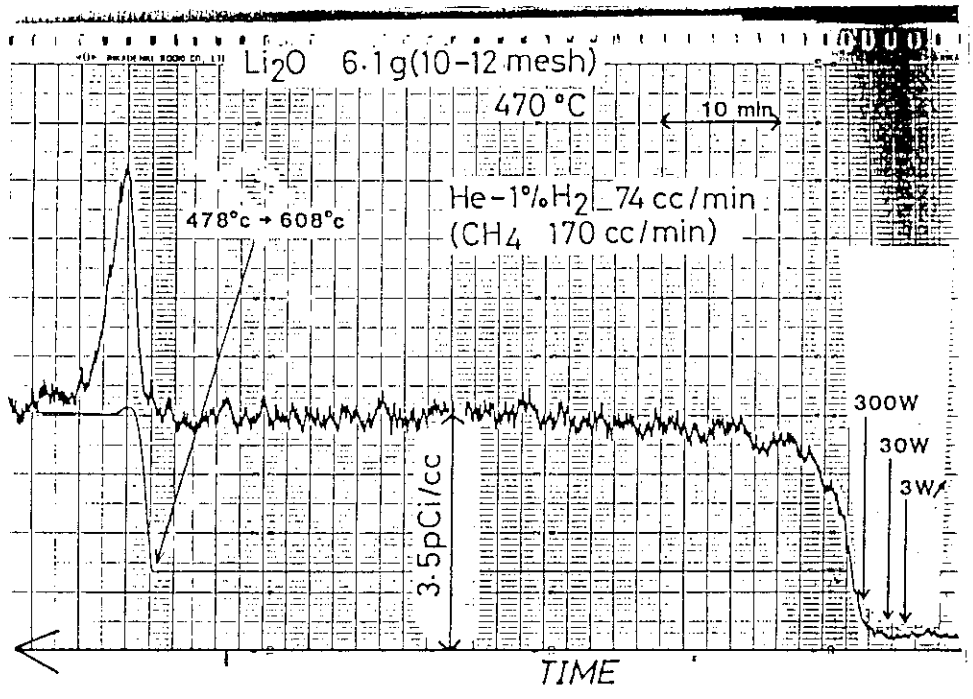

Fig. 15 Example of Tritium Release Rate (on-line monitoring)

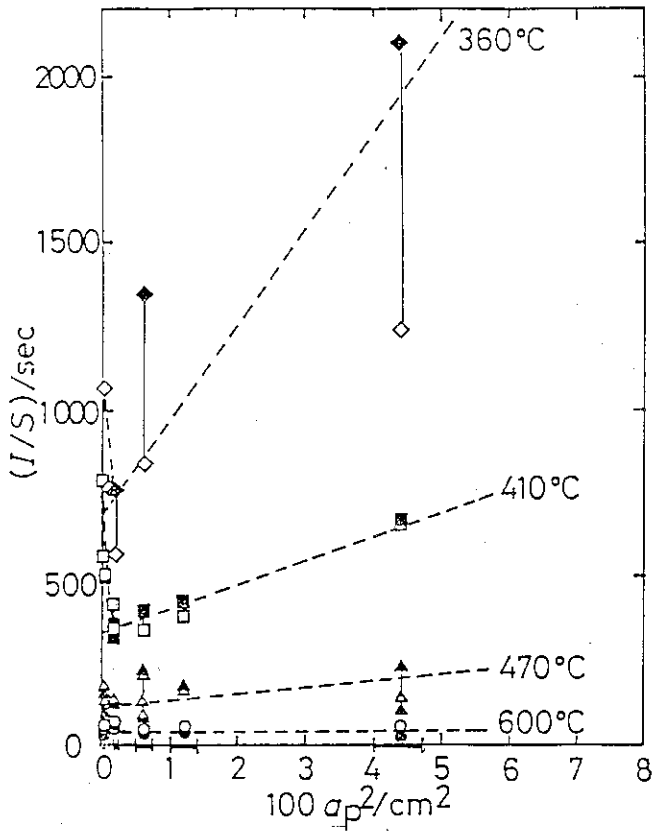

Fig. 16 Particle Size Dependence of Tritium Inventory
(Li_2O powder, solid symbol: analyzed from start-up, open symbol: analyzed from shut-down)

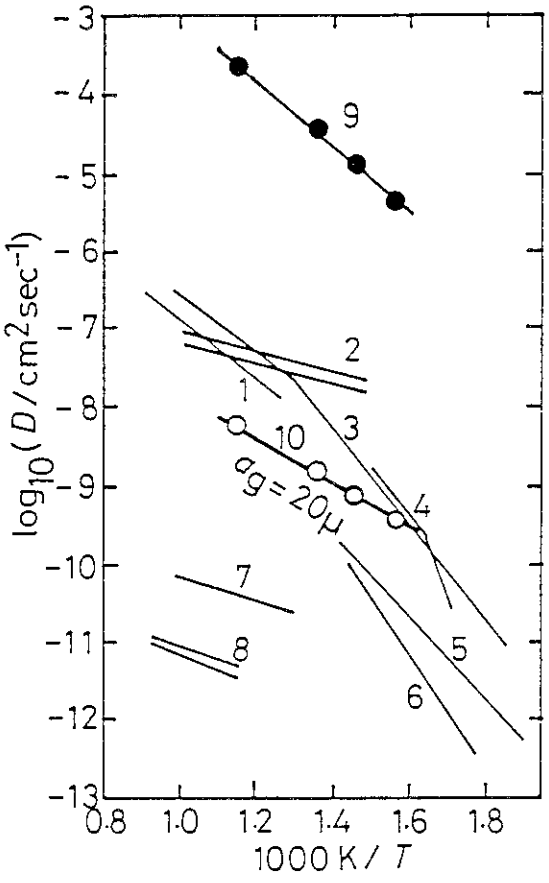

1. Single crystal (Guggi et al., 1983)
2. Solidified melt (Okula et al., 1984)
3. Single crystal (Tanifuji et al., 1983)
4. Powder (Vasilyev, 1979)
5. Powder (Hudo et al., 1981)
6. Sintered pellet (Okuno et al., 1983)
7. Powder (Guggi et al., 1979)
8. Sintered pellet (Matsuta et al., 1983)
9. Present work / D_{int}
10. Present work / D_g

$D_{int} = 1.61 \times 10^{2} \exp(-22700[cal/mol] / RT)$
$D_g = 1.27 \times 10^{-5} \exp(-13100[cal/mol] / RT)$

Fig. 17 Comparison of Diffusion Coefficients in Li_2O

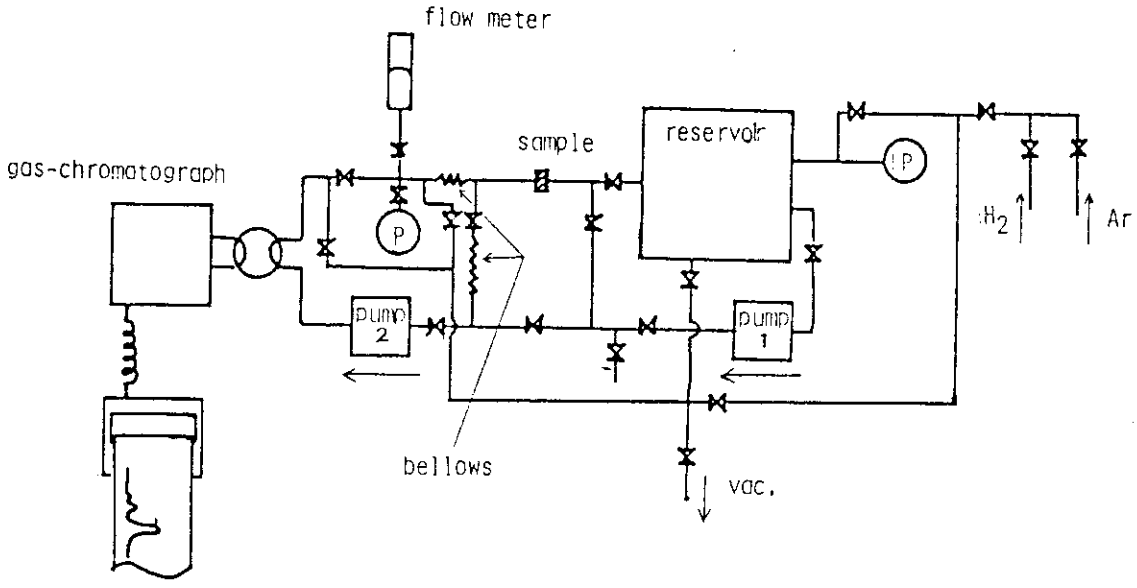

Fig. 18 Experimental Apparatus for Measuring Effective Diffusivity and Permeability through Interconnected Pores of Sintered Materials

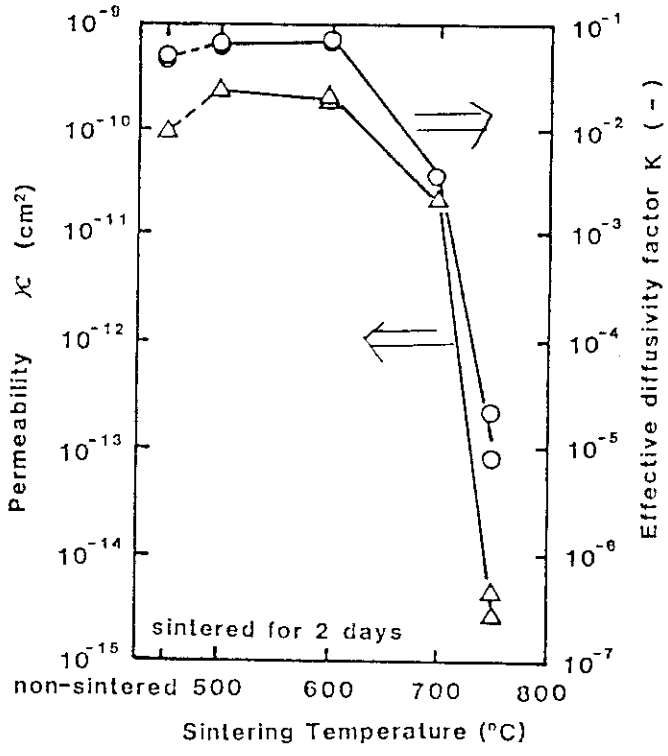

Fig. 19 Sintering-Temperature Dependence of Permeability and Effective Diffusivity Factor (LiF pellets)

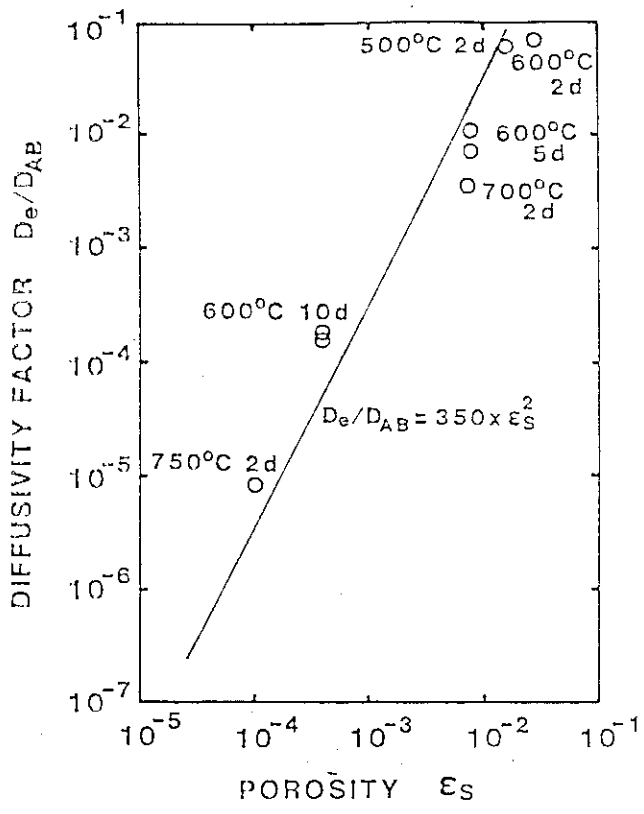

Fig. 20 Porosity Dependence of Diffusivity Factor (LiF)

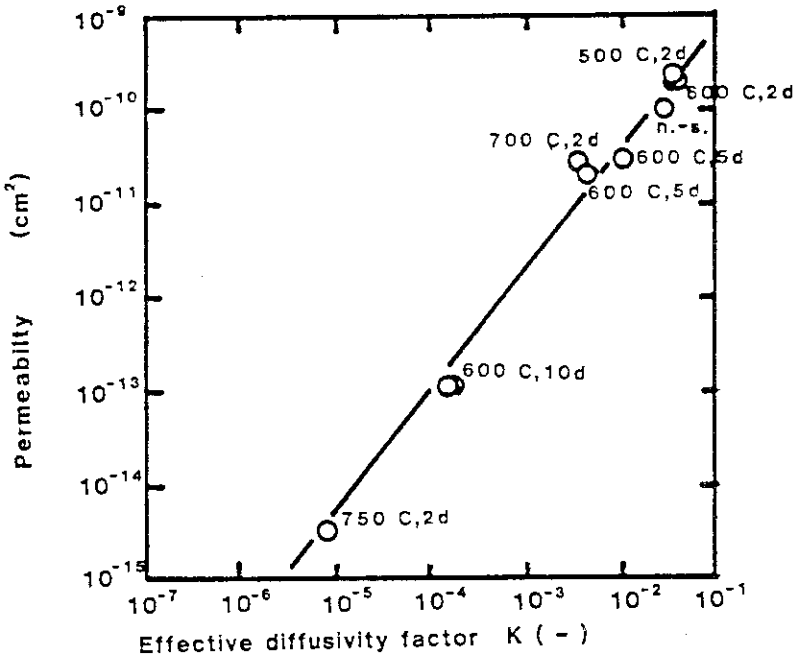

Fig.21 Effective Diffusivity Factor vs Permeability

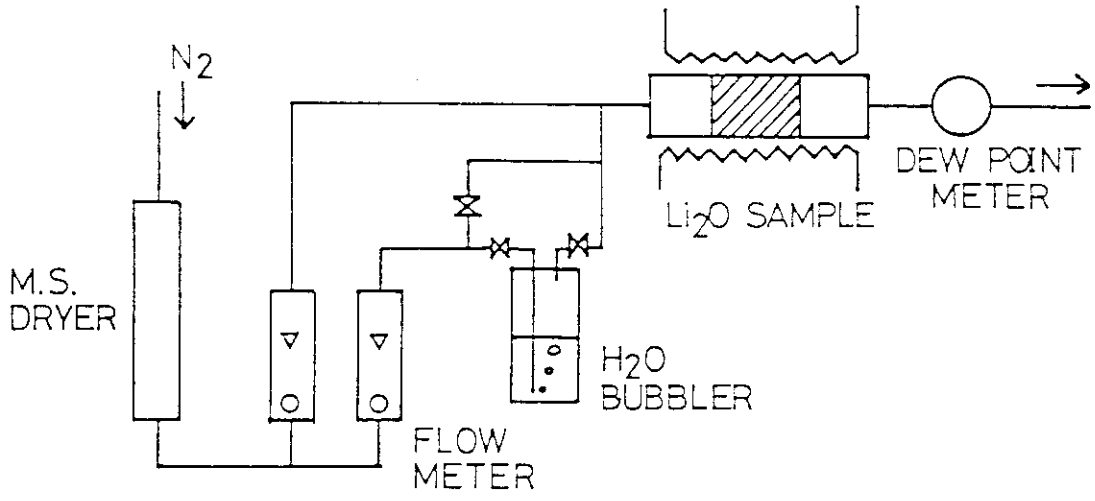

Fig. 22 Experimental Apparatus for Measuring H_2O Adsorption on Li_2O Powder

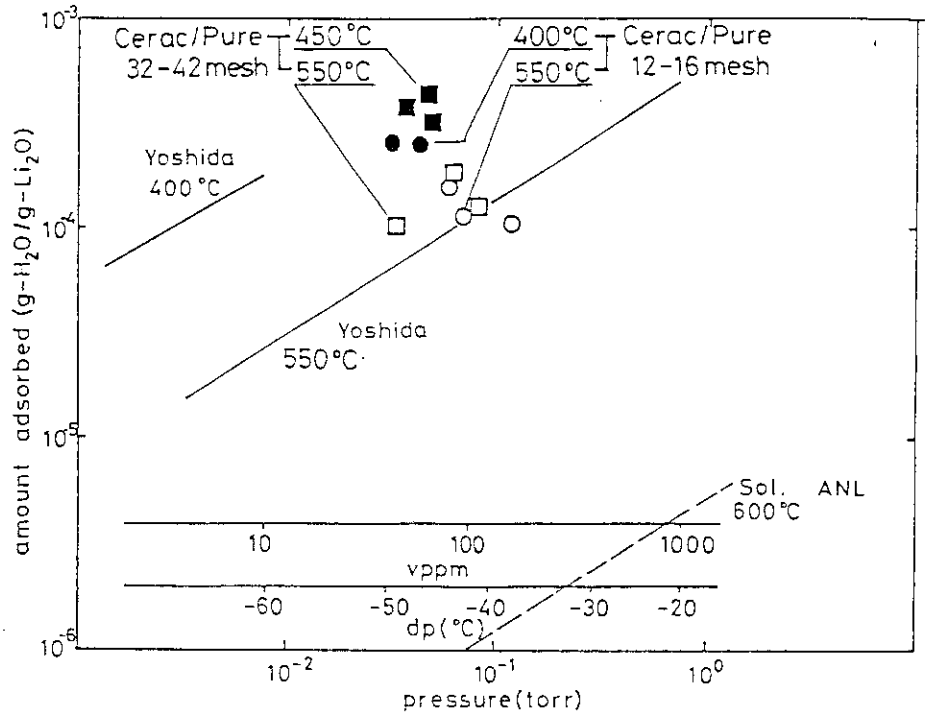

Fig. 23 Experimental Results of Amount Adsorbed for Li_2O Powder

No.10 OVERVIEW OF THE IN-SITU TRITIUM RELEASE EXPERIMENTS OF THE SOLID BREEDER MATERIALS

H. WATANABE, JAERI

ABSTRACT

The VOM series experiments have been conducted in the JRR-2 in order to examine the tritium release behavior from several kinds of breeding materials, mainly Li_2O, since 1981. It has undergone various improvements in capsules and measurements apparatus.

The chemical form of released tritium is mainly HTO and T_2O in pure helium sweep gas. On the other hand the tritium release is enhanced in deutrium-added helium gas and its form is almost DT and T_2.

In recent VOM -22H experiment, the operating behavior of Li_2O and $LiAlO_2$ spheres which were simultaneously irradiated was examined. The tritium release from Li_2O spheres is far better than in the $LiAlO_2$. Post irradiation examination of both materials revealed that their integrity was preserved. Some localized mass transfer of Li_2O spheres was observed on their surfaces at temperatures as high as 820°C.

Table 1 In Situ Tritium Recovery Experiments Condition

	VOM－15H	VOM－21H	TRIO (USA)
SAMPLE & WEIGHT (g)	Li_2O , 6.67	Li_2O , 2.03	$LiAlO_2$, 42.9
NEUTRON FLUX (n/cm^2·s)	1×10^{14}	0.9×10^{14}	4×10^{14}
TEMPERATURE (°C)	480－760	480－900	500－700
IRRADIATION TIME (h)	990	2655	2112
T GENERATION RATE (mCi/min)	0.53	0.30	0.3
SWEEP GAS	He	He, He-0.001, 0.01, 0.1% D_2	He-0.1% H_2

	VOM－22H		VOM－23H (BEATRIX)	
SAMPLE & WEIGHT	$LiAlO_2$, 4.24	Li_2O , 3.87	$LiAlO_2$, 34.9	Li_4SiO_4 , 17.8
NEUTRON FLUX	1×10^{14}		1×10^{14}	
TEMPERATURE	430－900	300－900	400－900	
IRRADIATION TIME	2050		1056	
T GENERATION RATE	0.33	0.30	0.77	0.40
SWEEP GAS	He, He-0.001, 0.01, 0.02, 0.1, 1% D_2		He, He-0.1% D_2	

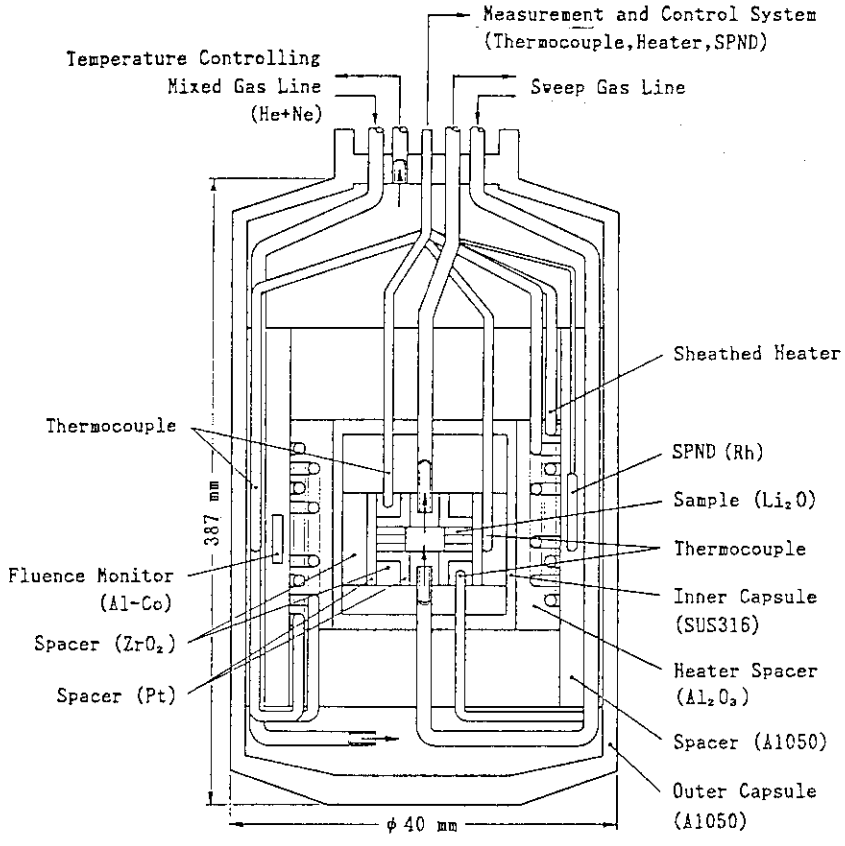

VOM-21H Experiment

Fig. 1 Schematic Diagram of the Capsule for the VOM-21H Experiment

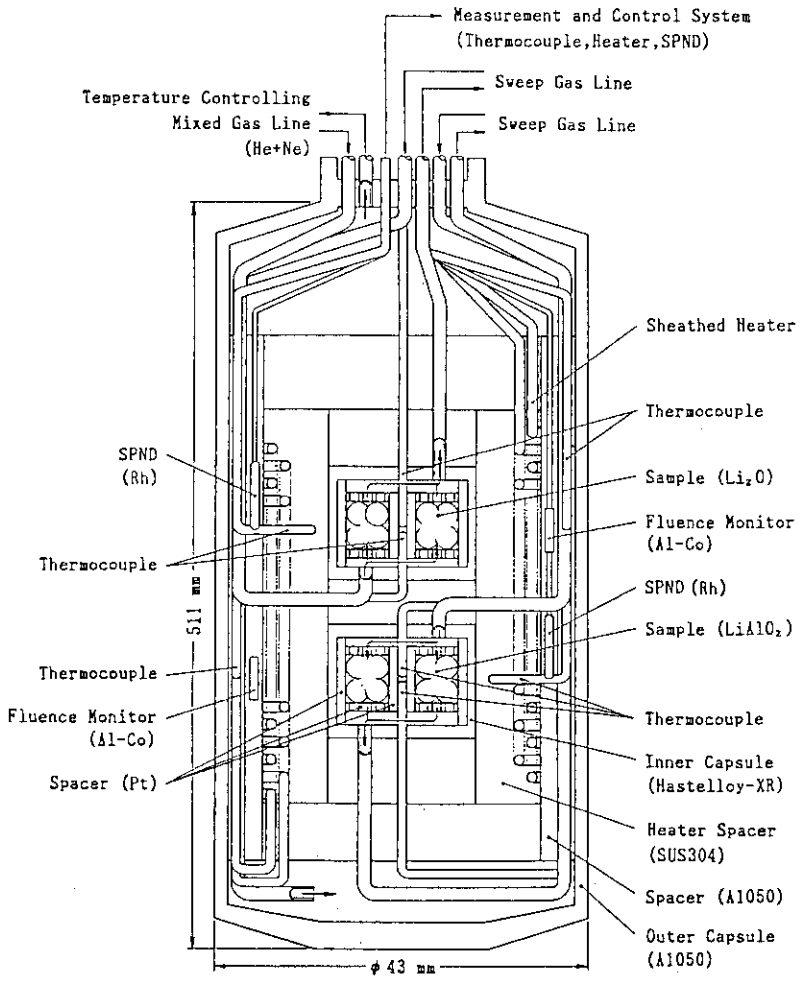

VOM-22H Experiment

Fig. 2 Schematic Diagram of the Capsule for the VOM-22H Experiment

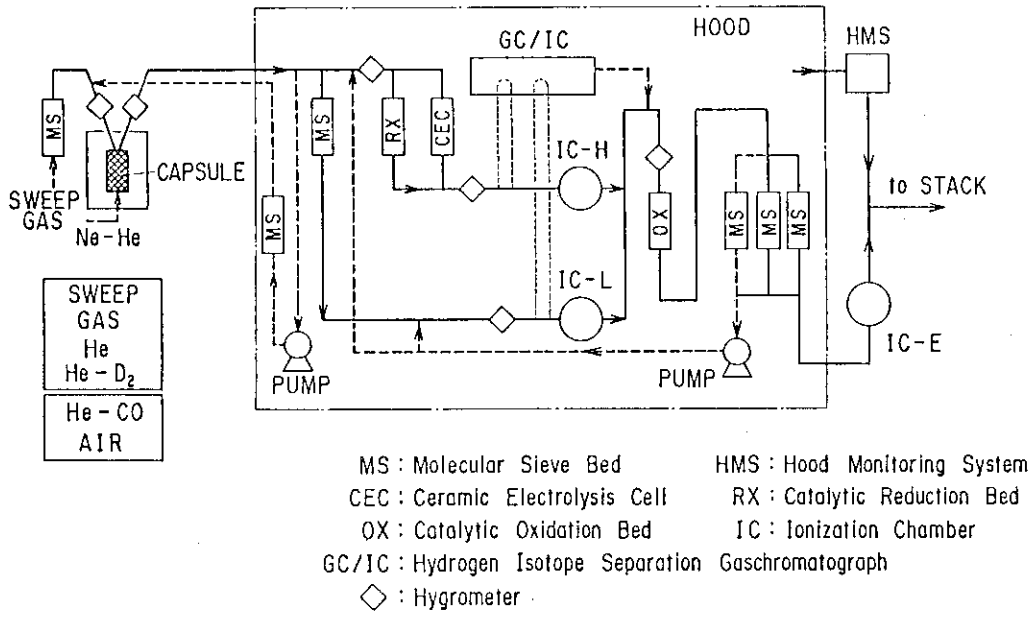

Fig. 3 Flowsheet of Apparatus for In Situ Tritium Recovery Experiment (VOM-21H)

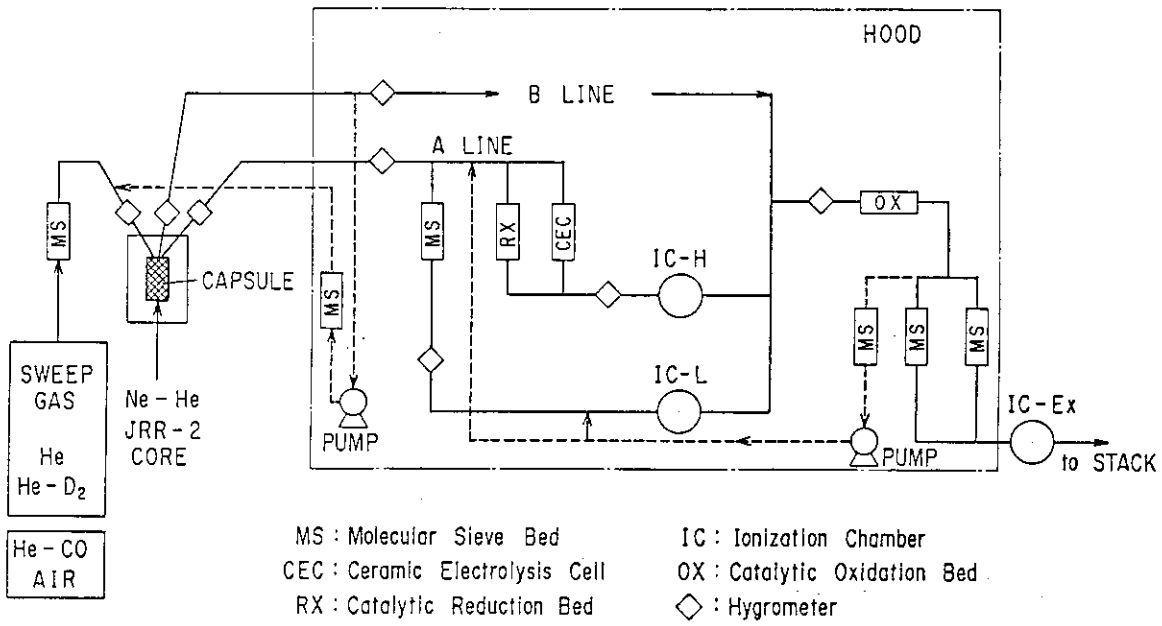

Fig. 4 Flowsheet of Apparatus for In Situ Tritium Recovery Experiments (VOM-22H & -23H)

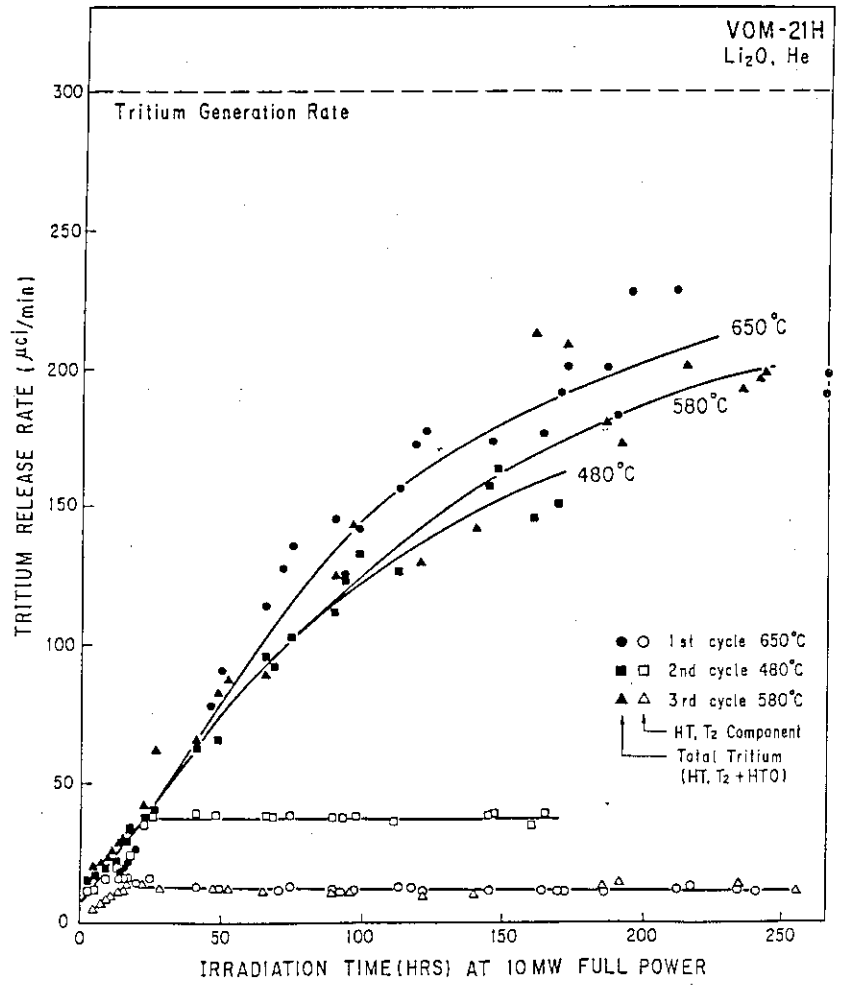

Fig. 5 Total Tritium and Gaseous Tritium Release from Li_2O Pellets Using Pure Helium Gas as a Sweep Gas (VOM-21H)

Table 2 Retained Tritium in Li_2O and $LiAlO_2$

Experiment	Material	^6Li Burn-up (%)	Temperature(°C)	Retained Tritium(wppm)	Remark
VOM-7H(JAERI)	Li_2O	$6x10^{-4}$	600	0.1	He 1%H_2 sweep
VOM-15H(JAERI)	Li_2O	0.24	760	0.5~0.9	He sweep
TRIO(ANL)	$LiAlO_2$	0.18	650	< 0.1	He-0.1%H_2 sweep
FUBR(HEDL)	Li_2O	0.43	500	85	Sealed capsule with Ce Getter
			700	28	
			900	13	
TULIP(ANL)	Li_2O	1	600	100~150	Sealed capsule
		3	600	75	

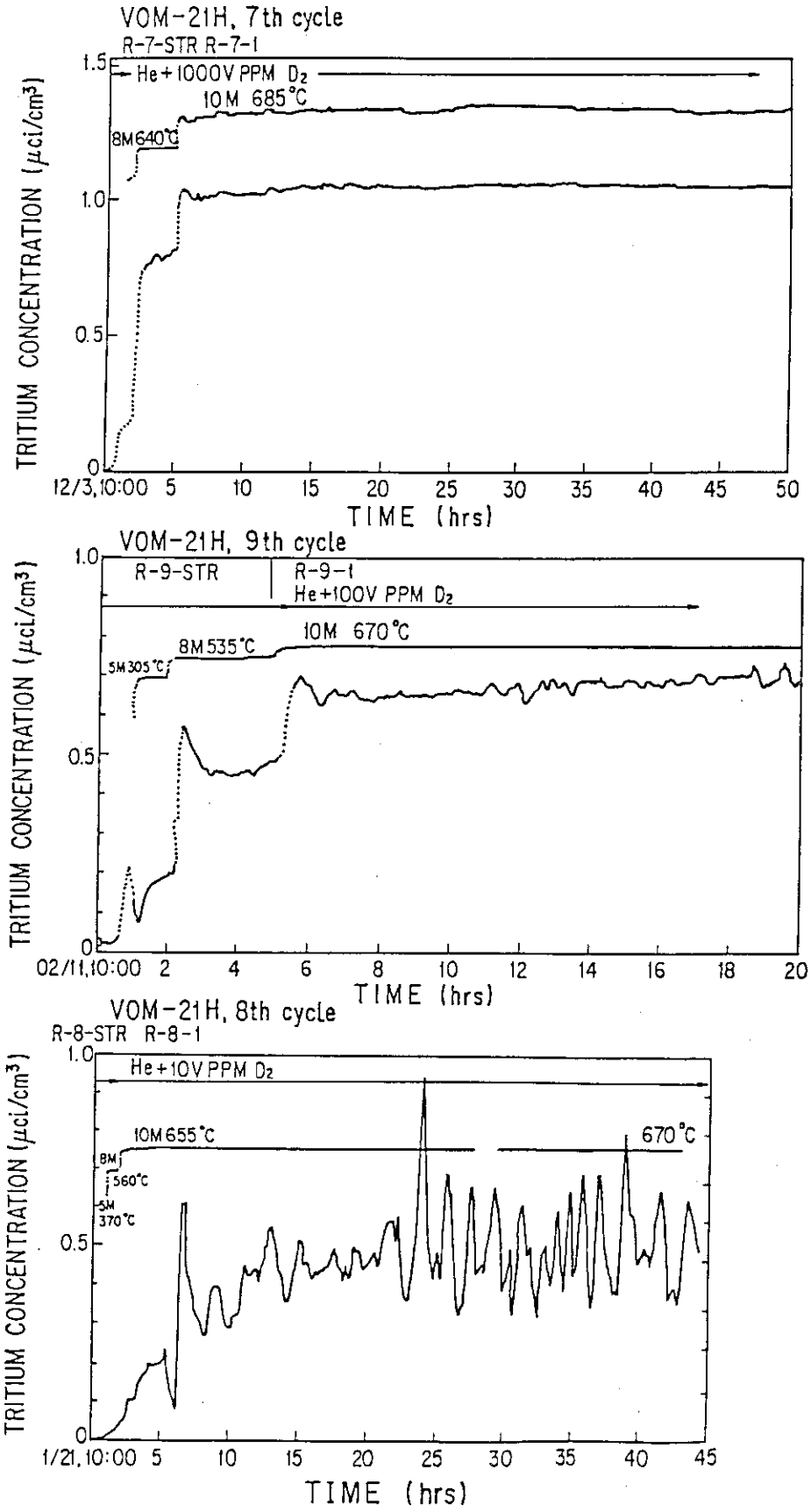

Fig. 6 Effect of Hydrogen Content of a Sweep Gas on Tritium Release at Start-Up (VOM-21H)

Table 3 Isotopic Composition of the Gas Component of Tritium Released from Li_2O as a Function of Hydrogen (D_2) Concentration in the Sweep Gas

D_2 concentration in the sweep gas (ppm)	Reactor cycle No.	Fraction of gas component*1 (%)	Isotopic composition of the gas component HT (mole %)	DT (mole %)	T_2 (mole %)
no addition	3	8	48	ND*2	52
"	5	4	58	ND	42
"	9	[12]	34	14	52
10	8	[60]	39	55	6
100	9	95	36	64	ND
1000	6	94 - 96	0.5	99.5	ND
"	7	"	2	98	ND
"	8	"	2	98	ND
"	9	"	29	71	ND
"	10	-	5	95	ND

*1 Steady state values except ones in brackets. Fractions were calculated based on the tritium generation rate (300 μCi/min).
*2 Not detected.

Table 4 The VOM-22H Spheres Specification

	Capsule A	Capsule B
Composition	$LiAlO_2$	Li_2O
Lithium-6 Enrichment	26 %	Natural
Initial Grain Size	10 μm*	10 μm*
Density	77 % TD	85 % TD
Mass	4.235 g	3.865 g
Diameter of spheres	4 mm	5 mm
Source	Mitsubishi Atomic Power Industries Omiya, Japan	Kawasaki Heavy Industries Akashi, Japan

* estimated, after irradiation grain growth will be measured.

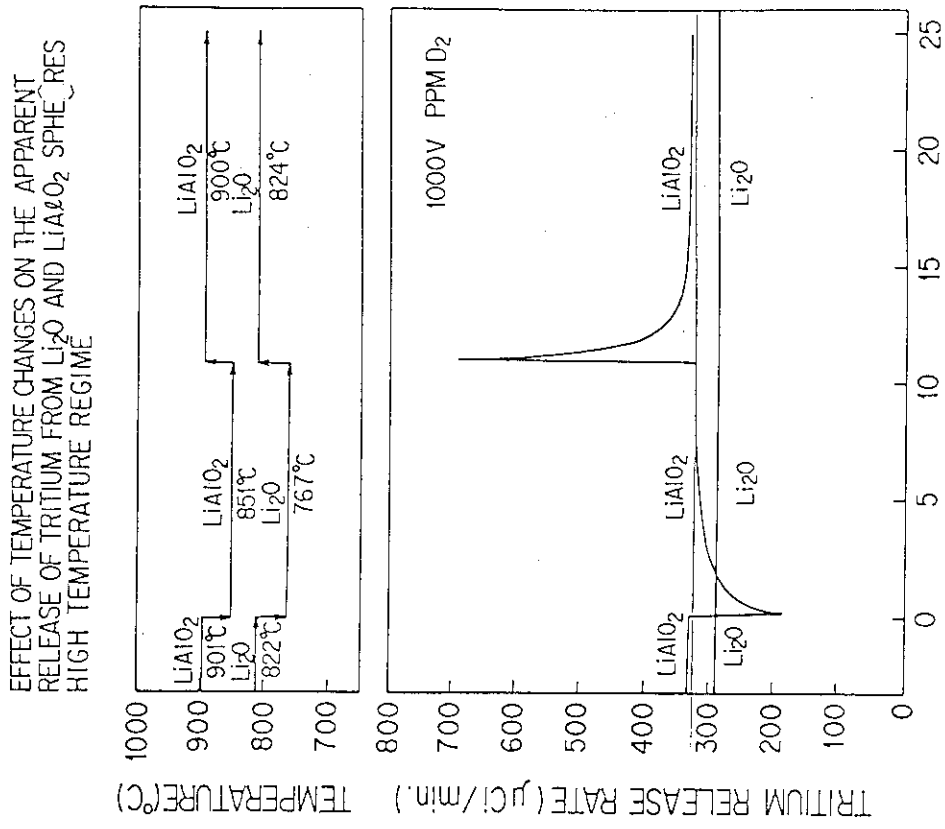
EFFECT OF TEMPERATURE CHANGES ON THE APPARENT RELEASE OF TRITIUM FROM Li2O AND LiAlO2 SPHERES HIGH TEMPERATURE REGIME
TEMPERATURE(°C)
TRITIUM RELEASE RATE (μCi/min.)
TIME (hr.)
LiAlO2 901℃
Li2O 822℃
LiAlO2 851℃
Li2O 767℃
LiAlO2 900℃
Li2O 824℃
1000V PPM D2
LiAlO2
Li2O

Fig. 8

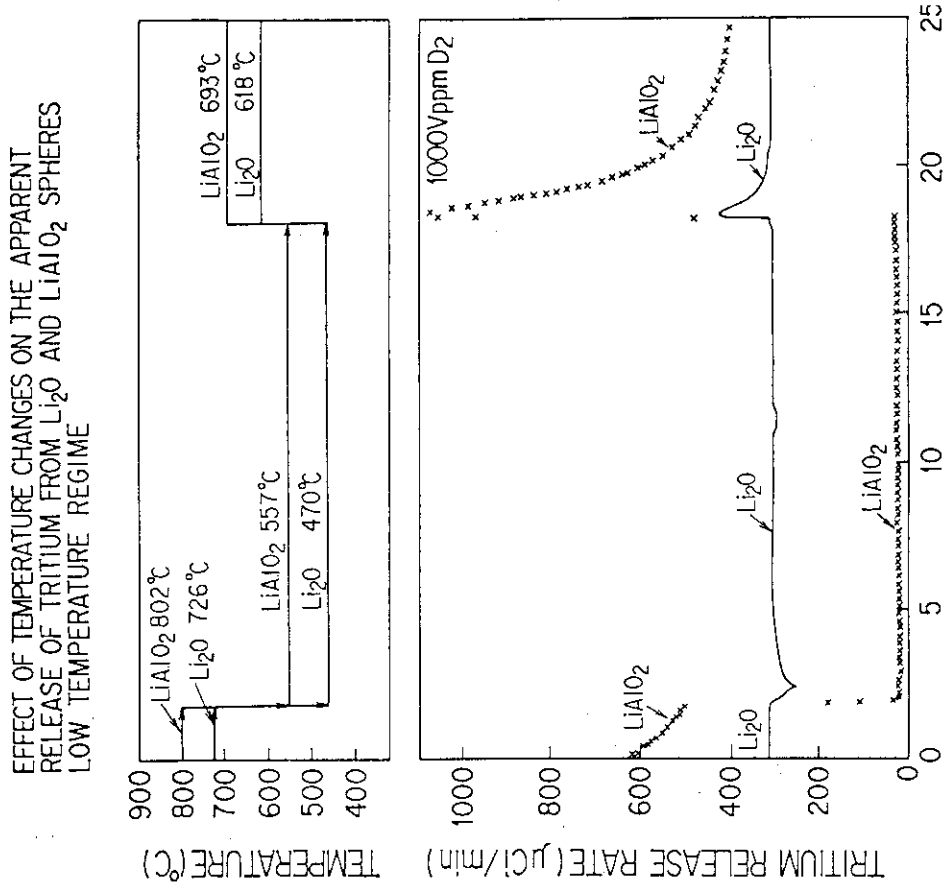
EFFECT OF TEMPERATURE CHANGES ON THE APPARENT RELEASE OF TRITIUM FROM Li2O AND LiAlO2 SPHERES LOW TEMPERATURE REGIME
TEMPERATURE(°C)
TRITIUM RELEASE RATE (μCi/min)
TIME (hr.)
LiAlO2 802℃
Li2O 726℃
LiAlO2 557℃
Li2O 470℃
LiAlO2 693℃
Li2O 618℃
1000Vppm D2
LiAlO2
Li2O

Fig. 7

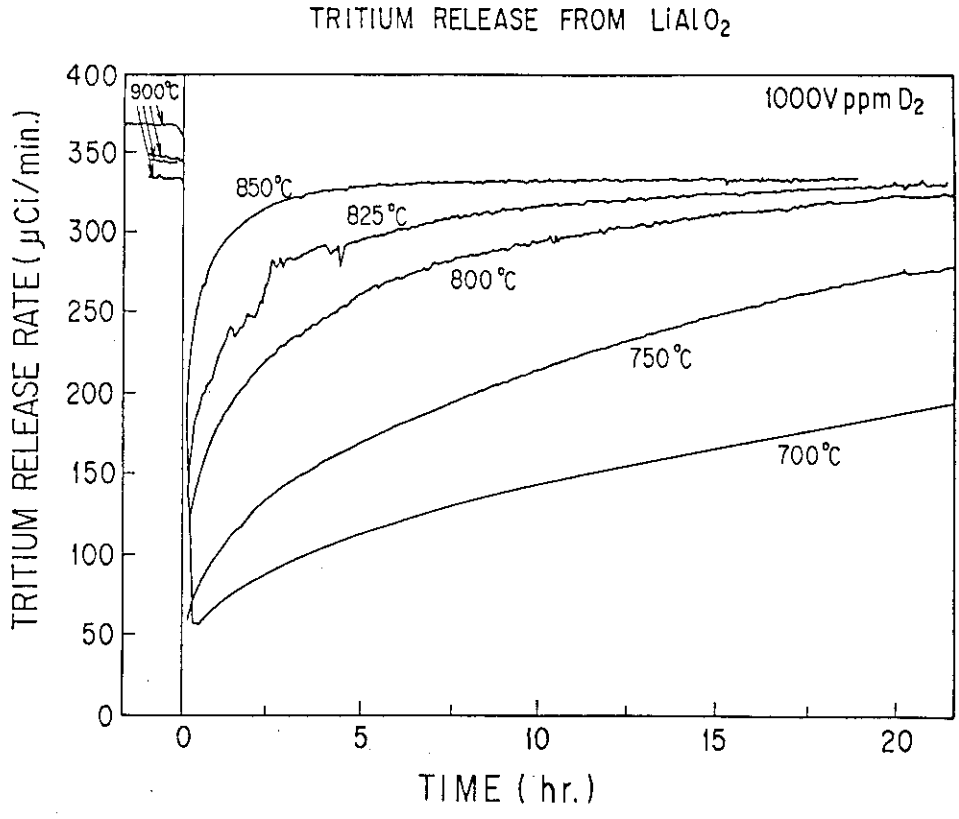
TRITIUM RELEASE FROM LiAlO2
1000V ppm D2
900℃
850℃
825℃
800℃
750℃
700℃
TRITIUM RELEASE RATE (μCi/min.)
TIME (hr.)
400
350
300
250
200
150
100
50
0
0
5
10
15
20

Fig. 9

P89 Japan-US
Tritium Technology
Workshop
Oct. 22(Wed.)-24(Fri.)
1986 at JAERI

No.11 $LiF-PbF_x$ Blanket System

Kazutaka KAWAMURA

Research Laboratory for Nuclear Reactors

Tokyo Institute of Technology

1. INTRODUCTION

In nuclear fusion reactor, which employ D-T fuel cycle, breeding of tritium(^{3}T) is required. While the consensus of many researchers is that Li is a most favorable element to breed tritium, selection of its chemical and physical forms have not been specified so far. Liquid Li compounds such as molten alloys(Li-Pb and Li-Bi-Pb), binary molten salt(LiF-BeF_2), and also liquid Li metal alone have been proposed as ^{3}T breeding materials, as well as solid ones. Liquid breeding materials are advantageous not to be suffered from radiation damage nor from phase transformation and to have high thermal conductivity. Although among them, molten salts seem to be minor candidates, they are still attractive, since they might offer much less pumping load than liquid metals under high magnetic field. Among salts containing Li, LiF is a prominent candidate as a molten blanket material. However, since LiF has a high melting point(842℃), another compound should be added to obtain a moderate operating temperature. As such additives, a compound containing a neutron multiplier, e.g. Be and Pb, is favorable. We proposed the liquid LiF-PbF_2 system as a candidate of the molten salt breeding materials. Since both of LiF and PbF_2 are not hygroscopic substantially, quality control of them is much easier than some other chemical forms such as Li_2O. It is, thus, the purpose of this paper to know the tritium release behaviour from the cold-pressed pellet, cold-pressed and sintered pellet and solidified pellet of LiF-PbF_2, to give the phase diagram of LiF-PbF_2 system and to show the corrosion resistant materials for molten LiF-PbF_2 system.

2. TRITIUM RELEASE BEHAVIOUR FROM COLD-PRESSED PELLET AND COLD-PRESSED AND SINTERED PELLET OF LiF-PbF_2 IRRADIATED BY THERMAL NEUTRON[1)]

Dimensions of these pellets are typically 1 cm diameter x 0.3 cm thickness. The pellets were irradiated with the neutron flux of 7×10^{11} $cm^{-2} \cdot s^{-1}$ for 10 min in Research Reactor TRIGA II at Musashi Institute of Technology. Isotope ratio of Li used in this work was determined by a mass spectrometer. Released tritium from irradiated pellet in an infrared image furnace was trapped as a condensed component at first cold trap. Released tritium broken through the trap was introduced to the oxydization bed containing Hopcallite II (60w/o MnO_2-40w/o CuO) and was trapped as a gaseous component at second cold trap. Residual component remained in the pellet after the release experiment was extracted from the crashed pellet by aqua regia. Each tritium component was analyzed by the scintillation counter. Experimental conditions and results are listed in Table 1. This reveals that the gaseous component is much less than the condensed one in all pellets, suggesting that the main product in the irradiated pellets is TF. Figure 1 shows the cold-pressed pellets release almost all tritium above 600℃ for 3 hrs. Although the pellets of pellet numbers〈10〉 and 〈11〉 were in the liquid state at 870℃ on tritium release experiment, their tritium release behaviour is not largely different from that of the pellet 〈3〉 and 〈4〉 in the solid state at 600℃ .

Tritium release curves of three kinds of the pellets at 700℃ are shown in Fig. 2. The cold pressed and sintered pellet containing PbF_2 ⟨9⟩ released more tiritum than one containing no PbF_2 ⟨8⟩, while both of the cold-pressed pellet containing PbF_2 ⟨6⟩ and no PbF_2 ⟨5⟩ released in the almost same way. The pellets ⟨5⟩, ⟨8⟩ and ⟨7⟩, theoretical densities of which are 68, 81 and 100%, respectively, have significantly different tritium release rate, that is, tritium release rate of the pellets containing no PbF_2 seems to increase with decrease of theoretical density at the same temperature, while they evolved same amount of tiritum within initial 5 min.

3. TRITIUM RELEASE BEHAVIOUR FROM SOLIDIFIED PELLET OF LiF-PbF_2 IRRADIATED BY THERMAL NEUTRON[2]

Samples melted in a Pt crucible were kept at ~727° k for 20 min and were allowed to cool at 4.7 k min^{-1} under He atmosphere. The solidified samples in the Pt crucible were sliced with a multiwire saw. Dimensions of the pellets are listed in Table 2. Total tritium product and its components are shown in Table 3. Gaseous component is considerably small in all experimental runs. Judging from the self-shielding factors[2], it might be conjectured that tritium was produced nearly uniformly in the pellets. From the initial concentration of tritium in pellet and the concentration of tritium in the pellet at time t, it is possible to determine the diffusion coefficient of tritium in LiF-PbF_2 system by nonlinear optimazation. The calculated values of diffusion coefficient of tritium are listed in Table 4. Arrhenius plots of diffusion coefficient against the reciprocal of temperature are shown in Fig. 3, which gives us an activation energy of diffusional process of tritium. The estimated activation energy of 0.51 eV is much smaller than that in the LiF single crystal (1.75 eV)[3] and the LiF powder[4] (2.2 eV), which implies diffusion mechanism of tritium in the LiF-PbF_2 system is different from that in the pure LiF. The diffusion coefficient at p=0.476 ($D=1.18\times10^{-10}$ $m^2\cdot s^{-1}$) is smaller than that at p=0.377 ($D=1.63\times10^{-10}$ $m^2\cdot s^{-1}$) at 673 K, where p is mole fraction of LiF. It has been shown that addition of PbF_2 to LiF in order to decrease melting point of the system and multiply neutron brings the increase of diffusion coefficient of tritium, which is favorable to decrease tritium inventory in the blanket.

4. PHASE DIAGRAM OF LiF-PbF_2 SYSTEM[5]

The fundamental knowledges of molten binary LiF-PbF_2 salt are still limited and remain to be less accurate. For example, it could be stressed from our preliminary experiment that the eutectic temperature of LiF-PbF_2 is about 580℃, being 80℃ lower than that published value[6]. Melts of LiF with PbF_2 were made up by weight directly in TG-DTA(Thermogravimetric Analysis-Differential Thermal Analysis) platinum sample pan. The most typical TG and DTA curves, together with the phase diagram, were shown in Fig. 4. A glance at Fig. 4 shows the appreciable change in weight at a temperature where both solid and melt can exist. The decrease in weight with increasing temperature has been attributed to the fact that

PbF_2 has a high vapour pressure at high temperature, in contrast with that of LiF, which was confirmed experimentally. It, thus, is necessary to correct the composition due to the vaporization of PbF_2 after each run of experiment. Combining the result of DTA with that of TG, we obtain the phase diagram of LiF-PbF_2 system as shown in Fig. 5. The obtained liquidus line for LiF-rich melt is almost identical with that reported previously, the liquidus line for PbF_2-rich melt, however, is more likely to be too low compared with published line. It, therefore, is apparent that the eutectic temperature for LiF-PbF_2 system at 580℃ gives the lower value than that at 660℃ reported previously and the eutectic composition of 60 mole % PbF_2 shows higher compared with the published eutectic composition of 53 mole % PbF_2.

5. CORROSION RESISTANT MATERIALS FOR LiF-PbF_2 MELT

It is most important to find out the corrosion resistant materials in order to apply LiF-PbF_2 melt to blanket for fusion reactor. From the results of the batch-typed corrosion test, in which the eutectic LiF-PbF_2 liquid of 10 gram in various metallic crucibles 1.23 cm in inner diameter and 3.6 cm high, as shown in Fig. 6, was kept under helium atmosphere at 740℃, it is found that the surface of copper crucible reduces only 1.5 μm in thickness for 70 hours, indicating that the copper is the corrosion resistant material for molten LiF-PbF_2 melt. The data of corrosion for copper is shown in Fig. 7, together with that of other materials, such as brass, stainless steel, nickel, monel and phosphons blonze. It should finally be stressed that the half-lives of nuclear rection products of copper are very short, that is, 12.7 h and 5.10 min.

REFERENCES

1) K. Ohashi, R. Takagi, M. Okamoto, and K. Kawamura; J. Nucl. Sci. and Tech., 21 152 (1984)
2) N. Saito, K. Tsunekawa, R. Takagi, and K. Kawamura; J. Nucl. Sci. and Tech., 23 253(1986)
3) H. J. Matzke; Phys. Stat. Sol., 18 317(1966)
4) H. Cohen and W. S. Diethorh; Phys. Stat, Sol., 9 251(1965)
5) N. Saito, K. Kawamura, H. Tanaka, and R. Takagi; Denki Kagaku(in press) (1986)
6) C. Margheritis, G. Flor and C. Sinistri; Z. Naturforsch., 30a 896(1975)

Table 1 Experimental conditions and results

Pellet No.	Pellet type	TD (%)	Release temperature (K)	PbF_2 content (mol%)	Total tritium production (μCi)	P_c	P_g (%)	P_r
1	C	69	673	0	7.00	71.6	4.1	24.3
2	C	76	673	30	2.65	75.5	2.6	21.9
3	C	68	873	0	6.57	95.6	3.8	0.6
4	C	72	873	20	3.94	96.7	2.8	0.5
5	C	68	973	0	10.52	96.2	3.8	0.0
6	C	76	973	14	3.01	86.4	11.3	2.3
7	M	100	973	0	5.72	52.3	0.5	47.2
8	S	81	973	0	3.14	90.3	0.8	8.9
9	S	85	973	10	3.46	96.6	3.2	0.2
10	C	69	1143	0	8.16	96.4	3.4	0.2
11	C	83	1143	30	3.75	96.3	3.7	0.0

C: Cold-pressed, M: Solidified, S: Sintered, TD: Theoretical density,
P_c, P_g, P_r: Fractional contribution of the codensed, gaseous and residual component to the total tritium production

Table 2 Dimensions of pellets of LiF-PbF_2 system and their self-shielding factors

Pellet No.	r[†1] (mm)	h[†2] (mm)	w[†3] (mg)	p[†4]	f[†5]
1	9.48	0.86	402.5	0.476	0.918
2	9.51	0.81	388.9	0.476	0.918
3	9.45	0.84	383.9	0.476	0.920
4	9.58	0.88	401.7	0.476	0.920
5	9.60	1.62	789.0	0.476	0.879
6	9.75	1.63	839.6	0.377	0.932
7	9.57	0.84	412.8	0.377	0.949
8	9.59	0.84	410.3	0.476	0.916

†1: Radius, †2: Thickness, †3: Weight
†4: Mole fraction of LiF
†5: Self-shielding factor

Table 3 Total ^3H product and its components

Pellet No.	T[†1](K)	H[†2](min)	C[†3](μCi)	P_C[†4](%)	P_G[†5](%)	P_R[†6](%)
1	503	90	2.316	47.02	0.04	52.94
2	583	60	2.357	96.52	0.13	3.35
3	673	60	1.971	98.88	0.36	0.76
4	673	90	3.941	99.34	0.10	0.56
5	673	50	3.892	99.05	0.13	0.82
6	673	50	3.414	99.00	0.12	0.88
7	673	60	2.236	98.88	0.18	0.94
8	773	60	3.261	98.90	0.18	0.92

†1: Release temperature, †2: Irradiation time, †3: Total ^3H product
†4: Fractional contribution of condenced component released
†5: Fractional contribution of gaseous component released
†6: Fractional contribution of residual component remained in pellet

Table 4 Diffusion coefficients of ^3H in $LiF\text{-}PbF_2$ system

Pellet No.	1	2	3	4	5	6	7	8
$D\times10^{10}(m^2\cdot s^{-1})$	0.031	0.153	1.332	1.015	1.183	1.565	1.695	1.657

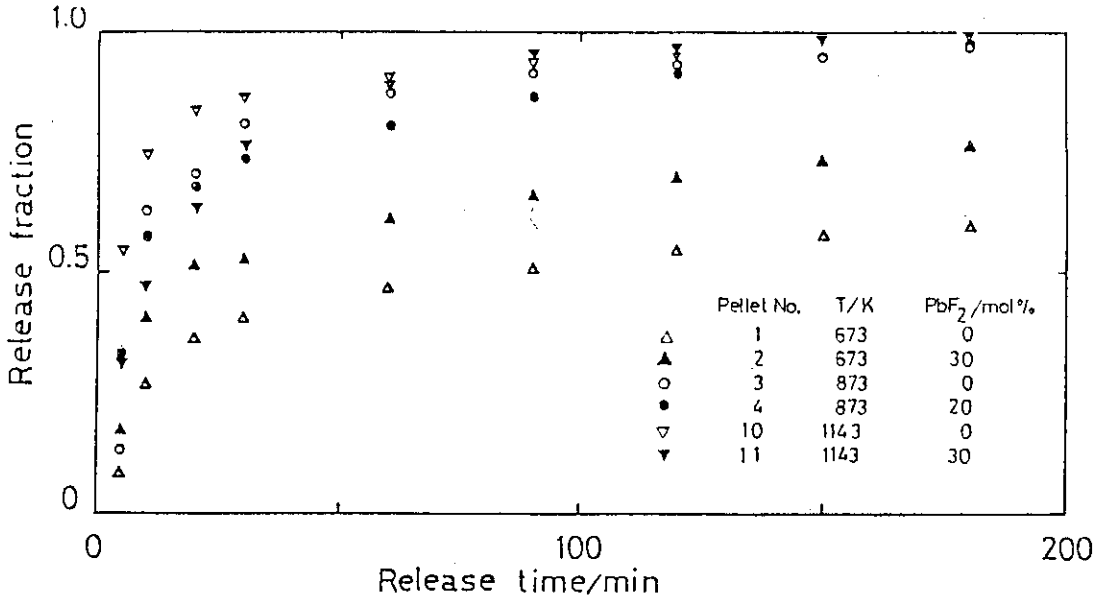

Fig. 1 Release fraction of condensed component of tritium from cold-pressed pellets

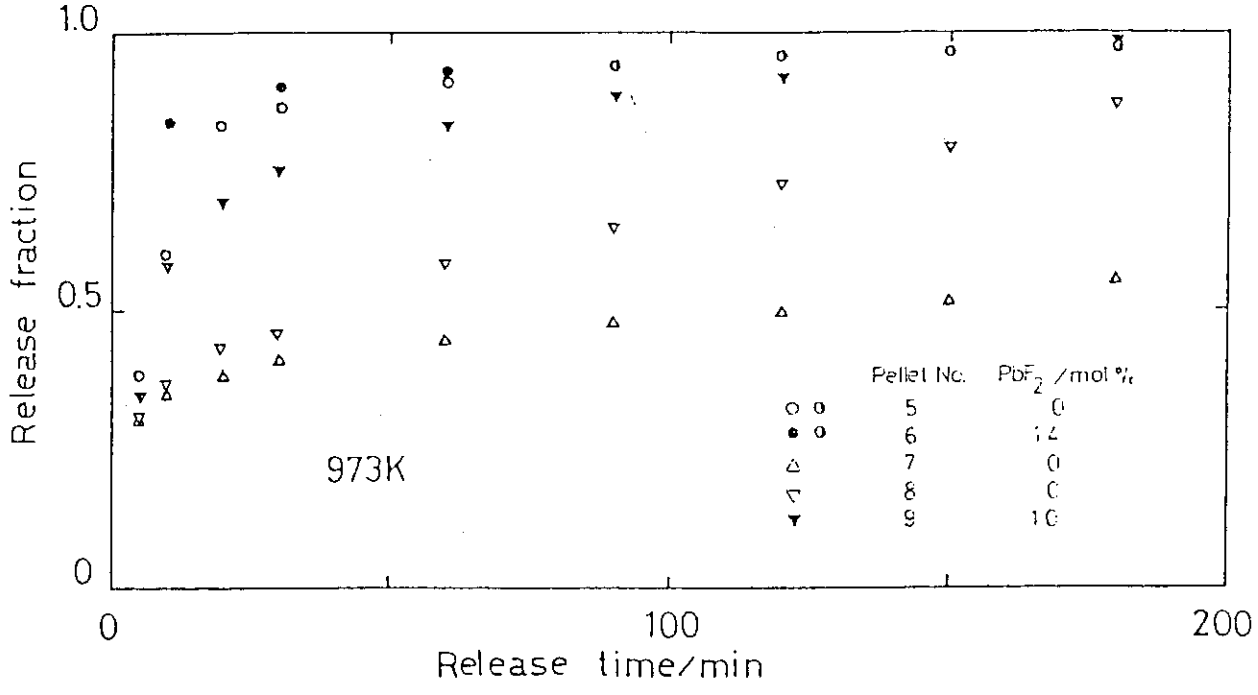

The symbol means that the pellets <5> and <6> have the same release amount eventually.

Fig. 2 Release fraction of condensed component of tritium from three kinds of pellets

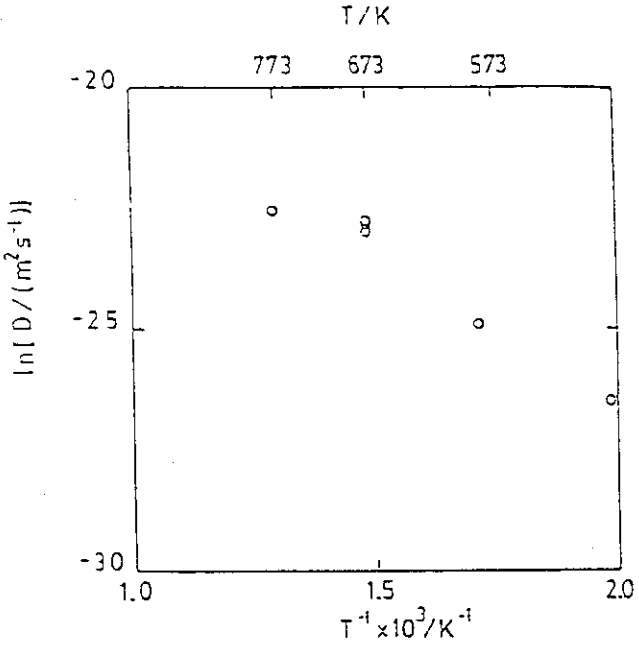

Fig. 3 Arrhenius plot of diffusion coefficient of ^3H in solidified $LiF\text{-}PbF_2$ pellet

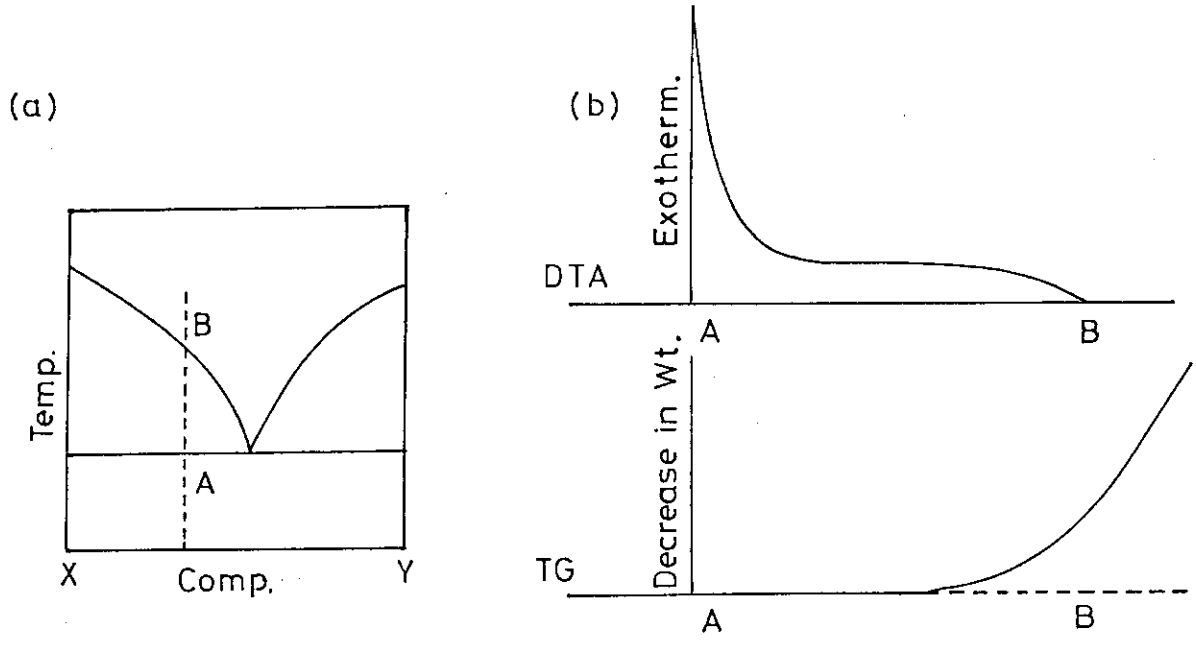

Fig. 4 (a) Phase Diagram and (b) TG-DTA Curve

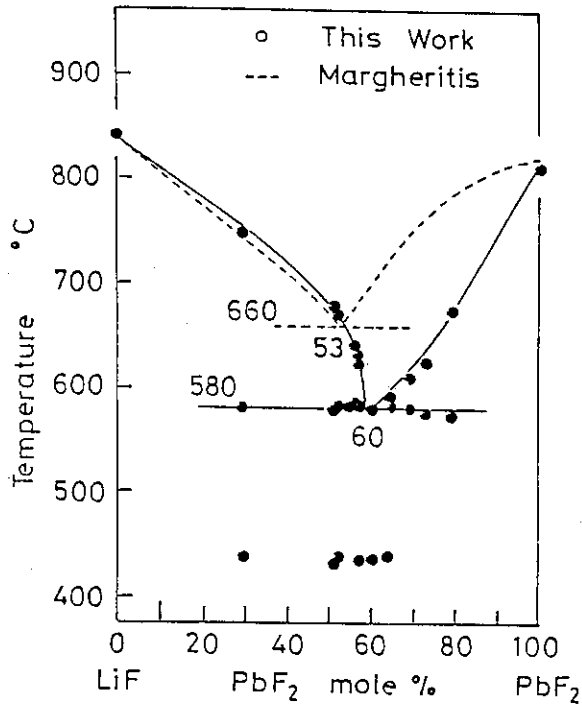

Fig. 5 Phase Diagram of $LiF-PbF_2$

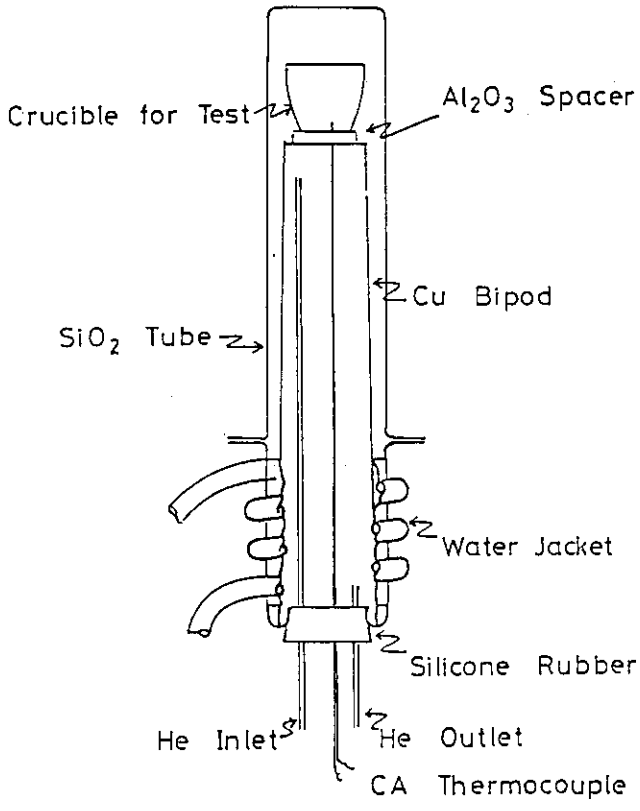

Fig. 6 Corrosion Testing Apparatus

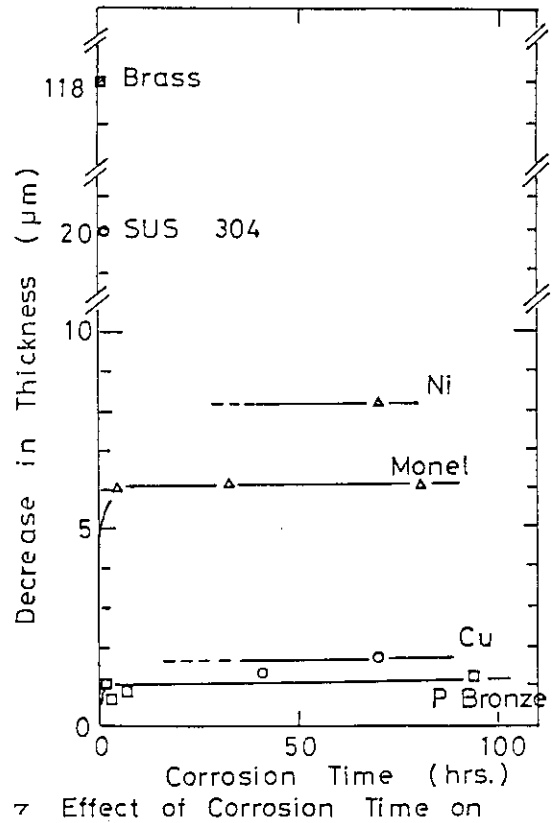

Fig. 7 Effect of Corrosion Time on Decrease in Thickness

No.12 Design Concept of Down Stream in Fusion Fuel Cycle

Presented

by

Hiroshi AMANO, Institute of Plasma Physics,
Nagoya University, JAPAN

at

Japan-U.S.A. Work-shop on Tritium Technology

on

23rd October, 1986 (JAERI Head-office, Tokyo, JAPAN)

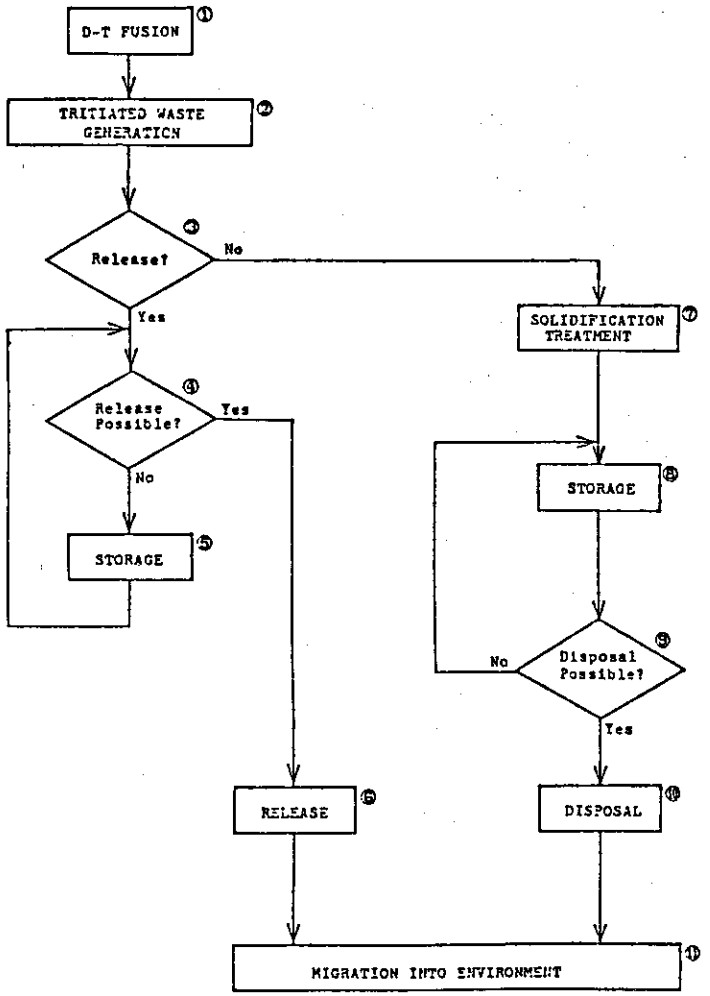

Notes:

① . Generation suppression
. TS/ARW mixture suppression

② . Clarification of classification level (non-radioactive waste/radioactive waste)

③ . Clarification of classification level (TS/ARW)

④ . Clarification of permissible mixture level

⑤ . Separating technology

⑥ . Chemical form, phase, condition
Ex. Recovery in gaseous phase

⑦ . Change in chemical form, phase, condition
Ex. Change to H_2O

⑧ . Combustible matter → incineration → concentration
. Oxidation, reduction (clarification of permissible mixture level of chemical form other than H_2O)
. Distillation → TS/Another

⑨ . Effort for lowering lower limit of recovery
→ Reduction in quantity of T waste generated
. Improvement in recovery efficiency

⑩ . Improvement in refining efficiency

. Is quantity excessive?
Suppression of waste generation ①
Improvement regarding lower limit of recovery ⑨

Fig. 1 Conceptual Logic on Treatment and Disposal of Tritiated Waste

Table 1 Definition of Tritiated Waste

1. Radioactive nuclides other than tritium are not included due to separation in advance.
2. Tritium is to be oxidized and to be the form of THO (water).
3. In disposal of tritiated waste, it is to be solidified and packaged.

Table 2 Concept of Waste Management

	Subject	Item	Detail	Selection
1	Management scenario	Concentrated disposal system		
		Self-concluding disposal system		o
2	Treatment system	Chemical form of TW	THO	o
		Treatment form	Solidification	o
3	Disposal system	Land disposal	Shallow-ground type	o
		Sea dumping		
4	Quantification of TW			

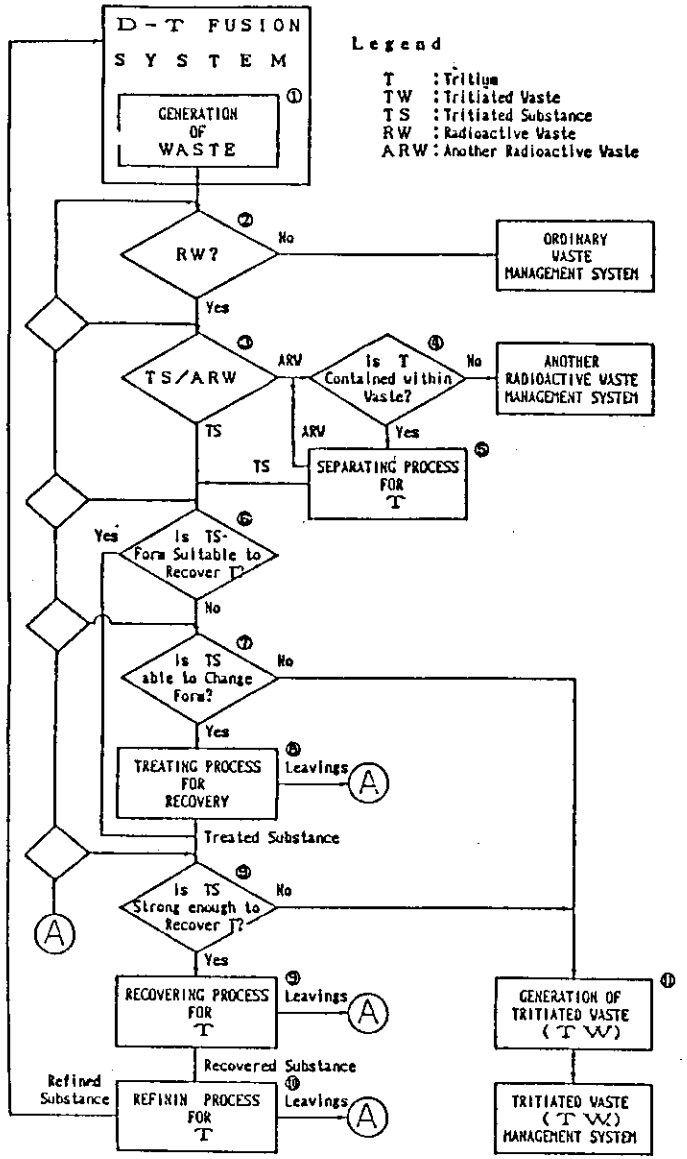

Notes:

① . Generation suppression
. TS/ARW mixture suppression
② . Clarification of classification level (non-radioactive waste/radioactive waste)
③ . Clarification of classification level (TS/ARW)
④ . Clarification of permissible mixture level
⑤ . Separating technology
⑥ . Chemical form, phase, condition
Ex. Recovery in gaseous phase
⑦ . Change in chemical form, phase, condition
Ex. Change to H_2O
⑧ . Combustible matter → incineration → concentration
. Oxidation, reduction (clarification of permissible mixture level of chemical form other than H_2O)
. Distillation → TS/Another
⑨ . Effort for lowering lower limit of recovery
→ Reduction in quantity of T waste generated
. Improvement in recovery efficiency
⑩ . Improvement in refining efficiency

. Is quantity excessive?
Suppression of waste generation ①
Improvement regarding lower limit of recovery ⑨

Fig. 2 Generation of Tritiated Waste

Table 3 Method of Proceeding with Safety Evaluation

	Topic	Remarks
1	Definition of components and subcomponents	
2	Evolvement of function of each subcomponent	Matrix of subcomponents and functions of each component
3	Evolvement of performance of each subcomponent	
4	Quantitative evaluation of effect by FTA	Predicated on probabilistic approach
5	Comprehensive evaluation of emvironmental safety	Defense with multi-barrier and in depth

Table 4 Relation of Tritiated Waste Generated and Number of Solidified Units Produced on Annual Basis

T Waste Generated (g/yr)	T Concentration in Treated Water[1] (Ci/ℓ)	Water Treated (ℓ)	Number of Solidified Units (Pc/yr)	T Concentration of Solidified Units[2] (Ci/ton)
10 (100,000 Ci)	100	1,000	10	25,000
	10	10,000	100	2,500
	1	100,000	1,000	250
	0.1	1,000,000	10,000	25
1 (10,000 Ci)	10	1,000	10	2,500
	1	10,000	100	250
	0.1	100,000	1,000	25
	0.01	1,000,000	10,000	2.5
0.1 (1,000 Ci)	1	1,000	10	250
	0.1	10,000	100	25
	0.01	100,000	1,100	2.5
	0.001	1,000,000	10,000	0.25

Note 1) The increase in volume due to solidification is twofold and the drum can capacity 200 ℓ/can. In effect, the quantity of treated water possible to solidify in one drum is 100 ℓ.

Note 2) The density of the solidified material is considered as 2.0 kg/ℓ.

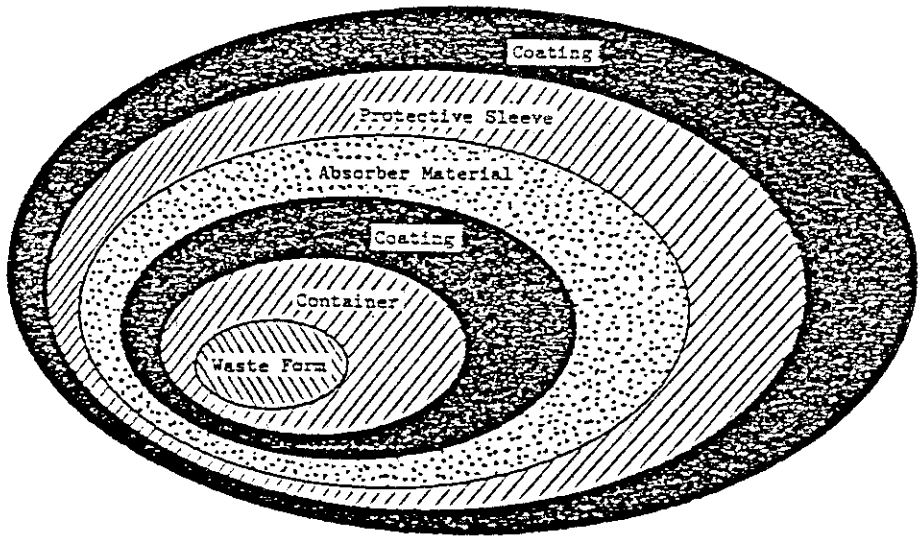

Fig. 3 Subcomponents of Waste Package

Table 5 Matrix of Subcomponents and Functions of Waste Package

		Waste Form	Container and/or Coating	Absorber Material	Protective Sleeve and/or Coating
1	Securing of immobility	○	△		
2	Securing of spatial isolation	△	○		○
3	Securing of retardation effect	△	○	○	○
4	Protection against water from outside	△	○	△	○
5	Protection against mechanical external forces	△	○	△	○
6	Securing of engineering operability	○	○		

o function absolutely necessary
Δ function desirable to have

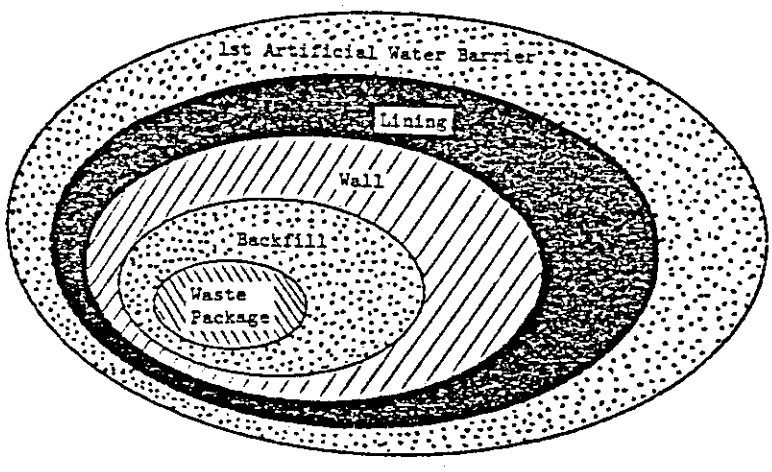

Fig. 4 Subcomponents of Repository

Table 6 Matrix of Subcomponents and Functions of Repository

		Back-fill	Wall and/or Lining	First Arti-ficial Water Barrier	Embank-ment (Vege-tation)
1	Protection against human external forces	△	○		△
2	Protection against natural external forces	△	○		
3	Retardation of groundwater movement	△	○	○	○
4	Retardation of tritium migration	○	△		
5	Securing of thermal dif-fusibility	○	△		

o function absolutely necessary
Δ function desirable to have

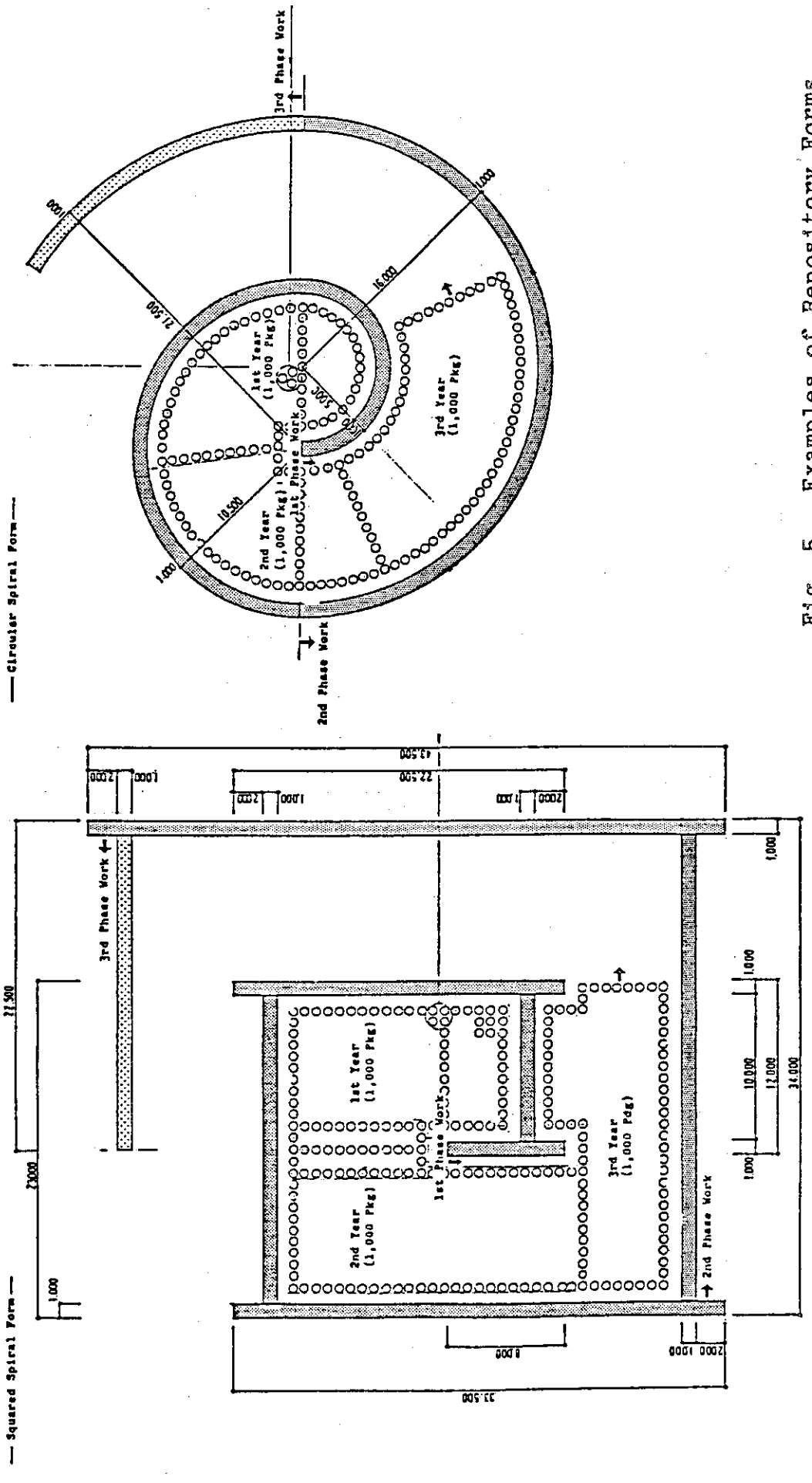

Fig. 5 Examples of Repository Forms

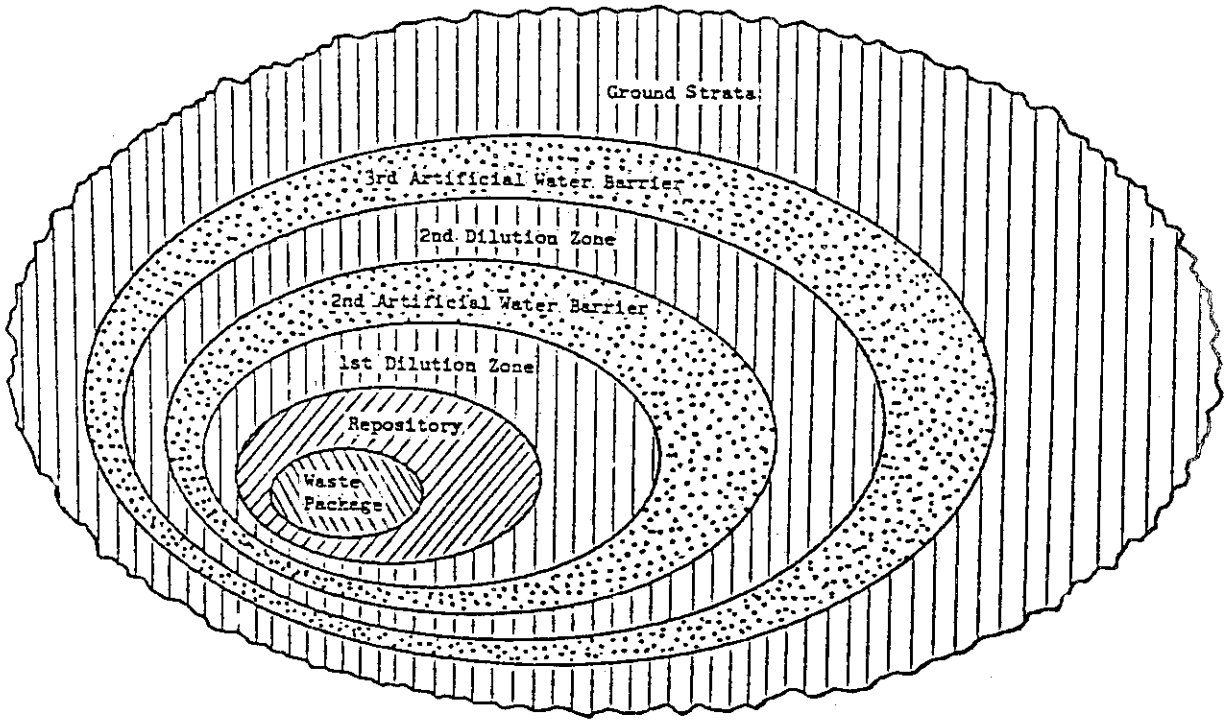

Fig. 6 Subcomponents of Environment

Table 7 Matrix of Subcomponents and Functions of Environment

		1st Dilution Zone/ 2nd Artificial Water Barrier (Vegetation)	2nd Dilution Zone/ 3rd Artificial Water Barrier (Vegetation)	Ground Strata Surrounding Repository	Exclusion Area of Ground Surface
1	Limitation of groundwater path	○	○	△	△
2	Reduction of concentration	○	△	△	
3	Protection of Waste Package and Repository				○
4	Partial transpiration		○	△	

o function absolutely necessary
Δ function desirable to have

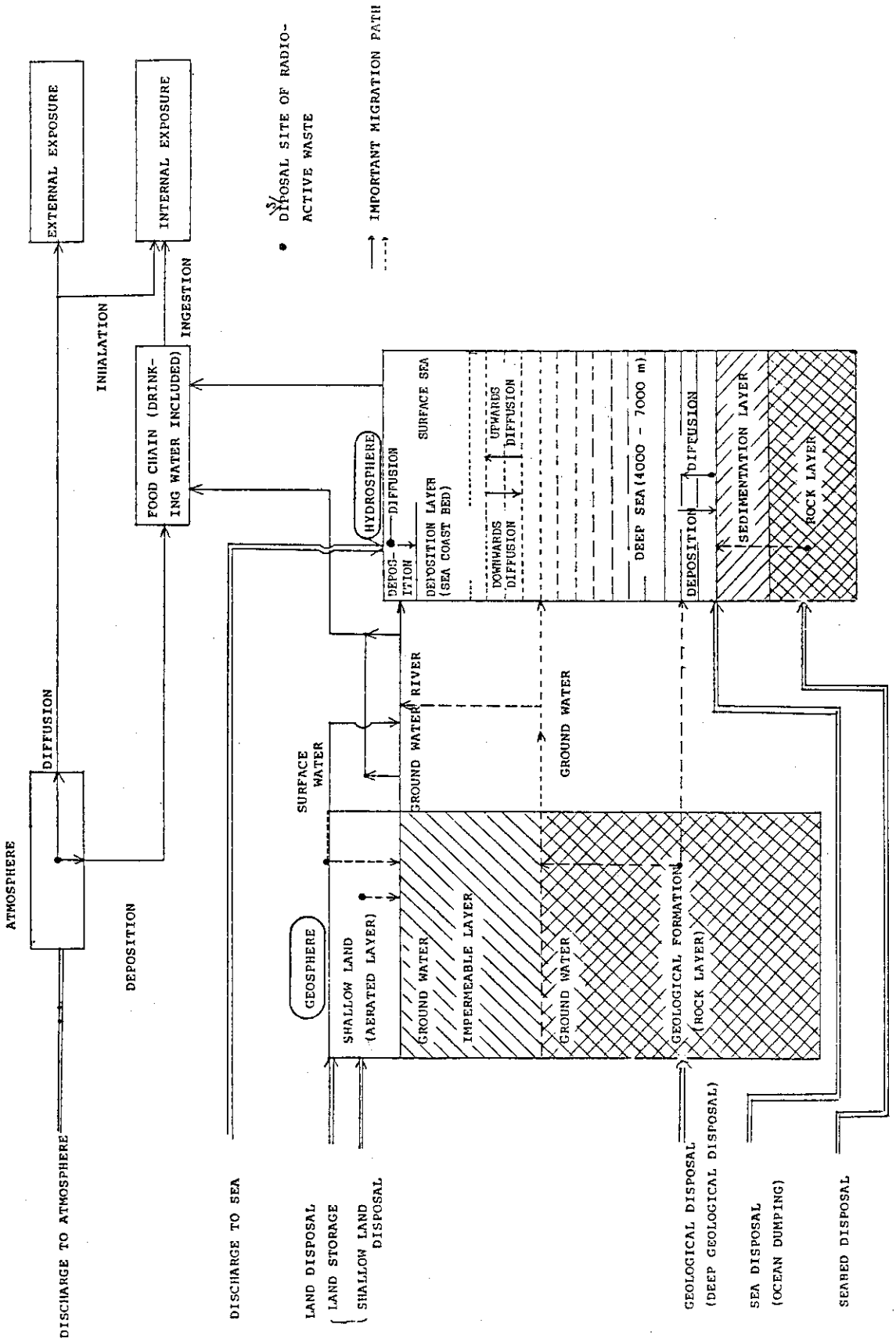

Fig. 7 Simplified Model for Migration Path of Radio-nuclides in Environment

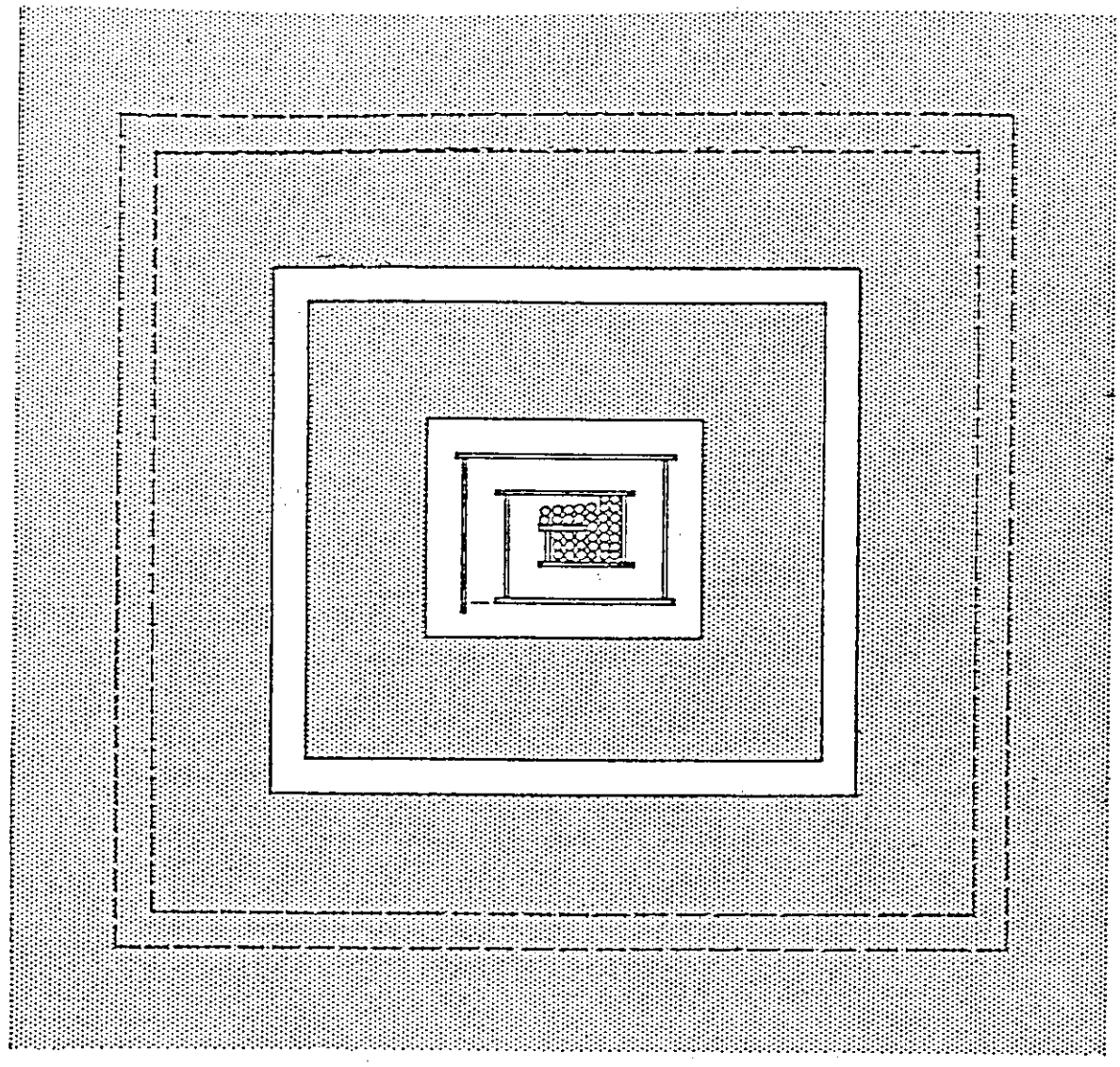

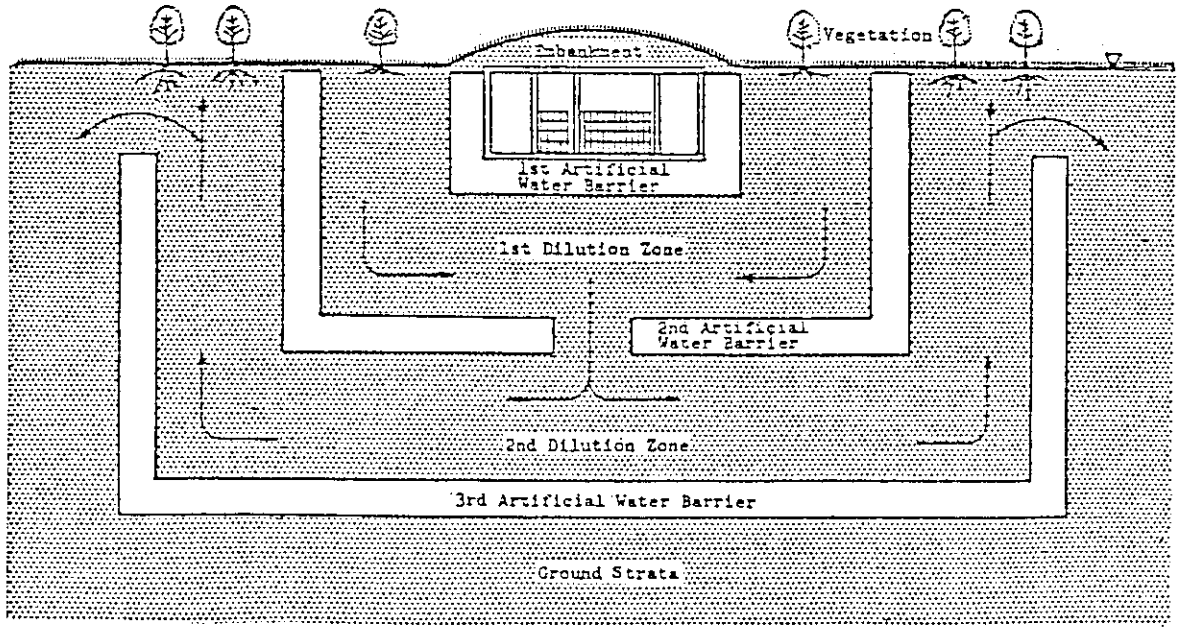

Fig. 8 Conceptual Drawing of Possible Disposal System for Tritiated Waste

Table 8 Classification of Components and Functions Assumed

No.	Component	No.	Subcomponent	Function Assumed
I	Waste Package	1	Waste Form	(1) Securing of immobility (2) Securing of engineering operability
		2	Container and/or Coating	(1) Securing of spatial isolation (2) Securing of retardation effect (3) Protection against water from outside (4) Protection against mechanical external forces (5) Securing of engineering operability
		3	Absorber Material	Securing of retardation effect
		4	Protective Sleeve and/or Coating	(1) Securing of spatial isolation (2) Securing of retardation effect (3) Protection against water from outside (4) Protection against mechanical external forces
II	Repository	1	Backfill	(1) Retardation of tritium migration (2) Securing of thermal diffusibility
		2	Wall and/or Lining	(1) Protection against human external forces (2) Protection against natural external forces (3) Retardation of groundwater movement
		3	1st Artificial Water Barrier	Retardation of groundwater movement
		4	Embankment (Vegetation)	
III	Environment	1	1st Dilution Zone/ 2nd Artificial Water Barrier (Vegetation)	(1) Limitation of groundwater path (2) Reduction of concentration
		2	2nd Dilution Zone/ 3rd Artificial Water Barrier (Vegetation)	(1) Limitation of groundwater path (2) Partial transpiration
		3	Ground Strata Surrounding Repository	
		4	Exclusion Area at Ground Surface	Protection of Waste Package and Repository

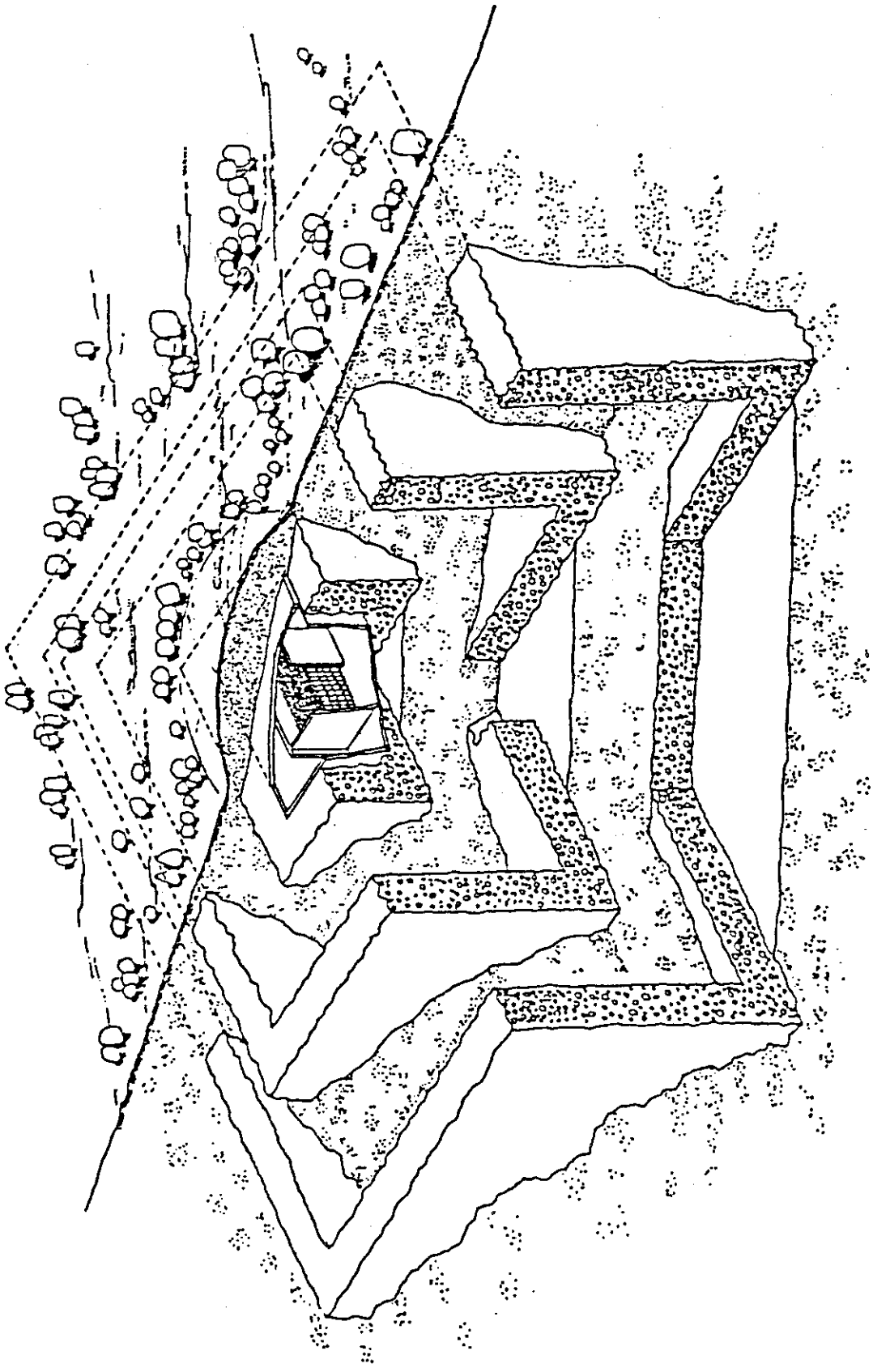

Fig. 9 Cut-off View of Disposal Site for Tritiated Waste

No.13 SWELLING OF LITHIUM CERAMICS DURING IRRADIATION

Glenn W. Hollenberg
Westinghouse Hanford Company
P. O. Box 1970
Richland, Washington 99352

I. INTRODUCTION

Lithium ceramics are being considered for the purpose of tritium production in D-T fusion power plants. One of the many issues which must be resolved before blankets containing lithium ceramics are brought into service is the degree of stability which can be expected from these new materials. Swelling of the solid breeder material can directly impact the design lifetime of the blanket. Accommodation of swelling in the design can correspondingly require compromises in the overall performance of the blanket.

Recently, an irradiation experiment was completed at moderate burnup levels in which swelling of solid breeder materials was observed. As will be discussed, the swelling of the Li_2O can be considerably more than that of the Li_4SiO_4. Li_2ZrO_3 and $LiAlO_2$. In addition, a degree of pellet cracking and fragmentation was observed which varied between the materials.

II. EXPERIMENTAL

Pellets of Li_2O, Li_4SiO_4, Li_2ZrO_3 and $LiAlO_2$ were irradiated in the fast neutron spectrum of the EBR-II reactor at temperatures of 500, 700 and 900°C for periods of 105, 192 and 297 full power days (FPD).[1] The pellets were 85% of theoretical density except for two sets of 95% TD $LiAlO_2$ pellets at 700 and 900°C for 105 and 192 FPD.

After irradiation, the pins were neutron radiographed in order to examine the solid breeder's configuration within the cladding. Later the pellets were removed from their capsules by cutting through the vacant end of the cladding in an argon flooded box located in the HFEF hot cells. In some cases, it was necessary to longitudinally slit cladding in order to extract the pellets. The saw at times penetrated into the pellets and made surface cuts which are visible on the pellets. Finally, the lithium-6 burnup was determined by measurement of retained helium in the pellets and the released helium in the pin.[1]

Before irradiation, the dimensions of the pellets (approximately 1 cm OD x 1.4 cm L) were measured to the nearest 0.0005 cm with a micrometer in an inert gas glovebox prior to capsule loading. Diametral measurements were made at the top, center and bottom of the pellet by making three individual measurements with a flat-faced micrometer 120 degrees apart. The lengths were measured by making three measurements near the circumference and one in the center with a

ball tipped micrometer. All measurements were then averaged to give the final values used for swelling computation.

After irradiation, the same mensuration method was attempted in an inert gas glovebox or, in the case of the more radioactive Li_2ZrO_3, in a hot cell. However, many pellets were fragmented into small pieces and thus sometimes measurements in the axial direction were not feasible as will be noted later. Most pellets were photographed after being transferred to inert gas gloveboxes, however, the radioactivity level of the Li_2ZrO_3 made it desirable to photograph and store these pellets in a hot cell until several half-lives (two months) had passed.

III. PELLET INTEGRITY

Figure 1 is a mosaic of photographs of the Li_2ZrO_3 pellets after irradiation to 192 and 297 FPD. These pellets appeared to survive the irradiation better than any other composition. Only at an exposure of 297 FPD at 900°C did the pellets crack and fragment and even then the cracking was limited to a separation of the pellets into shorter right cylinders. The origin of the surface spots on these pellets was not resolved. Ion microprobe analysis of the discolored areas did not reveal heavy metal contamination.

Figures 2a and 2b are of 85% and 95% TD Li_2AlO_2 pellets and 60% TD powder compacts after irradiation at temperatures from 500 to 900°C for exposures between 105 and 297 FPD. The 85% TD $LiAlO_2$ pellets irradiated at 500°C were not visibly cracked, but at 700 and 900°C the pellets appeared to not only be cracked but had also fragmented into many pieces. Cracking includes limited subcritical crack growth or extension which is contrasted with fragmentation which is indicative of crack propagation through the pellet and thus two or more fragments were recovered in a fragmented pellet. Both transverse and radial cracks were observed in these pellets.

In Figure 2b, the 95% TD $LiAlO_2$ pellets exhibited very little fragmentation or cracking at either 700 or 900°C. $LiAlO_2$ powder was simply compacted into the capsule in order to form the 60% TD $LiAlO_2$ material. This material was cut out of the surrounding cladding after irradiation and was amazingly tough considering it had never been sintered.

The lithium silicate in Figure 3 fragmented more extensively than any other material. Even in the pellets which did not fragment, obvious radial cracks were observed. In the other materials, i.e., $LiAlO_2$, Li_2ZrO_3, and Li_2O, it was difficult to observe fragmented pieces in postirradiation neutron radiographs taken while the pellets were still in the capsule. This observation could be used as an argument that in these materials cracks were present during irradiation and that fragmentation occurred during the cutting and manipulator operations in the hot cells. But in the Li_4SiO_4 capsules cracks could be easily distinguished in the neutron radiographs and material rearrangement of the fragmented pieces was observed.

The Li_2O pellets in Figure 4 primarily have radial cracks with large crack opening displacements. There is also some transverse cracking and fragmentation. On some of the pellets, the longitudinal saw cuts are visible which were made during deencapsulation.

IV. PELLET CRACKING CONSIDERATIONS

Although swelling gradients can contribute to pellet cracking, in these materials it is anticipated that thermal stresses are a more likely cause. It was recognized that the cracking did not appear to be burnup dependent and thus could have occurred at or shortly after the initial startup. Only limited thermal mechanical data are available on these particular materials. Hence, calculation of classical thermal stress parameters is not justified, but in Table I, some of the information on these pellets has been compiled. Since heat generation rates are similar between the materials, their thermal conductivity dominates in the predicted temperature gradients that are calculated. Notice that the high thermal conductivity of Li_2O results in a lower temperature difference. Similarly, higher density materials, i.e., 95% TD $LiAlO_2$, possesses higher thermal conductivities and lower temperature gradients. The Li_2O and Li_4SiO_4 possessed the highest thermal expansion coefficients, almost twice as large as those for $LiAlO_2$ and Li_2ZrO_3.

The overall thermal strain difference has been calculated which is the driving force for thermal stress fracture. Notice that the Li_4SiO_4 material with its low thermal conductivity and high thermal expansion has the highest thermal strain difference. Li_4SiO_4 exhibited the most cracking and fragmentation of these materials. Next highest is the Li_2O with its high thermal expansion coefficient. Li_2O also exhibited extensive cracking but with less fragmentation. Li_2O is known to exhibit plasticity at even very low temperatures ($T < 500^{\circ}C$) so the fact that stable subcritical crack extension occurred is not surprising.

The higher thermal condutivity of the 95% TD $LiAlO_2$ (in comparison to the 85% TD reference material) results in the lower thermal strain difference. This, coupled with the anticipated higher strength of this material, explains the improved integrity of the 95% TD material. Hence, there is a qualitative agreement between the thermal strain differences and the extent of cracking in these pellets. The strong temperature dependence of the thermal conductivity of $LiAlO_2$ results in the lower predicted temperature differences ($54^{\circ}C$) at $500^{\circ}C$ and consequently lower strain differences which are thought to be the reason behind the good pellet integrity of the 85% TD pellets irradiated at $500^{\circ}C$.

V. SWELLING

Swelling had previously been reported but was only from measurements on neutron radiographs.[1,2] Volumetric swelling results from mensuration measurements are presented in Figures 5-7 on $LiAlO_2$, Li_2ZrO_3 and Li_4SiO_4. Axial or length swelling and diametral or radial swelling was nominally the same in these materials.

In Figure 5, the swelling of 85% TD $LiAlO_2$ was observed to increase up to 8 x 10^{20} captures/cc, but was less than 0.5% for all data. The error bars which indicate the standard deviation for the measurements are quite large in comparison to the low swelling values in these pellets. Part of the error was thought to be associated with the internal cracks present in some of these pellets. In many cases the measurement of swelling in the axial direction was not possible. At both 2.5 x 10^{20} and 5.6 x 10^{20} captures/cm^3, the higher density $LiAlO_2$ pellets actually exhibited shrinkage. In Figure 6, the swelling of 85% TD Li_2ZrO_3 is almost as low ($\Delta V/V < .7\%$) as $LiAlO_2$ except for the 900°C data at the highest exposure. It should be pointed out that these 900°C pellets were the only Li_2ZrO_3 pellets that were fragmented (see Figure 1).

In Figure 7, the swelling of the Li_4SiO_4 pellets ($\Delta V/V < 1.6\%$) is almost twice that of the $LiAlO_2$ and Li_2ZrO_3. There appears to be an increasing trend of Li_4SiO_4 swelling with respect to burnup. In both Li_2ZrO_3 and Li_4SiO_4 the swelling at the intermediate burnup which corresponds to 192 FPD are on the average less than which might be interpolated from the lower and higher burnup data. In both cases the 192 FPD material was fabricated from a different batch of starting powder, but was made to the same specification as the other two. In all these materials, swelling appears to be relatively independent of temperature.

In Figure 8, the volumetric swelling of Li_2O at 700 and 900°C is much larger than in any of the other lithium ceramics, approximately 8% at 700°C. It appears that there is a nonlinear relationship between swelling and burnup at 700 and 900°C. When higher burnup data (BU > 12 x 10^{20} captures/cm^3) becomes available, the apparent saturation of the volumetric swelling at a level of about 7% will be better described.

At 500°C, the Li_2O pellets exhibited an overall volumetric contraction after irradiation. In Figure 9, a comparison of the volumetric swelling to its two components, axial and diametral swelling, reveals that the diametral swelling of the Li_2O at 500°C is slightly smaller than, but highly consistent with, the higher temperature data. However, the axial swelling is very negative at 500°C and is thus the source of the overall volumetric shrinkage. At 700 and 900°C, the axial swelling is actually more than the diametral swelling values.

VI. SWELLING DISCUSSION

Swelling in these ceramics is envisioned to have two components, a hard or high modulus component and a soft or low modulus component. The soft component is produced by internal macroscopic cracks as seen in Figures 1-4 and microcracks present at grain boundaries. The soft component is of less consequence since very low stresses can be induced into neighboring structural material from this type of swelling. The hard component is, however, almost incompressible in comparison and originates from swelling internal in the individual

crystallites. The data obtained cannot be quantitatively separated into these two components.

Swelling in irradiated materials is typically attributed to either Frenkel pair formation and vacancy agglomeration into voids or to gaseous transmutation product formation and agglomeration into bubbles. In this irradiation of lithium ceramics, it is anticipated that the gaseous transmutation products dominate because of the moderate lithium-6 neutron cross-section and the more permanent nature of these defects. In addition, atomic displacements occur not only from the direct knock-on events with neutrons but also from the transmutation products themselves. Displacement defects, i.e., vacancies and interstitials, need only annihilate while the helium and tritium must diffuse to a free surface in order to be eliminated from the crystals. Consequently, it is logical to correlate the retained helium and tritium to swelling. The low swelling of the $LiAlO_2$ and of the Li_2ZrO_3 were forcasted by the electron beam irradiations of Auvray-Gely et al.[3]

The helium and tritium are expected to take up different sites in the lattice. The inert helium atoms are expected to take up interstitial sites while the charged tritium ions can fill negatively charged lithium vacancies formed during the neutron capture process. Hence, the helium atoms are much more likely to introduce swelling as intersitials and have a higher driving force for bubble formation. Lui et al. have reported significant bubble formation in Li_2O irradiated under slightly different conditions.[4]

As reported earlier, the helium retention in 85% TD $LiAlO_2$ and Li_2ZrO_3 was much lower than in 85% TD Li_2O.[1] Of all the Li_2ZrO_3 pellets, the greatest amount of helium (0.21×10^{20} atoms/cc or 2.34%) was retained at 500°C and 297 FPD. The $LiAlO_2$ behaved in a similar manner with 0.23×10^{20} atoms/cc or 2.74% helium being retained at the lowest temperature (500°C) and at 297 FPD (8.5×10^{20} captures/cc). In contrast, the greatest amount of retained helium in the Li_2O pellets was reported to be 2.5×10^{20} atoms/cc or 22.5% at 700°C and at 297 FPD (11×10^{20} captures/cc). Thus the helium retained in the Li_2O is approximately 10 times greater than in either $LiAlO_2$ or Li_2ZrO_3. In order to appreciate how much helium induced swelling is possible, it is worthwhile to compute the retained helium volume per volume of solid breeder. For the maximum case discussed above, the volume of helium in Li_2O would be 30 cc/cc at 1 atm and 0.1 cc/cc at 300 atm of internal pressure at 700°C. Thus the volumetric swelling ($\Delta V/V < 10\%$) in the Li_2O at 700°C is qualitatively consistent with pressurized bubbles slightly larger than 300 atm of internal pressure at 700°C ($\Delta V/V < 10\%$). The radial swelling in Li_2O contains a soft swelling component as seen in Figure 4. The lack of significant swelling in the Li_2ZrO_3 and $LiAlO_2$ is consistent with the low helium retention in those materials.

The shrinkage of Li_2O at 500°C is far more difficult to explain. In Figure 9, the volumetric shrinkage is seen to result from axial shrinkage while radial swelling occurred in much the same manner as at the higher temperatures. Taken by itself, one simple explanation is

that dilational creep occurred with a compressive creep force being applied axially to the pellet and shear creep resulting in the diametral strain. The predicted, but unmeasured, stress from the plenum spring was approximately 187 KPa. Normally creep is expected to be a thermally activated process such that even more creep would be expected at 700 and 900°C. However, in polycrystalline studies [5] and even more clearly in single crystal creep experiments[6], it has been observed that Li_2O creep is not a simple thermally activated process at low temperatures. Perhaps the higher retention of tritium oxide or moisture at the lower temperatures provides for enhanced dilational creep rates at 500°C in comparison to the higher temperatures.

The shrinkage of the high density $LiAlO_2$ pellets is even more unusual. Although the error bands are proportionately large, there is measurable densification at both burnup levels. Sintering or creep could not be used to explain this densification since at 900°C $LiAlO_2$ does not normally sinter or creep. There was a net loss of lithium from the pellet of approximately 0.6% atomic, that is lithium burnup compared to total lithium, aluminum and oxygen atoms. It is possible that if complete defect annihilation and helium release occurred, this could lead to a reduced volume. The retained helium in the 95% TD $LiAlO_2$ was only 0.0179×10^{20} atoms/cc, which is less than either the 85% or even the 60% TD $LiAlO_2$ at 297 FPD. The growth of a $LiAl_5O_8$ second phase was reported by Auvray-Gely et al. after electron beam irradiation of $LiAlO_2$.[3] Depending on where a second phase is deposited in the mocrostructure, it could lead to shrinkage.

VII. CONCLUSIONS

The observed pellet integrity of the Li_2ZrO_3 pellets was best and could be explained by its moderate thermal conductivity and lower thermal expansion coefficient. Li_4SiO_4 appeared to have the most pellet fragmentation which was explained by its low thermal conductivity and high thermal expansion. The higher density $LiAlO_2$ had better thermal integrity than the 85% dense $LiAlO_2$ in part, because of its naturally higher thermal conductivity. The high plasticity of Li_2O provided it with a limited crack growth.

Pellet swelling was very low in Li_2ZrO_3 and $LiAlO_2$. Pellet swelling was slightly higher for Li_4SiO_4. Pellet swelling of Li_2O was very high at 700 and 900°C and is thought to be caused by the retained helium in these samples. Pellet shrinkage occurred in Li_2O at 500°C and could be caused by enhanced dilational creep.

Acknowledgments

The continued support of Drs. T. C. Reuther (USDOE, Office of Fusion Energy) and E. T. Weber and Mr. L. A. Pember is appreciated. The measurements made by D. L. Baldwin, W. E. Hart, V. N. Pearson, and D. E. Baker are also appreciated. The assistance in disassembly at the HFEF Hot Cells, especially R. Wisner, is appreciated.

References

1. D. L. Baldwin and G. W. Hollenberg, "Measurement of Tritium and Helium in Fast Neutron Irradiated Lithium Ceramics using High Temperature Vacuum Extraction," to be published in J. Nucl. Mater., presented at the Third International Conference on Fusion Reactor Materials, Chicago, Illinois, April 1986.

2. G. W. Hollenberg and D. L. Baldwin, "The Effect of Irradiation on Four Solid Breeder Materials, J. Nucl. Mater. 133 & 134 (1985) 242-245.

3. M. H. Auvray-Gely, A. Dunlop and L. W. Hobbs, "Irradiation Damage in Lithium Ceramics," J. Nucl. Mater. 133 and 134 (1985) 230-233.

4. Y. Y. Lui, R. F. Mattas, D. L. Smith, and D. L. Porter, "Microstructural Examination of Fast Neutron Irradiated Li_2O," J. Nucl. Mater. 133 & 134 (1985) 209-215. Ibid, D. L. Porter et al., ANL/FPP/TM-167 (1982), Argonne National Laboratory, Argonne, Illinois.

5. G. W. Hollenberg, "Creep of Li_2O," J. Nucl. Mater. 133 & 134 (1984) 216-220.

6. Kenji Noda, M. Arita, Y. Ishii, H. Saka, T. Imura, K. Kuroda and H. Watanable, "Mechanical Properties of Lithium Oxide at High Temperatures," to be published in J. Nucl. Mater., presented at the Third International Conference on Fusion Reactor Materials, Chicago, Illinois, April 1986.

Table 1

THERMAL STRAINS IN IRRADIATED LITHIUM CERAMIC PELLETS

Material	Density	T (C)	TCE (-6 cm/cm/C)	Maximum Strain Difference (%)*
Li_2O	85%	32 to 47	29.35	.137
Li_2ZrO_3	85%	67 to 114	9.97	.114
Li_4SiO_4	85%	54 to 105	27.1	.285
$LiAlO_2$	60%	130 to 144	12.0	.173
$LiAlO_2$	85%	54 to 102	12.0	.122
$LiAlO_2$	95%	40 to 78	12.0	.096

*Maximum thermal strain difference is calculated from the maximum temperature difference in the pellets and 500°C thermal expansion coefficient for the purpose of comparison.

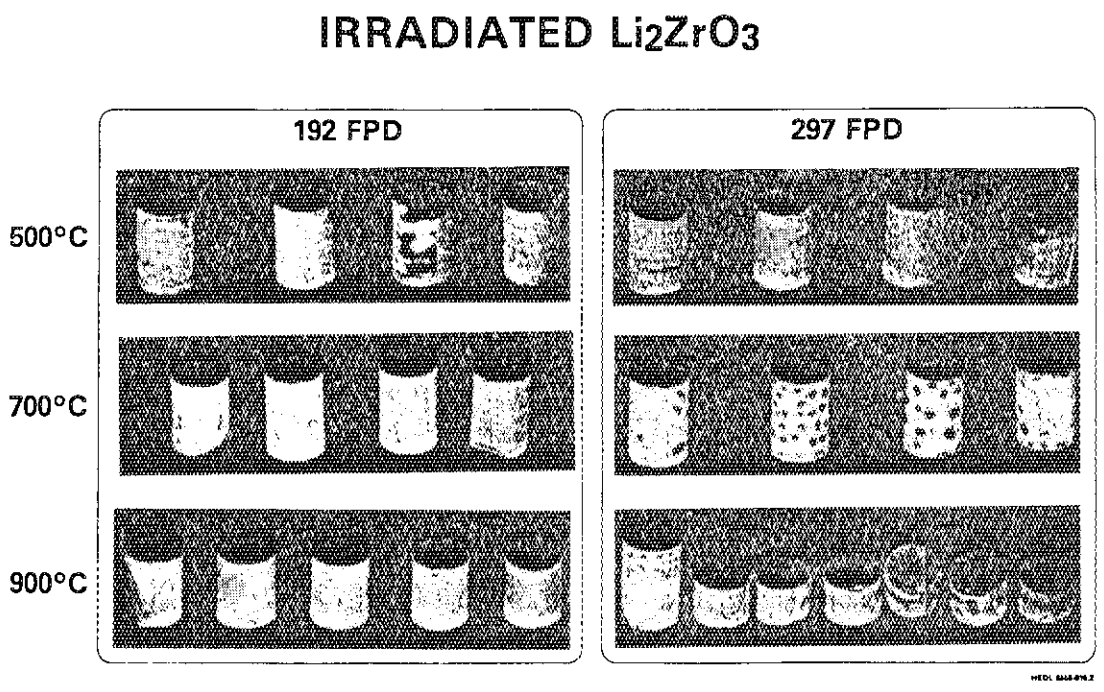

Fig. 1 Photographs of 85% TD Li_2ZrO_3 pellets after irradiation to 192 and 297 FPD at temperatures of 500, 700 and 900°C.

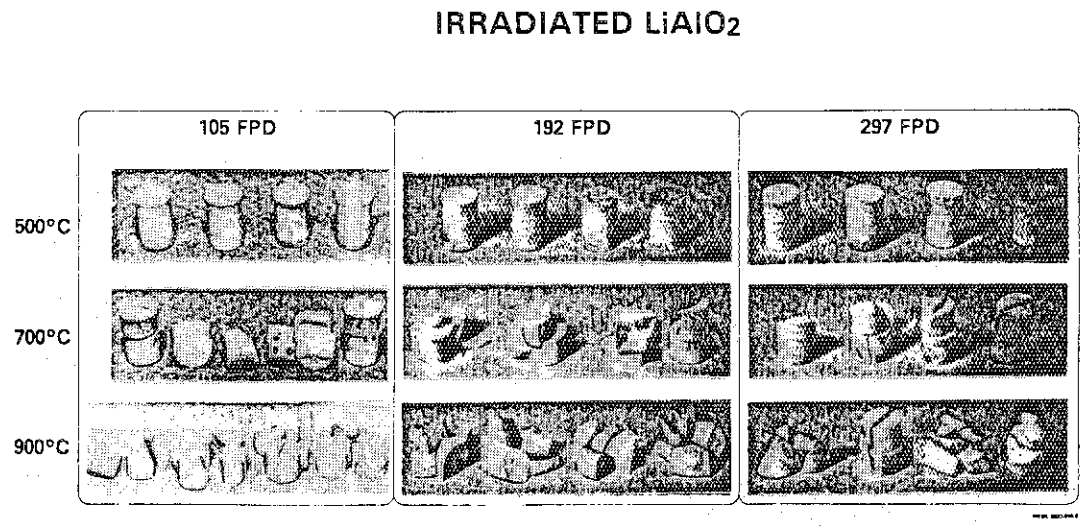

Fig. 2a Photographs of 85% TD $LiAlO_2$ pellets after irradiation to 105, 192 and 297 FPD at temperatures of 500, 700 and 900°C.

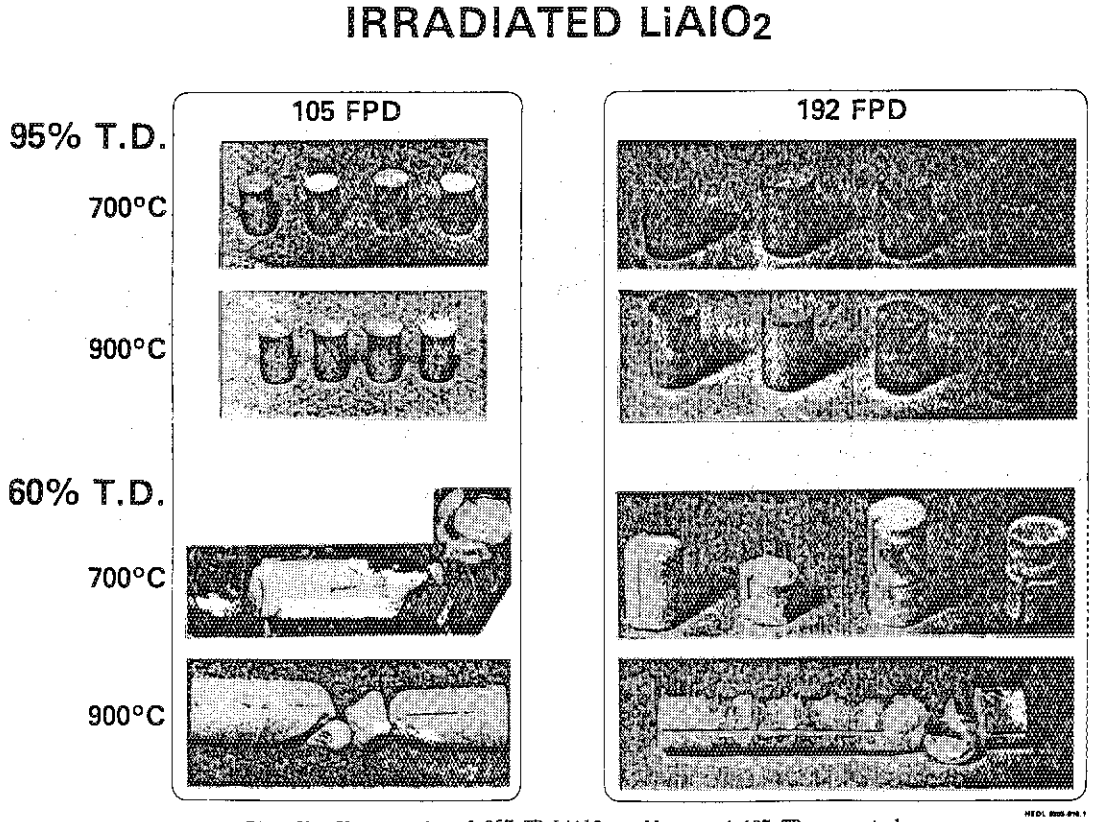

Fig. 2b Photographs of 95% TD $LiAlO_2$ pellets and 60% TD compacted $LiAlO_2$ powder after irradiation to 192 and 297 FPD at temperatures of 500, 700 and 900°C.

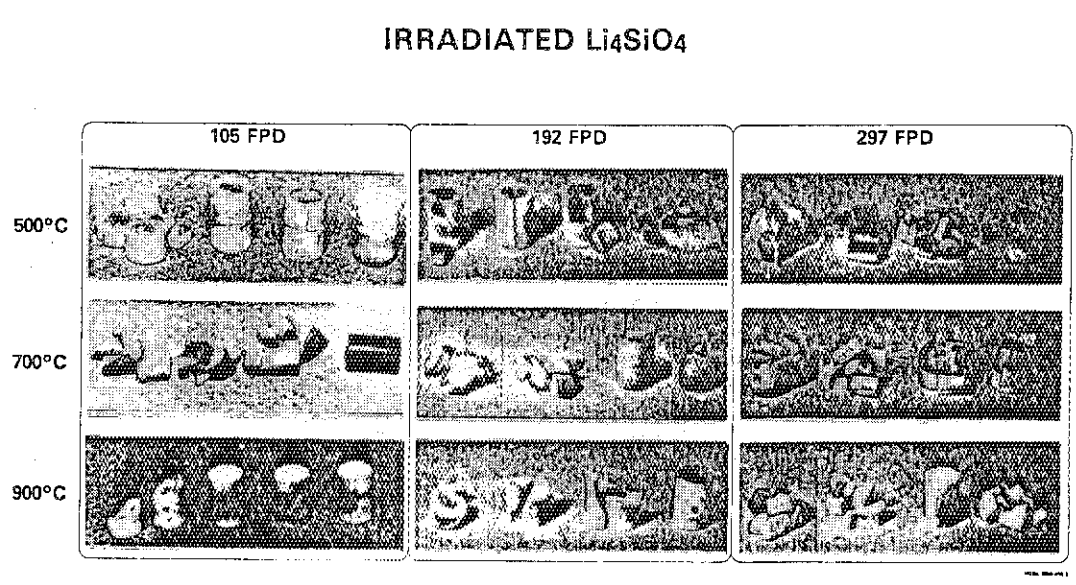

Fig. 3 Photographs of 85% TD Li_4SiO_4 pellets after irradiation to 105, 192 and 297 FPD at temperatures of 500, 700 and 900°C.

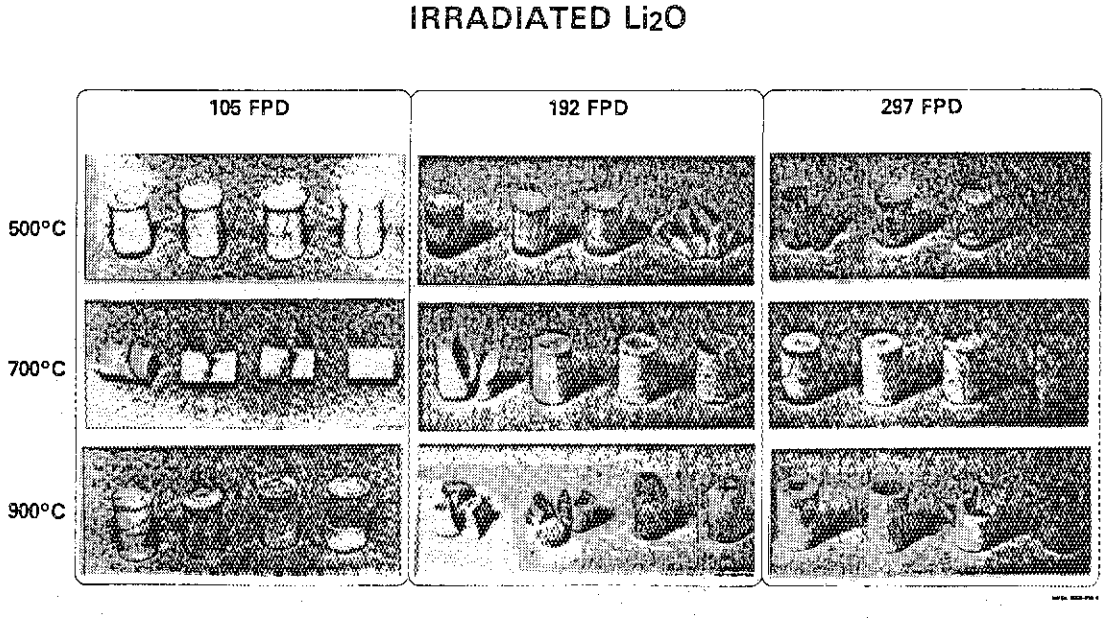

Fig. 4 Photographs of 85% TD Li_2O pellets after irradiation to 105, 192 and 297 FPD at temperatures of 500, 700 and 900°C.

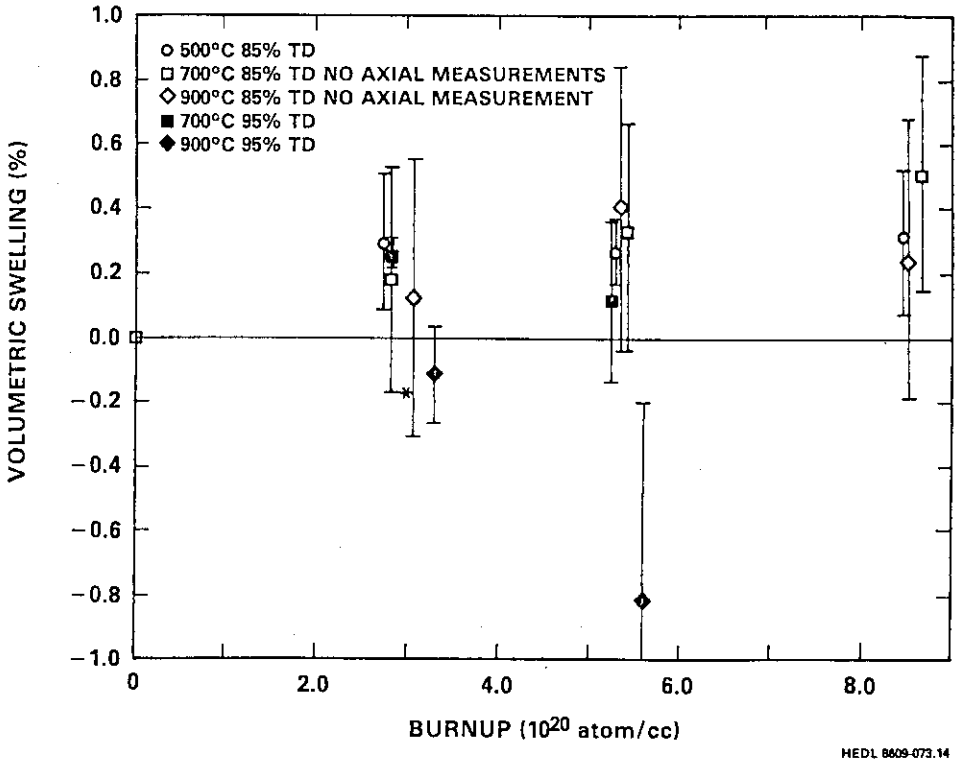

Fig. 5 The volumetric swelling of 85 and 95% TD $LiAlO_2$ at burnups up to 8.5 x 10^{20} captures/cc at temperatures from 500 to 900°C.

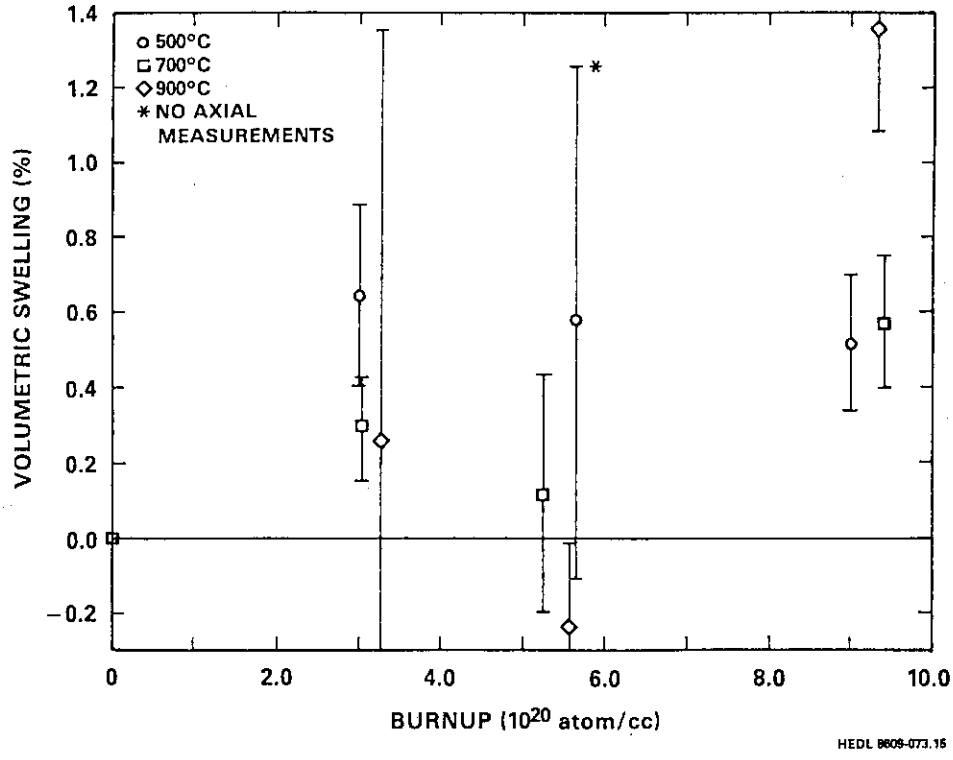

Fig. 6 The volumetric swelling of 85% TD Li_2ZrO_3 at burnups up to 9.5 x 10^{20} captures/cc at temperatures from 500 to 900°C.

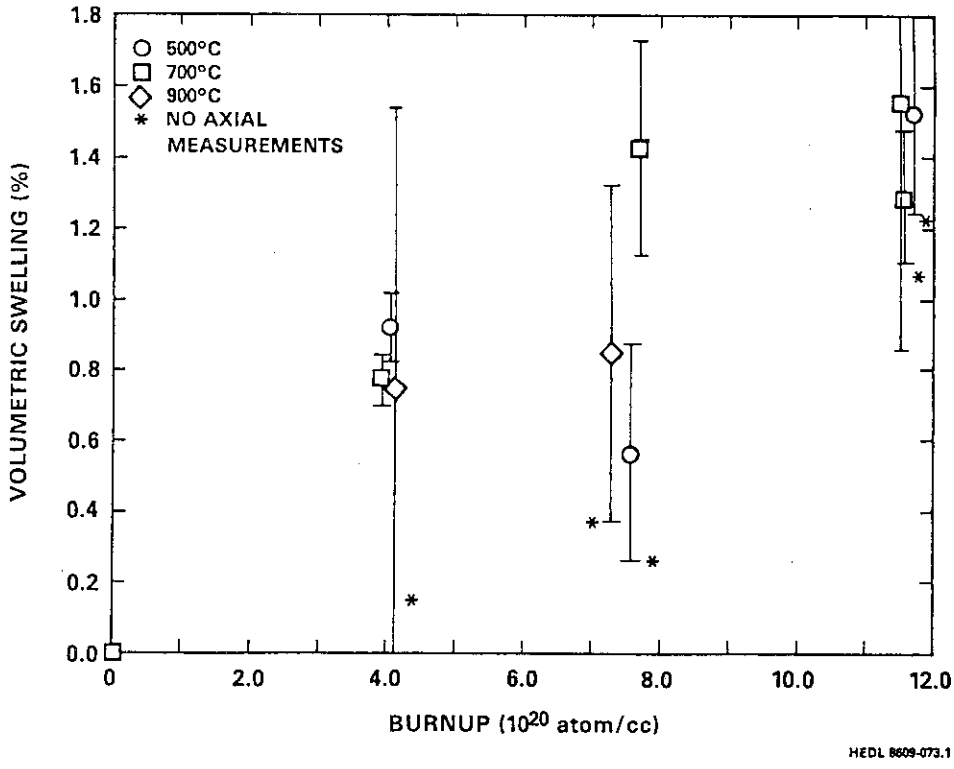

Fig. 7 The volumetric swelling of 85% TD Li_4SiO_4 at burnups up to 12 x 10^{20} captures/cc at temperatures from 500 to 900°C.

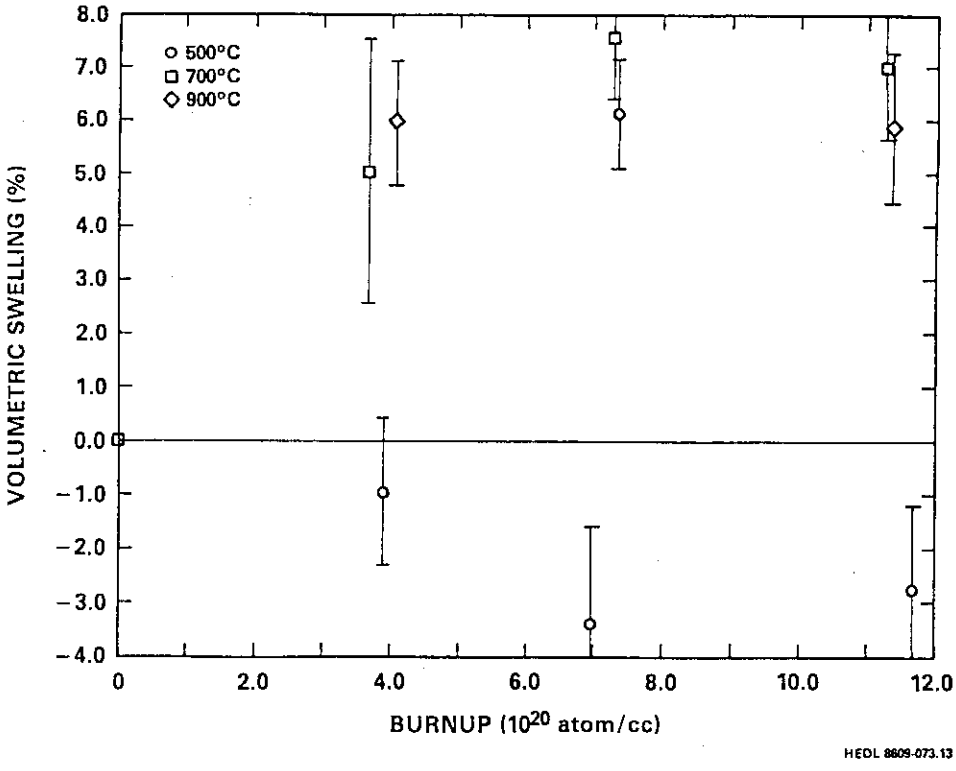

Fig. 8 The volumetric swelling of 85% TD Li_2O at burnups up to 12 x 10^{20} captures/cc at temperatures from 500 to 900°C.

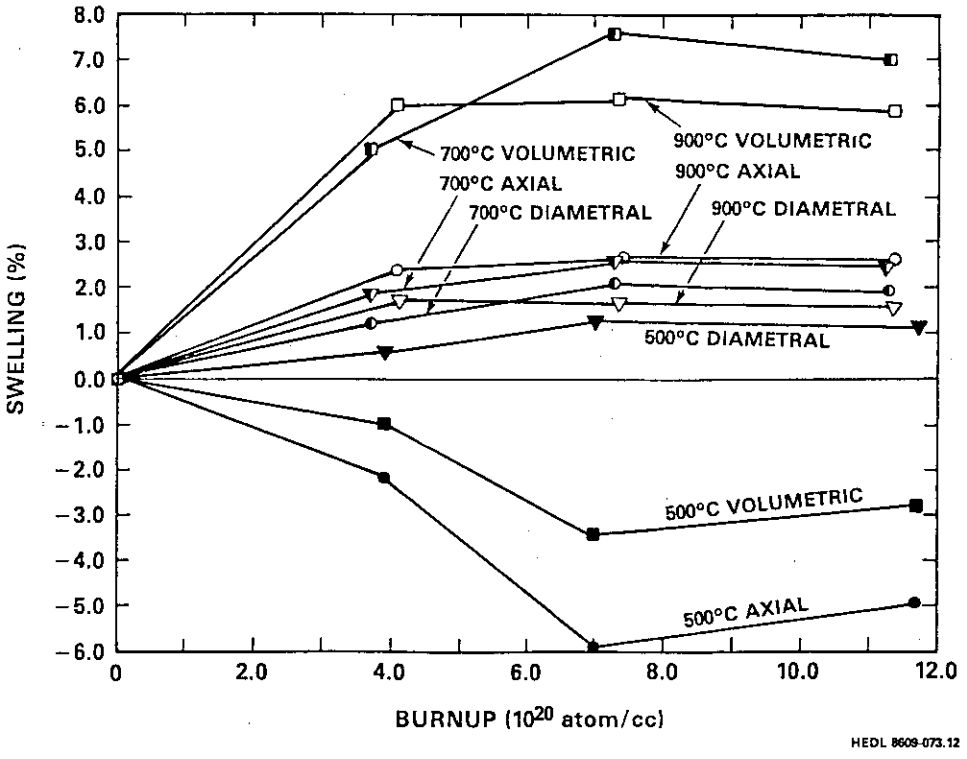

Fig. 9 A comparison of the volumetric swelling to the diametral and axial swelling of Li_2O after irradiation at burnups up to 12 x 10^{20} captures/cc at temperatures from 500 to 900°C.

No.14

Accumulation and Desorption of Hydrogen Isotopes Bombarded on Ti-coated Surface of Metals.

K.Higashi, K.Kitagawa, K.Mizushima,

M.Muraoka and H.Fujita

Department of Nuclear Engineering

Kyoto University

Yoshida, Sakyo-ku, Kyoto 606

I. INTRODUCTION

At present, titanium is often deposited on inner surface of plasma confinement devices. Coating with various low-Z materials has been also developed for the first wall of future plasma devices. For the research of hydrogen recycling and safety handling of tritium, it must be essential to examine the behaviors of hydrogen isotopes implanted in coated layers.

By using the depth-profiling technique of nuclear reaction $D(^3He,p)^4He$, we have observed the behavior of deuteriums implanted into Ti-deposition layer on substrates of SS304 stainless steel and nickel.

II. EXPERIMENTAL

Titanium was deposited on polished surface of SS304 stainless steel and nickel at a thickness of 0.4 to 1.8 μm. Implantation of deuterium ions was carried out at three different energies of <1KeV, 15KeV and 150KeV. The low energy implantation (< 1KeV) was performed by using the experimental set-up for plasma driven permeation of hydrogen (Fig.1). The details of the set-up was described previously[1),2)]. By keeping the probe voltage at 1KV, a metal specimen was exposed by a flux of deuterium ions of energy less than 1KeV. Since the set-up has no analyzing magnet, the specimens were irradiated by a mixture of D^+, D_2^+ and D_3^+ ions.

Implantation of 15 and 150 KeV ions was carried out by two different Cockcroft-Walton accelerators at The Radiation Lab. of Kyoto University. The metal specimen can be kept at around -150°C by liquid nitrogen during the implantation.

Probing for the depth-profile of deuteriums implanted in metal specimens was performed on the Van de Graaff accelerator at The Radiation Lab. of Kyoto University. A schematic diagram of the analyzing chamber is given in Fig.2. The incident beam of $^{3}He^{+}$ of 0.8 or 1.3 MeV was collimated to 1mm-diameter. A secondary electron shield (Faraday cup) encloses the sample holder which can hold four specimens. Those are kept cold by liquid nitrogen. To prevent the implanted deuteriums from dispersing due to heating by the ^{3}He beam, the current of the probing beam was maintained under 0.1 μA.

Two silicon detectors are placed at angles of 165 and 135 degree with respect to the incident beam to have energy spectra of protons and alpha particles. To probe deuteriums up to deep locations, energy spectrum of protons was mainly used for the profiling.

III. RESULTS AND DISCUSSION

An example of experimental results is shown in Fig.3. Titanium is deposited by ∿0.4 μm thickness on a substrate of SS304, which was irradiated by deuterium ions of energy less than 1KeV. Though the projected range of 1KeV deuteron is about 10^{-3} μm or less in SS304, you can see in Fig.3 that deuteriums develop their pofile into deeper location with the increase of irradiation dose at room temperature. However, it is difficult for deuteriums to diffuse into the endo-thermic substrates (SS304 and nickel). The interlayer acts as a barrier against deuteriums, and they accumulate within the Ti-deposition layer.

When the concentration of deuterium was lower than 50 $^{a}/o$, a peak in the depth-profile was formed near the surface. The concentration, however, increased homogenously throughout the Ti-deposition layer

as it becomes higher than 50 a/o.

At the beginning of irradiation, the amount of deuteriums in Ti-deposition layer tended to increase in proportion to the irradiation dose. The retention ratio of deuteriums, however, decreased rapidly with the dose, and the concentration could not become higher than 200 a/o.

The desorption behavior of deuteriums in Ti-deposition layer has been examined. An example of the results is shown in Fig.4. When an implanted specimen was annealed sequentially at various temperature, the depth-profile was changed discontinuously at narrow ranges of temperature. As seen in Fig.4, the concentration decreased down to ∿100 a/o by annealing at 100°C for 30 minutes. The profile, however, was kept unchanged during the successive annealing of 100°C/20min, 200°C/20min and 250°C/35min. Then, the concentration decreased suddenly down to∿ 50 a/o by annealing at 300°C for 35minutes. The concentration was maintained until the annealing at 400°C, when the profile changed into a shape as like carved off a part of surface side. By annealing at 450°C, deuteriums disappeared from the Ti-deposition layer. It may follow that there are at least three different energy states for deuteriums in Ti-deposition layer corresponding to three concentration ranges of <50 a/o, 50-100 a/o and≻ 100 a/o.

Now we know that deuteriums get away from the Ti-deposition layer by annealing at 450°C or higher temperature. However, it is still uncertain that the deuteriums desorb into the gas-phase or diffuse into the substrate. It may be important in relation to the hydrogen recycling and tritium permeation through the first wall.

Judging from the change of profile at 400°C in Fig.4, deuteriums seem to desorb into gas-phase through the surface. To confirm it, a thermal desorption experiment was performed. A deuterium-implanted specimen was heated gradually to detect the desorbed deuterium gas by QMA.

The result is shown in Fig.5. When the temperature reached around 400°C, deuteriums began to release into the gas-phase. The observed result seems to correspond well to the change of depth-profile by annealing at 400°C (Fig.4.)

It is very interesting to compare the hydrogen behavior in Ti-deposition layer on a endo-thermic substrate with that in Ti-metal itself. Deuterium ions of 15KeV were implanted into Ti-deposition layer by $3x10^{17}(D/cm^2)$. The specimen was cooled during the implantation. Fig.6 shows the change of depth-profile when it was annealed at 300°C for 30minutes. One may see that deuteriums develop the profile all over the deposition layer from the restricted location close to the surface.

On the other hand, deuterium ions of 150KeV were implanted into a titanium metal specimen by $3x10^{17}(D/cm^2)$. Before annealing, deuteriums distributed around the depth of projected range of about 1 μm. By the sequential annealing, a secondary peak near the surface was developed gradually. It showed that a significant fraction of deuteriums has moved towards the surface during annealing, and accumulated there. Such a migration of implanted hydrogen isotopes towards the surface has been also observed in some other metals which form hydrides with hydrogen[3),4)]. It may be clear that one cannot always speculate the hydrogen behavior in deposition layers from the results observed for those metals.

IV. CONCLUSION

Applying the depth-profiling technique using the nuclear reaction $D(^3He,p)^4He$, hydrogen behaviors in Ti-deposition layer on substrate of SS304 and nickel have been observed fairly in details. The experimental results may be summarized as follows:

i) It seems to be difficult for implanted hydrogen to diffuse into the endo-thermic substrate (SS304 or nickel). Implanted hydrogen tends to accumulate within the Ti-deposition layer. The upper limit of hydrogen concentration in Ti-deposition layer is ∿200 ^{a}/o.

ii) Concentration of hydrogen in Ti-deposition layer changes discontinuously by annealing within narrow ranges of temperature (< 100°C, ∿300°C and ∿400°C). There are three differnt energy states for hydrogen in Ti-deposition layer corresponding to concentration ranges of < 50 ^{a}/o, 50-100 ^{a}/o and > 100 ^{a}/o. By annealing at 450°C or higher temperature, all of hydrogen get out into gas-phase through the surface.

iii) Comparing Fig.6 with Fig.7, it should be noticed that the thermal behavior of hydrogen in deposition layer is quite different in some cases from that of the metal.

ACKNOWLEDGMENT

The authors wish to thank Drs. M. Sakisaka, F.Fukuzawa, M.Tomita and other staff of The Radiation Lab. of Kyoto University for their helpful discussions on the experiments. Also, they wish to thank Japan Vacuum Technology Co., Ltd. who had performed the deposition of titanium on the substrates of SS304 and nickel for us.

REFERENCES

1) I.Takagi, T.Komori, H.Fujita and K.Higashi, J. Nucl. Mater., 136, 287 (1985).

2) I.Takagi, T.Komori, H.Aoi, Y.Kondo, H.Fujita and K.Higashi, Proc. Intern. Symp. on Fusion Reactor Blanket and Fuel Cycle Technology, Tokyo Univ., Tokai-mura, Oct. 27-29, 1986.

3) K.Higashi, Y,Matsuno, H.Sakamoto, Y.Matsui and H.Fujita, Mem. Fac. Engng., Kyoto Univ., 44, 396 (1982).

4) K.Higashi, Y.Matsuno, H.Sakamoto, Y.Matsui, T.Yaegashi and H.Fujita, proc. Intern. Symp. on Effective Utilization of Surface Analysis Techniques in Plasma Surface Interactions, Sapporo, Japan, 308p.

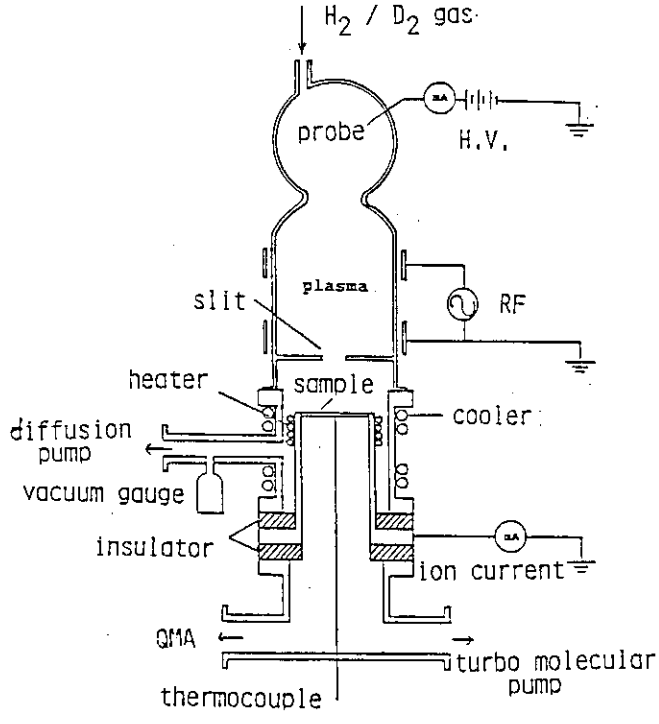

Fig.1 For the low energy implantation (< 1 KeV) of deuterium ions into Ti-deposition layer, the experimental set-up for plasma driven permeation (PDP) of hydrogen was used.

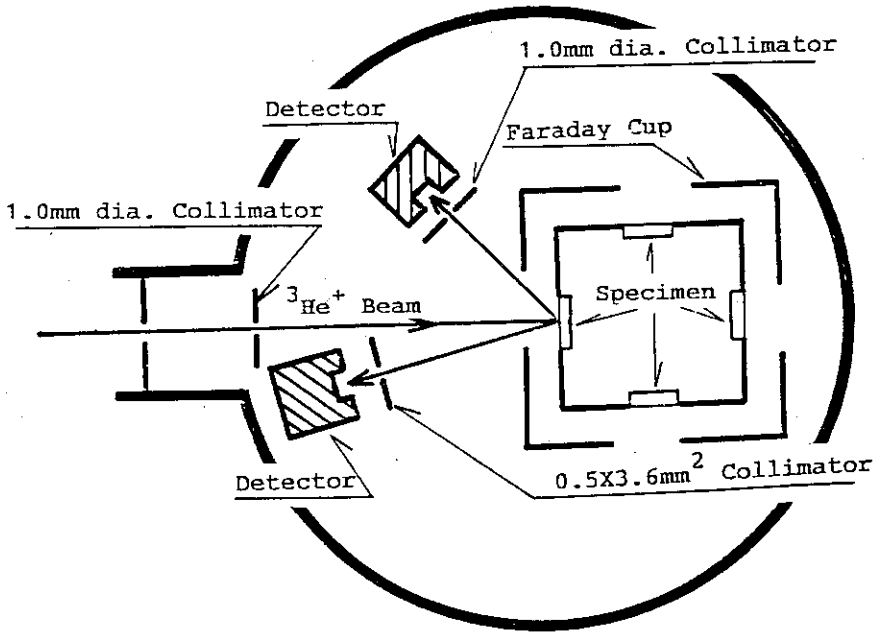

Fig. 2 Schematic diagram of ion-beam analyzing chamber for probing.

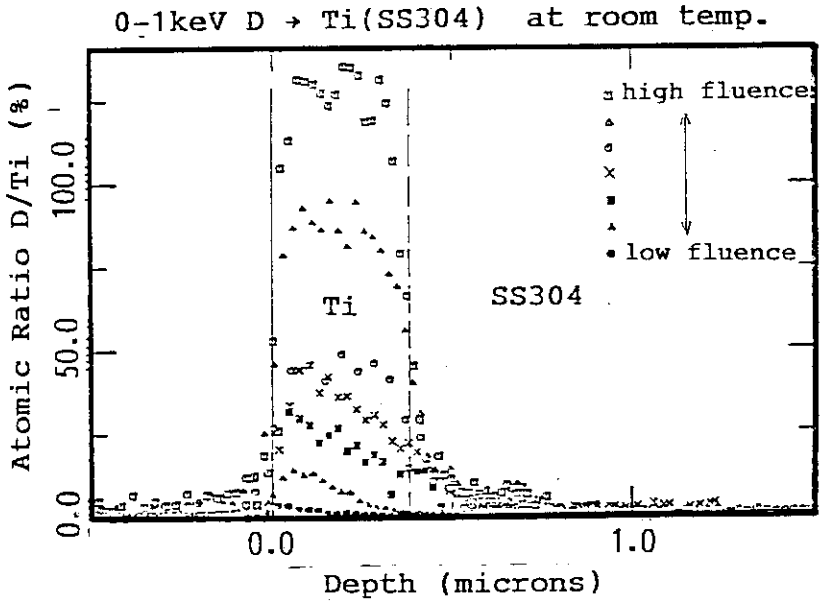

Fig. 3 Successive accumulation of implanted deuteriums within Ti-deposition layer on SS304 substrate. Implantation energy was lower than 1 KeV.

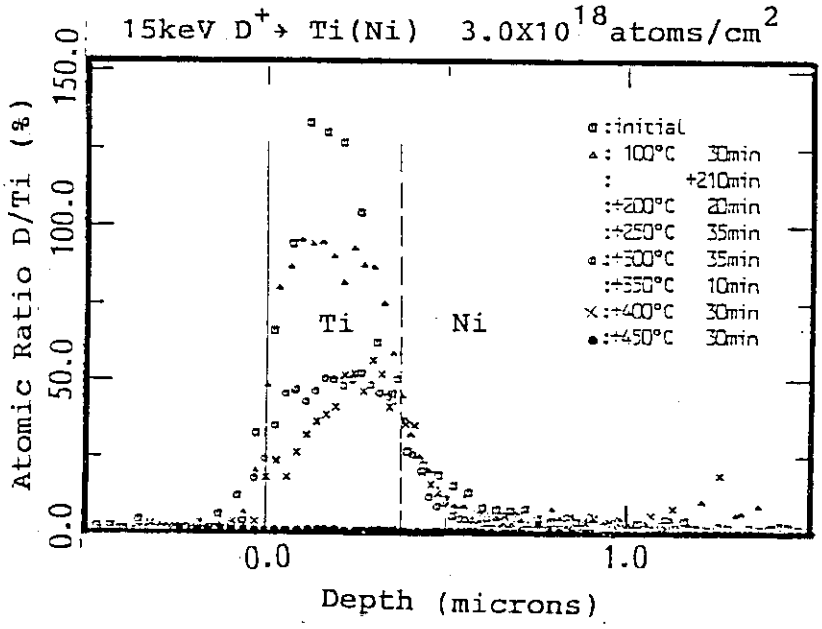

Fig. 4 Desorption of deuteriums out of Ti-desorption layer. Concentration in the layer changes discontinuously within narrow ranges of temperature.

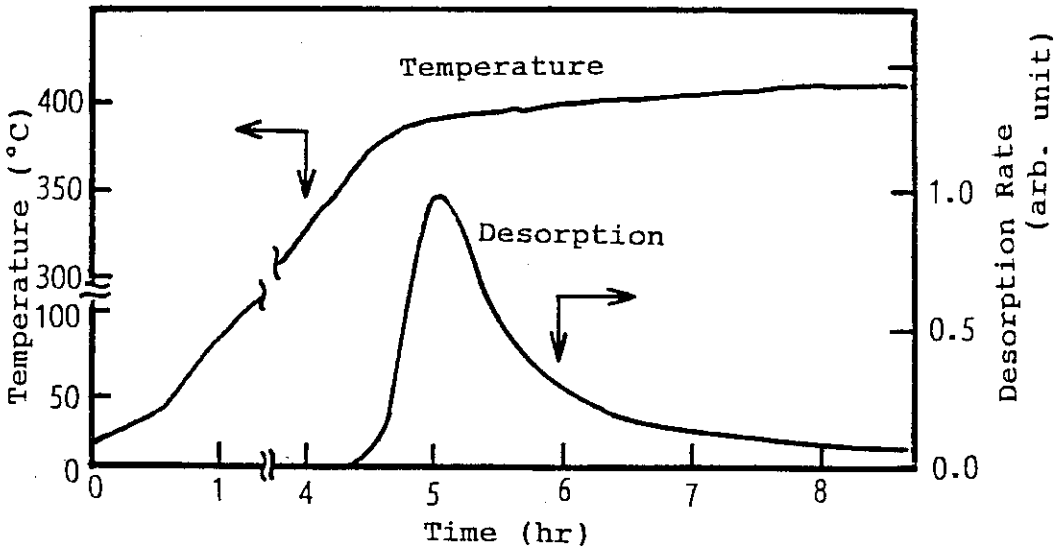

Fig. 5 An example of thermal desorption from Ti-deposition layer. When the temperature reached around 400°C, deuteriums began to release into the gas phase.

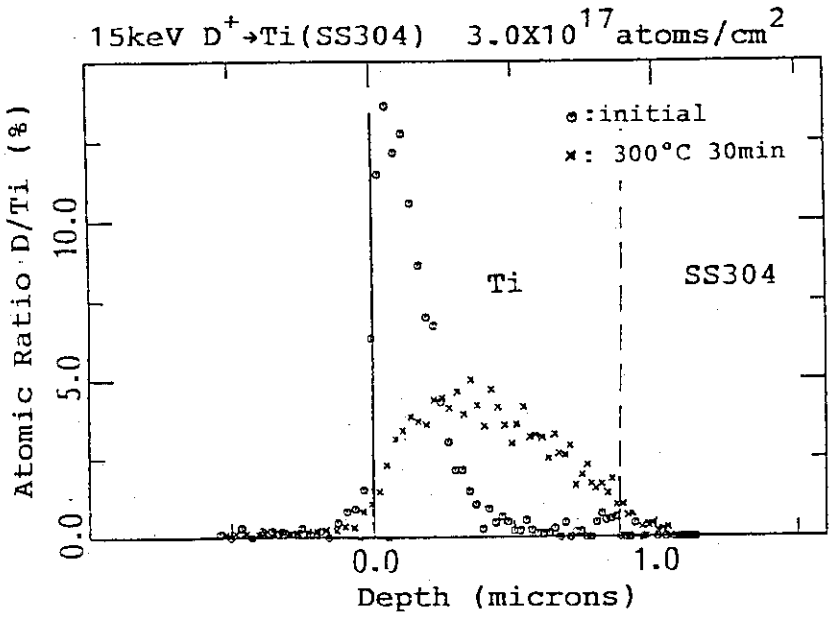

Fig. 6 In Ti-deposition layer, implanted hydrogen tends to disperse all over the layer when the temperature is raised.

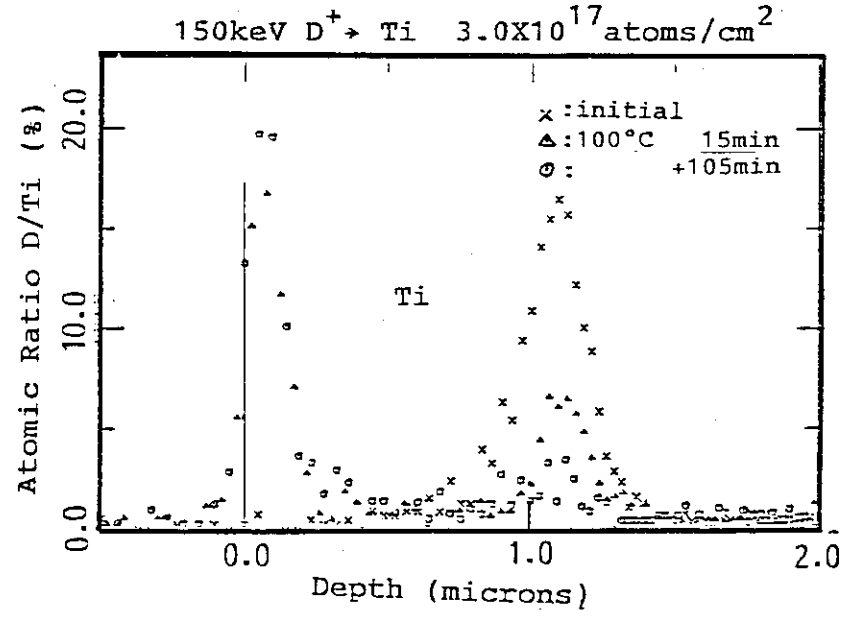

Fig. 7 In titanium metal, implanted hydrogen tends to migrate towards the surface when annealed.

No.15 IMPLICATIONS OF RECENT IMPLANTATION-DRIVEN PERMEATION EXPERIMENTS FOR FUSION REACTOR SAFETY*

G R. Longhurst, R. A. Anderl, and D. A. Struttmann
Idaho National Engineering Laboratory
EG&G Idaho, Inc.
Idaho Falls, ID 83415, USA

ABSTRACT

Experiments have been conducted to observe and investigate the implantation-driven permeation characteristics of several materials considered for fusion reactor structures. Materials tested include 304 and 316 stainless steels, Primary Candidate Alloy (a titanium modified 316 stainless steel), pure alpha iron and the ferritic steel HT-9, and the vanadium alloy V-15Cr-5Ti. Wafers of these materials each 0.5-mm thick were exposed to D_3^+ ions at energies and beam intensities representative of that seen by surfaces exposed to the plasma of a fusion reactor. The rates of permeation and reemission of deuterium from the target specimens were observed as was the spectrum of ion species sputtered from the target surface. From these experiments it was concluded that surface conditions strongly influence the implantation-driven permeation of hydrogen isotopes in these circumstances. The highest permeating fraction seen was in the vanadium alloy tests. This material showed about 750 times the permeating fraction of the austenitic steels and about 170 times that of the ferritic materials. To properly analyze the experimental results it was necessary to use a two-dimensional transport code. Analysis suggests that while beam-sputtering effects are important in all the materials tested, for the vanadium alloy, radial diffusion in the target also strongly influences the results. Safety implications are that while hydrogen isotope concentrations in fusion structures may not be large enough to alter their mechanical properties substantially, there will probably be tritium inventories in those structures sufficiently large that unmitigated release could be hazardous.

INTRODUCTION

Metal structures exposed to the plasma in tritium-burning fusion reactors will be subject to implantation-driven permeation (IDP) of tritium. This comes about because charge-exchange neutral atoms and some energetic ions strike the surface of the structure and become embedded in it. This is shown schematically in Figure 1. The resulting transport of the tritium follows rules which are becoming well understood, but it is significantly different from gas pressure driven permeation (GDP). Permeation rates for IDP in fusion structural materials are usually high

* Work supported by the U. S. Department of Energy Assistant Secretary for Energy Research, Office of Fusion Energy under DOE Contract No. DE-AC07-76ID01570.

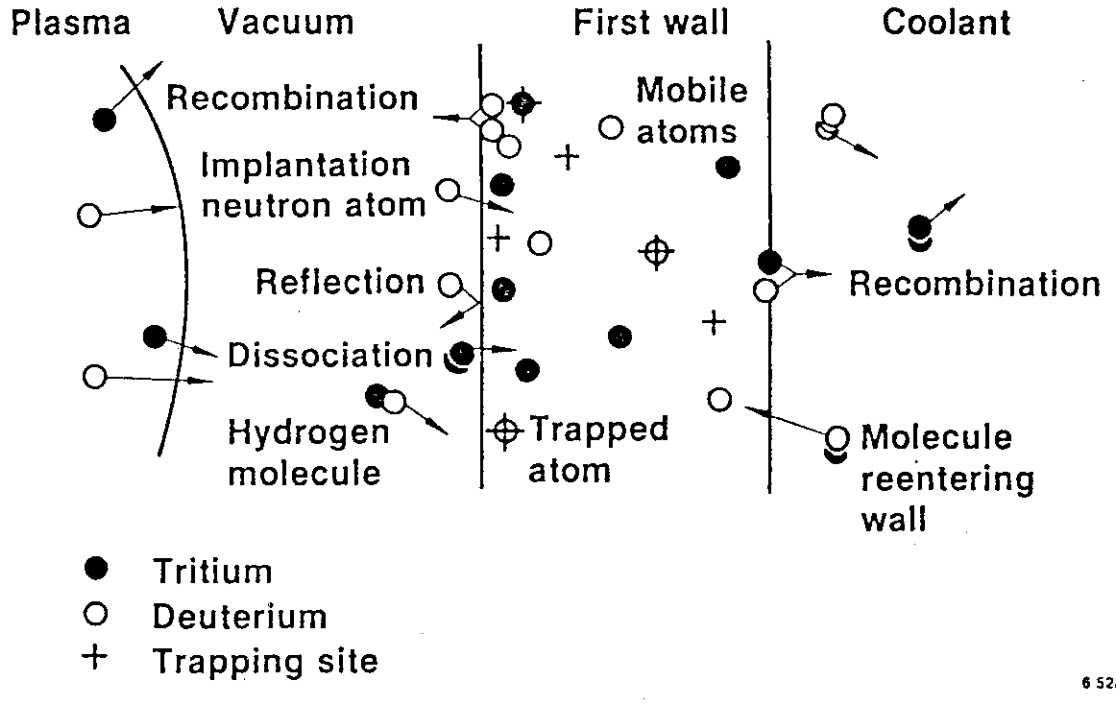

Figure 1. Various kinds of ion, neutral, and molecular interactions take place in a structure such as a first wall exposed to the plasma of a fusion reactor.

because the tritium atoms enter the material without having to go through the dissociation and solution steps required of tritium-bearing gas molecules. These surface processes, which may be rate limiting in GDP, actually enhance permeation in IDP by inhibiting the return of tritium to the plasma side of the structure.

Experiments have been conducted at the Idaho National Engineering Laboratory (INEL) to investigate the nature of IDP by simulating conditions experienced by structures exposed to the plasma. These experiments have shown that surface conditions are important to tritium permeation in materials endothermic to hydrogen solution such as austenitic and ferritic steels. In reactive metals such as vanadium, surface processes appear to totally control the permeation.

The purpose of this paper is to review the progress of those experiments and to discuss the implications that the results have regarding the tritium-related safety concerns of fusion reactors.

EXPERIMENTS

Apparatus

The apparatus used for conducting IDP experiments is shown schematically in Figures 2 and 3. Figure 2 shows the general layout of the facility. The key component is a 10-kV electrostatic accelerator with

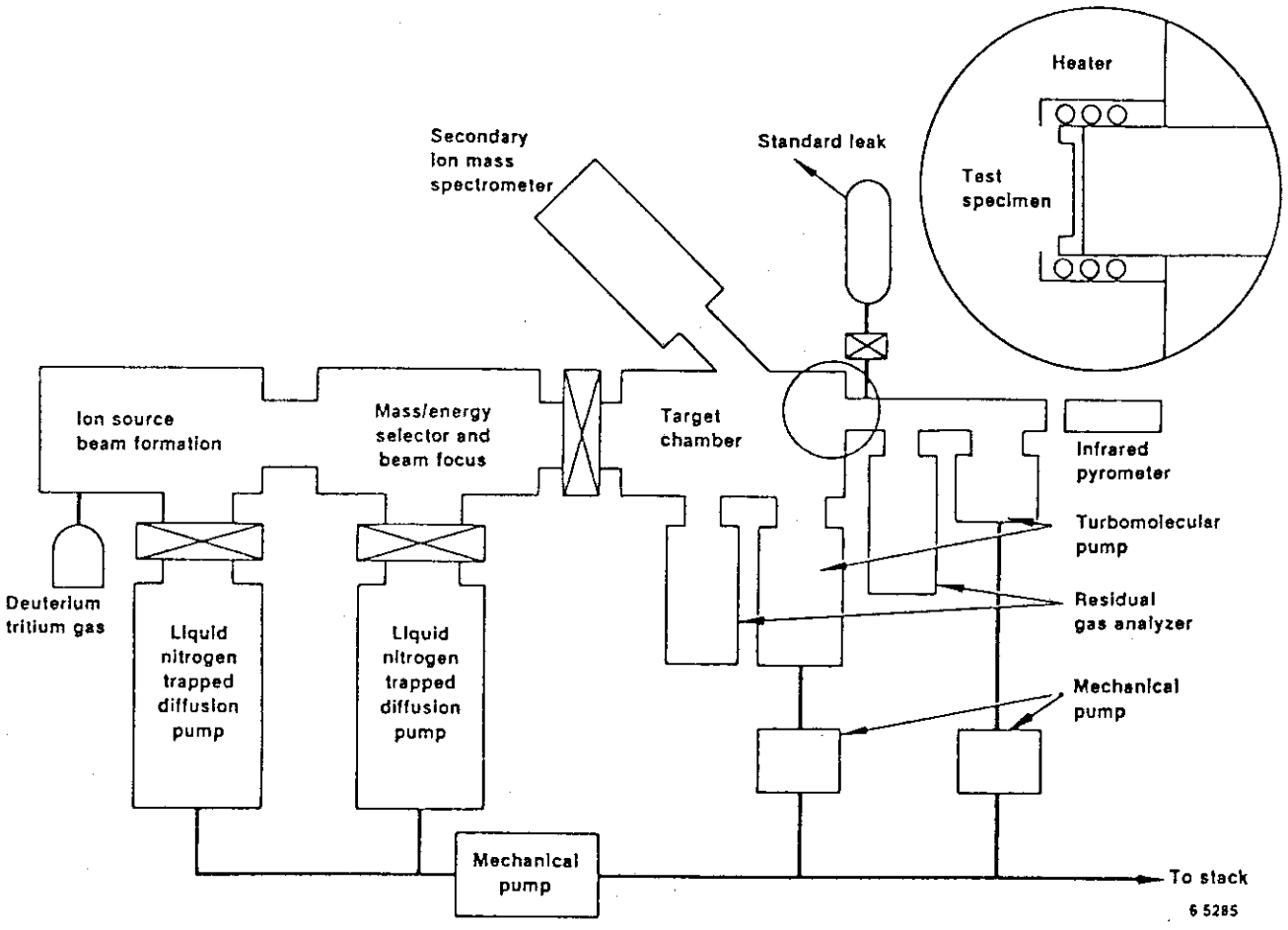

Figure 2. Schematic of apparatus used in conducting implantation-driven permeation experiments.

a duoplasmatron ion source which is used to produce deuterium ions that are mass analyzed, decelerated to the energy of interest, and focused onto a heated target specimen. D_2 gas is used in the ion source, and D_3^+ molecular ions are selected for implanting into the target. When used with net acceleration potentials of 1.5 - 3 kV, implantation energies of 250-500 eV/amu result. The ion beam is effectively Gaussian on the target with a full-width half-maximum radius of 2.7 mm.

Targets used are flange-mounted disks, 25 mm in diameter and usually 0.5 mm thick. Figure 3 shows the way in which these targets are mounted in the test fixture. The target and its supporting structure are electrically isolated from the housing to permit direct measurement of the implantation current. A Faraday cup is also used before and after implantations to calibrate ion current measurements and to correct for secondary electron emission.

Heating of the specimen is provided by a radiant electrical resistance heater. Target temperatures up to 773 K are routinely used, but some

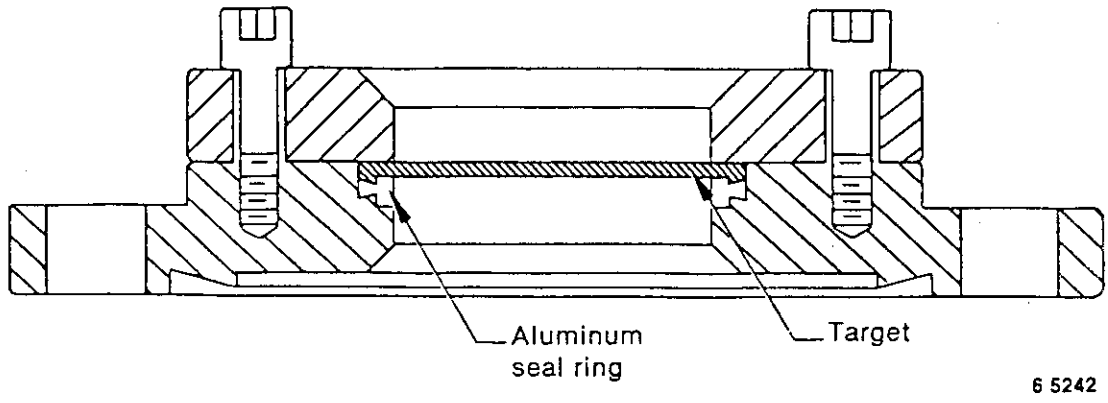

Figure 3. Method of clamping target specimens into the test fixture.

tests have reached 873 K. Chromel-alumel thermocouples measure temperatures of the heater housing, the target support flange and the target itself. Analysis and measurement of target temperatures have shown that the target temperature is spatially uniform to within 5 K even with the beam on.

Independent vacuum pumping systems maintain pressures of a few uPa over both upstream and downstream surfaces of the target. Deuterium reemission and permeation from the specimens are determined by monitoring respective chamber pressures using residual gas analyzers (RGAs). Mass peaks 2, 3, 4, and 19 are observed. Masses 2, 3, and 4 consistently have similar history profiles though their intensities are widely different. Most of the deuterium appears as D_2 with mass 4. There is enough residual hydrogen present that some appears as HD with mass 3. Some also appears as HDO (mass 19). This may be due to recombination of deuterium with hydroxyl ions at the surface or to exchange of deuterium with hydrogen atoms in water molecules elsewhere in the system. Upstream and downstream target chambers are each connected to calibrated D_2 leaks which are used to calibrate measurements of permeation and reemission rates made using the RGAs.

The facility is equipped with a secondary-ion mass spectrometer (SIMS) which samples either positive or negative ions emitted from the target allowing some indication of surface processes taking place during implantation. Important SIMS mass numbers monitored include 23 (Na), 27 (Al, C_2H_3), 28 (Si, N_2, CO, C_2H_4), 39 (K), 48 (Ti), 51 (V), 52 (Cr), 55 (Mn), and 56 (Fe). By monitoring the time histories of the various ion species concentrations, inferences can be made regarding surface composition changes. Then these may be correlated with permeation and reemission transient data.

A computer-based data acquisition system is used to acquire time history information for each monitored mass peak and for other experiment parameters. Signals recorded include time, masses and intensities for the RGAs and SIMS unit, thermocouple temperatures, beam current, and net accelerator voltage. Locally written software performs test data display, reduction and analysis.

During a typical test the sample is installed and annealed in vacuum for 12 to 24 hours. The RGAs are calibrated by valving in the calibrated D_2 leaks. The ion current is measured in the Faraday cup and the indicated beam current signal is compared with that when the beam strikes a shield masking the target. The shield is then withdrawn, and the beam is allowed to strike the target. In some tests the beam is interrupted for periods long enough that the transient behavior of the permeation and reemission flux signals can be observed.

Test Results

Experiments have been performed on pure alpha iron, on 304 stainless steel, on primary candidate alloy (PCA) which is a titanium modified type 316 stainless steel, on HT-9, a ferritic steel, and on the vanadium alloy V-15Cr-5Ti. Typical results are shown in Figures 4 - 6. Figure 4(a) shows permeation and reemission histories for a test of PCA at 753 K with 3-keV D_3^+ ions at 6.5×10^{19} $D/m^2 \cdot s$. Periods where the beam is turned off are clearly reflected in both permeation and reemission histories. Of particular note is the initially high value of the permeation flux. This has been observed by other investigators[1-3] and is interpreted to be due mainly to the enhanced reemission at the front surface resulting from erosion from the upstream surface of contaminants such as oxygen, carbon, and their compounds.[4] This conclusion is drawn from the correlation between the SIMS measurements of the depletion of these materials from the surface (Figure 4(b)) and the decay of the deuterium permeation flux. This intense transient can be regenerated by exposure of the hot surface to contaminants such as air and to a lesser extent by just letting the target remain heated for periods of several hours without an ion flux.

Figure 5(a) shows similar permeation and reemission histories for HT-9 under the same conditions. Figure 5(b) shows the SIMS data for that test. Not only did the permeating fraction in the initial transient far exceed the corresponding quantity in the PCA results, but the steady state permeation flux was about 0.09% of the implantation beam flux in the HT-9 as compared with 0.02% in the PCA case. The higher permeation fraction in the HT-9 is due principally to the greater diffusivity in the ferritic steel (bcc structure) as compared with that in the austenitic PCA (fcc structure).

Both these materials exhibit the same general tendency: an initially intense permeation transient followed by a much lower steady state value. A striking contrast is provided by Figure 6 which is for a similar test of V-15Cr-5Ti under the same conditions the same as for Figures 4 and 5. Figure 6(a) shows premeation and reemission flux histories while Figure 6(b) shows SIMS data taken on the same sample at a later time, after the upstream surface was allowed to regenerate. In this case, instead of the initially intense transient there is a much slower rise to steady state. The short-period variations in the curves result from fluctuations in ion beam intensity and focus. It is also typical of these tests on V-15Cr-5Ti that the reemission signal rises and falls more rapidly than does the permeation signal, but it is not so abrupt as is observed in tests of steels. SIMS data shown in Figure 6(b) indicate that most of the surface

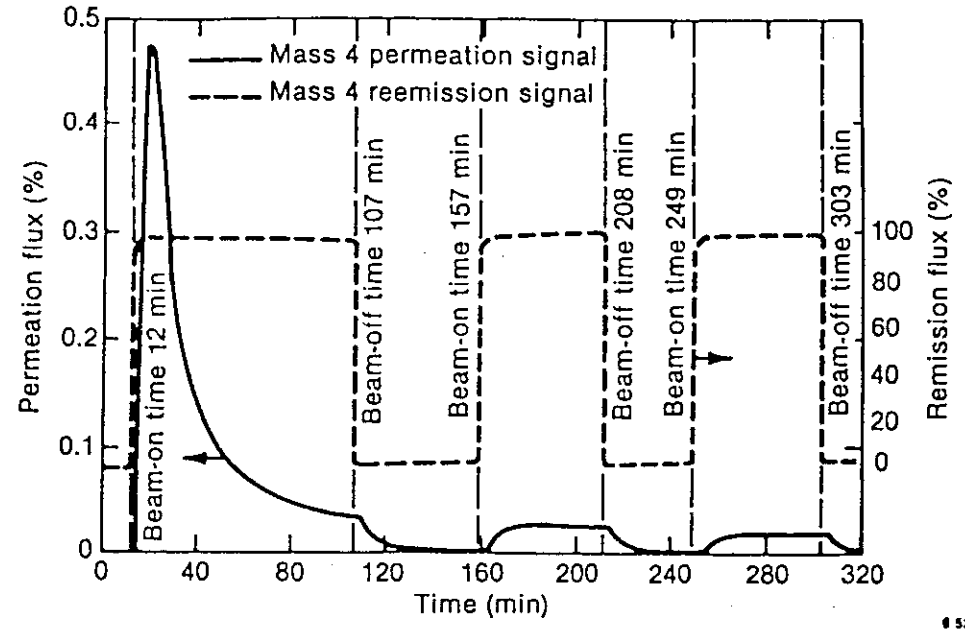

(a)

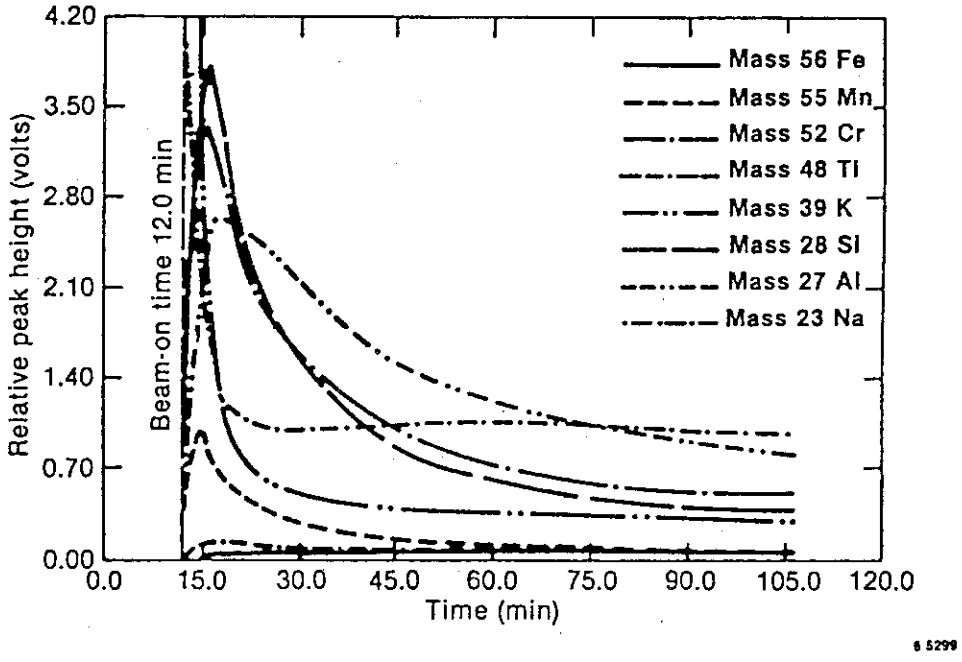

(b)

Figure 4. Results of implantation-driven permeation testing of PCA at 753 K with 3-keV D_3^+ ions; (a) permeation and reemission histories normalized to the implantation current of 1.5×10^{15} D/s, (b) SIMS measurements of emissions from the implantation side of the target for various mass numbers as indicated. Effective beam area (FWHM) was 0.23 cm^2.

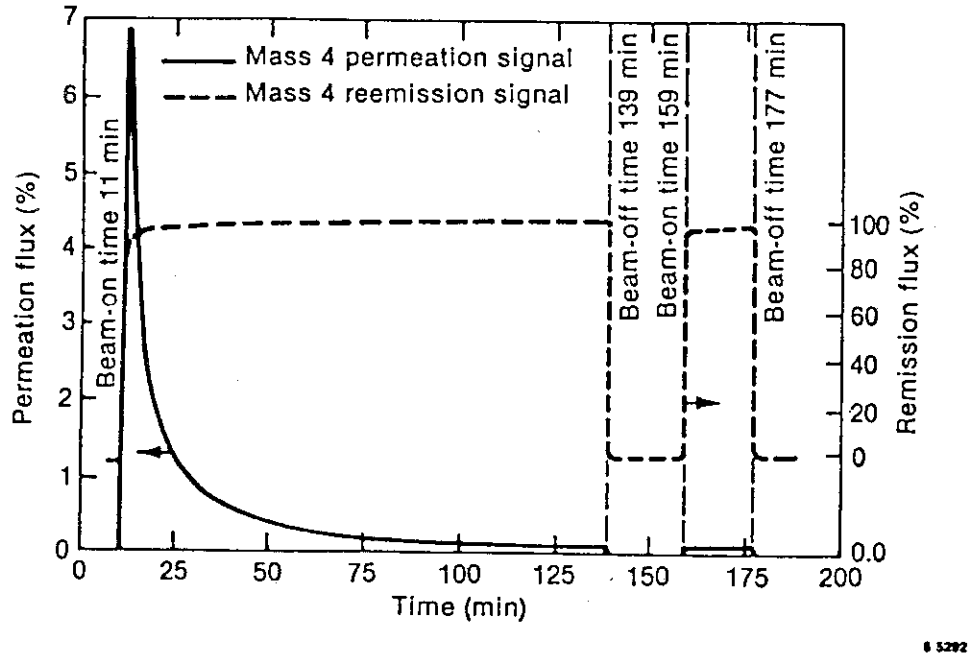

(a)

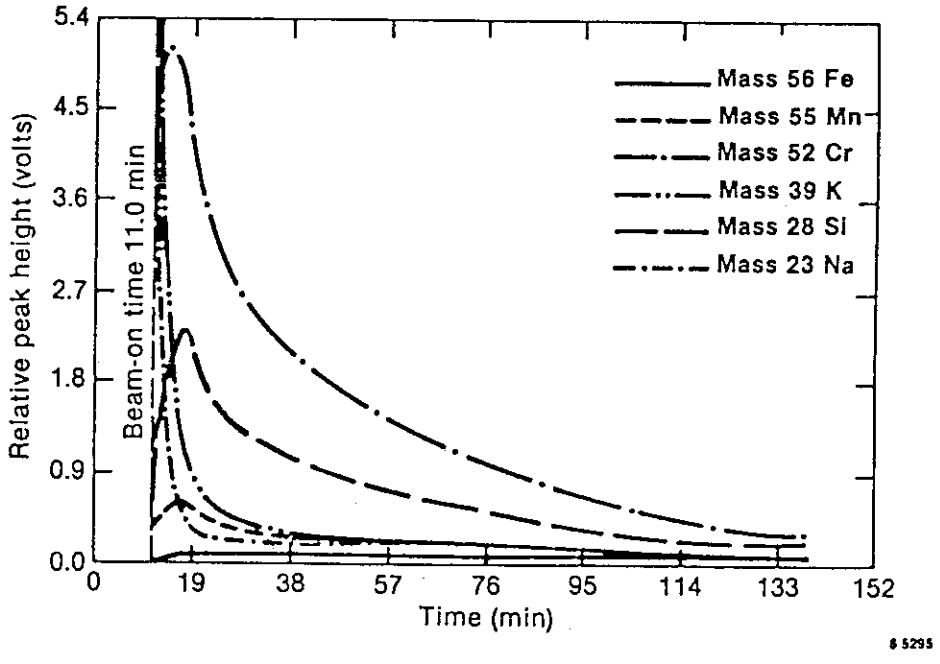

(b)

Figure 5. Results of implantation-driven permeation testing of HT-9 at 753 K with 3-keV D_3^+ ions; (a) permeation and reemission histories normalized to the implantation current of 1.5×10^{15} D/s, (b) SIMS measurements of emissions from the implantation side of the target for various mass numbers as indicated. Effective beam area (FWHM) was 0.23 cm^2.

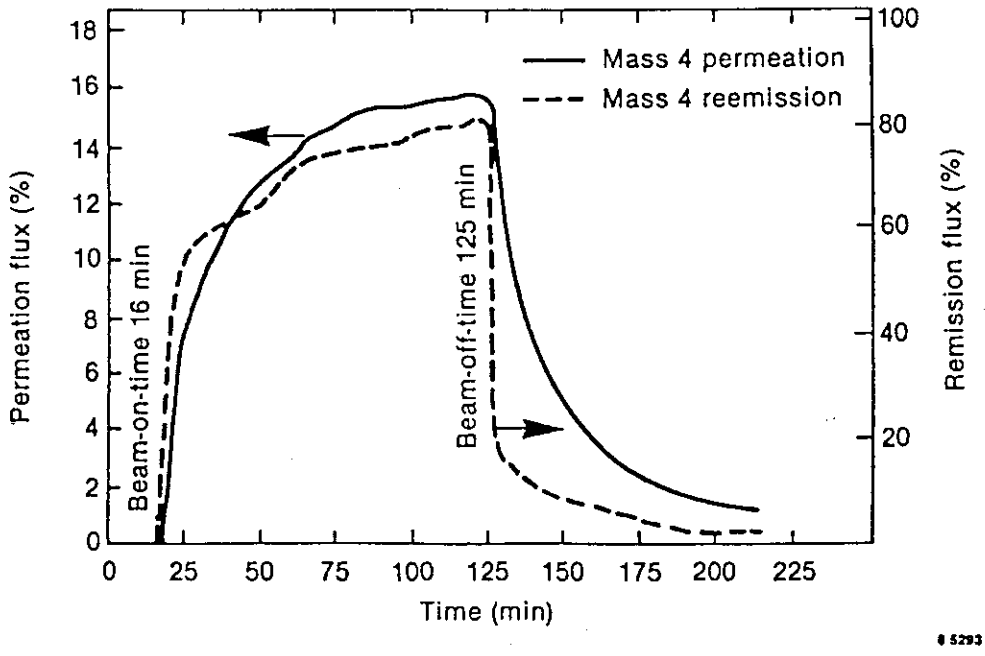

(a)

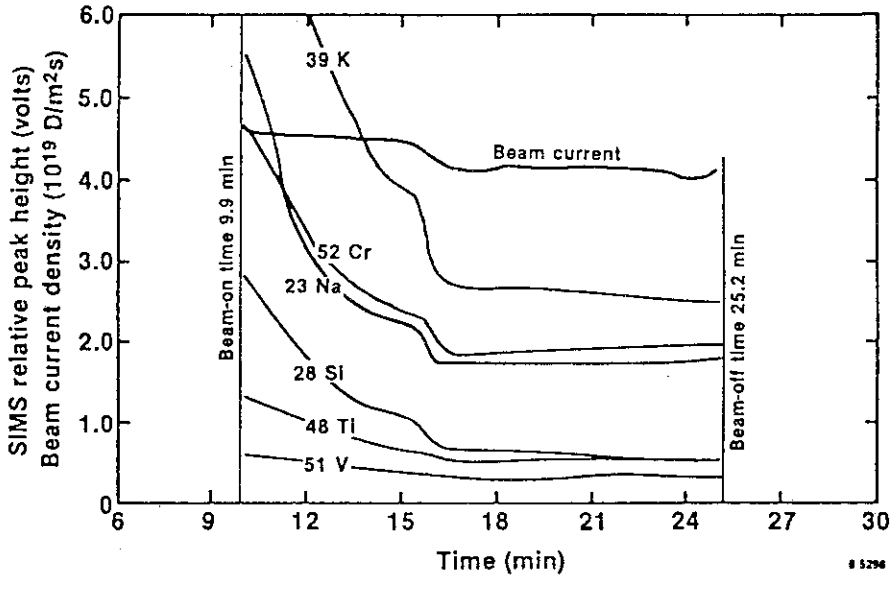

(b)

Figure 6. Test results for a test of V-15Cr-5Ti at 723 K using 3-keV D_3^+ ions; (a) permeation and reemission histories normalized to the implantation current of 1.5×10^{15} D/s, (b) SIMS measurements of emissions from the implantation side of the target for various mass numbers, as indicated, on a test similar to that shown in (a). Effective beam area (FWHM) was 0.23 cm^2.

contaminants are removed during the first seven minutes or so which is somewhat faster than for the steels.

Perhaps the most significant difference between the vanadium alloy and the steels is that for vanadium about 15% of the implantation flux permeates through the target at steady state, 750 times that coming through PCA under similar conditions even though the vanadium has only about 50 times the diffusivity of the PCA at these temperatures (for hydrogen, $D=6.32\times10^{-7}\ \exp(-5747/T)\ m^2/s$ for type 316 SS[5] and $D=8.9\times10^{-8}\ \exp(-1311/T)\ m^2/s$ for vanadium[6]).

ANALYSIS

To extend test results obtained in experiments to real-world applications, it is critically important that an analytical model capable of providing accurate scaling be available. Therefore, considerable effort has gone into the development and refinement of computer codes capable of dealing with IDP.[8-10] These are typically one-dimensional diffusion codes with non-linear boundary conditions which assume Fick's law diffusion of single atoms through a medium and second-order recombination[7] at the surfaces. Most are capable of dealing with one or more traps, and there are varying degrees of sophistication regarding the deposition of implantation atoms near the surface of the material.

When one is able to successfully analytically model the results of an experiment using the appropriate parametric constants, there is some confidence that the performance of a prototype may be predicted using the same model with altered dimensions and/or conditions. The accuracy of the prediction rests in the quality of the analytical model.

The modeling of IDP processes using TMAP,[8] an existing one-dimensional code, gives good results for cases where there is little or no radial diffusion compared with that in the direction of principal diffusive flow. Literature values for the diffusivity of deuterium in vanadium and estimates of the recombination coefficient that may be expected suggested that over the period of the tests there would be sufficient radial diffusion through the target that the entire surface area would be emitting deuterium in significant quantities. This had a substantial impact on interpretation of the results, so it was necessary to use a two-dimensional code to model the experiments. A code called DIF2D was written which uses two-dimensional versions of the same transport and surface process equations used in TMAP. Trapping was included for versatility, although that feature has not yet been needed to explain the results seen so far. An additional feature is a local-fluence dependent upstream recombination-coefficient sticking factor to account for the sputtering of the upstream surface by the beam.

Even though the permeation spike characteristic in the tests of the iron alloys did not appear in the vanadium alloy tests, it was evident that the ratio of permeation flux to reemission flux was changing during the course of the vanadium alloy tests. This is illustrated in Figure 6. On the time scale of the experiments the diffusion of deuterium within the material is effectively instantaneous. This is evident in the immediate response in the permeation flux to switching the beam on or off. Under

these conditions, if the recombination coefficients at both upstream and downstream surfaces were constant, even though they may not be equal, the normalized permeation and reemission curves would overlap. Instead what is seen is a significant difference in the shapes of the normalized curves during the implantation period. This is a compound effect resulting from the filling of the sample with deuterium, the modification of the upstream surface condition by the ion beam, and the radial diffusion of deuterium in the target.

Figure 7 illustrates the extent of this radial diffusion by presenting concentration profiles calculated with the DIF2D code for the experiment whose results are shown in Figure 6(a). The curves of Figure 7 are normalized concentration profiles calculated with DIF2D. Near the top of the tick-marked vertical axis in each plot is the maximum deuterium concentration fraction. The distribution is shown over half the cross section of the target with the centerline to the left. The axial and radial distance scales are different for clarity (recall that the target radius is 12.5 mm while its thickness is only 0.5 mm), with the radial axis extending to the right and the axial axis receding. At the top of each plot is the elapsed time in seconds labelled with "T", the permeation current (D/s) labelled with "JP", the reemission current (D/s) labelled "JR", the upstream centerline recombination coefficient value called "KR1(c/l)" having units of (m^4/s), the uniform downstream recombination coefficient (m^4/s) labelled "KR2", and the ratio (Ji/Jo) of the present beam current to the reference value.

Another interesting feature of the curves in Figure 6(a) is that the reemission flux drops precipitously upon interrupting the ion beam while the permeation flux takes much longer to decay. This may be explained qualitatively by again considering the profiles of Figure 7. The upstream surface is sputter cleaned by the beam whose profile is shown in the horizontal plane, for times when the beam is on, with the amplitude (D/s) given adjacent to the profile apex. The modeling of the change in recombination coefficient in the DIF2D code is

$$K_r = K_r^o + \Delta K_r \, [1 - \exp(-F/F_c)] \qquad [1]$$

where F is the local ion fluence received and F_c is an experimental constant related to the ability of the ion beam to modify the target surface. K_r^o is the initial value of the recombination coefficient, and ΔK_r is the change that takes place in K_r under the action of the ion beam. For large values of F, K_r is assumed to approach the value given by Baskes' model (Ref. 7) with a sticking factor near unity.

Late in the implantation period, when near steady-state conditions apply, the central part of the target has a much higher recombination coefficient than does the outer (major) part of the upstream surface or the downstream surface. Most of the reemission flux is coming through the part of the target impacted by the beam. The permeation flux, on the other hand, is coming from the entire downstream surface of the target. The higher concentrations toward the center of the target are offset by the larger area emitting deuterium at lower concentrations toward the outer edge of the target. The deuterium in the vicinity of the sputter cleaned surface leaves very quickly when the beam goes off because the

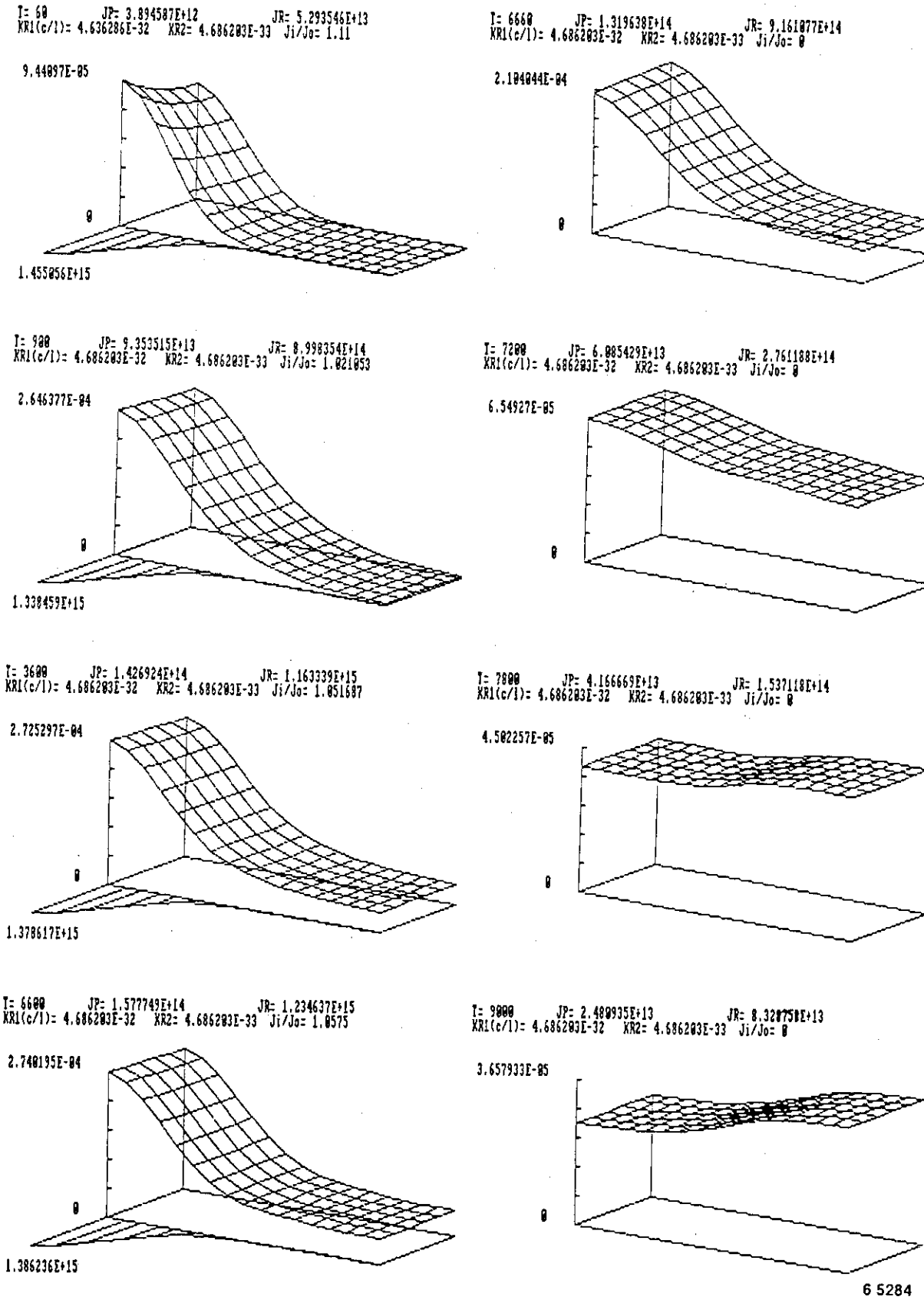

Figure 7. Calculated deuterium concentration profiles for the V-15Cr-5Ti target in the test shown in Figure 6(a) for the elapsed times indicated. The beam stopped at 6600 seconds.

recombination coefficient is so high there. Most of the deuterium in the outer periphery of the target then diffuses radially inward to get out. The permeation flux changes much more slowly because the area-average deuterium concentration remains high. Hence, when comparing permeation and reemission fluxes which have been normalized to their maximum values,he normalized permeation flux appears to remain high for a longer period than does the reemission flux.

The larger permeating area for the vanadium alloy experiments, when compared with the smaller permeating area in similar tests in steel where radial diffusion is minimal, contributes to the much higher permeation fraction in the vanadium alloy tests. This permeating fraction ratio could be reduced by roughly a factor of 10 if the whole surface of the target had been irradiated with the ion beam, making the transport one-dimensional,

The reemission and permeation histories of Figure 8 were calculated by DIF2D for the test conditions of Figure 6 and correspond with the deuterium density concentrations shown in Figure 7. Figure 8 is a fair approximation to the curves in Figure 6. (Note that the curves of Figure 6 were not fully normalized for clarity.)

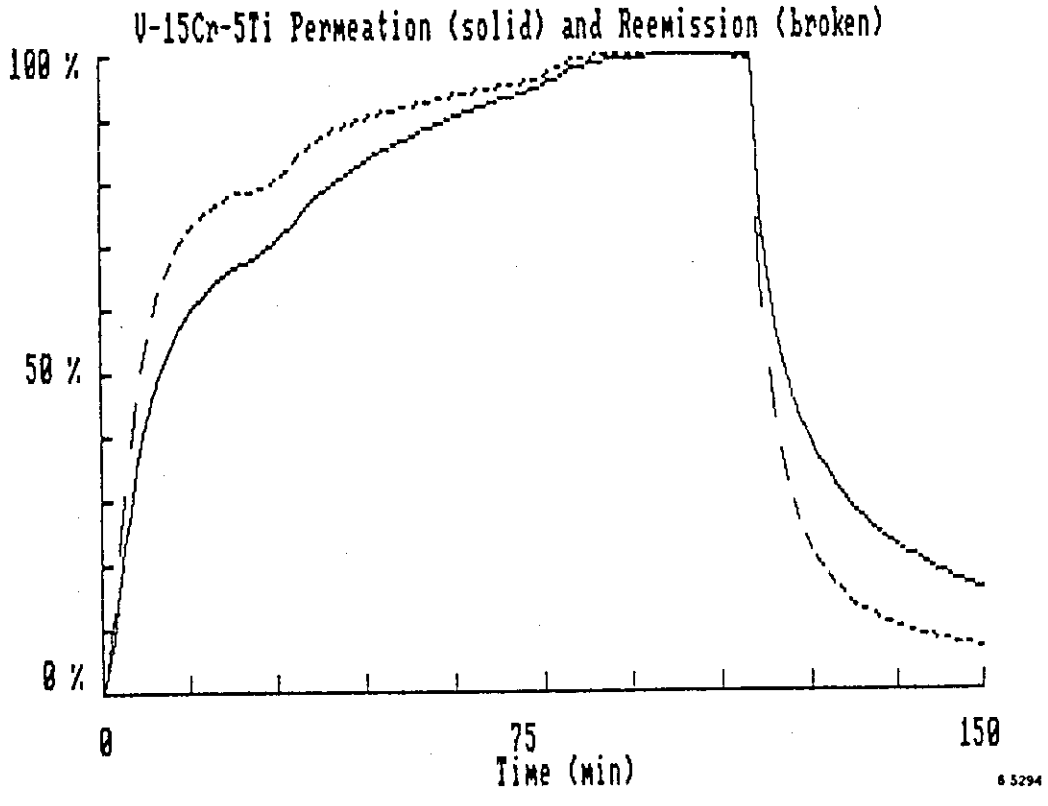

Figure 8. Calculated reemission and permeation histories for the test shown in Figure 5(a) using the DIF2D code.

The parameters for computations were obtained as follows: The diffusivity of deuterium in the material was estimated from permeation breakthrough times. Then the permeation and reemission histories were integrated and compared with beam fluence at the time the beam was stopped to give an estimate of the average deuterium concentration in the sample. The ratio of the reemission current to the permeation current, when divided by the estimated ratio of the sputter cleaned area to the target downstream area gives the approximate ratio of the upstream and downstream recombination coefficients. Those combined with the average deuterium concentration is sufficient to estimate the magnitude of each recombination coefficient. The critical ion fluence for sputter cleaning is then adjusted to give the appropriate approach rate to steady state. A check on the validity of the parameters is that the rise time and concentration both match well with experimental data.

SAFETY IMPLICATIONS

A principal concern for safety in fusion reactors is the assurance that there will be no significant hazard to site employees or to the public from exposure to tritium. Such exposure may come if tritium or tritiated materials or fluids are released from the fusion reactor or its associated equipment in unacceptable quantities. Some leakage is unavoidable under routine operating conditions. It comes as tritium slowly diffuses through structures, as tritiated water seeps from valves or fittings, or as gases containing trace quantities of tritium are vented to the stack. Loss rates for all these processes should be small, probably only a few curies per day. Achievement of such a low rate requires careful attention to detail in the design, fabrication, and maintenance of the fusion facility, particularly the tritium fuel processing systems.

Another concern is that some structures, such as a first wall or limiter, may acquire a large inventory of tritium which may be released in the event of an accident. This is possible in loss-of-coolant or loss-of-flow situations where the structure may undergo a severe thermal excursion. These possibilities make it important to accurately predict the permeation rate and inventory of tritium in fusion reactor structures, particularly those exposed to the plasma.

The experiments described here have helped us to better understand the processes occurring during implantation driven permeation of hydrogen isotopes. Among the things learned from these experiments are the following:

One concept supported by experiments on HT-9 and pure alpha iron was that the behavior of the alloy under IDP was very similar to that for the pure alpha iron. Also, the austenitics tested gave similar results to each other, though different from the ferritics. This is valuable because often detailed information on a particular alloy's permeation characteristics is not available. Use of data for the base material may provide a good substitute. The generality of this concept has yet to be proven, however.

Next, vanadium or its alloys, while desirable for their ability to withstand high temperature and high neutron fluences, will have much higher tritium permeation of charge exchange neutrals and plasma ions than will iron alloys. Likewise, the ferritic alloys will display greater permeation than will the austenitic alloys under similar conditions. To reiterate results quoted earlier, in these tests under similar conditions V-15Cr-5Ti was found to have about 750 times the permeation of PCA and about 170 times that in the HT-9. The two dimensional nature of the experiments appears partly responsible for the high permeation fraction in the vanadium, and the actual ratio in a triuly one-dimensional situation may be only about 100.

The deuterium inventories estimated from the calculations performed to model the experiments were in the range of 10 to 100 appm. The modeling done did not require the presence of traps in the bulk material to adequately represent the transients and steady state fluxes. While it is expected that radiation damage, both from the implanting particles and from neutrons, will result in the formation of traps, many of those traps will be annealed at working temperatures which should be similar to the ones used in these experiments. Tritium inventories in structures made of the materials tested will probably not be so large that material properties will be affected, however, an accident which results in the release of say 100 appm of tritium (70 g in a first wall 5 mm thick and 400 m^2 in area) would be significant. The highest concentrations were estimated for the vanadium alloy.

The presence of the permeation spike seen in the steel tests suggests that if a steel surface is continually cleaned by erosion of surface contaminants by the plasma, the permeating fraction of tritium implanted into the material will be the low steady state values. Coating of the plasma-side surface by a material with a high recombination coefficient should reduce permeation even further. However, if there is deposited on the steel surface a layer of other material which hinders recombination of implanted tritium, or if delays between plasma burns are sufficiently long that surface oxidation occurs, then higher permeation rates should be expected.

Finally,experience gained here suggests that for ferritic steels, alpha iron, vanadium alloys, or materials of similarly high diffusivity, it will be very important to use two or three dimensional transport codes to estimate tritium permeation. This will be particularly true in components such as divertor plates and limiters where loadings may be highly non-uniform.

REFERENCES

1. T. Tanabe, Y. Furuyama, and S. Imoto, "Reemission and Permeation of Deuterium Implanted into Metals," Journal of Nuclear Materials, 122 & 123, 1984, pp. 1563-1567.

2. J. Winter, F. Waelbroeck, P. Weinhold, and T. Schelske, "Permeation Probes for the Characterization of the Atomic Hydrogen Flux to a Tokamak Wall," Journal of Nuclear Materials, 111 & 112, 1982, pp. 243-247.

3. N. Saitoh, Y. Etoh, T. Tanabe, and S. Imoto, "Hydrogen Permeation and Diffusion under Ion Bombardment," Technology Reports of The Osaka University, 30, 1564, 1980, pp. 429-434.

4. R. A. Anderl, D. F. Holland, D. A. Struttmann, G. R. Longhurst, and B. J. Merrill, "Tritium Permeation in Stainless Steel Structures Exposed to Plasma Ions," Proceedings of the Eleventh Symposium on Fusion Engineering, Austin, Texas, November 18-22, 1985, IEEE CH2251-7, pp. 644-649.

5. T. Tanabe, Y. Yamanishi, K. Sawada, and S. Imoto, "Hydrogen Transport in Stainless Steels," Journal of Nuclear Materials, 111 & 112, 1984, pp. 1568-1572.

6. Y. Fukai and H. Sugimoto, "Diffusion of Hydrogen in Metals," Advances in Physics, 34, 2, March/April 1985, pp. 263-326.

7. M. I. Baskes, "A Calculation of the Surface Recombination Rate Constant for Hydrogen Isotopes on Metals," SAND 80-8860, April 1980.

8. J. L. Jones, B. J. Merrill, and D. F. Holland, "Predicting Tritium Movement and Inventory in Fusion Reactor Subsystems Using the TMAP Code," Proceedings of the Eleventh Symposium on Fusion Engineering, Austin, Texas, November 18-22, 1985, IEEE CH2251-7, pp. 631-636.

9. M. I. Baskes, "DIFFUSE: A Code to Calculate One-Dimensional Diffusion and Trapping," SAND 80-8021, January 1980.

10. P. Weinhold, M. Profant, F. Waelbroeck, and J. Winter, "Computer Code PERI for the Calculation of Recycling, Volume Distribution, and Permeation of Hydrogen in First Wall Materials of Tokamaks," Journal of Nuclear Materials, 93 & 94, 1980, pp.866-870.

No.16 : Permeation of Deuterium Implanted into Nickel

T. Nagasaki, R. Yamada, M. Saidoh, and H. Katsuta

Japan Atomic Energy Research Institute

Ⅰ. INTRODUCTION

While some models for plasma driven permeation(PDP) have been proposed —— for example Doyle et al. [1] ~ [3] have formulated hydrogen transport in materials using their simple model and classified the steady-state hydrogen transport by rate-limiting processes, there are not enough data to be compared with the models; Even the dependence of permeation flux on such parameters as temperature, incident flux, and incident energy has scarecely been measured systematically yet. Therefore we have been studying PDP experimentally with the following two objectives. One is to study how the permeation flux at steady state depends on parameters and the other is to identify the rate-limiting processes comparing the experimental results with a model.

Ⅱ. EXPERIMENTAL

For deuterium implantation was used a 5 kV accelerator with a duoPIGatron ion source, an analyzing magnet, and an electrostatic lens. Figure 1 is a schematic drawing of the sample head assembly, which was set up in the target chamber of the accelerator system. The base pressure in the target chamber was typically 2×10^{-6} Pa; it rose up to 8×10^{-5} Pa

during implantation. The deuterium permeation rate was measured with a quadrupole mass spectrometer.

The sample was 99.99% pure nickel foil of 15 mm in diameter and 0.124 mm in thickness.

Ⅲ. MODEL

In our experiments the rate of gas driven permeation (GDP) was comparable to that of PDP above ～300℃. Thus we have slightly modified Doyle's model [1] ～ [3] considering GDP to apply it to the experimental data.

We have obtained

$$J_P = \frac{K_2}{K_1 + K_2} \phi_P \tag{1}$$

when the rate of hydrogen transport in the material is recombination limited in both sides of the implantation plane(RR regime),

$$J_P \fallingdotseq \frac{D_2}{x_0} \sqrt{\frac{\phi_G}{K_1}} \left(\sqrt{1 + \frac{\phi_P}{\phi_G}} - 1 \right) \tag{2}$$

$$\fallingdotseq J_G \left(\sqrt{1 + \frac{\phi_P D_2^2}{K_1 x_0^2 J_G^2}} - 1 \right) \tag{3}$$

when it is recombination limited in the injection side and diffusion limied in the back side(RD regime), and

$$J_P \fallingdotseq \frac{D_2}{D_1} \frac{R}{x_0} \phi_P \tag{4}$$

when it is diffusion limited in both sides(DD regime),

where ϕ_G is the penetrating hydrogen flux from the gas, ϕ_P the penetrating hydrogen flux from the ion beam, J_G the flux of permeation driven by the hydrogen gas before and after hydrogen ion implantation, J_P the permeation flux increment

caused by implantation, x_0 foil thickness, R projected range, D_1 the diffusion constant in the injection side, D_2 the diffusion constant in the back side, K_1 the recombination coefficient at the injection surface, and K_2 the recombination coefficient at the back surface. It is noteworthy that J_P depends on J_G in the case of the RD regime.

Ⅳ. RESULTS AND DISCUSSION

・Temperature dependence of J_P

Temperature dependence of J_P was measured in the range from 100 to 1000℃ with 5 keV D_3^+. The results are shown in the lower part of figure 2. While J_P increases with increasing temperature above ～300℃, it is nearly constant below ～300℃.

・The dependence of Q_P on I

5 keV D_3^+ beam of 10 to 55 μA —— deuterium atomic flux of 0.2×10^{15} to 1.1×10^{15} $cm^{-2}s^{-1}$ —— was directed onto the sample, and the increment $Q_P(\propto J_P)$ of the permeation rate was measured as a function of the beam current $I(\propto \phi_P)$. The results are shown in figure 3. The values n are gradients of the fitted lines, that is, $J_P \propto \phi_P^n$. n is 0.7～0.8 above 400℃, while n is larger than 1 below 300℃. The temperature dependence of n is shown in the upper part of figure 2. The transition region of n is corresponds to that of J_P. We think that the transition results from that of the rate-limiting processes for deuterium transport in the

sample. According to equations (1)～(4) it is in the RD regime that n can be smaller than 1. Figure 4 shows normalized J_P calculated by equation (2) as a function of normalized ϕ_P. Since J_P/J_G in the experiments falls in the region indicated in the figure, we think the calculation for the RD regime reproduces the I dependence observed above 400℃.

・The dependence of Q_P on Q_G'

Deuterium gas was feeded into the target chamber to increase the rate Q_G' of GDP before and after implantation, and was measured the increment Q_P of the permeation rate caused by 5 keV D_3^+ implantation at atomic flux of $1.1\times10^{15}cm^{-2}s^{-1}$. The results are shown in figure 5. Q_P decreases with increasing Q_G' above 400℃, while it remains approximately constant at 270℃. According to equations (1)～(4) it is in the RD regime that $J_P(Q_P)$ can decrease with increasing $J_G(Q_G)$. Figure 6 shows normalized J_P calculated by equation (3) as a function of normalized J_G. Since J_P/J_G in the experiments falls in the region indicated in the figure, we think the calculation for the RD regime qualitatively reproduces the Q_G' dependence observed above 400℃.

・The dependence of J_P on E

3 keV D_3^+, 4 keV D_3^+, 5 keV D_3^+, and 5 keV D_2^+ were directed onto the sample at deuterium atomic flux of 5×10^{14} $cm^{-2}s^{-1}$, and J_P was measured. The results are shown

in figure 7 as a function of the incident energy E per deuterium atom. J_P hardly depends on E at 600 and 900℃, while it increases with increasing E below 400℃. The model predicts that J_P is independent of E(R) in the RR and RD regimes and that J_P increases with increasing E(R) in the DD regime. Therefore we think that the transport regime below ～400℃ is basically DD.

From the above discussion we conclude that the transport regime is basically RD above ～400℃ and DD below ～300℃.

V. SUMMARY

The dependence of $J_P(Q_P)$ on T, I, Q_G', and E was measured for nickel foil with deuterium ions of 3～5 keV. The transport regime was found to be basically RD above ～400℃ and DD below ～300℃ under our experimental condition.

REFERENCES

[1] B. L. Doyle, J. Nucl. Mater. 111/112(1982)628.

[2] D. K. Brice and B. L. Doyle, J. Nucl. Mater. 120(1984)230.

[3] B. L. Doyle and D. K. Brice, Rad. Effects 89(1985)49.

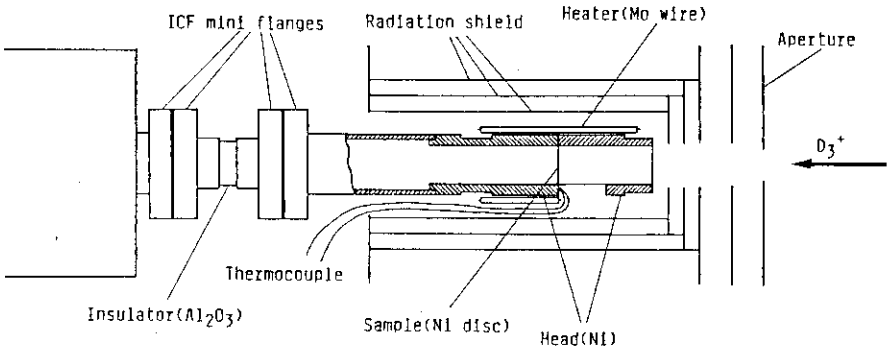

Figure 1 Schematic drawing of the sample head assembly.

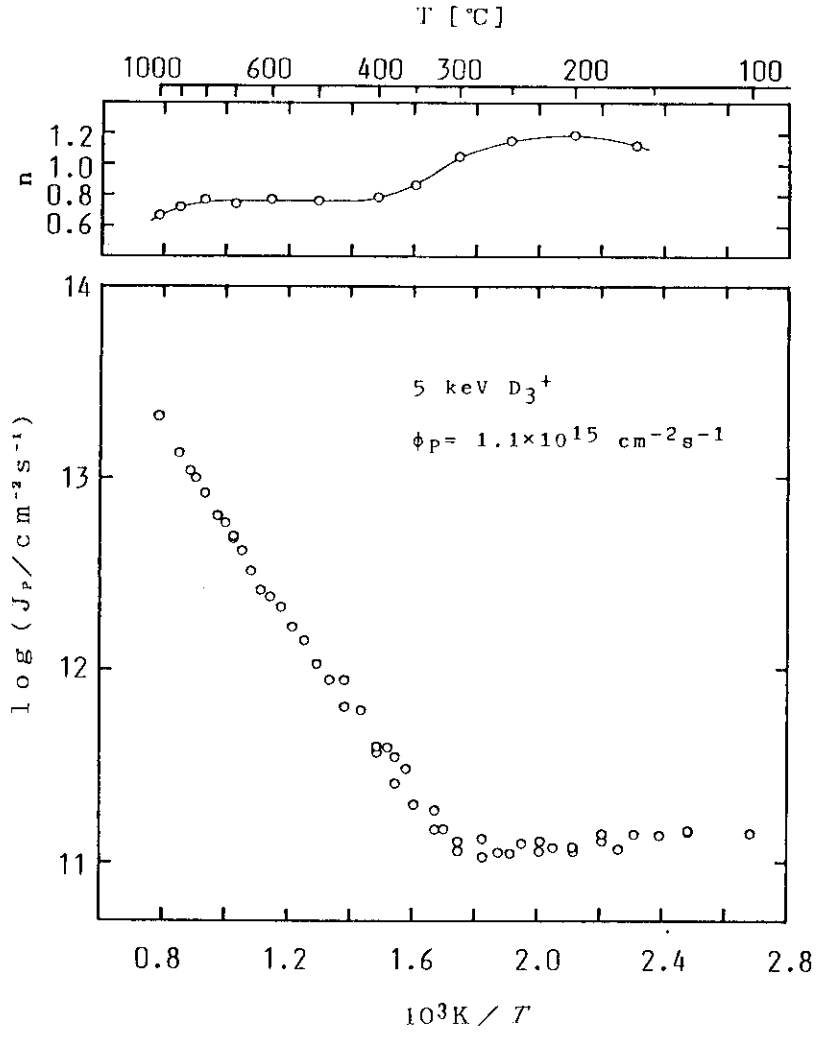

Figure 2 Temperature dependence of increment J_P of the permeation flux caused by deuterium ion implantation, and the power n(see text and figure 3).

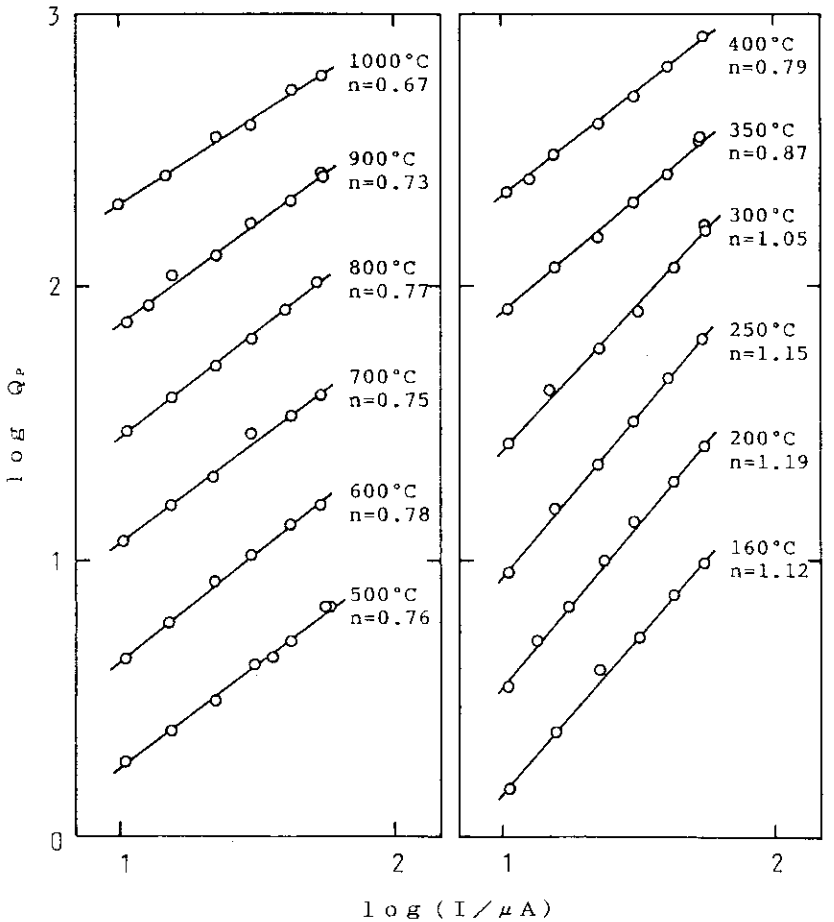

Figure 3 Increment Q_p of the permeation rate caused by deuterium ion implantation as a function of the beam current I. $Q_p/A=J_p$, where A is the implantaion area, and $I \propto \phi_p$. n is the gradient of fitted line, that is, $J_p \propto \phi_p^n$.

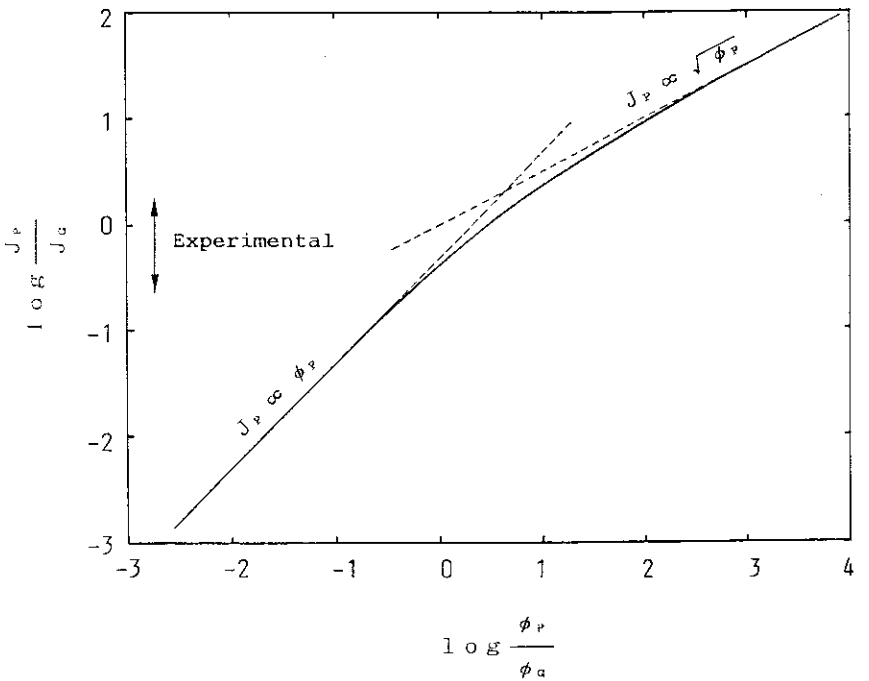

Figure 4 Normalized J_p as a function of normalized ϕ_p calculated by eq.(2). J_p/J_d in the experiment falls in the region indicated in the figure.

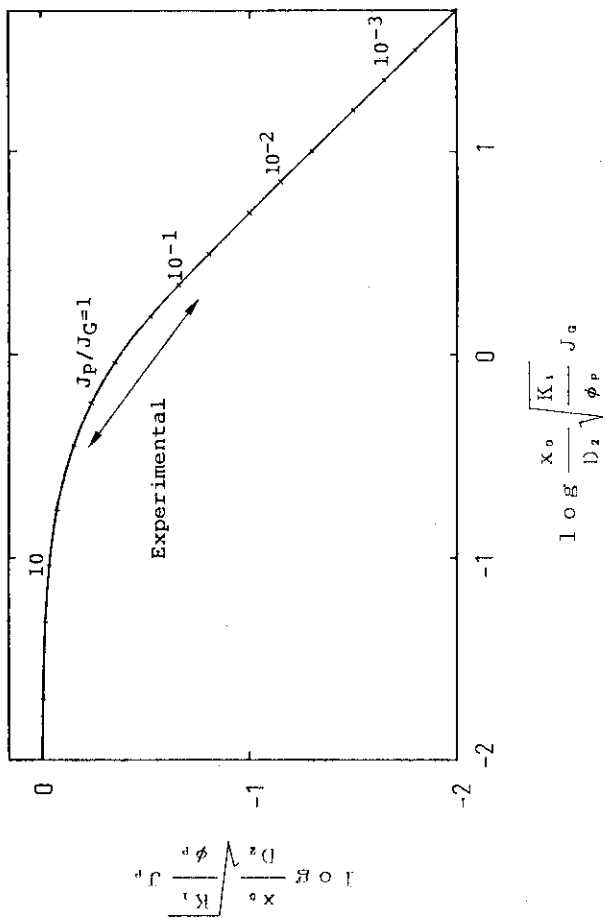

Figure 6 Normalized J_P as a function of normalized J_G calculated by eq.(3). J_P/J_G in the experiment falls in the region indicated in the figure.

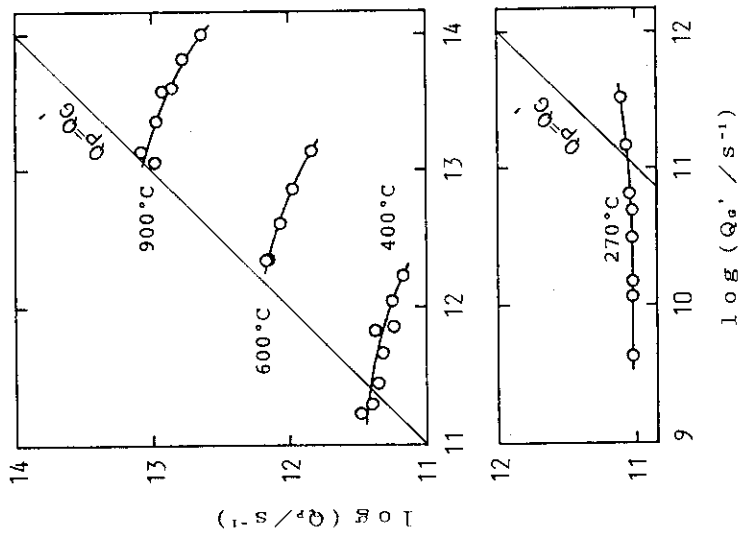

Figure 5 Increment Q_P of the permeation rate caused by ion implantation as a function of rate Q_G' of the permeation driven by gas before and after implantation. Q_G' includes the deuterium permeating through the region besides the implantation area so that $Q_G' > Q_G \equiv J_G A$.

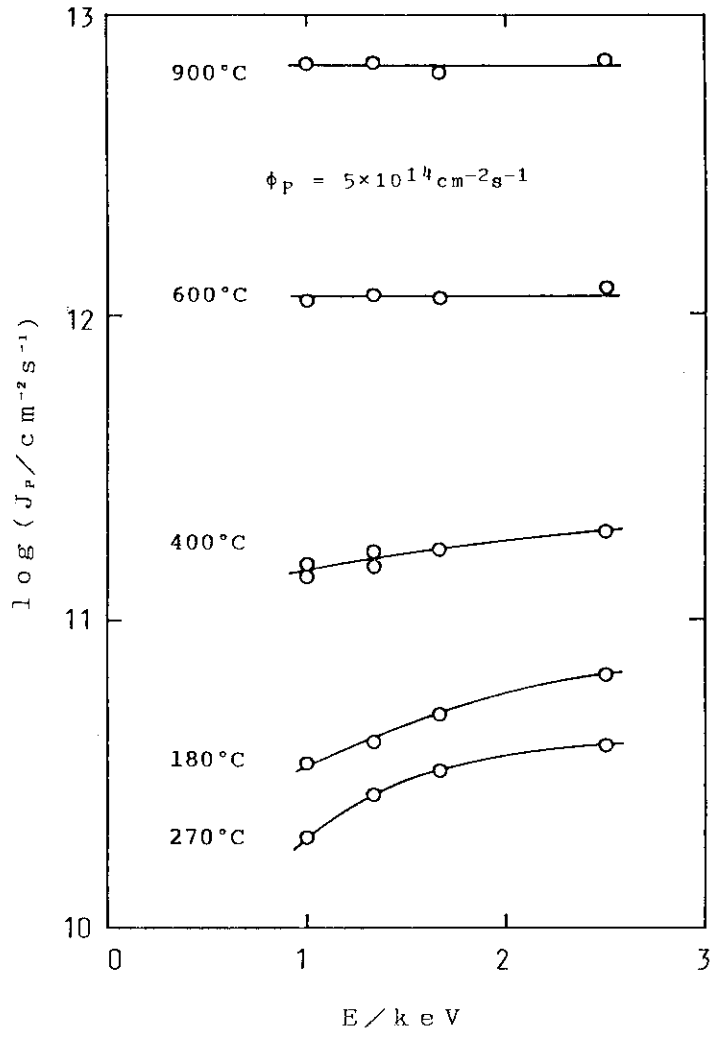

Figure 7 Increment J_P of the permeation flux caused by deuterium ion implantation as a function of the incident energy E per deuterium atom.

No.17
TRITIUM DIFFUSION IN METALS UNDER THERMAL GRADIENT

Masayasu Sugisaki
Department of Nuclear Engineering, Faculty of Engineering
Kyushu University, Fukuoka, Japan

The heat of transport Q* of H, D and T was determined in V, Nb, Ta and Ti by measuring the redistribution of hydrogen isotopes induced by the thermal gradient. The large isotope dependence of Q* was observed in V, Nb and Ta, but not confirmed in Ti.

The heat of transport Q* of hydrogen isotopes in other metals and alloys such as Ni, α-Fe, V-Nb, V-Cr and V-Ti reported by other investigators was reviewed and the common trend of isotope dependence of Q* such that $Q_T^* > Q_D^* > Q_H^*$ was pointed out for hydride-forming metals and alloys.

The influence of the thermomigration upon the tritium permeation through metals and alloys was discussed on the basis of the experimental data of Q* and the general formulation of tritium recycling and permeation.

It was pointed out that the tritium permeation was considerably enhanced by the thermomigration in the case of hydride-forming metals and alloys and suppressed in the case of non hydride-forming metals and alloys, and that the isotope dependence of the enhancement cannot be neglected.

1. Introduction

In a future power fusion reactor, the first wall may be exposed to a severe thermal gradient, so the tritium recycling and permetation processes may be influenced by this thermal gradient. We have pointed out the importance of taking into consideration of the thermomigration of tritium for estimation of tritium permeation through a wall exposed to the thermal gardient.[1]

Recently, the importance of taking into consideration of the non-isothermal condition for the estimation of the tritium permeation has been recognized and some general formulations have been developed.[2-5] However, the experimental data of a heat of transport Q*, which represents the magnitude and direction of the thermomigration, are scarce even for H and D in metals and alloys, in particular the data for tritium are very scarce. So, we have been carrying out the measurement of Q* for H, D and T in metals and alloys in series.

In the present paper, we shall report our recent data of Q* of hydrogen isotopes in some metals and review the data of Q* reported by other investigators. On the basis of these data of Q* and the general formulation of tritium transport through a first wall, we shall discuss the tritium permeation processes through some metals and alloys subjected to the thermal gradient, and explain the important role of the thermomigration.

2. Principle of Measurement of Q*

The diffusion of hydrogen isotopes in metals under the thermal gradient can be expressed by the equation,

$$J = -D\left(\frac{dC}{dx} + \frac{CQ^*}{RT^2}\frac{dT}{dx}\right) \qquad (1)$$

where J is the diffusion flux; D the diffusion coefficient; Q* the heat of transport; C the concentration; T the temperature; X the space coordinates; and R the gas constant.

When a metal, in which hydrogen isotopes are uniformly dissolved, is subjected to the thermal gradient, the diffusion flux is brought about due to the thermal gradient (a second term in eq(1)) in spite of the situation that the concentration gradient does not exist initially. Then, the concentration gradient is gradually built up in the direction either down or up the thermal gradient dependent upon the sign of Q*; simultaneously the ordinary diffusion (a first term in eq.(1)) starts in the direction such that the induced concentration gradient is cancelled; and finally those two diffusion fluxes are counterbalanced and the stationary concentration distribution is built up. Then, the magnitude of Q* can be determined by measuring the built-up concentration distribution.

In the present experiments, the rod-shaped specimens of V, Nb, Ta and Ti were used, the dimension of which was 2 mm in diameter and 50 mm in length. They were loaded with tritium with a gas absorption method, in which the tritiated hydrogen gas was used. The specific activity of tritium of the gas was 870 μCi/mol. The atomic ratio of hydrogen

isotopes to metal was adjusted to be about 0.01. The overall surface of the hydrogenated specimen was coated with a Cu film (0.1 mm in thickness) by electrodeposition from a $CuSO_4$ aqueous solution in order to prevent the leak of tritium out of the specimen at high temperatures. The thermal gradient was imposed in an axial direction of the specimen and its magnitude was adjusted to be about 10°C/cm.

After the diffusion, the specimen was quenched down to room temperature and cut in halves. The tritium content in each half was measured by use of liquid scintillation counting, the details of which was previously reported.

According to the theory of the thermal diffusion the redistribution of tritium in the specimen is expressed by the following equation,

$$\frac{n_L - n_H}{n_L + n_H} = \tanh\left(\frac{Q^*\Delta T}{4RT^2}\right)\left\{1 - \exp\left(-\frac{\pi^2 Dt}{l^2}\right)\right\}, \qquad (2)$$

where n_L and n_H represent the tritium contents in the lower and higher temperature halves of the specimen; T is the temperature difference between the ends of the specimen; l is the length of the specimen; and t is the time for which the thermal gradient is imposed. Then, the values of Q* and D can be determined by measuring the left-hand side of eq.(2) as a function of the time t.

3. Experimental data of Q*

In this section, we shall briefly explain our experimental data of Q* for H, D and T in V, Nb, Ta and Ti and review the data of Q* reported by other investigators. Pincipally, the value of Q* can be classified into two cases; one is a positive value of Q* and the other is a negative value. So, we shall explain the data of Q* in each case.

3.1. Case of positive Q*

The value of Q* for hydrogen isotopes is positive in all previously measured hydride-forming metals. In Fig. 1, our experimental data of Q* for V, Nb and Ta are summarized.[6-8] The values of Q* for H and D in these metals were also measured by Peterson and Smith[9] and the both data are in good agreement. In Fig. 2, our experimental data of Q* of tritium in Ti[10] are shown in comparison with the data reported by Kitada & Koda.[11]

In Figs. 3, 4 and 5 the experimental data of Q* for H and D in V-Nb, V-Cr and V-Ti alloys reported by Peterson and Smith[12] are shown.

The characteristic point of Q* in these matals and alloys is the large isotope dependence such that $Q_T^* > Q_D^* > Q_H^*$.

3.2. Case of negative Q*

The cases of negative values of Q* previously reported are α-Fe and Ni.[13] Their values are shown in Fig. 6. The isotope dependence of Q* in these metals is not clear; i.e. $|Q_D^*| > |Q_H^*|$ in the case of Ni and $|Q_D^*| < |Q_H^*|$ in the case of α-Fe.

4. Contribution of thermomigration to tritium permeation

The energetic D and T ions and neutral atoms escaping from the plasma penetrate into the inside of the first wall and accumulated near the front surface of the wall. These D and T atoms thermally diffuse in both directions of the front and back surfaces of the wall as is schematically shown in Fig. 7.

When the first wall is subjected to the thermal gradient, these diffusion fluxes are inevitably influenced by the thermal gradient. As is shown in Fig. 8, the ordianry diffusion flux due to the concentration gradient is enhanced by the thermal gradient in the case of $Q^*>0$ and suppressed in the case of $Q^*<0$ under the usual reactor condition. We shall evaluate these effects on the basis of the experimental data of Q^* and the general formulation developed by Doyle and Brice.[2]

Before discussing the thermomigration effect, we have to distinguish the rate-determining processes of tritium transport; the first situation is that the diffusion process controls the recycling and permeation processes; the second is that the recombination process at the front surface controls the tritium recycling and the diffusion process controls the tritium permeation; and the third is that the recombination process at front and back surfaces controls the tritium recycling and permeation. The predominace of these processes is determined by the interrelation between the recombination and diffusion rates, and dependent upon the temperature and in some cases also upon the surface condition and the existence of trapping effect inside the wall.

On the basis of the experimental data of diffusion coefficient and recombination coefficient of hydrogen isotopes, the rate-determinig processes are calculated in Fig. 9, in which R represents the recombination-controlled process and D stands for the diffusion-controlled process.

In Fig. 10, the tritium permeation fraction is calculated under an isothermal condition. In Fig. 11, the tritium permeation fraction is calculated under a thermal gradient, in which the temperature at the outer surface is kept 100°C and the temperature at the inner surface is varied. In this calculation, the contribution of the thermomigration is not taken into consideration.

In Fig. 12, tritium permeation fraction is calculated under a thermal gradient by taking into consideration of the thermomigration. As is seen in these figures, the tritium permeation is enhanced by the thermomigration in the case of hydride-forming metals and suppressed in the case of non hydride-forming metals.

In Fig. 13, the isotope dependence of hydrogen isotopes permeation fraction is shown. As is seen in this figure, the tritium permeation fraction is very large compared to other hydrogen isotopes. Therefore, if the contribution of the thermomigration is neglected, the tritium permeation fraction would be underestimated.

5. Conclusions

(1) The heat of transport Q* of H, D and T has been measured and the large isotope dependence has been confirmed.

(2) Summarizing our data of Q* and those reported by other investigators, the common trend of the isotope dependence such that

$$Q_T^* > Q_D^* > Q_H^*$$

has been pointed out for hydride-forming metals and alloys.

(3) The tritium permeation rate is considerably enhanced by the thermomigration in the hydride-forming metals and alloys and suppressed in the non hydride-forming metals.

(4) The isotope dependence of enhancement of the tritium permeation cannot be neglected, so the data of Q* of tritium need to be accumulated for a large number of metals and alloys.

REFERENCES

1) M. Sugisaki, K. Idemitsu, S. Mukai and H. Furuya, J. Nucl. Mater., 103(1982)1493.

2) D. K. Brice and B. L. Doyle, J. Nucl. Mater., 120(1984)230
B. L. Doyle and D. K. Brice, J. Nucl. Mater., 122/123(1984)1523.

3) M. I. Baskes, Sandia National Laboratories Report, SAND83-8231 and SAND80-8201.

4) P. Wienhold, I. Ali-Kahan, K. J. Dietz and F. Waelbroeck, J. Nucl. Mater., 85/86(1979)1001, and P. Wienhold, M. Profant, F. Waelbroeck and J. Winter, Rep. Jul-1825(1983)

5) K. Ashibe and K. Ebisawa, J. Nucl. Mater., 128/129(1984)739.

6) M. Sugisaki, S. Mukai, K. Idemitsu and H. Furuya, J. Nucl. Mater., 115(1983)91.

7) M. Sugisaki, S. Mukai and H. Furuya, J. Less-Common Metals, 107(1985)79.

8) M. Sugisaki and H. Furuya, Z. fur Phys. Chem., Neue Folge, 145(1985)251.

9) D. T. Peterson and M. F. Smith, Met. Trans., 13A(1982)821.

10) M. Sugisaki and H. Furuya, J. Nucl. Mater., 128/129(1984)734.

11) M. Kitada and S. Koda, Scripta Met., 3(1969)583.

12) D. T. Peterson and M. F. Smith, Met. Trans., 14A(1983)871.

13) O. D. Gonzalez and R. A. Oriani, Trans. Met. Soc. AIME, 233(1965)1878.

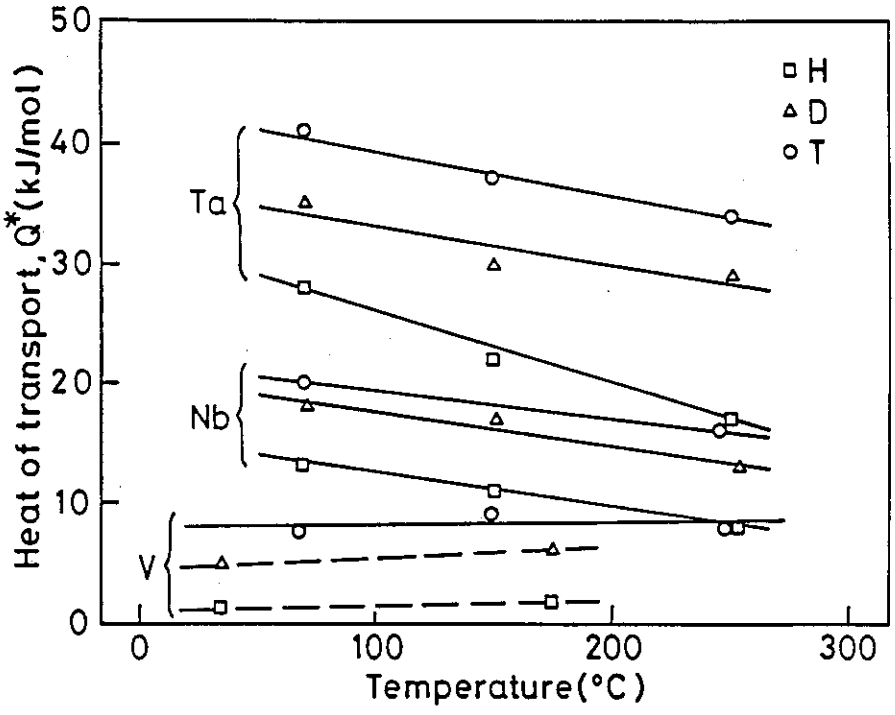

Fig. 1. Experimental data of Q* for H, D and T in V, Nb and Ta

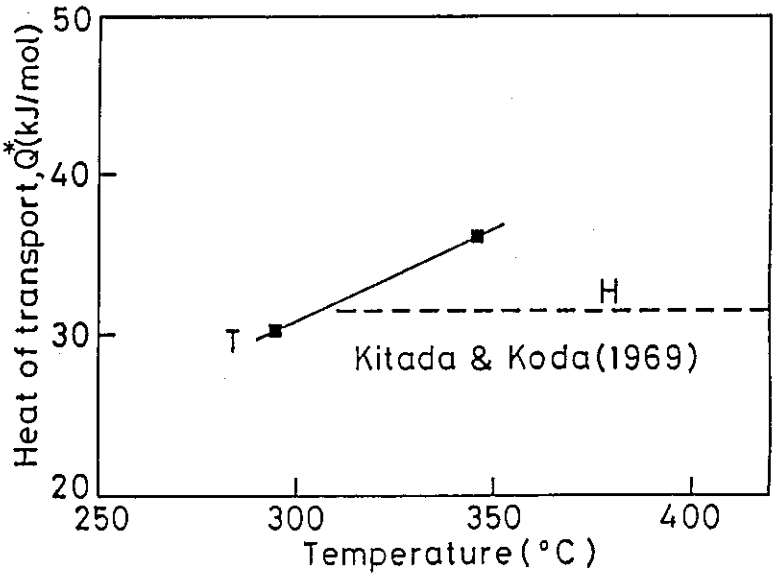

Fig. 2. Experimental data of Q* for H and T in Ti.

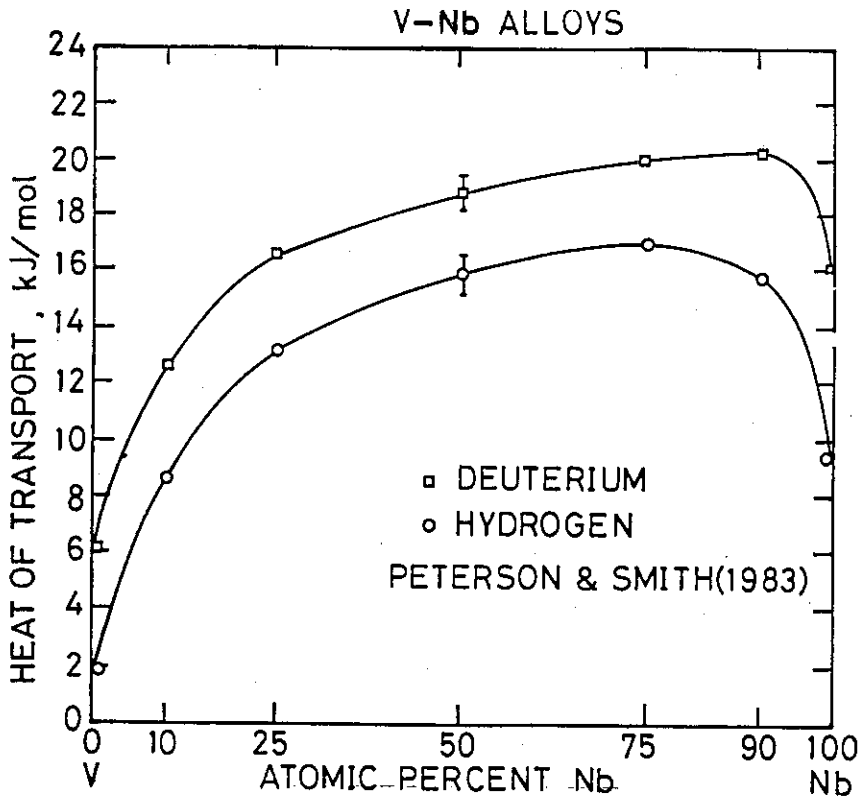

Fig. 3. Experimental data of Q* for H and D in V-Nb alloys reported by Peterson and Smith

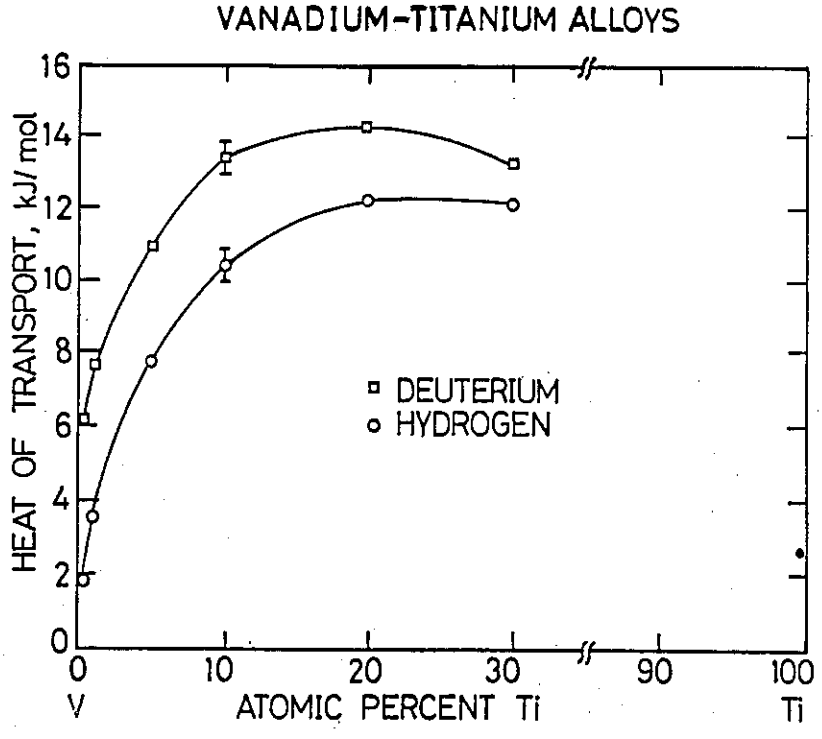

Fig. 4. Experimental data of Q* for H and D in V-Ti alloys reported by Peterson and Smith

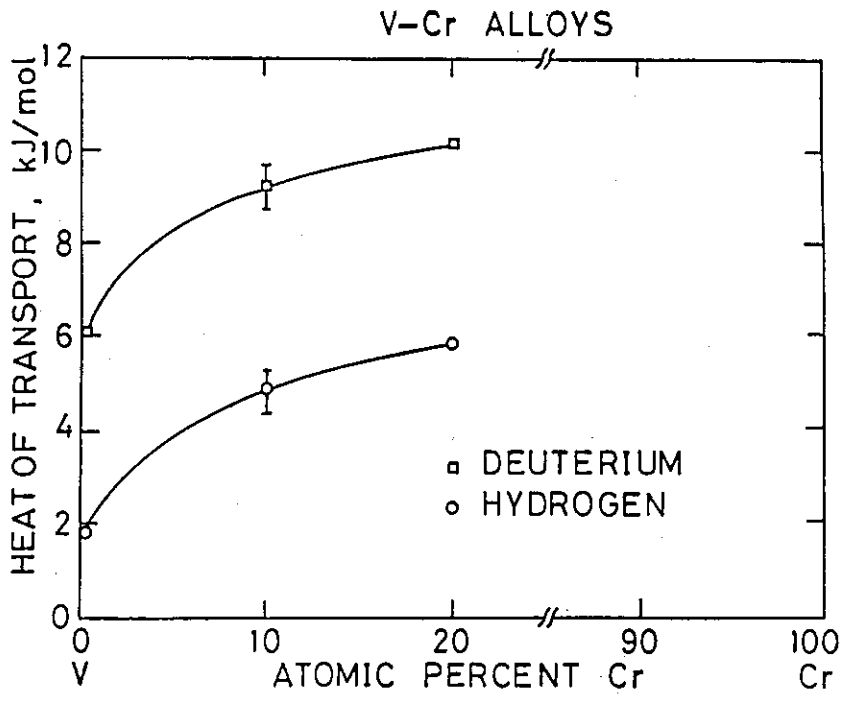

Fig. 5. Experimental data of Q* for H and D in V-Cr alloys reported by Peterson and Smith

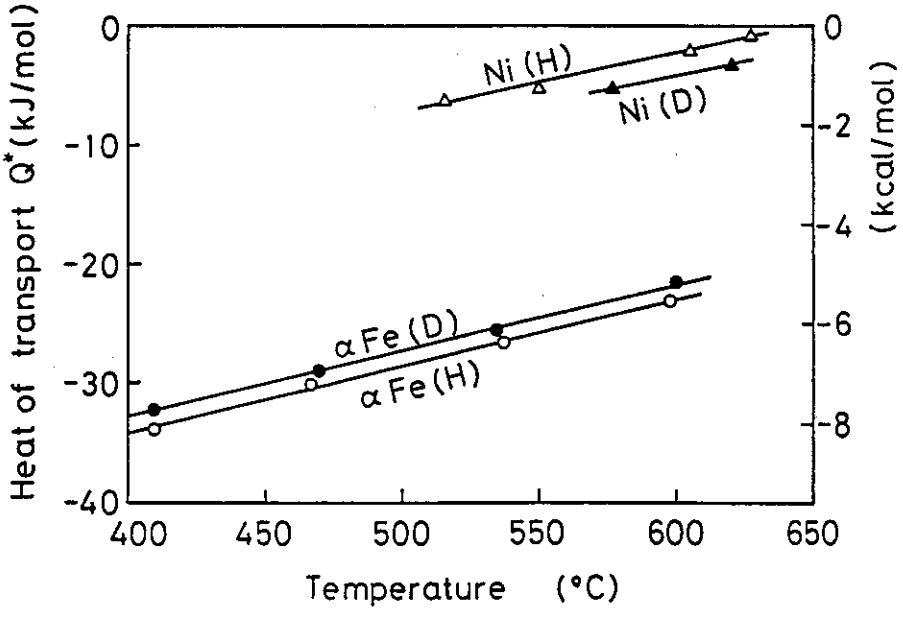

Fig. 6. Experimental data of Q* for H and D in α-Fe and Ni reported by Gonzarez and Oriani

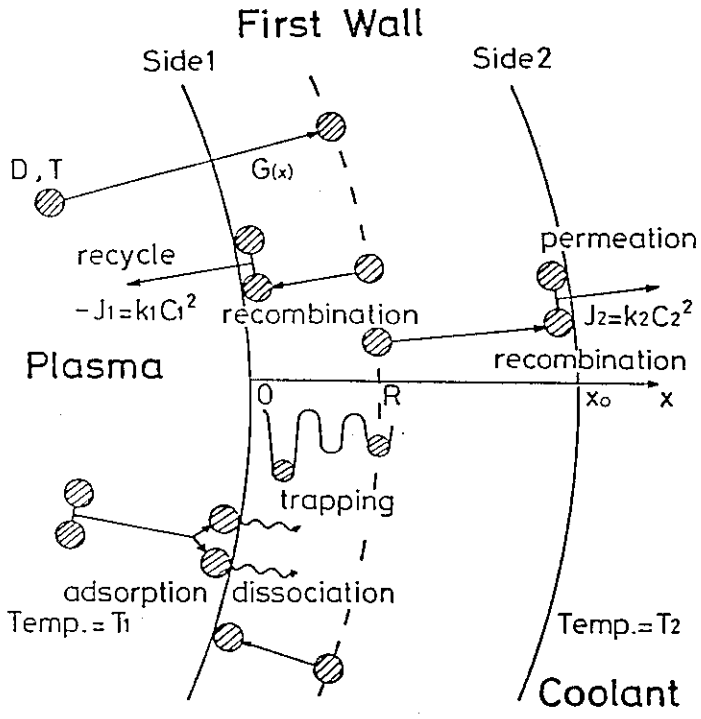

Fig. 7. Schematic description of hydrogen isotopes recycling and permeation in a first wall

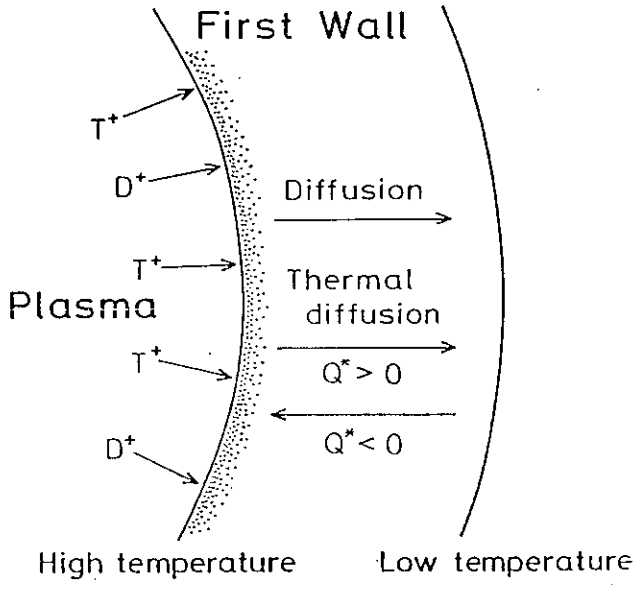

$$J = -D\left(\frac{dc}{dx} + \frac{cQ^*}{RT^2}\frac{dT}{dx}\right)$$

Fig. 8. Influence of the thermomigration upon the tritium recycling and permeation

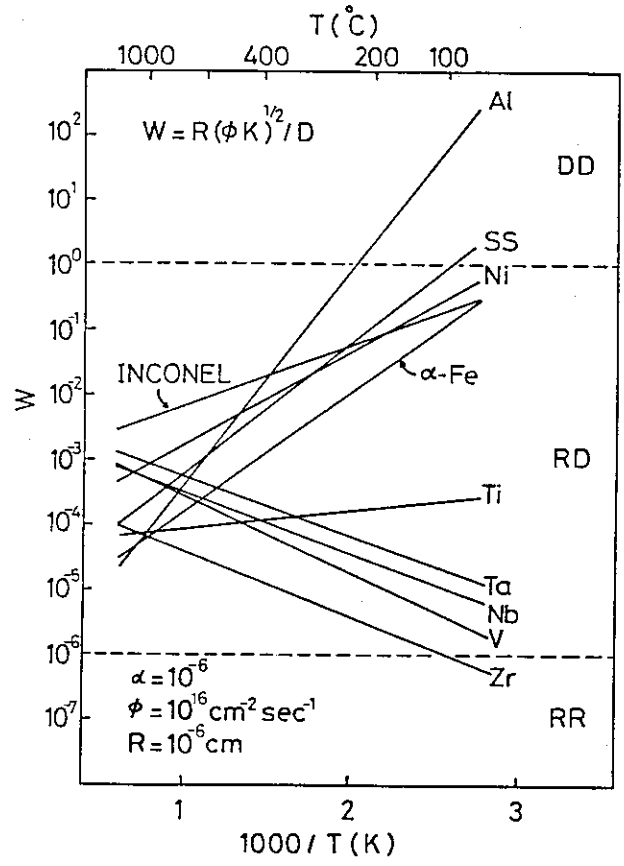

Fig. 9. Temperature dependence of the rate-determining processes for tritium recycling and permeation

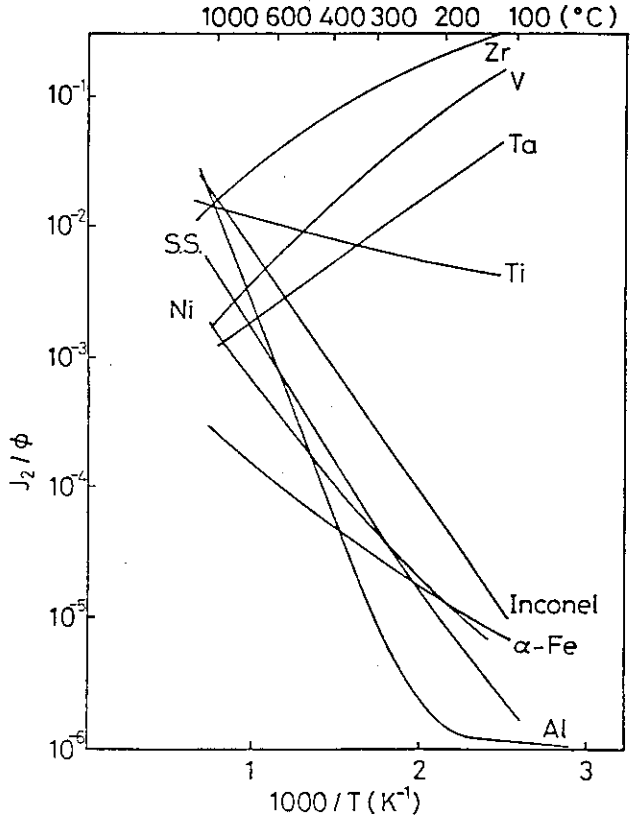

Fig.10. Tritium permeation fraction under an isothermal condition

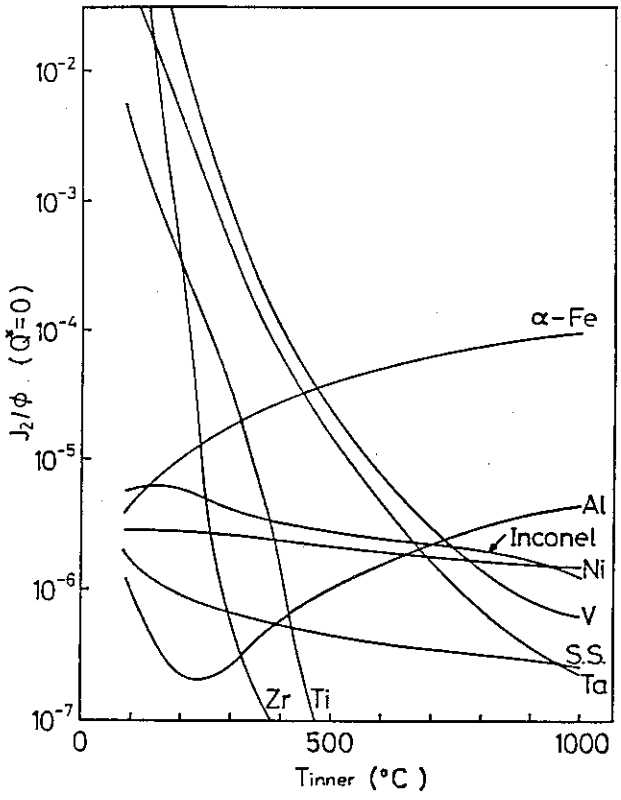

Fig.11. Tritium permeation fraction under a thermal gradient where the contribution of the thermomigration is not taken into consideration

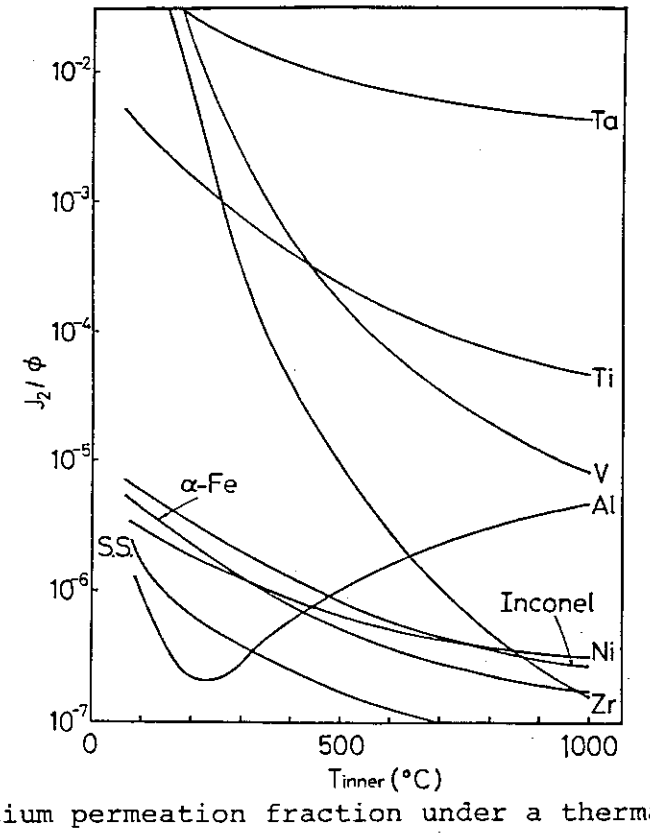

Fig.12. Tritium permeation fraction under a thermal gradient where the contribution of the thermomigration is taken into consideration

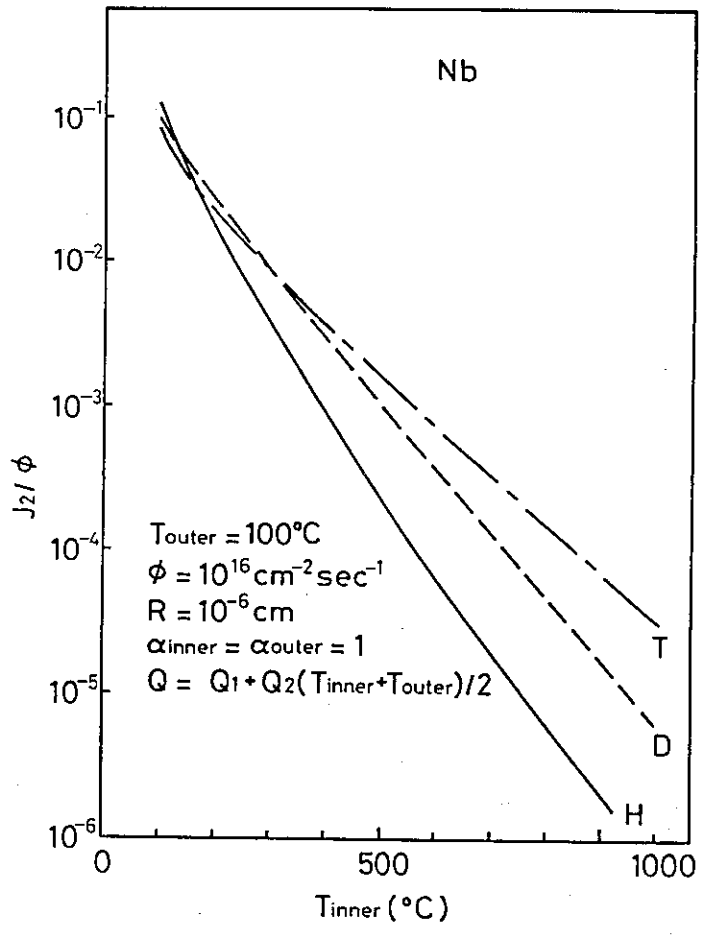

Fig.13. The isorope dependence of hydrogen isotopes permeation fraction in Nb.

No.18 Tritium Retention in Graphite*

R.A. Causey and K.L. Wilson
Sandia National Laboratories
Livermore, California 94550

The hydrogen isotope retention for samples exposed to a high fluence of 100 eV deuterons and tritons has been measured for the graphites ATJ-2000, Great Lakes H-451, Schunk and Ebe FE-159, and FMI 4-D weave carbon composite. These measurements were performed at a series of temperatures, and results were compared to earlier results for POCO AXF-5Q graphite. Both grain size and amount of open porosity were found to affect the amount of retention.

1. Introduction

Graphite has recently emerged as one of the more important materials for use in present-day fusion reactors. Its use as a limiter effectively lowers the amount of high-Z impurities in the plasma; however, there may soon develop a problem with tritium inventories as today's machines begin to experiment with D-T plasmas. As a limiter material, graphite will be exposed to very high fluences of energetic tritium ions and charge exchange neutrals. Because graphite normally has a very high specific surface area and a known affinity for hydrogen isotopes, it is quite likely that it will pose a problem for machines with limited on-site tritium inventories.

This paper presents the results of an experimental study on the retention of deuterium and tritium in several different graphites exposed to very high fluences of 100 eV ions. The graphites tested were ATJ-2000, Great Lakes H-451, Schunk and Ebe FE-159, and FMI 4-D weave carbon composite. The results are compared to those for POCO AXF-5Q,

*This work supported by U.S. Department of Energy.

a graphite whose tritium retention properties were given in an earlier report[1].

2. Experimental Procedures

All experiments were performed in the Tritium Plasma Experiment (TPX), which has been described in detail elsewhere[2]. It is a plasma discharge apparatus utilizing rf heating and magnetic confinement where the energy of the ions striking the sample is controlled by applying a negative bias to the electrically isolated sample holder. The plasma feed gas used to keep the system at the required 0.66 Pa was 99% deuterium and 1% tritium. Besides singly charged diatomic ions, the fluxes and fluences listed in this report include low energy neutrals. These occur in approximately equal proportions in this experimental apparatus. The flux was maintained at 3.7×10^{16} D/cm^2-s for 1.5 hours to yield a fluence of 2.0×10^{20} D/cm^2. The graphite samples were 1.0 cm wide, 1.5 cm long, and 0.1 cm thick. Sample preparation consisted of ultrasonic cleaning in alcohol, followed by an anneal at 1273 K for 1 hour in vacuum. After plasma exposure the samples were dissolved in chromosulfuric acid. The acid solution was then partially distilled to yield a small tritiated water sample for liquid scintillation counting. Calibration was performed by adding known amounts of a tritiated water standard to the acid solution during dissolution of uncontaminated graphite samples. The deuterium content of the samples were determined by multiplying the tritium content by the isotope ratio in the plasma.

3. Results and Discussion

Figures 1 through 4 show the comparison of the deuterium-tritium retention in the different graphites to that reported earlier for POCO

grains, the atoms have to diffuse relatively large distances to uniformly load the sample. Because these experiments were limited to 1.5 hours, there was not time for this to occur even at the highest temperature of 1473 K. This would explain the lower retention in the carbon composite where the individual strands are small, but the porosity is also small. The lower retention in the Great Lakes H-451 graphite is due to a similar effect. Its grain size of 700 um, about 70 times that of POCO graphite, prevents even approach to equilibrium during the 1.5 hour exposure. The limited retention in the other two graphites at the higher temperatures is not understood at this time. Both materials are thought to have moderate grain size and porosity. As the effect of impurities on the retention has yet to be investigated, it is not possible at this time to conclude that this was the determining factor.

Work will be continued on the measurements of tritium and deuterium retention in graphite. The ultimate goal of this research is the ability to predict the hydrogen isotope retention in any type of graphite if the grain size, amount of open porosity, and impurity levels are known. This knowledge along with an understanding of hydrogen and carbon codeposition will allow fairly accurate projections for tritium inventories in present and future fusion reactors.

4. Conclusions

Of the five different graphites tested in this research project for deuterium and tritium retention due to plasma and gas exposure, POCO AXF-5Q retains the highest amount at the higher temperatures, and ATJ-2000 retains the highest quantity at lower temperatures. The FMI 4-D weave carbon composite

showed consistently low retention at all temperatures. Both grain size and amount of open porosity appear to affect the amount of retained hydrogen isotopes.

1. R.A. Causey, M.I. Baskes, and K.L. Wilson, J. Vac. Sci. Technol. A, 40 (1986) 1189.
2. R.A. Kerst, J. Vac. Sci. Technol., 20 (1982) 1267.
3. R. A. Causey and K. L. Wilson, J. Nucl. Mater. 138 (1986) 57.
4. D.K. Brice, B.L. Doyle, and W.R. Wampler, J. Nucl. Mater. 111/112, (1982) 598.

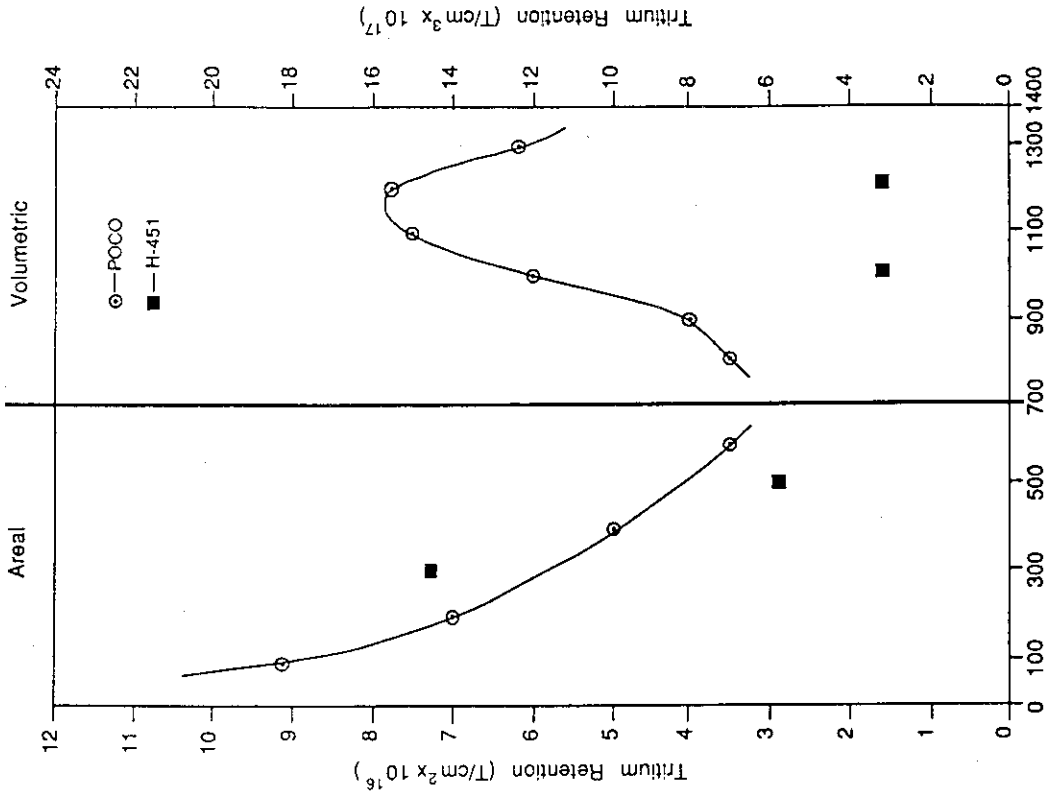

Fig. 2. Comparison of D-T Retention in Great Lakes H-451 Graphite to that in POCO AXF-5Q Graphite.

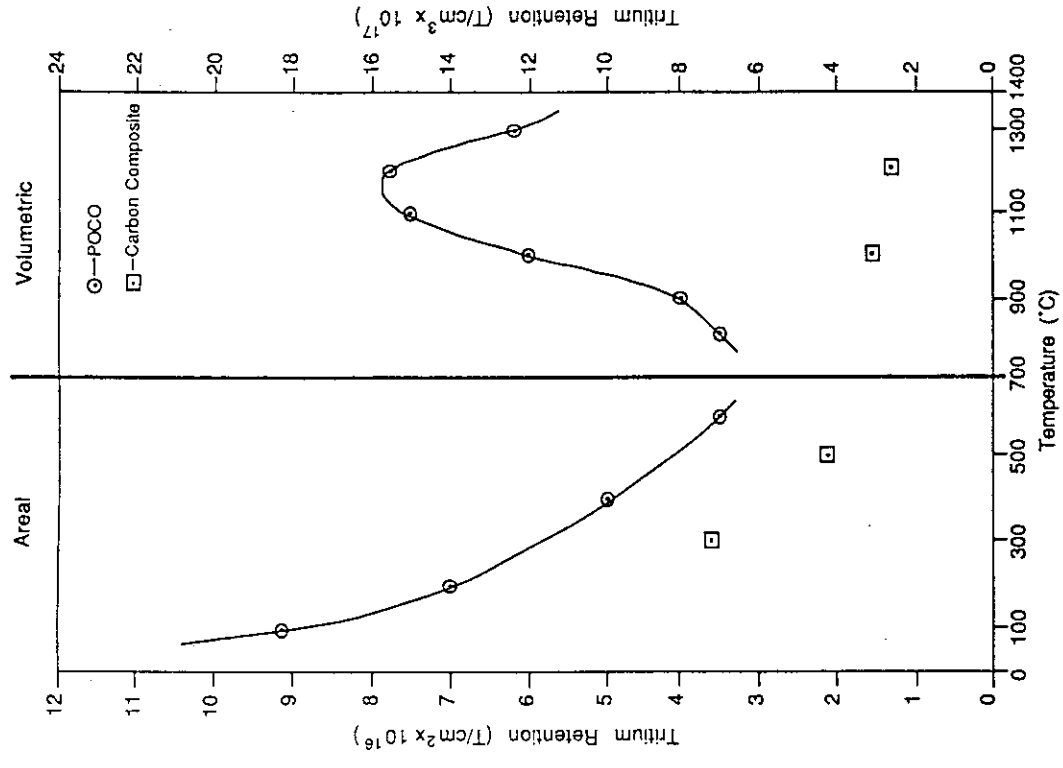

Fig. 1. Comparison of D-T Retention in FMI 4-D Weave Carbon Composite to that in POCO AXF-5Q Graphite.

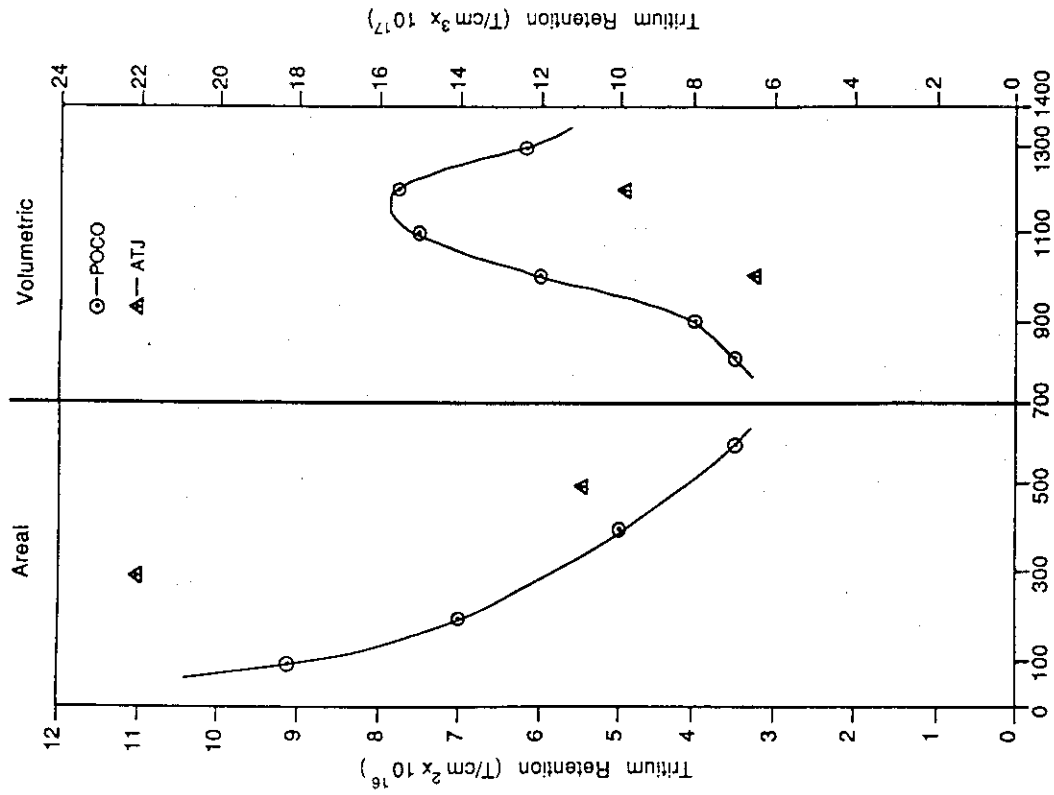

Fig. 4. Comparison of D-T Retention in ATJ-2000 Graphite to that in POCO AXF-5Q Graphite.

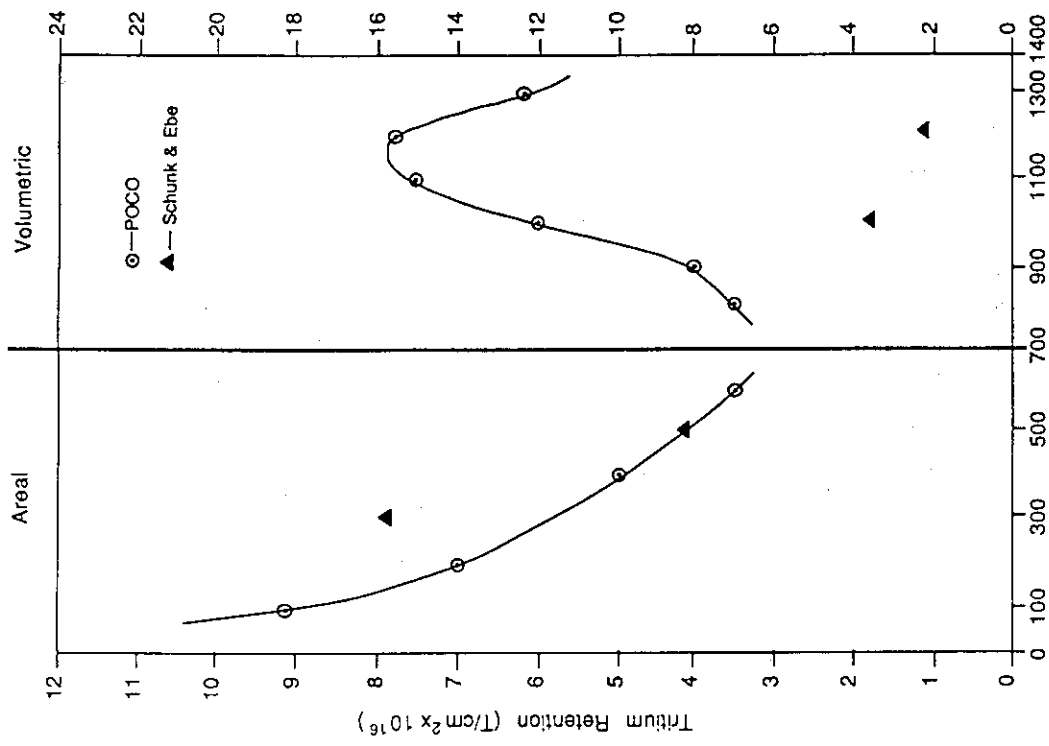

Fig. 3. Comparison of D-T Retention in Schunk & Ebe FE 159 Graphite to that in POCO AXF-5Q Graphite.

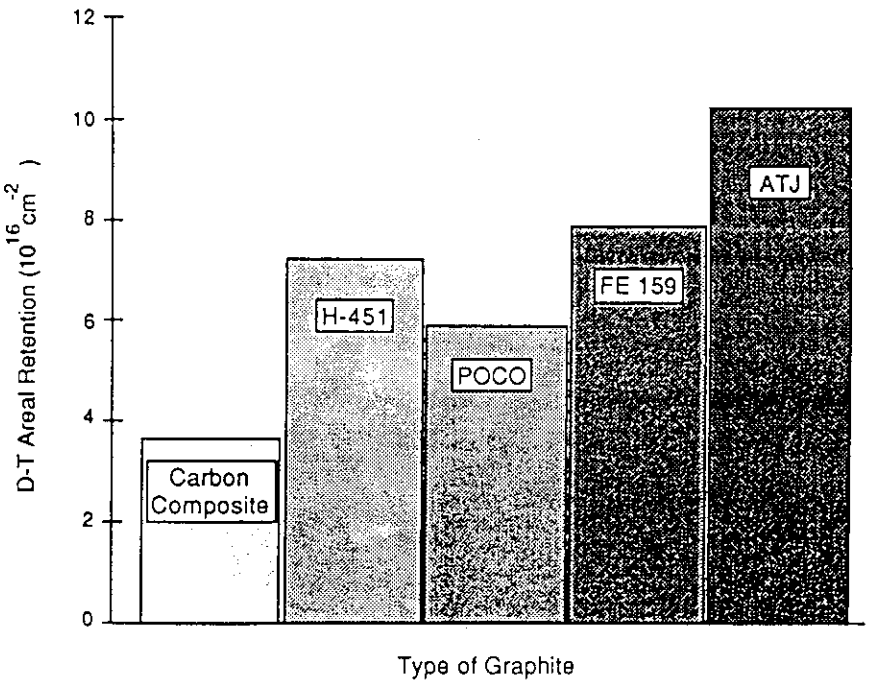

Fig. 5. Comparison of D-T Retention in Several Graphites at 573 K.

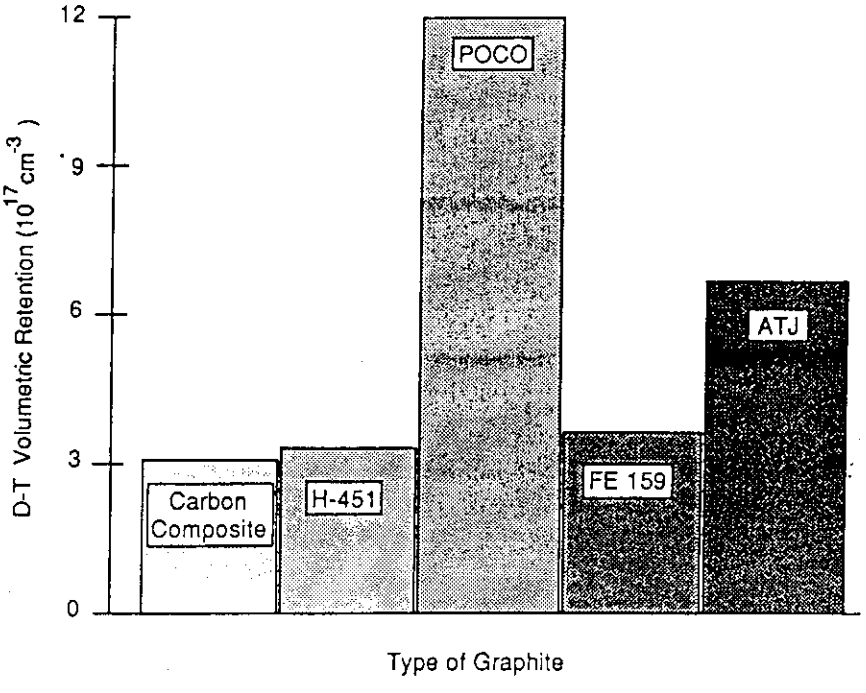

Fig. 6. Comparison of D-T Retention in Several Graphites at 1273 K.

No.19 Conversion of Tritium Gas to Tritiated Water at Low Tritium Concentration*

H. Noguchi[1], C. E. Easterly[2], and M. R. Bennett[3]

[1]Department of Health Physics
Japan Atomic Energy Research Institute
Tokai-mura, Naka-gun, Ibaraki-ken, 319-11, Japan

[2]Health and Safety Research Division
[3]Chemistry Division
Oak Ridge National Laboratory
Oak Ridge, Tennessee 37831, U. S. A.

ABSTRACT

The conversion reaction of tritium gas (T_2) to tritiated water was studied experimentally at initial tritium concentrations between 2.6×10^{-4} and 1.3 Ci/m^3 in air. Effects of water vapor and catalysts on the conversion reaction were also examined. The potential catalysts, stainless steel, copper, paint and platinum black were used.

It was found that first-order rate constants for the reaction in air are independent of initial tritium concentration, and that there is no effect of water vapor on the reaction. The conversion was insensitive to the presence or absence of stainless steel and copper. Paint, which did not influence the rate constant, sorbed T_2 and HTO, but the latter was desorbed from the paint by heating. Platinum black produced a remarkable increase of the rate constant.

* Research conducted at the Oak Ridge National Laboratory under the U.S.A.-Japan Fusion Cooperation Program. Partial support provided by the Fusion Safety Program, EG&G Idaho, under Martin Marietta Energy Systems, Inc., Contract DE-AC05-OR21400 with the U.S. Department of Energy.

INTRODUCTION

Tritium gas can be converted into tritiated water owing to various environmental factors. Since tritiated water is about 25,000 times more radiotoxic than tritium gas [1], the conversion reaction produces an increased radiological hazard for workers and the public.

The conversion inside a building (e.g. a fusion reactor room) is different from that in the natural environment. The former is mainly due to tritium β-ray induced reactions and catalytic reactions. A dominant reaction in the environment is probably oxidation by microorganisms in soil [2].

In the design of a fusion reactor room and in particular an air detritiation system, it is essential to determine a conversion rate of tritium gas to tritiated water at low tritium concentration. The tritium concentration in the reactor room is estimated at ~1 Ci/m^3 under accident condition. Adsorption/desorption of tritiated water vapor at the wall surface of the reactor room will influence the flow rate of the air detritiation system [3].

Conversion of tritium gas in the gas phase, which is related to a reaction inside a building, has been studied by several workers over a tritium concentration range of 10^{-3} to 10^{6} Ci/m^3 [4-8]. Dorfman and Hemmer [4] found that conversion of tritium gas in a mixture of hydrogen and oxygen is first-order concentration dependent for tritium concentrations between 9.4×10^{4} and 3.2×10^{5} Ci/m^3. Casaletto et al. [5] described that both conversion reactions in dry air and in oxygen were second-order dependent for the concentration between 10 and 10^{3} Ci/m^3 and that the conversion was caused by β particles emitted from tritium. Belovodskii et al. [6] observed that the conversion reaction had a 5/3 power dependence on concentration over a concentration range of 1 to 600 Ci/m^3 in humid air and in a mixture of oxygen and argon. At lower tritium concentrations, our previous data [7,8] indicated that the rate constants of the conversion reaction in air and in nitrogen are independent of initial T_2 concentration over a tritium concentration range of 10^{-3} to 1 Ci/m^3.

On catalytic conversion reaction, Eakins and Hutchinson [9] found that steel, aluminum and platinum increase the rate constants for the

conversion in dry air by factors of 7.5, 7.0 and 43, respectively, at an initial tritium concentration of 20 Ci/m^3.

We have measured the rate constants for the T_2 conversion reaction at a low initial concentration of 2.6×10^{-4} Ci/m^3, which is lower than the concentration in our previous experiment by about one order of magnitude, and have also examined the reaction at initial T_2 concentrations between 10^{-3} and 1 Ci/m^3 to confirm the previous data. Further, the isotopic exchange reaction of T_2 with water vapor and the catalytic reaction on surfaces of stainless steel, copper, platinum black and paint were studied at low concentrations.

EXPERIMENTAL

Two types of reaction flasks were used in the experiment: (1) Pyrex spherical flasks (about 320 cm^3), and (2) Pyrex spherical flasks (about 360 cm^3) which separate at the equator and have ground-glass flanges to maintain the integrity of the system [8,10]. The former were used for the gas phase reactions and the latter for the catalytic reactions. The flasks are shown in Fig. 1. Both flasks have a cylidrical branch to capture produced HTO with liquid nitrogen.

After evacuating to ~10^{-4} Pa, the flasks were filled with the desired amount of T_2 gas. They were then filled to atmospheric pressure with either room air (RH 15-60 %) or humidity controlled air (RH ~0 and ~100 %). In the catalytic reaction studies, catalysts were inserted into the flasks before introducing T_2 gas. Stainless steel, copper, platinum black and paint (oil base semi-gloss enamel) were chosen as catalysts in the experiments. The stainless steel and copper foils were cleaned with carbon tetrachloride and were then dried before inserting into the flask. Powdery platinum black of 7 g attached to a stainless steel foil with epoxy resin and enamel painted on a stainless steel foil were used as the catalysts. The characteristics of these catalysts are shown in Table 1.

Stopcocks and ground-glass joints were lubricated with Apiezon H grease. High vacuum silicone grease was used for the flanges.

The flasks prepared for the gas phase and the catalyst experiments were kept at a room temperature for periods ranging from 1 day to

3 months and were then assayed for both reacted and unreacted tritium using a sampling apparatus depicted in Fig. 2. The branch of the flask was immersed in liquid nitrogen to capture produced HTO. Helium gas was then passed through the flask to sparge T_2 gas which was then oxidized to HTO by passage through a bed of copper oxide at ~600 ℃. The HTO was then captured in liquid nitrogen trap No. 3. After the helium was passed through for ~1 hour, hydrogen gas was added to produce non-radioactive water in sufficient volume to allow more efficient removal of the trace amounts of HTO in trap No. 3 by acting as a diluent.

Concentrations of initial T_2 and produced HTO were obtained by measurement of the corresponding activities in a liquid scitillation counter. Percentage of conversion, F, was calculated using these concentrations as follows:

$$F = 100[HTO]/[T_2]_0 = 100\{1-\exp(-kt)\}, \quad (1)$$

where [HTO] is the radioactive concentration of HTO produced, $[T_2]_0$ is the initial radioactive concentration of T_2, k is the first-order rate constant, and t is the time. The conversion percentage was kept below 3 % in most cases. Therefore, equation (1) was approximated by

$$F = 100kt. \quad (2)$$

RESULTS AND DISCUSSION

1. Conversion of low concentration T_2 in air

The conversion percentage of T_2 in air at an initial concentration of 2.6×10^{-4} Ci/m^3 is shown in Fig. 3 as a function of time. The percentage was directly proportional to the elapsed time. The rate constant was found to be 2.3×10^{-9} s^{-1}, using equation (2) and the method of least squares. The straight line in the figure was not drawn through the origin. The increase on the ordinate from the origin was most likely caused by a contamination of small amount of tritiated compound that entered into the flasks during the preparation.

In the present experiment, six rate constants were obtained over the initial T_2 concentration range of 2.6×10^{-4} to 1.3 Ci/m^3. In Fig. 4, the rate constants are plotted agaist the initial tritium concentration. Experimental data obtained by other workers under the condition of higher

tritium concentrations in air also plotted in Fig. 4 with our previous data. Our previous results have indicated that the rate constants for the conversion of low concentration T_2 are independent of initial T_2 concentration. Agreement between the present and the previous results verifies that this conclusion is true down to an initial T_2 concentration of 2.6×10^{-4} Ci/m^3. The average of the rate constants including our previous data was $(1.8\pm0.5)\times10^{-9}$ s^{-1}.

It should be noted in Fig. 4 that the rate constants increase with initial tritium concentration above ~10 Ci/m^3 but are constant below the concentration. This suggests that dominant mechanisms on the conversion at high tritium concentration differ from those at low concentration. At high tritium concentrations, β particles emitted from tritium would induce the conversion of T_2 [5,11]. As we discussed in the previous report [8], at low T_2 concentrations, THe^+ produced following T_2 decay would play the most important role for the production of tritiated water because of the agreement of the physical decay constant (1.78×10^{-9} s^{-1}) of tritium and the measured rate constant.

2. Conversion of T_2 in the presence of water vapor

The effect of water vapor on the rate constant was studied at an initial concentration of ~1.3 Ci/m^3. The results are shown in Fig. 5. The rate constants calculated using equation (2) were 1.3×10^{-9}, 1.5×10^{-9} and 1.5×10^{-9} s^{-1} for RH ~0, 40 and ~100 %, respectively. These data indicate that water vapor has no effect on the conversion, that is, an isotopic exchange reaction of T_2 with water vapor does not proceed at low tritium concentration.

Casaletto et al. [5] observed that while water vapor in oxgen increased the conversion rate constant by a factor of 3 at a relatively high tritium concentration, the rate constant in actual breathing air was approximately the same as in dry air. Eakins and Hutchinson [9], however, described that the rate constant in humid air was about 5 times larger than in dry air at a tritium concentration of 20 Ci /m^3. Our present results are in agreement with the observation of Casaletto et al. [5]. Further experiment on the isotopic exchange reaction is required for a wide range of tritium concentration.

3. Effect of catalyst on the conversion

In Fig. 6, conversion percentages for the reactions in the presence or absence of the stainless steel (type 309) foil are plotted as a function of time at an initial T_2 concentration of 0.2 Ci/m^3. It can be seen that the tritium conversion is insensitive to the presence of the foil, since a normal rate constant of 1.4×10^{-9} s^{-1} was obtained from this experiment. As a follow-up experiment, after produced HTO was removed by washing the surface of the foil, the foil was heated at 600 ℃ to desorb tightly bound tritium. However, no additional tritium was detected.

Table 2 summarizes the rate constants of the T_2 conversion reaction in the presence of the catalysts shown in Table 1. The rate constants for stainless steel and copper were the same as the average constant (1.8×10^{-9} s^{-1}) in air alone within experimental error. Thus, stainless steel and copper had no effect on the tritium conversion.

For the paint sample, it was observed that both amounts of T_2 and HTO recovered from the flask after ten days from the T_2 filling, were considerably less than expected ones. It was hypothesized that the paint absorbed T_2 and HTO. Hence, an experiment was designed to capture T_2 and HTO which were desorbed from the paint by heating at 250 ℃, with liquid nitrogen. The amount of desorbed HTO was more than twice as much as that of HTO recovered initially. However, no additional T_2 was recovered from the paint suggesting the possibility that the T_2 reacted with the paint to form a chemically stable compound. The rate constant for the paint sample in Table 2 was calculated using the combined total amounts of the initially recovered HTO plus the desorbed HTO and the initial T_2 concentration estimated from other flasks. No significant change in the rate constant was found for the paint sample compared with that for air alone. In addition to the tritium conversion in gas phase, the adsorption and desorption of tritium on painted surface would complicate behavior analysis of tritium released in a building.

As expected, there was a marked increase in the rate constant for platinum black by factors of ~300 to ~1600 over that in air alone. This indicates that in the catalytic experiments, a diffusion process of T_2 molecules from air to the surface of the catalyst is not a rate-deter-

mining step. The conversion percentages for the platinum black experiment were 61 and 59 % for the periods of 4 and 18 days, respectively. This may imply that the conversion reaction reaches an equiliblium.

Eakins and Hutchinson [9] observed that steel, aluminum and platinum catalysts increased the rate constants of the tritium conversion in dry air at an initial tritium concentration of 20 Ci/m^3 and that the catalytic effect was further enhanced in humid air. Our experimental data for platinum black show a similar tendency to that of Eakins's result for platinum. However, our data for the stainless steel and copper, which had no catalytic effect, were different from Eakins's results for steel and aluminum. This may be attributed to a difference in the catalysts and the tritium concentration between the present and Eakins's study.

CONCLUSION

The results of these experiments on the conversion reaction of tritium gas (T_2) to tritiated water (HTO) indicate that the rate constants are independent of initial T_2 concentration down to 2.6×10^{-4} Ci/m^3, which is lower than the previous concentration by about one order of magnitude. The average of the rate constants was $(1.8\pm0.5)\times10^{-9}$ s^{-1}; this value equals the tritium decay constant.

Isotopic exchange reaction of tritium gas with water vapor was negligible at low tritium concentrations.

No effect of stainless steel and copper on the conversion reaction was observed at an initial tritium concentration of ~0.2 Ci/m^3. Platinum black, however, increased the rate constant remarkably. Oil-base enamel paint, which did not influence the rate constant, sorbed T_2 and HTO in rather large quantities, but only the latter was easily desorbed from the paint by heating. The adsorption and desorption of tritium on painted surfaces would complicate behavior analysis of tritium released in a building.

REFERENCES

[1] INTERNATIONAL COMMISSION ON RADIOLOGICAL PROTECTION; ICRP

Publication 30, Part 1, Pergamon, Oxford (1979).

[2] J. C. McFARLANE, R. D. ROGERS and D. V. BRADLEY Jr.; Environ. Sci. Technol., 13, 607 (1979).

[3] IAEA, International Tokamak Reactor, Phase Two A, Part 1, IAEA, Vienna (1983).

[4] L. M. DORFMAN and B. A. HEMMER; J. Chem. Phys., 22, 1555 (1954).

[5] G. J. CASALETTO, L. H. GEVANTMAN and J. B. NASH; USNRDL-TR-565 (1962).

[6] L. F. BELOVODSKII; V. K. GAEVOI, V. I. GRISHMANOVSKII and N. V. NEFEDOV; Translation of Atomnaya Energiya, 38, 379 (1975).

[7] C. E. EASTERLY and M. R. BENNETT; Nucl. Technol. Fusion, 4,. 116 (1983).

[8] C. E. EASTERLY, H. NOGUCHI and M. R. BENNETT; Fusion Technol., 8, 2564 (1985).

[9] J. D. EAKINS and W. P. HUTCHINSON; "Tritium" (A.A. MOGAHISSI, M.W. CARTER eds.), p.392, Messenger Graphics, Phoenix (1973).

[10] J. E. PHILLIPS and C. E. EASTERLY; ORNL/TM-7670 (1982).

[11] P. J. PAPAGIANNAKOPOULOS and C. E. EASTERLY; Int. J. Chem. Kinetics, 14, 77 (1982).

Table 1 Characteristics of the catalysts

catalyst	shape	surface area (cm^2)	weight (g)	thickness (mm)
stainless steel (type 309)	foil	200	-	0.076
copper	foil	200	-	0.10
enamel paint	foil	200	-	-
platinum black	powder	-	7	-

Table 2 Rate constants for the tritium conversion reaction in the presence of catalysts

catalyst	initial T_2 concentration (Ci/m^3)	relative humidity (%)	rate constant (s^{-1})
stainless steel	0.22	60	1.4×10^{-9}
copper	0.33	60	1.6×10^{-9}
enamel paint	0.30	60	2.2×10^{-9}
platinum black	0.30	60	2.8×10^{-6}
platinum black	0.23	60	5.8×10^{-7}

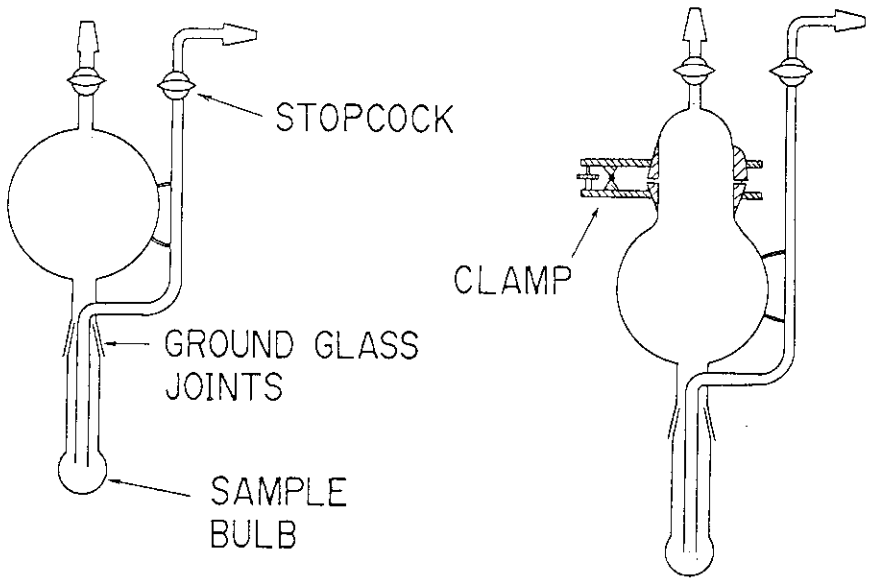

(a) For gas phase experiment. (b) For catalyst experiment.

Fig. 1 Reaction flasks for studying conversion of tritium gas to tritiated water.

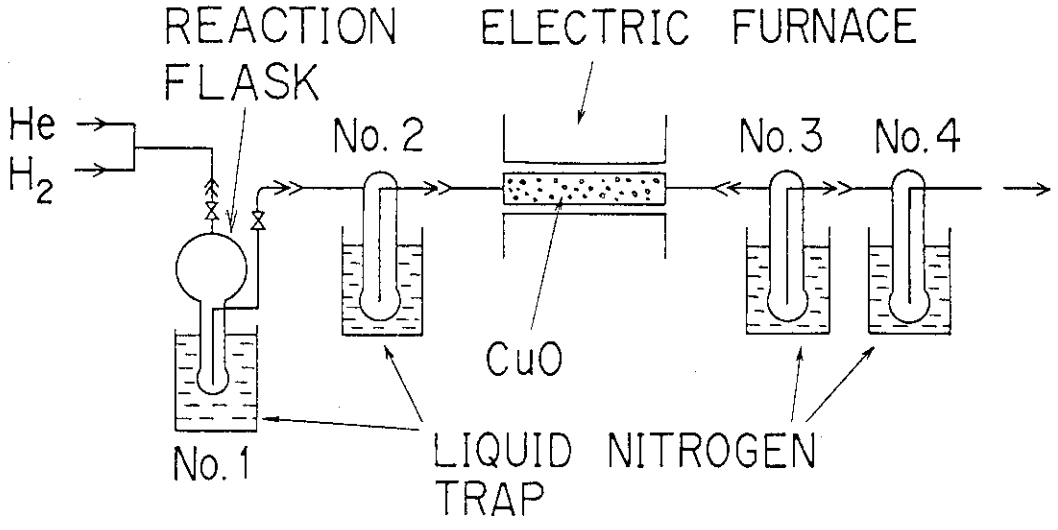

Fig. 2 System for sampling tritium gas and tritiated water in a reaction flask.

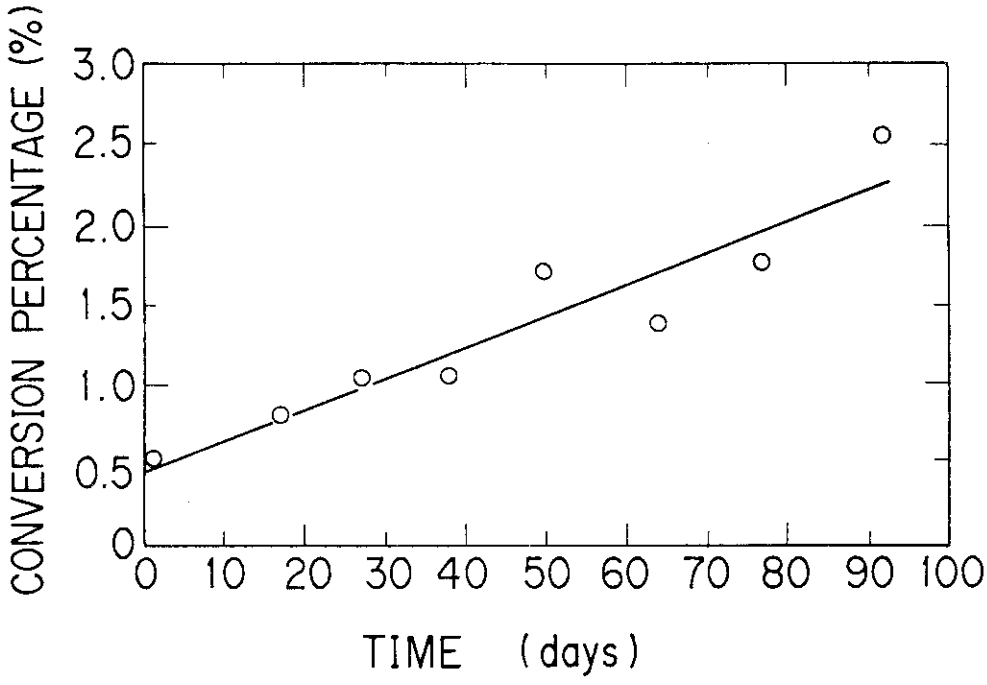

Fig. 3 Percentage of conversion of tritium gas to tritiated water in air at an initial tritium concentration of 2.6×10^{-4} Ci/m^3 as a function of time.

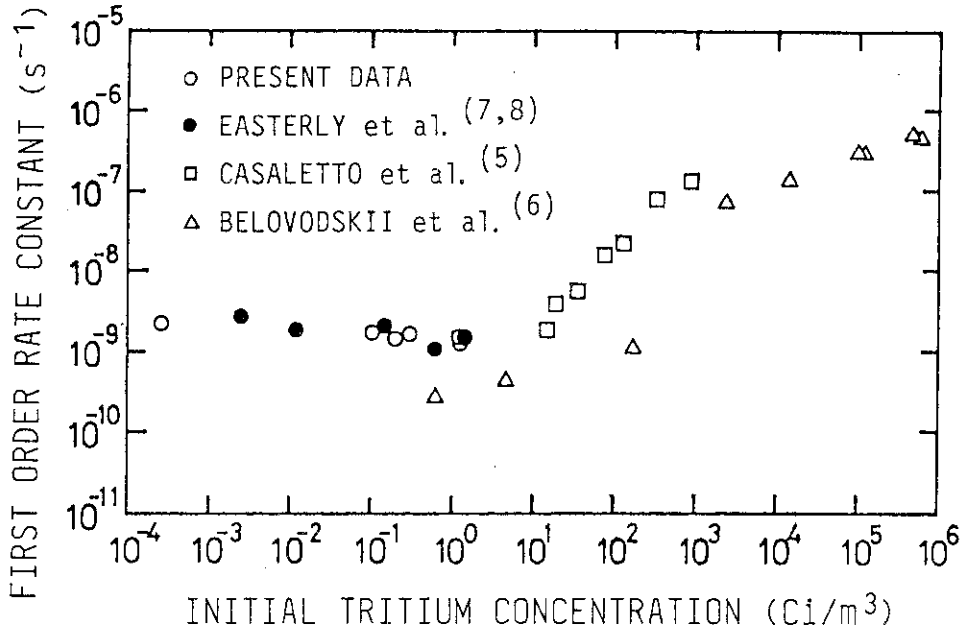

Fig. 4 First-order rate constant as a function of initial tritium concentration.

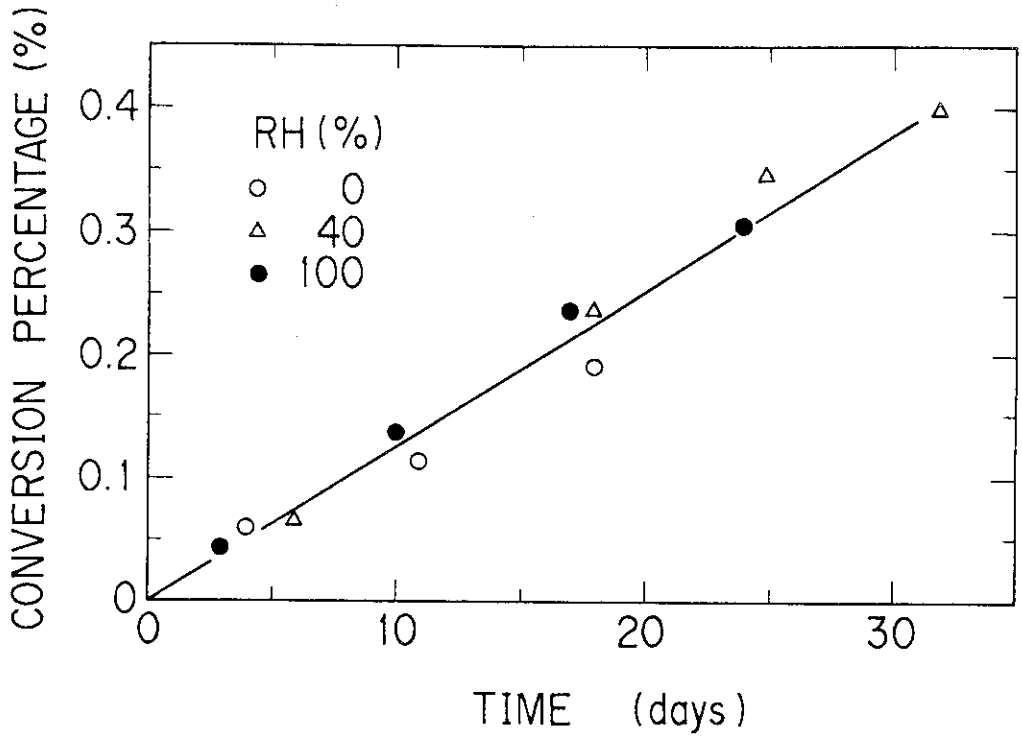

Fig. 5 Effect of water vapor on the tritium conversion reaction for initial T_2 concentrations of ~1.3 Ci/m^3.

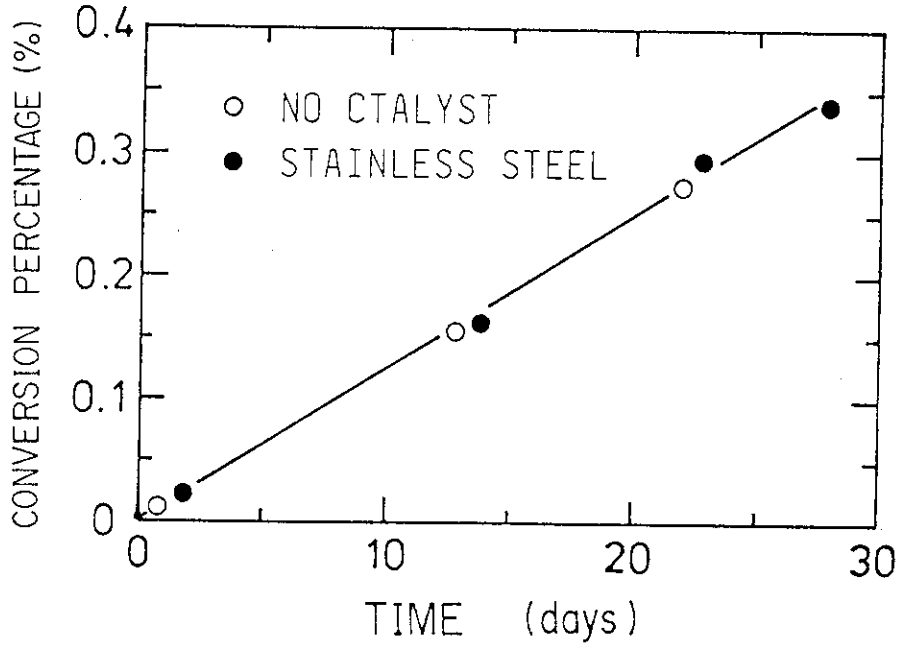

Fig. 6 Percentage of tritium conversion in the presence and absence of stainless steel for initial T_2 concentrations of ~0.2 Ci/m^3.

No.20

Analysis and Measurement of Tritium by Mass Spectrometer, Ionization Gauge and Secondary Electron Multiplier

M. Matsuyama, H. Miyake, K. Ichimura, and K. Watanabe

Tritium Research Center, Toyama University

Gofuku 3190, Toyama 930, Japan

ABSTRACT

To apply mass spectrometers and ionization gauges to D-T burning experiments in magnetic fusion devices, we examined the performance and sensitivity of a quadrupole mass spectrometer and B-A gauges for hydrogen isotopes(H_2, D_2, T_2, etc). In addition, we also examined the utility of a secondary electron multiplier(Ceratron) as a pressure gauge of tritium.

It was revealed that the relative sensitivities of the mass spectrometer for each isotope molecules with respect to H_2 was essentially the same as those of B-A gauges except T_2. It was also found that the relative sensitivities of B-A gauges for the isotopes were very close to unity except HD and T_2. With regard to Ceratron, the count rate was proportional to the partial pressure of tritium in a rage from 1.3×10^{-6} to 1.3×10^{-3} Pa.

1. INTRODUCTION

Accurate pressure gauges for tritium are required for D-T burning experiments in magnetic fusion devices as well as tritium handling systems. Mass spectrometers and ionization gauges will be used for this purpose. In addition, secondary electron multiplier can be applied as a pressure gauge of tritium, because the number of tritium β-rays is proportional to the density of tritium in gas phase. However, one must know in advance the sensitivity of them for tritium and its isotopes to determine the total and partial pressure of tritium. A convenient way to measure the pressure by these devices is to determine in advance the relative sensitivities of these gauges for them with respect to some standard gases, because the relative sensitivity is believed to be only a weak function of the operating conditions of these devices.

With respect to mass spectrometers, there is only on report on the relative sensitivities of the mass spectrometer of magnetic deflection type for hydrogen isotopes such as H_2, D_2, T_2, HD, and HT [1]. As for the ionization gauges, Nakao has reported the sensitivity for D_2 differs considerably from that of H_2 [2]. There is no other report on the relative sensitivities for other hydrogen isotopes. Therefore, we measured the relative sensitivities of B-A gauges and a quadrupole mass spectrometer for all of the hydrogen isotope molecules with the aid of a membrane manometer.

With respect to the secondary electron multipliers, Malinowski has reported that the count rate of a channeltron and

Cu-Be multipliers is proportional to tritium pressure [3]. We examined the properties of another type of multiplier, a ceramic channeltron type one.

2. EXPERIMENTAL

Figure 1(a) shows the schematic diagram of the experimental apparatus used for the measurement of the relative sensitivities of the quadrupole mass spectrometer and B-A gauges for hydrogen isotopes. The vacuum system was equipped with a sputter ion pump and mercury diffusion pump backed with an oil-sealed rotary pump. Since the system was not baked out, the residual pressure was routinely about 1×10^{-5} Pa.

A membrane manometer(MKS Baratron) was used as a standard pressure gauge. Two types of B-A gauges were used in this study: UGS-1A and UGD-1S purchased from ANELVA Co. The difference in the two gauges lies in the bake out process of the grid: that is, electron bombardment(UGS-1A) and ohmically heating(UGD-1S). The quadrupole mass spectrometer was purchased from ULVAC Co. (MSQ-150A). A Faraday cup was used as an ion detector to avoid the impairment of its performance due to the adsorption of tritium [4].

The purities of hydrogen and deuterium used in the present study were 99.999 and 99.8%, respectively. Tritium gas in a glass ampoule(5 Ci) purchased from New England Nuclear Co. was purified using a Zr-V-Fe getter [5], and was stored with the getter after the purity tests of tritium gas.

In the case of the calibration for hydrogen isotopes

containing tritium, the gases were introduced into the system from gas reservoir through a variable leak valve. The reservoir was used for temporary storage of the hydrogen isotopes released from the getter by heating. On the other hand, pure hydrogen and deuterium were introduced into the system from gas reservoir through a variable leak valve without using the getter. The tritiated gases introduced into the system was pumped out continuously with the sputter ion pump. On the other hand, non-radioactive gases were pumped out using either of the mercury diffusion pump or sputter ion pump, depending on the pressure.

Figure 1(b) shows the schematic diagram of the experimental apparatus for the partial pressure measurement of tritium by a secondary electron multiplier [6]. The multiplier used was Ceratron purchased from Murata Manuf. Co. In this case, the partial pressure of tritium was determined by the mass spectrometer of magnetic deflection type(VG-Gas Analysis, MM6).

The same kind of getter as mentioned above was also used for the storage and supply of tritium gas. The tritium gas was directly introduced into the system from the getter heated at given temperatures.

3. CALIBRATION OF THE MASS SPECTROMETER

The operating parameters of the quadrupole mass spectrometer were as follows: emission current(I^e)=0.5 mA, electron acceleration voltage=70 V, resolution(ΔM at 10% peak height)=0.6 for M/e=2 and 0.61 for M/e=3~6. The ion source was of Nier type. Under these conditions, the peaks of triatomic ions (H_3^+, D_3^+,

T_3^+, etc) and atomic ions (H^+, D^+, T^+) were negligible [7].

(1) PURE GASES

The sensitivities of the mass spectrometer for pure gases such as H_2 and D_2 can be determined using the membrane manometer as following,

$$S^x=(I^x/I^e)/P^x \qquad (1)$$

where S^x is the sensitivity of the mass spectrometer for molecular ions, x. I^x and I^e are the ion current and the emission current of electrons, respectively. P^x is the pressure of species x.

(2) GAS MIXTURES

Pure heteronuclear molecules such as HD, HT, and DT were not obtained. In addition, we could not obtain high purity tritium gas. Therefore, the sensitivities for those species were determined as the followings.

(A) H_2-HD-D_2 mixture

Partial pressure of HD is described as

$$P^{HD}=P_{total}-(P^{H2}+P^{D2})$$
$$=P_{total}-[(I^{H2}/S^{H2})+(I^{D2}/S^{D2})]/I^e \qquad (2)$$

where P_{total} is the total pressure measured by membrane manometer. Partial pressure of P^{H2} and P^{D2} were evaluated from the ion currents measured by the mass spectrometer using the eq. (1). Consequently, the sensitivity for HD, S^{HD}, can be obtained from eq. (1).

(B) H_2-HT-T_2 mixture

In determining the sensitivity for HT, S^{HT}, we employed the principally similar method to the case of HD. However, the

sensitivity for T_2, S^{T2}, could not be determined in advance from the eq. (1) because pure T_2 was not obtained. Therefore, we applied an alternative method in which mixtures of two isotope species with various compositions were used as sample gas. The typical gas mixtures were those as $P^{H2} > P^{HT} >> P^{T2}$ (Fig. 2) and $P^{H2} \simeq P^{HT} \simeq P^{T2}$ (Fig. 3). In the former case, the contribution of P^{T2} was neglected at first. Then, the tentative sensitivity for HT, $S^{HT(1)}$, was determined from the following equation and eq. (1).

$$P^{HT} = P_{total} - P^{H2}$$
$$= P_{total} - (I^{H2}/S^{H2})/I^{e} \quad (3)$$

From the latter conditions, the tentative value of S^{T2}, $S^{T2(1)}$, was obtained from the following equation.

$$P^{T2} = P_{total} - (P^{H2} + P^{HT})$$
$$= P_{total} - [(I^{H2}/S^{H2}) + (I^{HT}/S^{HT})]/I^{e} \quad (4)$$

where $S^{HT(1)}$ was used for S^{HT}. The sensitivity for T_2 in this step, however, was overestimated in comparison with the true value because the partial pressure of tritium was neglected in the eq. (3). Therefore, the calculation of S^{x} was repeated for the mass spectra observed for the mixture gases mentioned above using the tentative sensitivity factors such as $S^{HT(1)}$ and $S^{T2(1)}$. By these procedures, refined values of S^{T2} were obtained. Furthermore, these procedures were repeated until the sensitivities for HT and T_2 became invariant with the repetition.

(C) D_2-DT-T_2 mixture

The determination of sensitivity for DT, S^{DT}, was carried out by quite similar procedures to the case of H_2-HT-T_2 mixture. The details of the procedures have been described elsewhere [7].

4. CALIBRATION OF THE B-A GAUGES

The operating parameters of the B-A gauges were as follows: emission current(I^e)=0.94 mA for UGS-1A and 1.00 mA for UGD-1S, filament voltage=45 V, grid voltage=180 V and ion collector=0 V (grounded).

(1) PURE GASES

The sensitivities of the B-A gauges for pure gases(H_2 and D_2) could be determined by using similar equation to eq.(1). In this case, however, S^x in eq.(1) is the sensitivity of the B-A gauge for isotope species x, and I^x and I^e are the ion current at a pressure P^x and emission current, respectively.

(2) GAS MIXTURES

(A) H_2-HD-D_2 mixture

The ion current from HD is described as

$$I^{HD}=I_{total} - (I^{H_2} + I^{D_2})$$
$$=I_{total} - (S^{H_2}P^{H_2} + S^{D_2}P^{D_2})I^e \quad (5)$$

where the partial pressure of each species can be determined using the mass spectrometer. Consequently, I^{HD} is uniquely determined from eq.(5), because the S^{H_2} and S^{D_2} have been previously determined. Consequently, S^{HD} is obtained from eq.(1).

(B) H_2-HT-T_2 and D_2-DT-T_2 mixtures

The ion currents of HT and DT are described as

$$I^{HT}=I_{total} - (S^{H_2}P^{H_2} + S^{T_2}P^{T_2})I^e \quad (6)$$
$$I^{DT}=I_{total} - (S^{D_2}P^{D_2} + S^{T_2}P^{T_2})I^e \quad (7)$$

The unknown parameters in the eqs.(6) and (7), S^{HT}, S^{DT} and S^{T_2}, can be determined with similar manner as that for the calibration

of the mass spectrometer. As a result, the sensitivities for all of hydrogen isotopes can be determined.

5. RESULTS AND DISCUSSION

Figure 4 shows the calibration results for HT in H_2-T_2 mixtures as an example. The HT pressure is the one which was determined by the mass spectrometer after the sensitivities of all of the isotope species were determined. The sensitivity of the mass spectrometer, S^{HT}, was determined as $(8.55\pm0.45)\times 10^{-5}$/Pa in the range from 1×10^{-3} to 5×10^{-3} Pa of the HT pressure. It was constant within the experimental errors. This was also true for the B-A gauges. The sensitivities of UGS-1A and UGD-1S for HT were determined as $(2.23\pm0.08)\times 10^{-2}$/Pa and $(2.78\pm0.08)\times10^{-2}$/Pa, respectively. Although the calibration could not be carried out below 1×10^{-3} Pa because of the sensitivity limit of the membrane manometer, it is believed that the calibration curves can be extrapolated to lower pressures. Above the total pressure of 3×10^{-2} Pa, on the other hand, the calibration curves of both the mass spectrometer and B-A gauges convexly deviated from the linear relations. The exact reasons are not apparent: however, it is considered due to space charge effect, decrease in the mean free path of ions, recombination of ion-electron pairs and so on.

The results of the calibration of the mass spectrometer for hydrogen isotope molecules are summarized in Table 1, where the sensitivity for each isotope species is normalized to that for H_2. It is denoted as the relative sensitivity: $R_M^x = S_M^x / S_M^{H_2}$.

The statistical errors of them were within 6%. The values agree quite well with those of the mass spectrometer of magnetic deflection type reported by Dibeler et al. [1].

The results for the B-A gauges are also summarized in Table 1, where the relative sensitivities ($R_B^x = S_B^x / S_B^{H_2}$) of two gauges were averaged. It should be mentioned here that the relative sensitivities of the B-A gauges were very close to unity except S_B^{HD} and $S_B^{T_2}$: the former appears a little larger and the latter does a little smaller than unity. On account of the close correlation between the sensitivity of ionization gauges and ionization cross section [3], this is considered due to the difference in the ionization cross section from that of H_2.

It is seen in the table that the relative sensitivities of the B-A gauges for hydrogen isotopes were very close to those of the mass spectrometer except T_2. This feature indicates that the additivity assumed for the ion current of the B-A gauges is valid. In addition, it is understandable if we assume that the relative ionization cross section of a given isotope molecules with respect to that of H_2 does not change appreciably with the electron energy under the conditions in the present study.

As for the lower relative sensitivity of the mass spectrometer for T_2, Dibeler et al. have explained their results as mass discrimination. This is considered also true for the present results, because the ratio, $R_M^{T_2}/R_B^{T_2}$ (=0.93), was alone smaller than unity: for other isotope molecules, the ratio R_M^x / R_B^x was essentially equal to unity. The ratio, $R_M^{N_2} / R_B^{N_2}$ (=0.29), observed in the present study is consistent with this

explanation.

In contrast to the ionization gauges, the relative sensitivities of the mass spectrometer may not be applicable to other instruments, because the magnitude of the mass discrimination and the resolving power at which it becomes significant are dependent on the design of the mass spectrometer [8]. In fact, it was observed that the mass discrimination was almost negligible upto M/e=136 for a quadrupole mass spectrometer having parbolic rods(MSQ-500, ULVAC Co.) [9]. In such an instrument, therefore, it is expected that the mass discrimination does not play a role in the relative sensitivities for hydrogen isotopes. It should be mentioned, however, that the use of a secondary electron multiplier caused a significant change in the relative sensitivity, depending on its operating conditions.

Figure 5 shows the calibration curve of Ceratron against the tritium pressure [10]. In this case, the count rate was measured by applying a potential of −3.5 kV. It should be mentioned here that the abscissa represents the pressure of tritium calculated from $P^{T_2} = P_M^{T_2} + 1/2\ P_M^{HT}$ where $P_M^{T_2}$ and P_M^{HT} are the partial pressure of tritium species measured by the mass spectrometer (MM6). It is clear in the figure that the count rate of Ceratron is proportional to the pressure of tritium in a wide range. The sensitivity for tritium gas was determined from the slope of the calibration curve as P (Pa) = 2.1×10^{-8} R (cps) [6]. This value agrees quite well with that of channeltron reported by Malinowski [3].

To use the secondary electron multipliers as a tritium pressure gauge, however, one must take account of the contamination of them due to tritium irreversibly adsorbed on their surfaces [6,10]. The tritium adsorbed on the multiplier surfaces causes a certain number of count rate irrespective of tritium pressure. The count rate due to this species is denoted as noise level. The noise level increased with increasing exposure to tritium and eventually the pressure measurement by Ceratron became impossible. Similar phenomena have been observed for channeltron and Cu-Be multipliers by Malinowski [3]. Some part of the irreversibly adsorbed tritium was desorbed by heating in vacuo or in air. However, we found that photon irradiation was more effective to remove the irreversibly adsorbed tritium [10]. With use of this technique, one can use Ceratron as a pressure gauge for tritium gas. However, a standard β-ray source will be needed for this application, because the gain of secondary electron multipliers changes with time and depends on the conditions under which they are used.

6. CONCLUSIONS

The relative sensitivities of B-A gauges and a quadrupole mass spectrometer for hydrogen isotopes were determined. It was observed that those of the B-A gauges for hydrogen isotopes are essentially equal except HD and T_2. This is considered to be predominantly due to the difference in the ionization cross section. There is a similar trend for the relative sensitivities of the mass spectrometer for the isotopes. However, the

sensitivity for T_2 was appreciably smaller than that for H_2, being due to the mass discrimination.

With respect to the secondary electron multipliers, the count rate was proportional to tritium pressure. However, the irreversibly adsorbed tritium caused a considerable increase in the noie level. With the aid of some decontamination techniques such as photon irradiation, Ceratron can be also applied as a tritium pressure gauge.

Table 1. Relative sensitivities of the mass spectrometer(R_M^X) and B-A gauge(R_B^X) for hydrogen isotopes.

	Mass spectrometer(R_M^X)	Ionization gauge(R_B^X)	R_M^X/R_B^X
H_2	1.00	1.00	1.00
HD	1.09 ± 0.06	1.08 ± 0.05	1.01
D_2	0.99 ± 0.03	0.99 ± 0.01	1.00
HT	1.06 ± 0.06	1.03 ± 0.04	1.03
DT	0.96 ± 0.04	0.97 ± 0.03	0.99
T_2	0.88 ± 0.03	0.95 ± 0.02	0.93

REFERENCES

[1] V.H. Dibeler, F.L. Mohler, E.J. Well, Jr., and R.M. Reese J. Res. Natl. Bur. Standards, 45 (1950) 288.

[2] F. Nakao, Vacuum, 25 (1975) 201, 431.

[3] M.E. Malinowski, J. Nucl. Mater., 93/94 (1980) 96.

[4] K. Ichimura, N. Inoue, K. Ashida, M. Matsuyama, H. Miyake, and K. Watanabe, RADIOISOTOPES, 34 (1985) 83.

[5] K. Ichimura, M. Matsuyama, K. Watanabe, and T. Takeuchi Fusion Technology, 8 (1985) 2407.

[6] K. Ichimura, M. Matsuyama, K. Watanabe, K. Nisizawa, and J. Fujita, Ann. Rept. Tritium Res. Centr. Toyama Univ., 3 (1983) 17.

[7] K. Watanabe, H. Miyake, and M. matsuyama, being submitted to J. Vac. Sci. Technol.,

[8] W.E. Austin, A.E. Holme and J.H. Leck, in "Quadrupole Mass Spectrometer and Its Application", ed. P.H. Dawson, Elsevier, Amsterdam, 1976.

[9] S. Nakamura, private communication.

[10] K. Ichimura, K. Watanabe, K. Nishizawa, and J. Fujita, Nucl. Instruments Methods Phys. Rev., 226 (1984) 470.

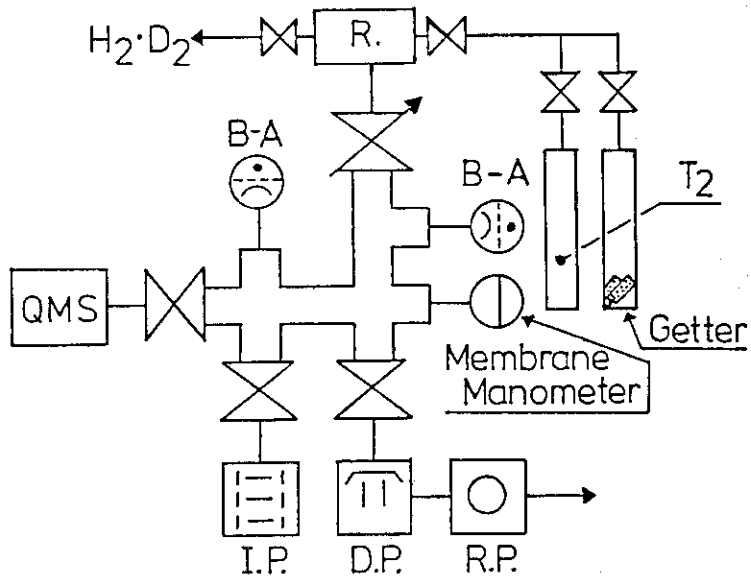

Fig. 1(a) Schematic diagram of the apparatus for calibrating QMS and B-A gauges.

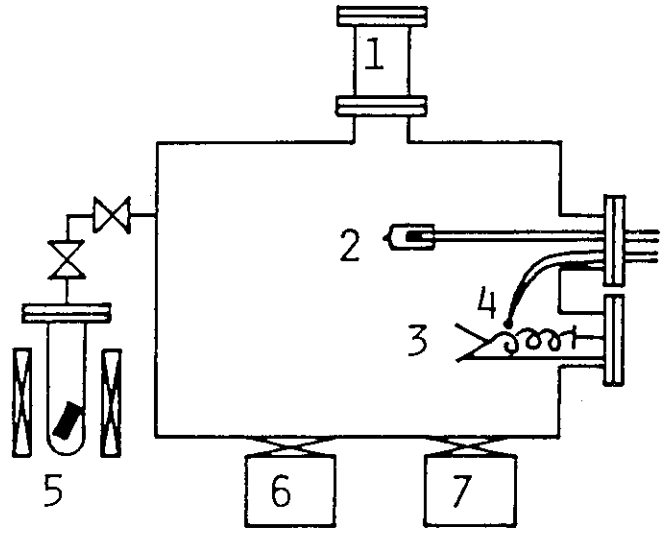

Fig. 1(b) Schematic diagram of the apparatus for tritium partial pressure measurement by Ceratron.
1. MM6 Mass analyzer 2. Halogen lamp
3. Ceratron 4. CA thermocouple
5. Zr-V-Fe getter 6. Cryogenic pump
7. Turbomolecular pump

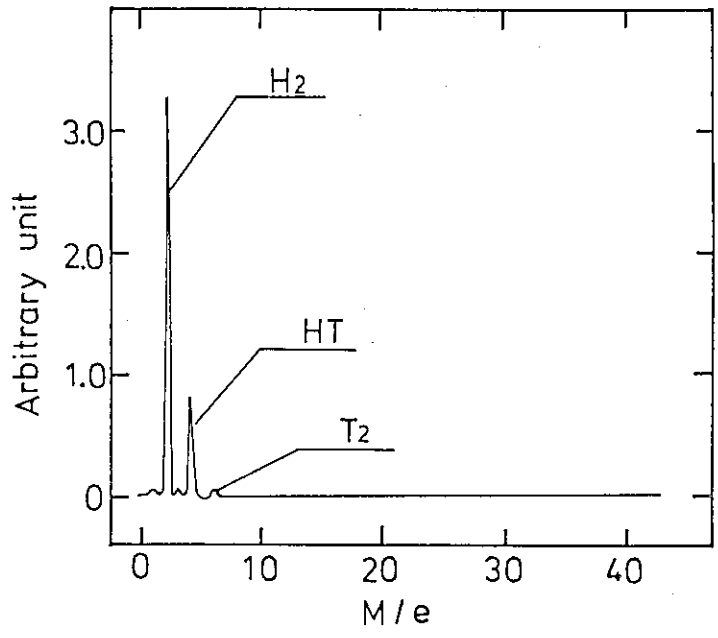

Fig. 2 Example of the mass spectra for H_2 - T_2 system.
($p^{H_2} > p^{HT} \gg p^{T_2}$)

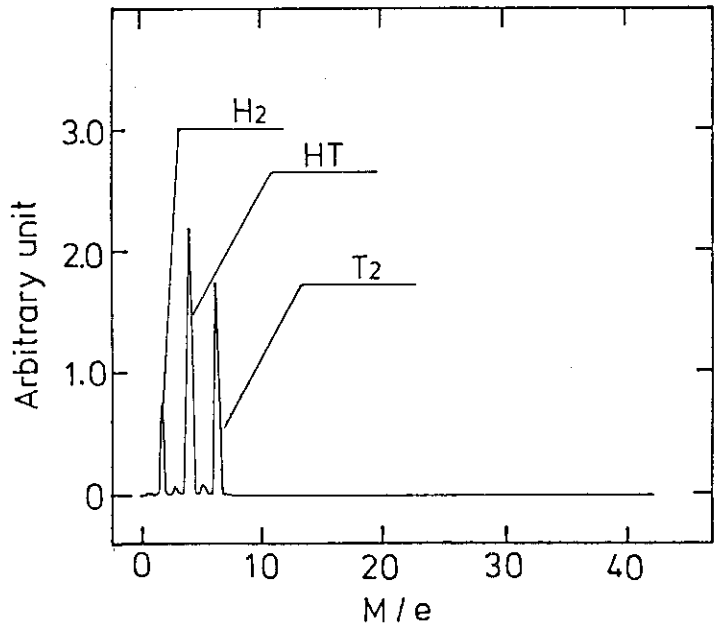

Fig. 3 Example of the mass spectra for H_2 - T_2 system.
($p^{H_2} \simeq p^{HT} \simeq p^{T_2}$)

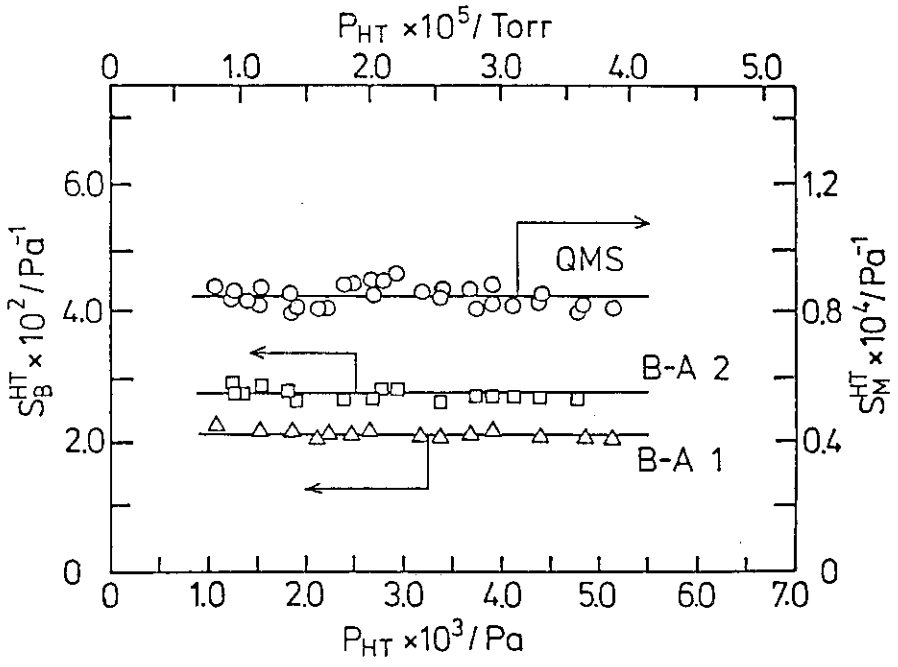

Fig. 4 Calibration curves of the mass spectrometer and B-A gauges for HT.

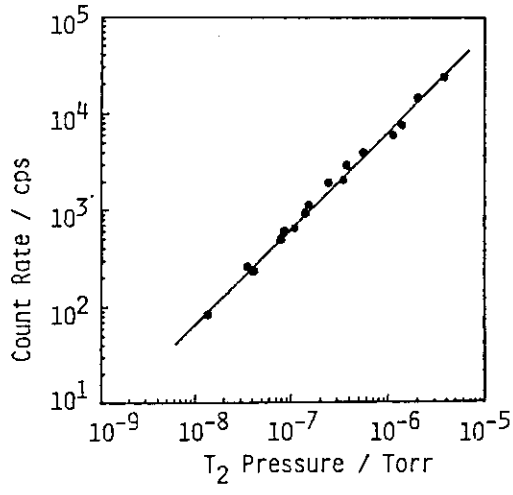

Fig. 5 Tritium partial pressure measurement by Ceratron.

No.21

Hydrogen Isotope (Tritium) Separation by Infrared Multiple-Photon Dissociation

A.Yokoyama, K. Suzuki, G. Fujisawa, and N. Ishikawa

Division of Chemistry, Japan Atomic Energy Research Institute, Tokai, Ibaraki, 319-11 Japan

M. Iwasaki

Institute of Atomic Energy, Kyoto University, Uji, Kyoto, 611 Japan

1. Introduction

Laser isotope separation has a greater advantage than other methods for enriching very small concentrations of isotopes, because a very high enrichment factor can be obtained in comparison with the other methods. We have investigated the laser isotope separation for the purpose of lowering tritium leakage to the environment from nuclear facilities and obtained high tritium enrichment factor exceeding 570 by the isotopically selective multiple-photon dissociation of $CTCl_3$ in $CHCl_3$ using a CO_2 laser-pumped NH_3 laser[1]. The tritium removal from waste water based on the isotopically selective multiple-photon dissociation of $CTCl_3$ can be accomplished through two successive processes: the tritium transfer process from water to chloroform and the laser tritium separation process. The results of the T/H separation by the selective infrared multiple-photon dissociation of $CTCl_3$ and the base catalyzed tritium exchange reaction between chloroform and water are described.

2. T/H separation by the selective infrared multiple-photon dissociation of $CTCl_3$

When a mixture of $CTCl_3$ and $CHCl_3$ was irradiated with 816, 828,

and 833 cm^{-1} radiations from a CO_2 laser-pumped NH_3 laser, $CTCl_3$ decomposed selectively. On the other hand, the decomposition of $CHCl_3$ was not observed even after 10000 laser pulses irradiation. The single-step tritium enrichment factor in photo-products produced by one laser pulse irradiation, which was defined by the ratio of the T/H fraction in the photo-products to that in the initial chloroform, was found to be greater than 570 at chloroform pressure of 2 torr. The laser fluence required for the decomposition of every $CTCl_3$ molecule, which was called as saturation fluence, was about 28 J/cm^2 at 2 torr. The saturation fluence increased with increasing chloroform pressure as a result of energy transfer from excited $CTCl_3$ to $CHCl_3$ within a laser pulse duration (about 1 μ sec). Therefore, a shorter pulse laser is necessary for the laser T/H separation at higher chloroform pressure.

3. Base catalyzed tritium exchange reaction between chloroform and water

Under the coexistence of water and chloroform phases, tritium exchange reaction between chloroform and water proceeds predominantly in the water phase through the following reactions:

$$CHCl_3 + OH^- \underset{k_{-1}}{\overset{k_1}{\rightleftharpoons}} CCl_3^- + H_2O \qquad (1)$$

$$CCl_3^- + HTO \underset{k_{-2}}{\overset{k_2}{\rightleftharpoons}} CTCl_3 + OH^- \qquad (2)$$

The exchange rates were measured at different hydroxide-ion concentrations, mole ratios of chloroform to water, and reaction temperatures. The values of de-tritiation rate constant, k_{-2}, and equilibrium constant, K_{eq}, defined by eq.(3) are summarized in Table 1.

$$K_{eq} = \frac{k_1 k_2}{k_{-1} k_{-2}} = \frac{[CTCl_3][H_2O]}{[CHCl_3][HTO]} \qquad (3)$$

Since the isotopic fractionation factor, which is defined by the ratio of the T/H fraction in the chloroform to that in the water and equals to $2K_{eq}$, is larger than unity, the tritium is enriched in the chloroform.

References

(1) A. Yokoyama, K. Suzuki, G. Fujisawa, N. Ishikawa, and M. Iwasaki: Appl. Phys. B **38**, 99 (1985).

Table 1. De-tritiation rate constant (k_{-2}) and equilibrium constant (K_{eq}).

Temp. (℃)	k_{-2} ($l \cdot mole^{-1} \cdot s^{-1}$)	K_{eq}
25.0	0.185 ± 0.003	0.535 ± 0.006
35.1	0.580 ± 0.007	0.538 ± 0.004
39.5	0.98 ± 0.02	0.521 ± 0.006

No.22

PROGRAM OF TRITIUM EXPERIMENTS AT THE TPL IN JAERI

Hiroshi YOSHIDA

Tritium Engineering Laboratory
Department of Thermonuclear Fusion Research,
Naka-Fusion Research Establishment

R & D Program of Tritium Technology in JAERI

I. Significance of the Tritium Technology Program

Establishment of tritium handling technology is one of the critical issues in the fusion reactor program in JAERI. Japan have no technology as well as handling experience for processing a large amount of tritium as the fuel in a fusion reactor.

R & D program of tritium technology in JAERI have been conducted on the philosophycal stand point that original and strong efforts of tritium technology should be evolved without delay for the smooth and successfull progress of the fusion reactor programm in Japan.

II. Important Technical Issues

Essential tritium technology to the fusion reactor are the following;

* Processing technology for the evaluation and selection of the suitable processes for the fusion fuel cycle,
* System technology integrating variuos processes,
* Tritium production technology for initial loading,
* Blanket material and tritium recivery tecnology,
* Safe handling and monitoring,
* Waste processing technology, and so on.

III. Schedule in JAERI

Several steps of R & D efforts of the tritium technology have been provided for the master plan of next D-T burning machine in JAERI.

STEP-I : Construction of Tritium Processing Laboratory(TPL)
The facility covers the basic engineering items such as the tritium processing technology and safe handling.

STEP-II : Construction of Tritium Engineering Laboratory
This facility will cover the following areas;

* D-T fuel gas recycling loop for the fusion fuel cycle. The loop will include vacuum system, purification system, cryogenic distillation cascade, refuelling system, etc.,
* Blanket engineering facility for PIE of neutron irradiated materials, for thermohydraulic study of solid breeder blanket modules, etc.,
* Tritium extraction and purification,
* Waste processing,
* Safety for a large amount of tritium.

STEP-III : Construction of a mockup D-T circulation loop, which meets the design and operating conditions of a next D-T burning machine. The objects of this facility are,(i) to demonstrate the full performance of the integrated system, and (ii) to demonstrate the safety controll systems.

STEP-IV : Coupling the D-T mockup loop with a next D-T burning machine.

IV. Present Activity in JAERI

Initiation of the STEP-I has been determined by 1980, and the construction of the Tritium Processing Laboratory has started at 1982. Completion of the construction and lisencing, and the start of various tritium process studies with 10 grams of T_2 are scheduled to be in the latter half of 1987.

The detailes of the TPL scheme are described in the following view graphs.--- the attached copies.

V. International Cooperation in Tritium Technology

(1) JAERI's Standpoint

In order to realize the fusion reactor, tremendous efforts in the budjet, manpower and term are needed. Majority of the technology are those of an unknown fields of mankind. Therefore, international cooperation of this matter will be effective and indispensable for their successfull execution in each nation.

(2) JAERI-US Cooperation

Successfull cooperation between TPL-JAERI and TSTA-LANL has been carried out in the last six years under the Japan-US Fusion Technology Cooperation Program. Several cooperation experiments, that is "Testing of Small Scale Pd-diffuser and Ceramic Electrolysis Cell with Tritium", have also been performed since 1984. This collaboration is now being expected to shift into a new stage based on each program.

(3) JAERI-CANADA Cooperation

Cooperation program between TPL-JAERI and CFFTP-CANADA will start at 1986 in the level of staff and information exchanges, which include the participation of experimental works conducted by both side institutes. Several joint R & D projects will also be initiated in the future.

(4) JAERI-EC Cooperation

Information exchange for the TPL-EC cooperation has just started.

3. Facility

(1) Schedule

* Design : 1977 -
* Construction
  - Building and Utilities : 1982 - 1984(May)
  - Safe Handling Systems : 1983 - 1985
  - Experimental Apparatus : 1986

(2) Specifications

(i) Buliding Structure

* 3 Floors(Ground Area; 1400m^2, Total Floor Area; 2300m^2)
* Reinforced Concrete (Withstand 300Gal Seismic Force)
* 1st Floor : Glovebox Room, Detritiation Systems Room, Semi-hot Experiment Room, Utility Room
* 2nd Floor : Semi-hot Experiment Room
* Basement : Waste Processing Room, Waste Storage Tank Room

(ii) Tritium Handling Capacity

* Glovebox : 2 - 3 g / Glovebox-Block
* Storage : 10 g (maximum)

(iii) Uranium Metal(Tritium Gettering)

: 20 kg

(v) Tritium Containment System(Threefold Containment)

* Primary Containment : Experimental Apparatus
* Secondary Containment : Gloveboxes
* Tertiary Containment : Glovebox Room and Detritiation Systems Room

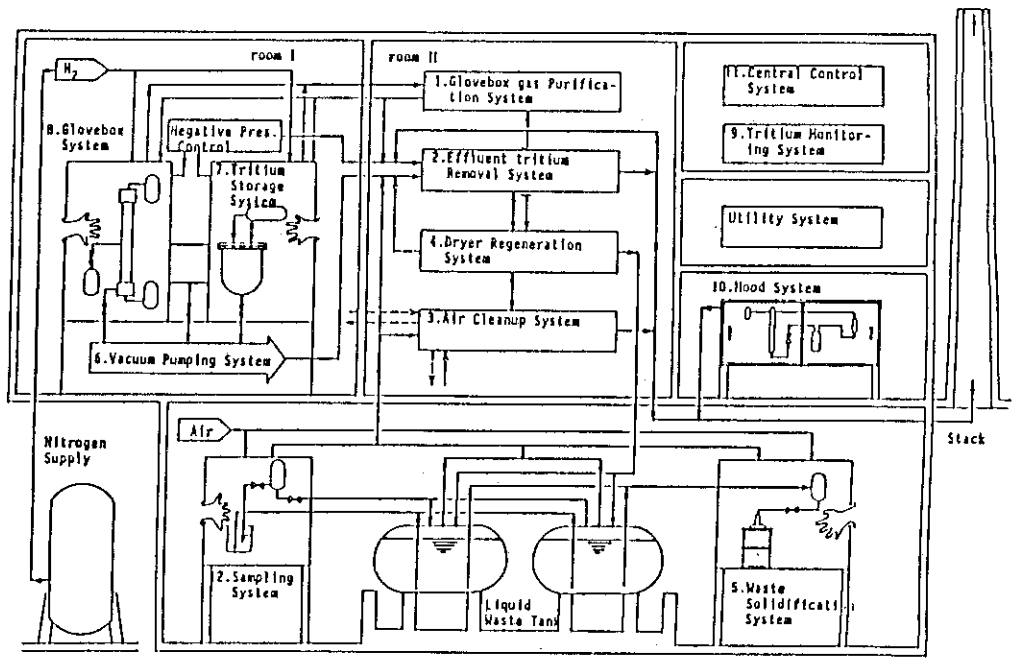

Subsystems of the Triitum Process Laboratory(TPL)

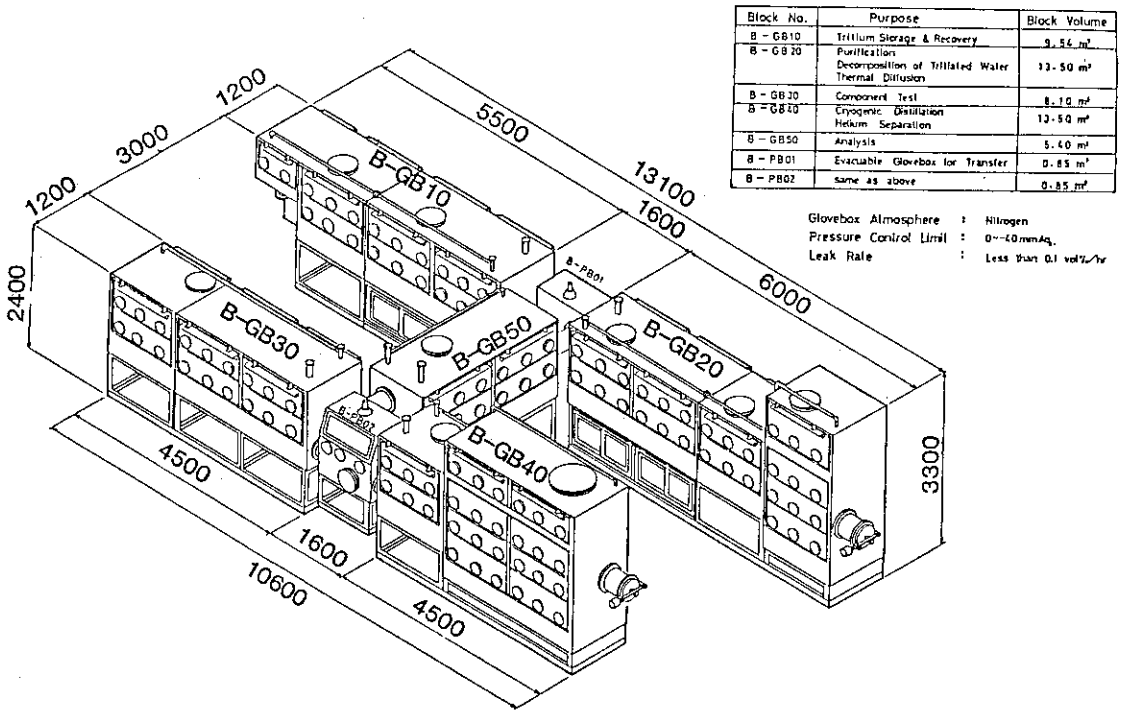

Block No.	Purpose	Block Volume
B－GB10	Tritium Storage & Recovery	9.54 m³
B－GB20	Purification Decomposition of Trifiated Water Thermal Diffusion	13.50 m³
B－GB30	Component Test	8.10 m³
B－GB40	Cryogenic Distillation Helium Separation	13.50 m³
B－GB50	Analysis	5.40 m³
B－PB01	Evacuable Glovebox for Transfer	0.85 m³
B－PB02	same as above	0.85 m³

Glovebox Atmosphere : Nitrogen
Pressure Control Limit : 0～-40mmAq.
Leak Rate : Less than 0.1 vol%/hr

OVERVIEW OF GLOVEBOXES
IN TRITIUM PROCESS LABORATORY

Tritium Processing R & D Work for Fusion Fuel System

Item	Process	Method/Component
Fuel Cleanup	* Fuel/Impurity Separation	Hydrogen Permeation through Pd-alloy Membrane Cryogenic Falling Liquid Film Helium Separator
	* Impurity Conversion to Tritiated Water	Catalytic Oxidation with Pd(Pt)-catalyst Bed
	* Tritium Recovery from Tritiated Water	Water Vapor Electrolysis with Ceramic Electrolysis Cell Water Vapor Reduction with Catalytic Reducing Bed (catalyst: $CuO.ZnO.Cr_2O_3$)
	* Tritium Gettering	Hydrogen Absorption/Desorption with Metal Bed(U, ZrNi,Pd,etc.)
Isotope Separation	* Multi-component Hydrogen Isotope Separation	Cryogenic Distillation with Packed Column Thermal Diffusion with Hot-wire and Hot-tube Type Column
Safety	* Tritium/Material Interaction	Low Energy Tritium Implantation/Permeation Study (T-ion energy:10～500eV, T_2 inventory:1～10^4Ci)
	* Tritium Removal	Catalytic Oxidation and Water Vapor Adsorption with Pd(Pt)-catalyst Bed and Mole Sieve Bed

Progress in Tritium Processing Laboratory Program

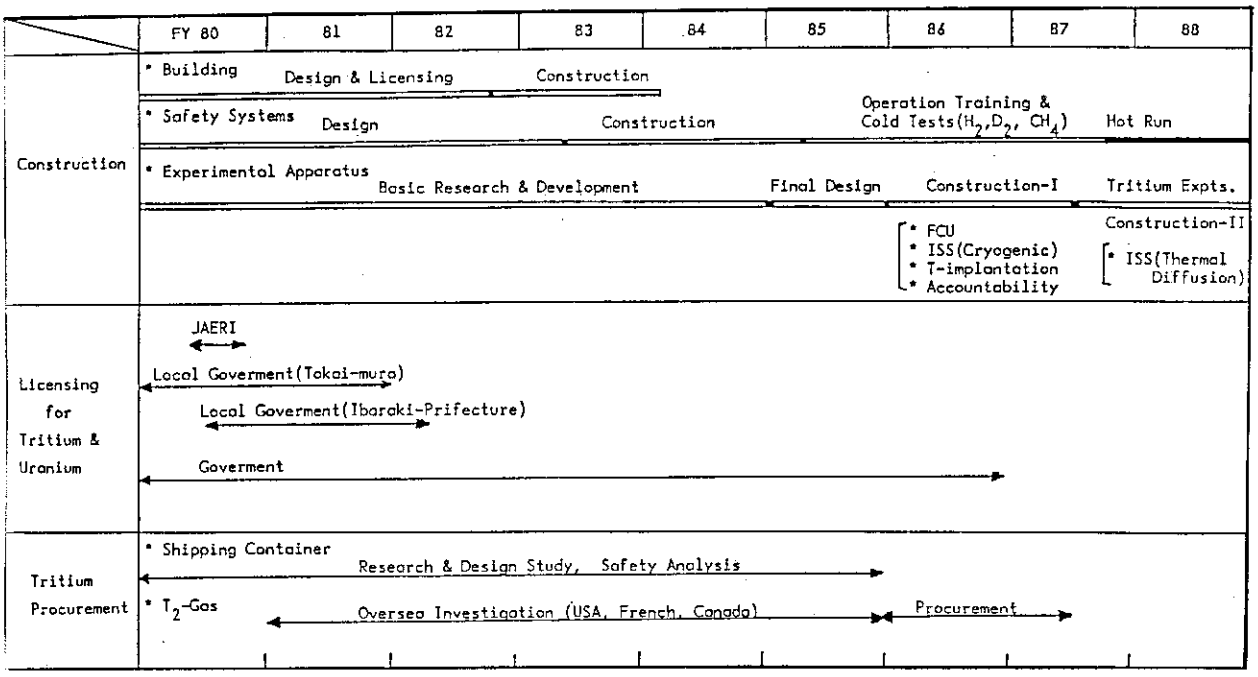

No.23

BRIEF DESCRIPTION OF EXPERIMENTAL APPARATUS FOR FUEL CLEANUP PROCESS

Satoshi KONISHI, Hiroshi YOSHIDA and Yuji NARUSE

Tritium Engineering Laboratory
Department of Thermonuclear Fusion Research
Japan Atomic Energy Research Institute

ABSTRACT

An experimental apparatus for the development of Fuel Cleanup System is being designed and fabricated at the Tritium Process Laboratory. The function of the system is continuous processing of a simulated plasma exhaust and separation of hydrogen isotopes and impurity elements in it. Main components are palladium diffusers, a catalytic reactor, freezers, an electrolysis cell and zirconium-cobalt beds. The apparatus will be installed in a glovebox in summer, 1987 and tests with tritium will initiate early in 1988.

INTRODUCTION

The Tritium Process Laboratory (TPL) at the Japan Atomic Energy Research Institute is charged with development of processing and safe handling technology of tritium related to a fusion fuel cycle. The experiments on purification and recovery. isotope separation, tritium permeation studies. analysis and accountability. are planned to be performed with 1 gram of tritium each. In the present paper, a program and experimental device for the study of the "Fuel Cleanup System", the process for purification and recovery of tritium are described.

OBJECTIVES

In the primary fuel cycle of fusion reactor system, the process of purification and recovery of tritium, that is, separation of hydrogen isotopes from other impurity elements are essential. The exhaust from the core of magnetic fusion reactor is assumed to contain various kinds of light element impurities. and high concentration of unburnt DT fuel that should be reprocessed and recirculated. Objectives of the "Fuel Cleanup", where plasma exhaust is chemically reprocessed are, (1) to supply pure hydrogen isotopes to Isotope separation system. and (2)exhaust impurity elements as tritium-free compounds.

Since prior techniques that have been proposed for this purpose have some disadvantages. the activities on this process in this laboratory are focused on the development of some

new techniques and components. Some of the major components are developed and tested with H_2 and D_2 in JAERI, and tests with high concentration of tritium have been performed at the Tritium Systems Test Assembly in Los Alamos National Laboratory under the US-Japan Cooperative program.

The test loop described in the following section will be used for the next step of the study of these techniques at the TPL. The objectives of this experiment are as follows:

to test the processing components with tritium,
to design, fabricate and operate a prototype system suitable for processing plasma exhaust,
to study the behaviors of the integrated loop, and
to establish an engineering basis of the fusion reactor fuel systems.

PROCESS SELECTION

As shown in the simplified flow of the Fuel Cleanup in the figure 1, the major components of the apparatus are, palladium diffusers, a catalytic reactor, freezers, an electrolysis cell and zirconium-cobalt beds. The letter X stands for the mixture of hydrogen isotopes, H, D and T in this paper. Feed stream to the palladium diffuser is a simulated plasma exhaust contains DT mixture and impurities of helium, water, methane and ammonia. Hydrogen isotopes are fed from the zirconium-cobalt beds and circulate in the system, while impurity elements are processed in once-through flow and exhausted to the Effluent tritium Removal

System of the TPL. Processes are selected under following considerations.

The impurity concentration in the DT product and tritium concentration in the exhaust impurity stream should be as low as possible. High purity of the product is desirable for the safe operation of cryogenic distillation column that is the primary candidate of the isotope separation process without troubles such as blockage in tubing. Tritium content in the exhaust should also be minimized to reduce tritium loss from the system and eventual tritium release to the environment.

Continuous processing in gas phase, low tritium inventory, and minimum switch-over operation or replacement of components are requirements related each other. Processes such as molecular sieve beds, hot metal beds, freezer or condenser usually requires batch processing and switch-over operation for regeneration, which makes the system and its operation more complicated, and thus increases possibility of hazards. These components also have larger tritium inventory in the form of liquid, solid, compounds or sorbed water/hydrogen.

Palladium diffuser is chosen as the front-end component of the Fuel Cleanup and separates pure hydrogen and impurities continuously. The advantages of this process are the purity of product and continuous separation. The impurity stream is processed by catalytic oxidation followed by freeze out at 160K. This process is expected to minimize the tritium loss from the outlet. Tritiated water will then be sent to the electrolysis cell and split to streams of hydrogen and oxygen. This process

decomposes tritiated water vapor continuously with little tritium inventory and generation of waste. Thus two separation components, palladium diffuser and electrolysis cell eliminates alternatives such as molecular sieve beds or hot metal beds which require switch-over operations.

The selected process is featured by these advanced components which made the system simple. Some of the processes have not been proven for continuous tritium service in a loop. This system is in contrast with the Fuel Cleanup in TSTA at LANL, where more conservative processes are chosen to demonstrate a fuel cycle of fusion reactor to be proven.

SYSTEM DESCRIPTION

Schematic flow diagram of the experimental apparatus is shown in the Fig.2. The loop consists of four subsystems; (1)Gas feed subsystem, (2)Purification subsystem, (3)Recovery subsystem, (4)Water decomposition subsystem.

Gas feed subsystem supplies hydrogen isotopes and impurity for experiments. D_2 and T_2 are supplied respectively from a gas bottle and an uranium bed for initially loading. They will be recovered by zirconium-cobalt bed for reuse. CH_4, NH_3 and He are continuously fed to the system from outside of the glovebox. Tritiated water is synthesized from DT and O_2 at the catalytic reactor. The hydrogen isotopes and these impurities are mixed to simulate plasma exhaust and fed to the next process, Purification subsystem. Ptium in these impurity compounds will be

accumulated in the system. Excess hydrogen isotope gas will be stored in the zirconium-cobalt bed so that the amount of hydrogen isotopes in the loop will be kept stable.

The purification subsystem is composed of a palladium diffuser and vacuum pumps. Gas mixture from the gas feed system is separated to pure hydrogen stream and bleed stream where impermeable impurities are concentrated. The permeated side of the palladium membrane is evacuated to below 10 torr in order to reduce hydrogen concentration in the bleed gas. Pure hydrogen is pressurized and recirculated to the gas feed subsystem. Bleed is sent to the recovery subsystem.

Bleed gas from the palladium diffuser is then processed in the Recovery subsystem. Hydrogen isotopes X in the form of X_2, CX_4 and NX_3 are oxidized to X_2O at the catalytic reactor. The reactor is operated at 550°C so that conversion ratio of CX_4 is expected to be higher than 10^6. Twice as much oxygen as required for oxidation is fed to the reactor from the electrolysis cell as well as gas bottle.

Exhaust of the reactor subsequently passes through freezers for separation of X_2O and tritium-free species. The operat temperature of 160K is the lowest temperature at which CO_2 will not be frozen out. Water vapor pressure at the outlet is expected to be lower than 0.1 ppm. Gas from the freezer contains He, CO_2, N_2 and O_2 is sent to the Effluent tritium Removal System (ERS) of the TPL for final detritiation before release to the environment. Trace of CX_4 and X_2O that failed to be processed in the loop will be the dominant loss of tritium from the apparatus

and the amount is expected to be less than 10 ci/y. A part of the freezer exhaust is recirculated to the catalytic reactor inlet to dilute combustible species. A molecular-sieve bed at room temperature is a back up of the freezers.

The freezers are periodically regenerated by inert stream and tritiated water X_2O is decomposed in the Water decomposition subsystem. This subsystem consists of a ceramic electrolysis cell, a small palladium diffuser and a vacuum pump. Mixture of inert and X_2O from the regenerating freezer is split to pure oxygen flow and a mixture of X_2 and He at the cell. Hydrogen gas is purified by a second diffuser followed by a vacuum pump. A part of this pure hydrogen stream is recirculated to maintain stable flow rate in the loop and excess is sucked by zirconium-cobalt beds. Diffuser bleed contains He, small amount of X_2 and X_2O is recirculated to the catalytic reactor feed.

An example of the material balance in the system is shown in the table 1. Processing rate of the simulated plasma exhaust is 3 mol/h of X_2 and impurities up to 15%. Tritium inventory in the system of 1g will make DT mixture contains tens of % of T.

Gas analysis system for this experiment is shown in the Fig.3. Three gas chromatographs are used for the seven samples taken periodically from the loop. Thermal conductivity detector and ion chamber will be used. Hygrometers will measure vapor concentration at the inlet and outlet of the diffuser, the catalytic reactor, freezers and the electrolysis cell. An ion chamber monitors total tritium flow to the ERS.

The system is operated from the local panel. Pressures, flow rate and temperatures are controlled automatically with manual set values. Major valves that will control main flow of the loop are operated pneumatically from the panel while minor ones are manual. Some interlocked actions will be operated automatically for the off-normal cases such as loss of power or malfunction of components.

Data will be processed and recorded by a 16 bit desk top computer. CAMAC interface is applied to transfer the data on the pressure, flow rate, temperature, and status of the system to the computer.

MAJOR COMPONENTS

(1) Palladium diffuser

Figure 4 shows the structure of the palladium diffuser for this apparatus. The palladium tubes of 60cm long are contained in the double stainless steel jacket. A couple of heater wire are wound on the inner shell. Permeated tritium from the inner shell is contained in the outer shell. Approximately 3 mol/h of hydrogen isotopes is purified by this diffuser. The operation temperature is 300°C and pressure at the feed and permeated side of the membrane is 760 torr and 10 torr respectively.

(2) Electrolysis cell

Figure 5 is an example of the structure of the electrolysis cell. In the figure, 10 zirconia tubes are contained in the

double stainless steel jacket. Heater wires are wound on the copper tubes where zirconia tubes are inserted one by one. The operation temperature is 600°C. Total 2.5mol/hr of gas will flow in the cell and 0.18 mol/hr of water will be decomposed. Cell voltage of up to 2.0V is supplied and controlled by potentiostat so that 1.3 V of Ir-free voltages are maintained.

(3) Zirconium-cobalt bed

The structure of the zirconium cobalt beds for recovery, storage and supply of hydrogen isotopes are shown in the Fig.6. Seven sintered stainless steel filter tubes contains activated powder of intermetallic compound ZrCo mixed with copper grains for heat sink and placed horizontally in the copper heater block. The capacity of each bed is approximately 200 litter of hydrogen gas. Hydrogen gas is recovered at room temperature and released at 400°C. Mixture of hydrogen and inert gas can be processed by recycling operation through this bed configuration.

(4) Catalytic reactor

A catalyc reactor operated at 550°C processes palladium diffuser bleed at flow rate of 3 mol/h. Precious metal catalyst is loaded. Double jacket will contain the permeated tritium at high temperature.

(5)Freezers

Three freezers are operated alternatively to freeze out 0.18 mol/h of tritiated water continuously. Fluorocarbon will be used for coolant.

(6)Pumps

Metal-bellows sealed oil free pumps (reciprocating pump and/or Scroll pump) are used for evacuation of palladium diffuser and gas transfer.

OTHER ENGINEERING REQUIREMENTS

This apparatus requires following items in design and fabrication for tritium service.

The apparatus should be completely leak tight. Whole plumbing and components are tested with helium leak detector.

The piping and components are made of stainless steel or copper. Joints should be welding, VCR fittings or conflat flanges with metal gaskets. Components operated at high temperatures should be doubly contained in order to prevent tritium permeation.

No organic materials can be exposed to tritium in the apparatus except for some minor components where very low tritium concentration is expected and will not be used often. Oils should not be used in any place to avoid contamination.

Configuration of the apparatus should be carefully designed so that it will fit in the glovebox and manual valve operation and maintenance work through gloves will be easy. The apparatus

will be operated from outside. Remote controle and data aquisition system is required.

Minimize tritium inventory.

SCHEDULE

The final design and fabrication of some components are being performed. The whole apparatus will be installed in the summer, 1987. Experiment with tritium is scheduld from the beginning of 1988 after the check out and testing without tritium.

Table 1 Example of mass balance in the apparatus.

	1	2	3	4	5	6	7	8	9	10	11	12	13	14	15	16	17
X_2		2.955 85.0	2.898 100	0.057 9.9		0.082 0.7	§	§	§	§		0.159 5.1		0.134 100	0.025 1.0	0.0315 100	0.102 100
He	0.45 95.0	0.45 13.0		0.45 78.3		11.80 97.2	11.80 97.6	11.80 98.9	2.95 98.9	8.85 98.9	2.50 94.0	2.50 94.9			2.50 99.0		
CX_4	0.009 2.0	0.009 0.3		0.009 1.6		0.009 0.1	§	§	§	§							
NH_3	0.009 2.0	0.009 0.3		0.009 1.6		0.009 0.1	§	§	§	§							
X_2O		0.045 1.3		0.045 7.8		0.045 0.4	0.159 1.3	§	§	§	0.159 6.0	0.0001 0					
N_2	0.0045 1.0	0.0045 0.1		0.0045 0.8		0.0315 0.3	0.036 0.3	0.036 0.3	0.009 0.3	0.027 0.3							
O_2					0.079 100	0.121 1.0	0.055 0.5	0.055 0.5	0.013 0.5	0.042 0.5			0.079 100				
CO_2						0.027 0.2	0.036 0.3	0.036 0.3	0.009 0.3	0.027 0.3							
TOTAL	0.473 100	3.473 100	2.898 100	0.575 100	0.079 100	12.125 100	12.086 100	11.927 100	2.982 100	8.946 100	2.659 100	2.659 100	0.079 100	0.134 100	2.525 100	0.0315 100	0.102 100

MOL/H
%

§ : TRACE, DETECTED WITH ION CHAMBER

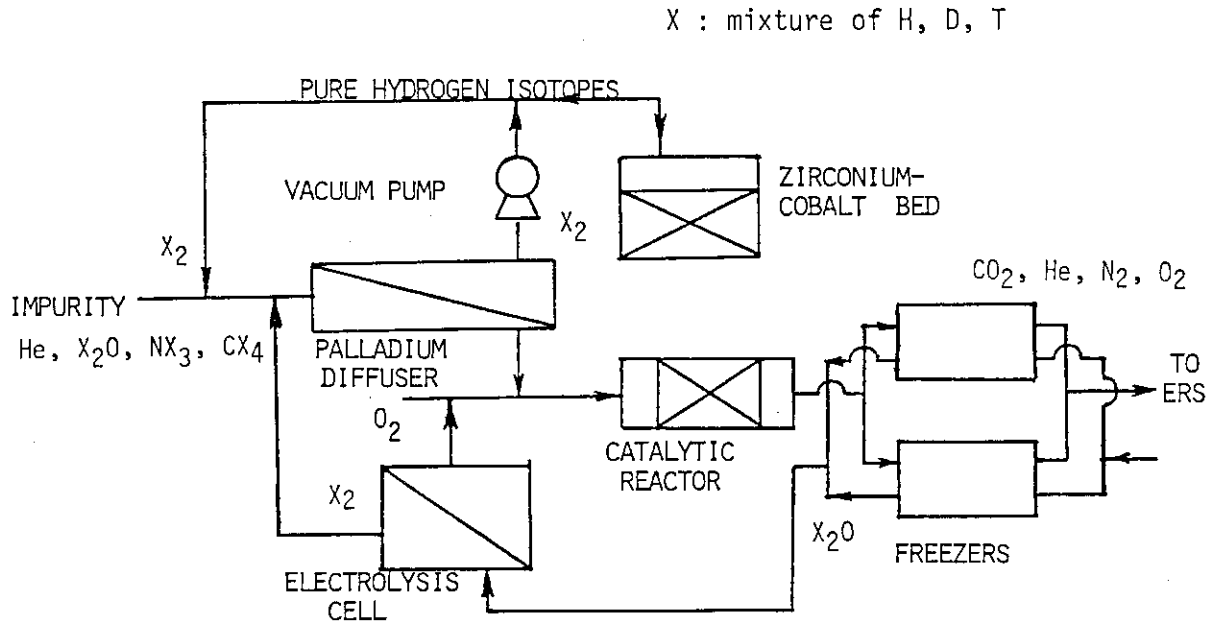

Fig.1 Simplified flow of the Fuel Cleanup System.

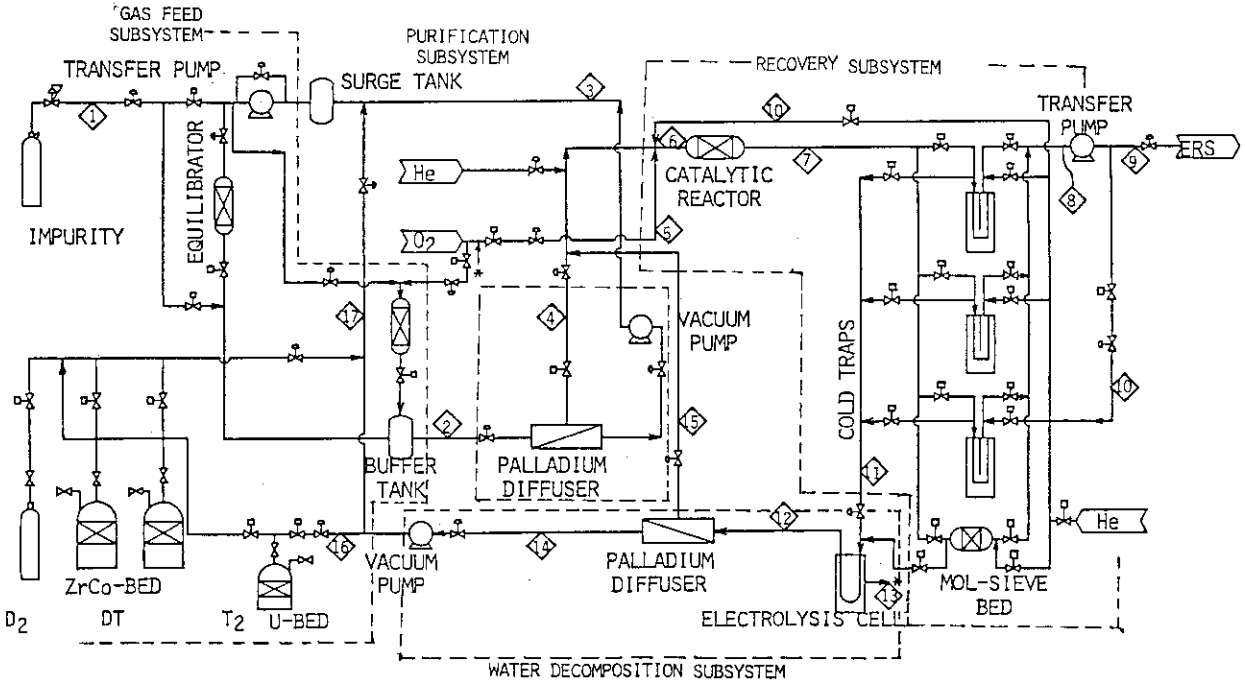

Fig.2 Schematic flow diagram of the experimental apparatus for the Fuel Cleanup. It consists of four subsystems.

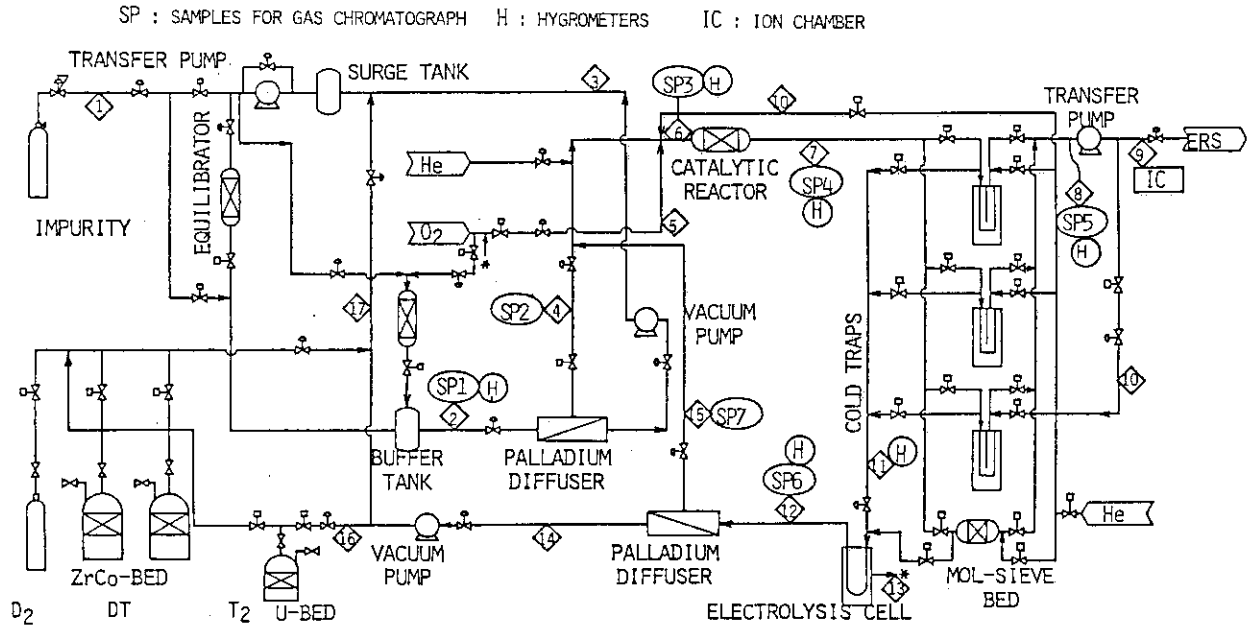

Fig.3 Gas analysis system for the experiment. Seven sampling points for gaschromatography, six hygrometers and an ion chamber are indicated.

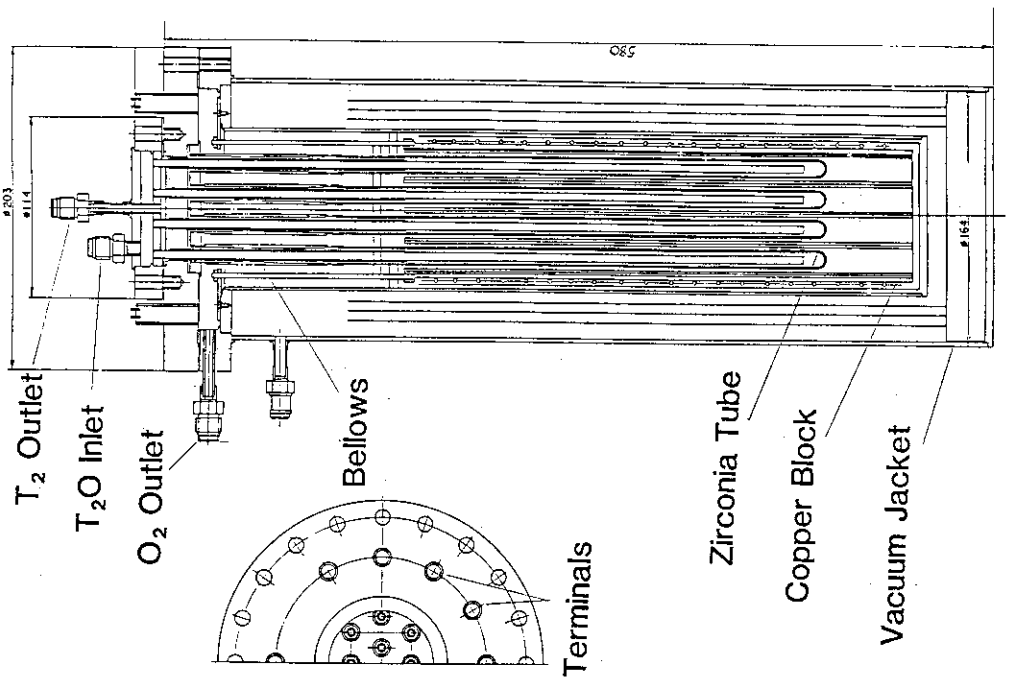

Fig.5 Structure of the electrolysis cell for decomposition of tritiated water vapor.

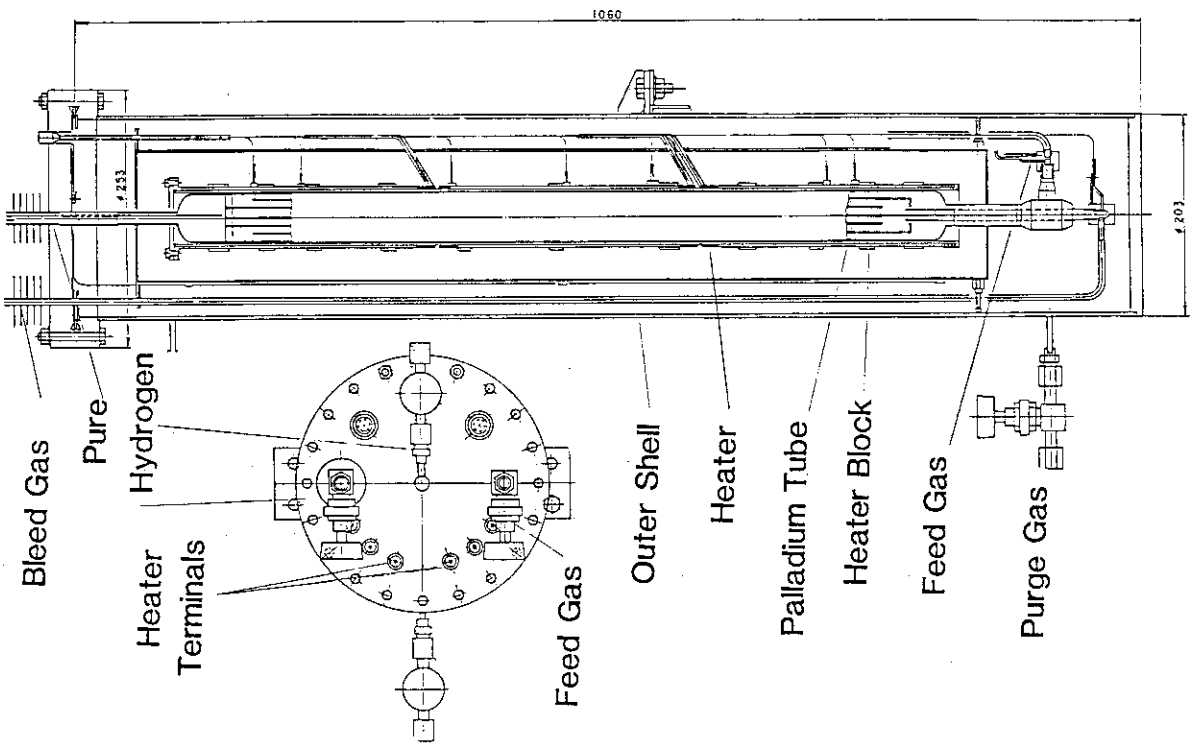

Fig.4 Structure of the palladium diffuser for purification of hydrogen isotopes.

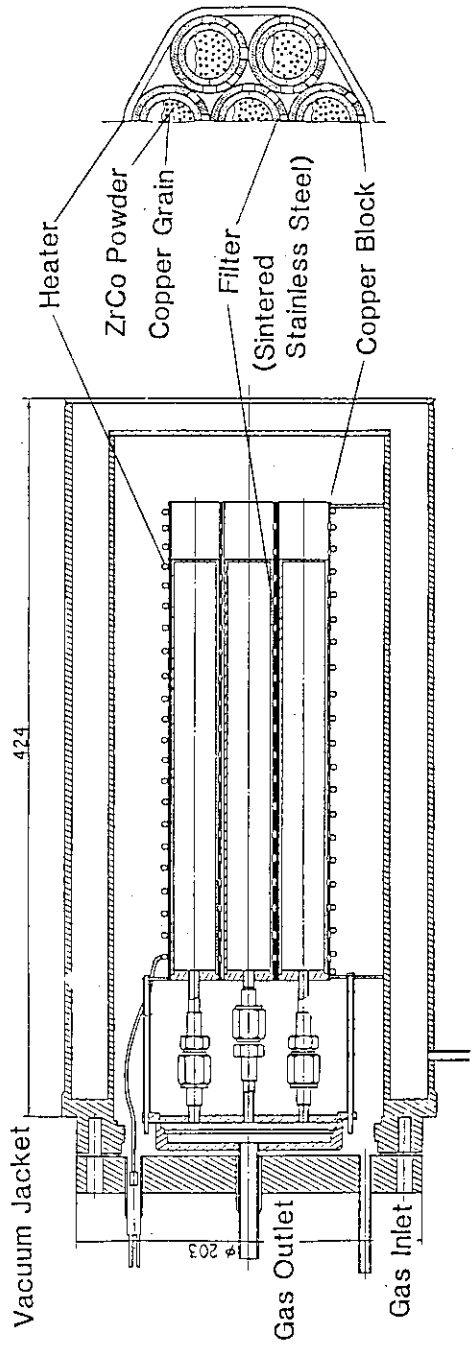

Fig.6 Structure of the zirconium-cobalt bed for recovery, storage and supply of hydrogen isotopes.

No.24

Brief Description of Experimental Apparatus for Hydrogen Isotope Separation by Cryogenic Distillation

Toshihiko YAMANISHI

Department of Thermonuclear Fusion Research,

Naka Research Establishment, JAERI

ABSTRACT

A design study has been performed for an experimental apparatus for hydrogen isotope separation by cryogenic distillation. The experimental apparatus handles hydrogen isotope mixture of all six molecular species (H_2, HD, HT, D_2, DT and T_2). The major items in the design study are to draw a flow schematic of the system, to determine the structures of the components and to examine operation and control modes.

INTRODUCTION

Separation of hydrogen isotopes by cryogenic distillation has various advantages : a comparatively large processing flow rate even with a compact scale device, high separating performance and negligible tritium permiation owing to the cryogenic operating temperature. Hence, it appears that cryogenic distillation is best suited to the needs in the mainstream fuel circulation system for fusion reactors.

Computer simulation studies for hydrogen isotope distillation columns were performed by Sherman & Bartlit[1], Wilkes[2] and Kinoshita[3]~[5]. Although these studies produced much useful information, the experimental data previously reported for the cryogenic distillation column is limited. Additionally, detail information is not given for the experimental condition[6][7]. Thus, further experimental studies are desired.

As the first stage of a research program to explore the characteristics of the cryogenic separation system, the author initiated an experimental study for hydrogen/deuterium distillation column. Some fundamental engineering data such as the HETP, liquid holdup and pressure drop will be obtained by the study. As the next step of the research program, a design study has been performed for an experimental apparatus separating hydrogen isotope mixture containing tritium. The major purpose of the experiment are to study separation characteristics of the

column and to examine the static and dynamic behavior of the apparatus.

The present paper gives a brief description of the above-mentioned experimental apparatus : the flow diagram of the apparatus, structures of the principal components and the operation and control modes are reported.

Brief Description of Experimental Apparatus

The feed gases to the experimental apparatus is mixture of protium, deuterium and tritium isotopes. Maxium amount of tritium used for experiment is 10^4 Ci.

A simplified flow diagram of the experimental apparatus is illustrated in Fig. 1. The apparatus has two distillation columns with room temperature equilibrators. Each column can independently be operated, addionally, two cascades can be tested. The flow diagrams under the above three operation modes show bold lines in a series of figures (Fig. 1~3). In the all operation modes, output streams from the columns or cascades are recycled as seen in the figures.

Figure 4 shows a brief system diagram of the experimental apparatus. The apparatus consists of the following system.

(i) cryogenic distillation system
(ii) gas circulation system
(iii) gas supply and recovery system
(iv) refrigeration system
(v) sampling system
(vi) vacuum system

Functions and principal components of the above-mentioned systems are as follows.

(1) Cryogenic distillation system

The present system consists of two cryogenic distillation columns and heat exchangers which refrigerate feed gases to about 20 K. The above components are set in a vacuum chamber in order to shield against thermal radiation and conduction.

(2) Gas circulation system

The functions of the present system are to remove impurities of the output streams from the columns or cascades and to recycle them. The principal components of the system are four equilibrators, two cryosorption and adsorption beds and two circulation pumps. The system is equiped a recovery tank and rupture disks for protection against overpressure due to loss of refrigeration.

(3) Gas supply and recovery system

The functions of the present system are to supply hydrogen isotope mixture to the columns and to recover the holdups within the cryogenic distillation and gas circulation systems. The principal components of the system are hot metal beds and a mixing chamber.

(4) Refrigeration system

The function of the present system is to supply the refrigeration for the two distillation columns and heat exchangers by the helium refrigerator as shown in Fig. 4.

(5) Sampling system

Figure 5 shows a simplified flow diagram of the present system. The system comprises two gaschromatographs and a liquid nitrogen bath used for strage of sampling gases withdrawn from the two distillation columns. The distillation columns has eight sampling points as shown in Fig. 4 (S1A~D, S2A~D), and five measuring tubes are attached to a point.

(6) Vacuum system

The function of the present system is to evacuate the vaccum chamber (10^{-5} Torr), the distillation columns (10^{-3} Torr), the measuring tubes (10^{-2} Torr) and vacuum enclosure of pipe lines for heat insulation (10^{-5} Torr) by an turbo molecular pump.

Design of Principal component

Hydrogen distillation columns operate at a nominal temperature of 20~24 K. In addition to the design requirements imposed by the cryogenic temperatures, the process gas contains radioactive tritium which imposes an additional set of constraints. As a result, all components and material of them are designed or selected to be compatible with low temperatures and tritium service in terms of reliability and safety. In addition, since the experimental apparatus is set in the glove box, design concepts must include ease of operation and maintenance. All the circulation pumps are doubly contained, within the inert gas jecket as the outer containment. All joints for piping are either welded or flanged, and all valves and components requiring maintenance are installed with "VCR" fittings on all process connections.

The design parameters for the principal components are presented in Table. The two distillation columns having inside diameters of 2 and 1 cm and packed heights of 50 cm are filled with 3 and 1.5 mm Dixon Ring, respectively. Helium refrigerator whose capacity is about twice as much as that required for the two columns (130 W) is selected for the experimental apparatus.

The basic structures of the principal components are as follows.

(1) Distillation column

Figure 6 shows a schematic diagram of the distillation column. The volumes of the reboilers are designed that the holdup within them are adequately larger than those within the columns lost by sampling. The condensers are refrigerated by helium streams at approximately 20 K with the gases flowing in tubes soldered to the exterior of the condenser. Copper fins are used within the condensers to provide ample condensation area for column reflux.

(2) Vacuum chamber

Figure 7 shows a schematic diagram of the vacuum chamber. The two columns and heat exchangers are attached to a central support and this assembly wrapped with multilayer insulation. The column assembly is enclosed within a thermal radistion shield cooled by liquid nitrogen. The vacuum chamber hauses helium control valves, heaters and temperature sensors wrapped with multilayer insulation. All critical heaters and temperature sensors located within the chamber are redundant.

(3) Gaschromatograph

Figure 8 shows a flow diagram of the gaschromatograph. The gaschromatograph comprises the separation column packed with alumina coated with $MnCl_2$ (inner diameter and length are 0.5 cm and 200 cm, respectively), thermal conductivity detector, ion

chamber and instruments for automatic analysis. The separation column is cooled to liquid nitrogen temperature.

The sample gases stored in the measuring tubes are automatically analyzed in order. The time required for analysis of a sample is about 54 min.

Control System

The experimental apparatus provides for complete manual control and local automatic control with manual set point. Condenser pressures of two columns are under automatic control varing helium temperature, and reboiler heat control is set manually since the rates of the feed and output streams are kept constant by mass flow controller.

REFFERENCES

(1) J. R. Bartlit, R. H. Sherman, and R. A. Stutz : Cryogenics, 19, 275 (1979)

(2) W. R. Wilkes :Proc. Int. Conf. Radiation Effects and Tritium Technology for Fusion Reactors. Gatlinburg, Tenessee, September 30-October 5, 1975, CONF-750989, IV, 266 (1976).

(3) M. Kinoshita, et al. :J. Nucl. Sci. Technol., 18, 7, 525 (1981).

(4) M. Kinoshita and Y. Naruse :Nucl. Technol./Fusion, 2, 410 (1982).

(5) M. Kinoshita :Doctoral Dissertation, Kyoto University (1983).

(6) W. R. Wilkes :MLM-2502, p. 10, Mound Laboratories, Miamisburg, Ohoi (1978).

(7) R. H. Sherman, J. R. Bartlit, and W. H. Denton :Proc. 3rd Topical Mtg. on Technol. of Controlled Nuclear Fusion, Santa Fe, NM, May 9-11, 1978.

Table　Design parameters for principal components

Distillation columns		Column No.1	Column No.2
	Pressure	about 360～1120 Torr	about 360～1120 Torr
	Temperature	about 20～ 25 K	about 20～ 25 K
	Dimensions (packed section)	20 mm (inner diameter) 500 mm (packed height)	10 mm (inner diameter) 500 mm (packed height)
	Packing	Dixon ring ϕ3 mm (dimension) SUS316 (material)	Dixon ring ϕ1.5 mm (dimension) SUS316 (material)
	Reboiler heat duty	100 W	30 W
Sampling system	Gaschromatograph Ion Chamber	Thermal conductivity detector 0.5 μCi ～ 50 mCi (range)	
Helium refrigerator		Refrigeration output 240 W (at 20 K) Helium pressure 2.4 atm	
Circulating pump	Double bellows pump	900 Nℓ/hour (max.) 225 Nℓ/hour (max.)	
Helium leak rate		1×10^{-8} Acc/sec (one joint) 1×10^{-6} Acc/sec (whole apparatus)	

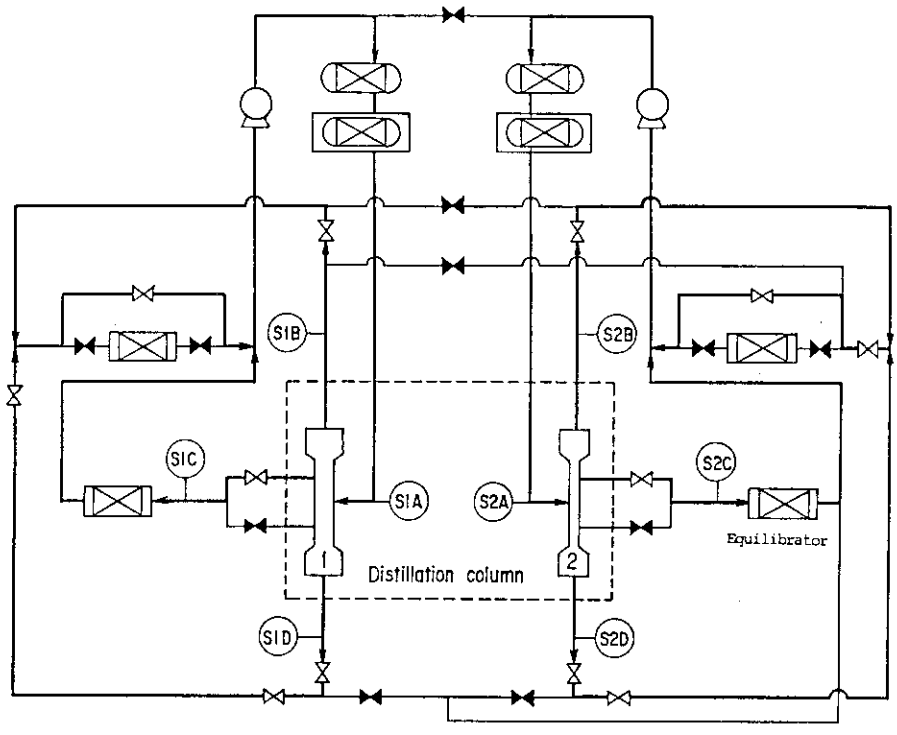

Fig. 1 Simplified flow diagram of experimental apparatus
Bold lines show flow diagram in the case where the two columns with feedback streams are independently operated.

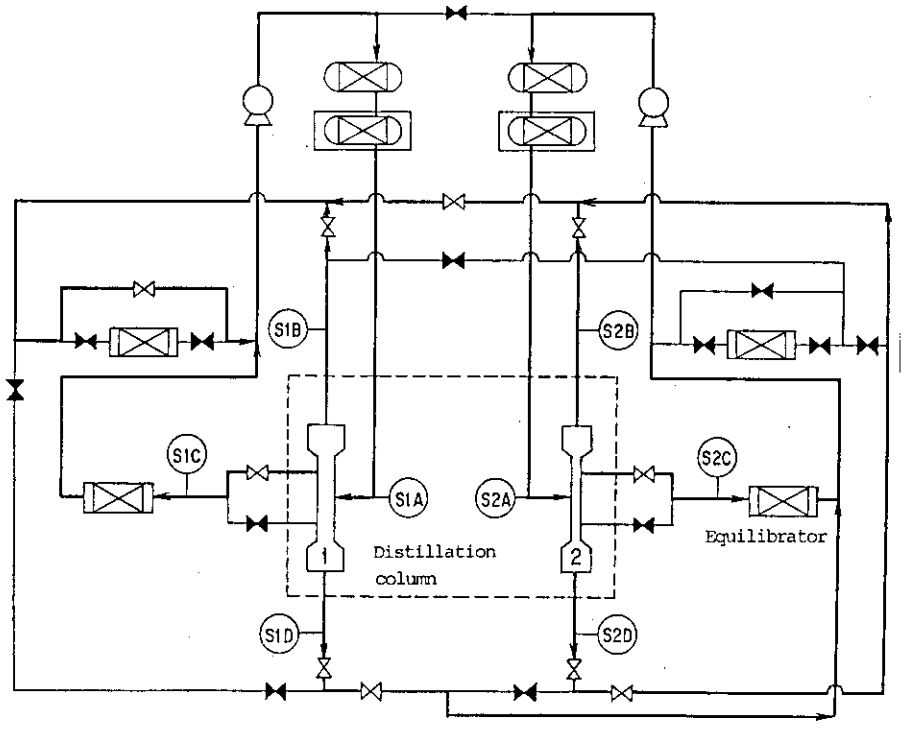

Fig. 2 Flow diagram of column cascade (2)

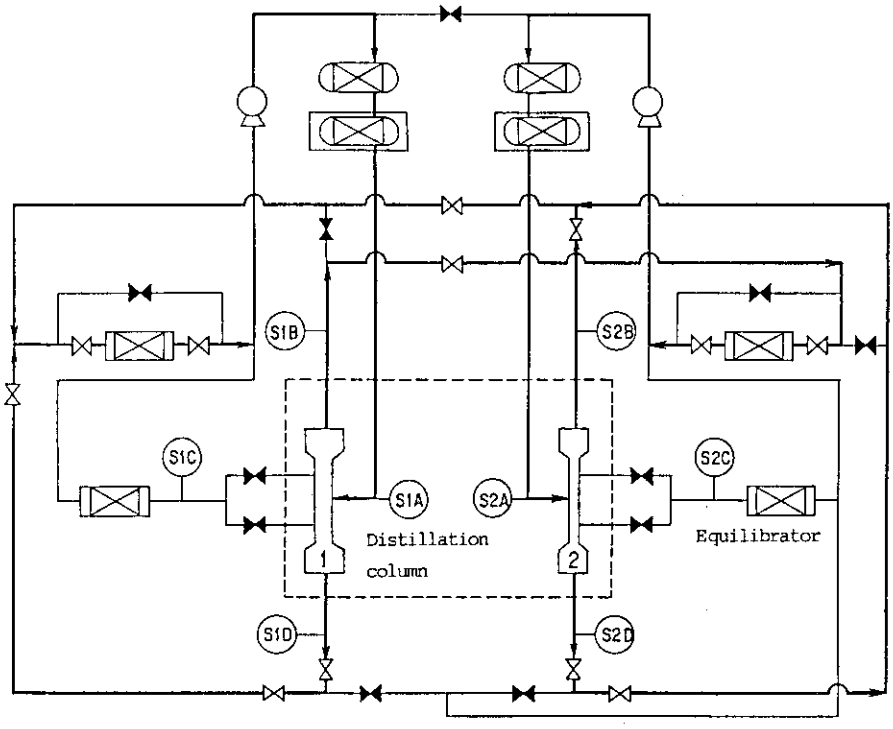

Fig. 3 Flow diagram of column cascade (1)

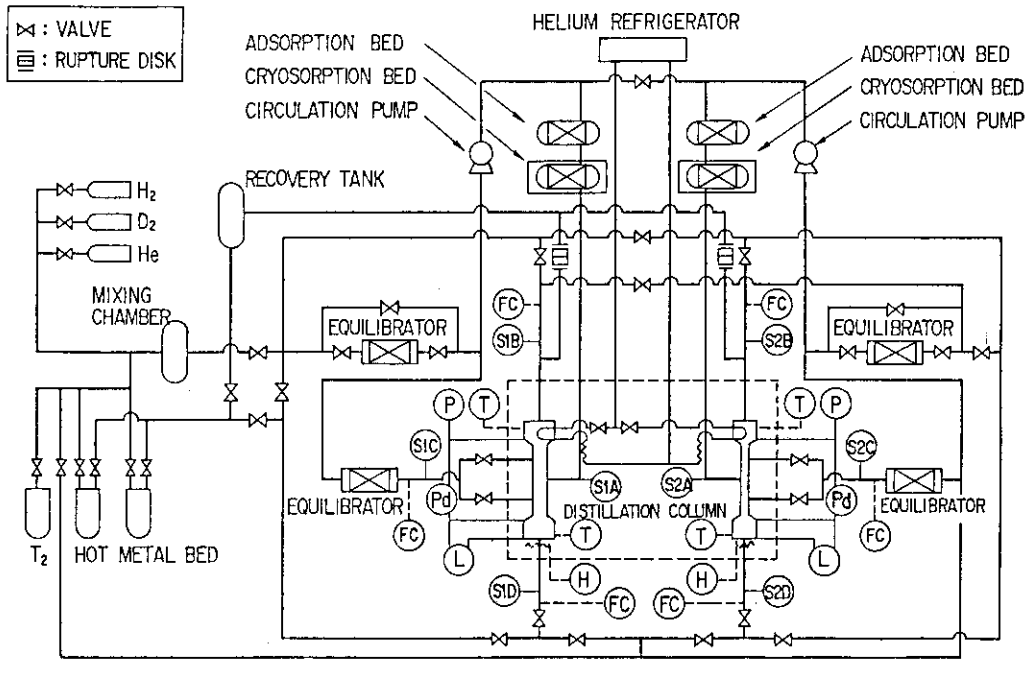

Fig. 4 Brief system diagram of experimental apparatus

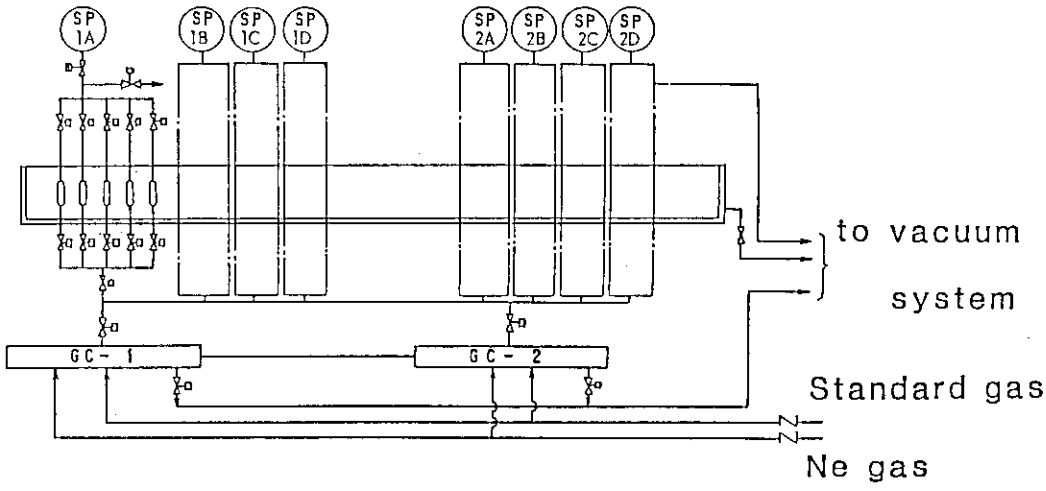

Fig. 5 **Flow diagram of sampling system**

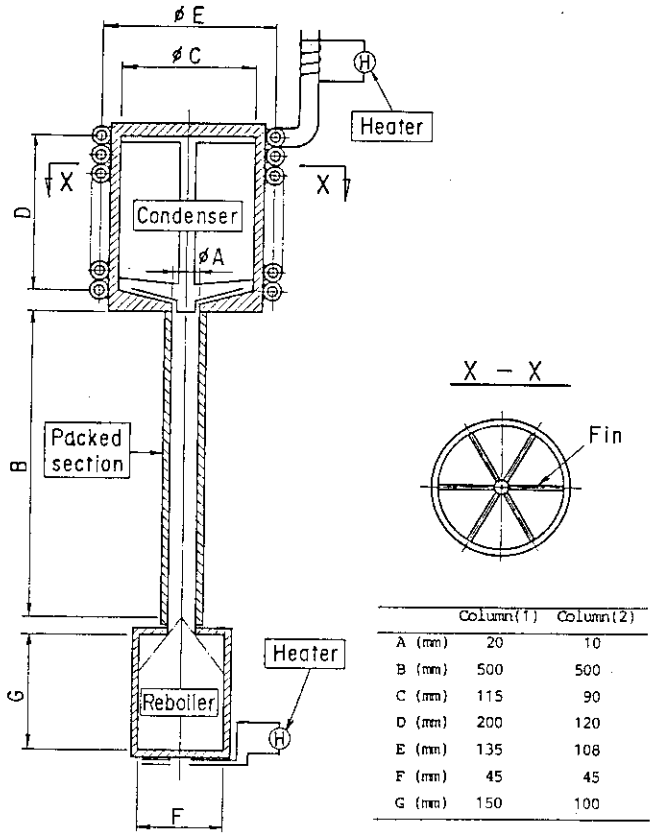

	Column(1)	Column(2)
A (mm)	20	10
B (mm)	500	500
C (mm)	115	90
D (mm)	200	120
E (mm)	135	108
F (mm)	45	45
G (mm)	150	100

Fig. 6 Schematic diagram of distillation column

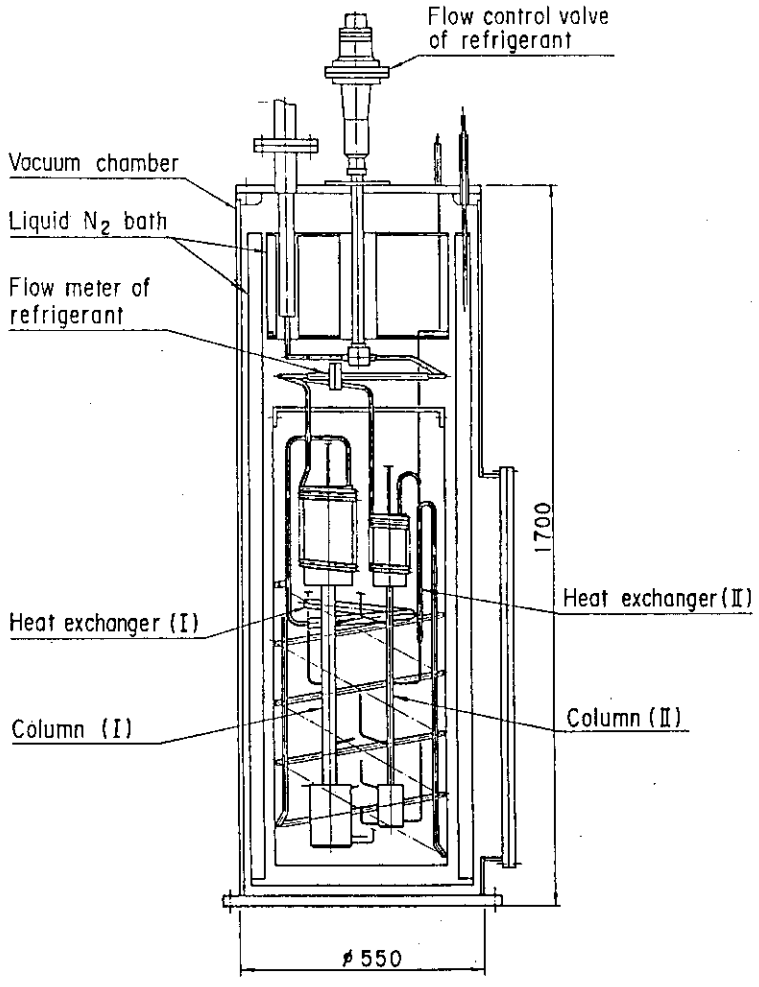

Fig. 7 Schematic diagram of vacuum chamber

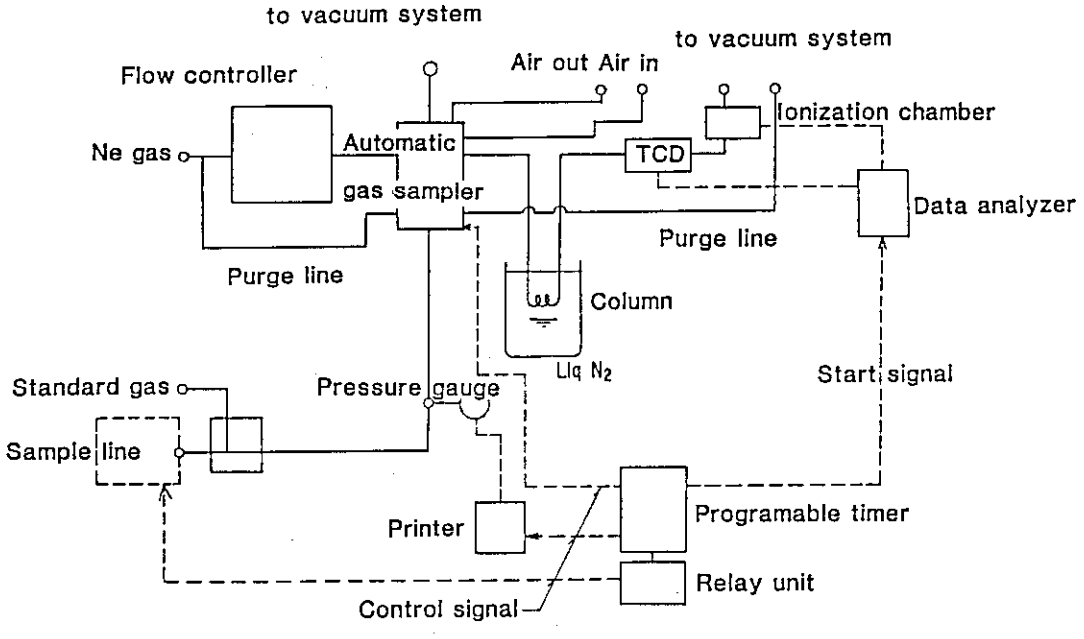

Fig. 8 **Flow diagram of analyzing system**

No.25

BRIEF DESCRIPTION OF EXPERIMENTAL APPARATUS FOR TRITIUM PERMEATION STUDIES

Kenji OKUNO, Shigeru O'HIRA, and Masahiro MISUMI

Tritium Engineering Laboratory
Department of Thermonuclear Fusion Research
Japan Atomic Energy Research Institute

abstract: An experimental apparatus for tritium permeation study is now under development in JAERI. Major characteristics of the apparatus are that (a) tritium experiment is available; (b) high flux of ion beam at low energy (<1KeV) is attainable to simulate realistic bombardment; and (c) simultaneous measurement of the sputtered ions from the front surface with a secondary ion mass spectrometer.

1. Introduction

For D-T fusion reactors, a key safety issue is the release of tritium implanted into first walls and limiters. We are especially interested in permeation of implanted tritium through the first walls and limiters into coolants. Although a number of experimental and theoretical studies on implantation-driven-permeation have been undertaken extensively, there are considerable uncertaities in prediction of tritium permeation behavior under actual operation conditions of the fusion rectors. In the previous experimental studies, hydrogen and deuterium ion beams were used to simulate the tritium bombardment on the first wall of fusion reactors. To progress the understanding of the permeation behavior of the implanted tritium, an advanced experimental approach is needed, involving tritium ion bombardment on the candidate materials of first walls.

In this situation, we have designed an experimental apparatus for tritium ion implantation-driven-permeation studies. Since the design is now under way, a summary of present status is briefly described here.

2. Overall objectives

1) To confirm the extrapolation of H/D data to T for plasma driven permeation.
2) To assess the permeation barrier effect of coating

materials.

3) To investigate the correlation between bulk/surface conditions and permeation/retention behavior.

4) To confirm calculation models to predict reemission, retention, and permeation of implanted tritium.

3. Design of experimental apparatus

3.1 Basic design requirements

Basic design requirements relating to tritium handling are as follows.

1) The experimental hardware are to be placed in the glovebox ($4.5m^{L}x1.2m^{W}x1.5m^{H}$) in TPL.

2) The maximum amount of tritium permitted to use for one batch operation is 1g(10,000 Ci).

3) Vacuum plumbing must be made up of all metal construction, and metal gasket must be used to make vacuum seals at all connections.

4) Oil-free type vacuum pumps must be used.

5) The tritium gas exhausted from the main pump must be recovered by use of tritium getter.

3.2 Design description

The schematic diagram of experimental apparatus designed for implantation driven permeation experiment is illustrated in Figure 1. The apparatus consists of (1) ion source for

production of intense ion beam, (2) main chamber system for ion implantation into specimen and for measurement of experimental parameters, (3) downstream system for measurement of permeated gas through the target specimen (4) evacuation system, and (5) tritium gas supply and recovery system. The schematic flow diagram of the apparatus is shown in Figure 2.

(1) Ion source

The first wall and limiter will be bombarded by a flux of 10^{15} to 10^{17} atoms/cm^2.s of charge exchange neutral tritium at relatively low energies below 200 eV. To simulate the high flux and low energy implantation, we have adopted the newly developed powerful hydrogen ion source.

The ion source is a modification of the quartz capillary duoPIGatron proton source developed by Isoya and Inoue (Kyushu University)[1]. Conceptual drawing of the ion source is shown in Figure 3. A dense narrow plasma is generated by the duoplasmatron and PIG discharge mechanism(duoPIGatron) in a quartz tube to which a strong magnetic field is applied along the tube axis and very high density of ion current is obtainable from the narrow exit hole at the end of tube with a high proton percentage as large as 90%. The extraction of ion beam is achieved by an extraction grid which is positioned just downstream of the exit hole. Ion beam energy is varied by the extraction grid from about 20 eV to 1 keV continuously. The beam energy is representative of implan-

tation energies expected on the first wall. Ion flux larger than 0.2 mA/cm ^{2} for 200 ev D^+ and 2 mA/cm^2 for 1KeV is expected at the target.

Gases are fed to the ion source at a required rate by use of a mass flow controller unit. Deuterium and hydrogen gases are supplied from gas cylinders and tritium gas is supplied from a metal getter through a reservoir tank.

(2) Main chamber system

The main chamber is a vacuum vessel that contains target sample-holder assembly and various diagnostic tools to measure experimental parameters. The cross section view of the main chamber is shown in Figure 4. The vacuum vessel is a type-304-ss cylindrical chamber which is about 50 cm long and 40 cm in diameter. The ion source is connected to one end of the cylinder. The sample-holder assembly which is connected to a separate vacuum line (downstream system) is inserted to the chamber interior.

The target sample holder is illustrated in Figure 5. The target specimen for permeation test is a 0.1 to 1mm thick membrane disk with a diameter of 2 cm which is welded to the support. A halogen lamp is located in the back side of the target to heat the target specimen(<700°C), and a thermocouple is attached to the support to monitor the target temperature. The sample support is electrically isolated from the base flange by an insulator to enable measurement of incident ion current.

For the purpose of in-situ analysis of front surface, Auger Electron Spectrometer(AES) and Secondary Ion Mass Spectrometer(SIMS) are incorporated in the system. In particular, measurements of the surface property by SIMS is simultaneous with the measurements of permeating gas.

Beside the surface analyzers, a variety of analytical tools are to be equipped with the main chamber. Nude ionization gauges are used to measure system pressure in the high vacuum regime and pirani gauges are used for low vacuum regime. Residual gas composition in the target chamber is measured with a QMS head of SIMS. The ion beam current is measured by use of a Faraday cup and the ion energy distribution can be measured applying retarding method. A high speed shutter plate for stopping the ion beam is equipped at the exit of ion source to measure the permeation response to ion implantation.

In addition to the target holder for permeation measurements, a sample manipulator is equipped in the main chamber. Sample materials provided for surface analysis are delivered to the sample manipulator by a sample transporter. To facilitate the sample exchange, sample loading chamber is coupled to one of the ports of the main chamber. This sample loading chamber is isolated by a gate valve and connected to the rough line of the vacuum system. By use of this sample loading system, quick exchange of sample is available without affecting the high vacuum of the main chamber.

(3) Downstream system

In the course of permeation experiment, the back side of the target specimen is exposed to a vacuum. A 80 l/s (N_2) ion pump is used to maintain the vacuum of downstream line. The measurement of the permeating gas will be accomplished by a quadrapole mass spectrometer(QMS) and the permeating rate will be calibrated with a standard leak. In the series of tritium operation, the permeating rate will be quantitatively determined most accurately by use of tritium monitors.

(4) Evacuation system

To facilitate the recovery of exhausted tritium gas, a cryopump unit (3600 l/s, H_2) is used to maintain the vacuum of the main chamber. And a sputter ion pump(80 l/s,N_2) is used to keep the downstream vacuum line at a high vacuum. A turbomolecular pump is provided for rough pumping of the whole vacuum system including the target loading chamber. This turbomolecular pump is backed by the exiting vacuum pump system (VPS) of TPL. The exhausted gas is to be processed by effluent tritium recovery system (ERS).

As already stated, vacuum line is of all metal construction. Metal gaskets are used at all connections wherever possible. And bakeable valves and metal bellows valves are used wherever necessary.

A conceptual flow diagram to illustrate the system opera-

tion mode under tritium permeation experiment is shown in Figure 6.

(5) Tritium gas supply and recovery system

Two metal getters are to be used to supply and to recover tritium gas. Tritium gas released from a metal getter into the reservoir tank will be fed to the ion source at a required rate through a mass flow controller. And the tritium gas storaged in cryopump is recovered by another metal getter.

Plumbing is of all metal construction, and metal gasket is used to make seals at all connections. And valves are of all metal bellows valves.

Figure 7 shows the flow diagram of the system during tritium recovery operation.

(6) Layout plan

The experimental hardware of this apparatus are to be placed in a glovebox ($4.5m^{L}x1.2m^{W}x1.5m^{H}$) of TPL. Figure 8 shows the layout plan of this apparatus in the glovebox. Control electronics to operate the apparatus are to be packaged into a instrument rack which is placed outside the glovebox.

4. Safety analysis

The potential of radiation hazard of this apparatus under normal operation has been evaluated.

The possible radiation hazards of this apparatus will come from the following:

i) Tritium leakages from the experimental hardware,

ii) X-ray emission due to bremsstrahlung in target sample, and

iii) 14 MeV Neutron emission from target sample due to $D(T,n)^4He$ reaction.

Calculated results are listed in Table 1. The maximum tritium leakage rate to the glovebox atmosphere under normal operation is estimated to be 2.5×10^{-3} Ci/hr, which is lower than the design commitment value op TPL: 0.01 Ci/hr for one glovebox. X-ray emission yield due to bremsstrahlung is estimated to be 2.5×10^{10} photons/sec. Fortunately, the energy of the bremsstrahlung x-ray is so small that the chamber structure works as a enough shield. If deuteron (or triton) is implanted onto tritium (or deuterium) containing sample, 14 MeV neutron emission occurs through $D(T,n)^4He$ nuclear reaction. This neutron production rate is roughly estimated to be 0.36 neutron/sec. at most. The corresponding dose rate at the outer surface of main chamber is only 1.1×10^{-5} mrem/hr.

Based on the above evaluations, we have confirmed that the health and safety of workers will not be affected by

operation of this apparatus.

5. Schedules

The time schedule of this R&D program is shown in Figure 9. The final design activities are now underway. The construction is going to start in the end of next January in earnest. Installation into the glovebox will be completed in the end of September 1987.

Reference

[1] A Isoya and T Inoue, " A proton source for high-intensity Lamb-shift-type polarized ion source ", Inst. Phys. Conf. Ser. No.54:Chapter 7.

Table 1. Safety analysis

1. Neutron Dose Rate from $d(T,n)^4He$ Reaction
   - Total Neutron Generation Rate : 0.36 n/sec
     D^+ flux : 0.4 mA/cm^2
     T in S.S. : 5×10^{21} T/cm^3
     D^+ energy : 1 keV
     Cross Section : 10^{-8} barn
   - Dose Rate on the Outside Surface of Main Chamber :
     1.1×10^{-5} mrem/hr

2. Bremsstrahlung Radiation from Specimen
   - Bremsstrahlung Yield : 2.5×10^{10} photons/sec
   - Dose Rate on the Outside Surface of Main Chamber : ～0 R/hr
     Gamma energy : 18 keV
     Wall Thickness : 5 mm

3. Tritium Transportation Rate to GB Atomosphere (Normal Condition)
   - Tritium Permeation : 1.1×10^{-5} Ci/hr
   - Tritium Leakage : 2.5×10^{-3} Ci/hr
     Leakage Rate of Equipment : $< 10^{-6}$ Acc/sec

4. Tritium Transportation Rate to GB Atomosphere (During Maintenance)
   - Without Baking : 0.14 Ci (During 8 hrs')
   - Baking at 300 C for 24 hr : 0.0014 Ci (During 8 hrs')

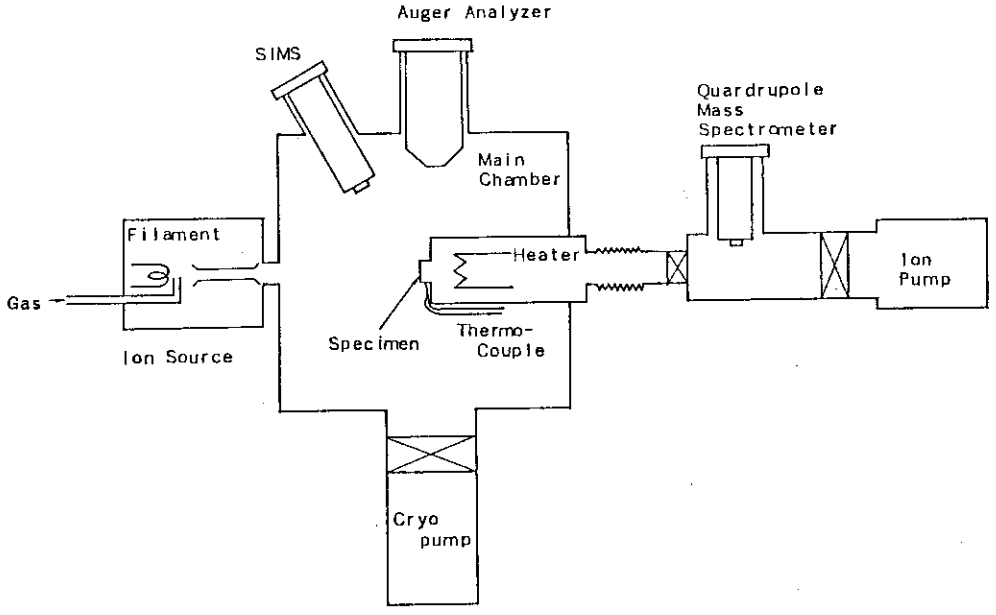

Figure 1. Schematic illustration of the experimental apparatus.

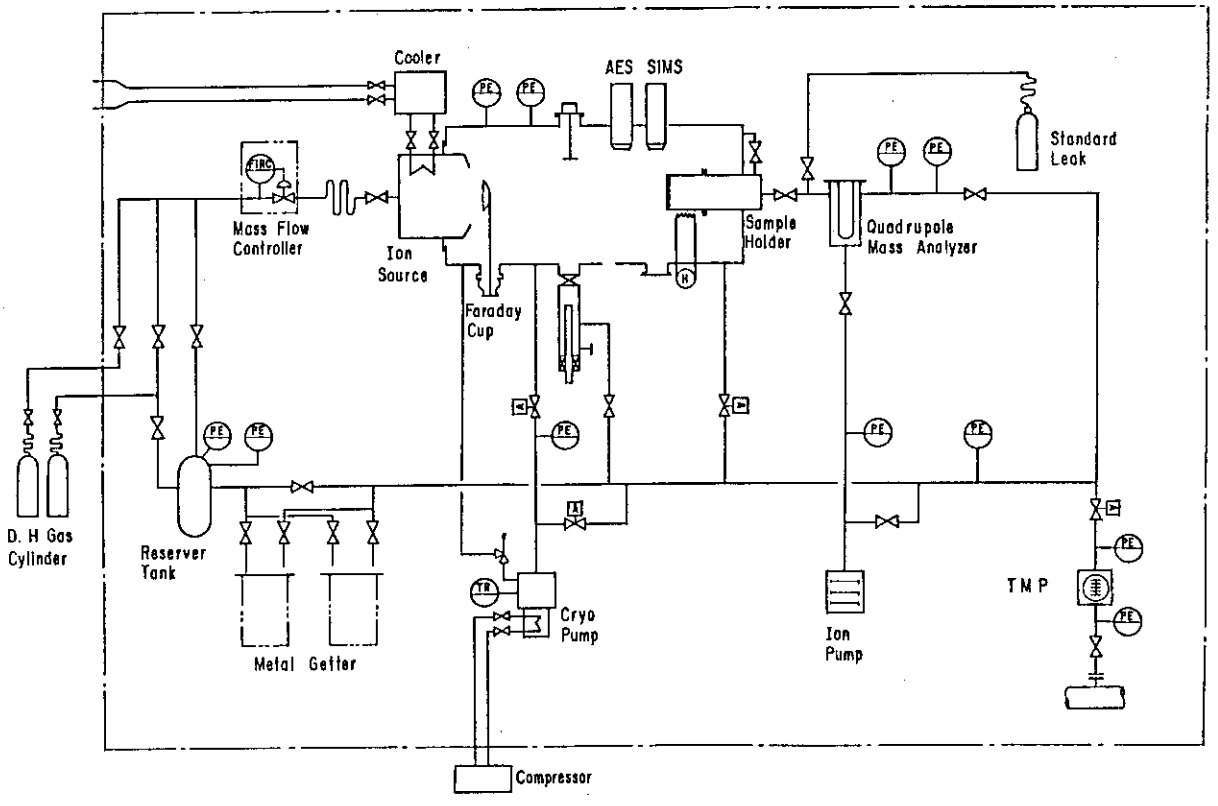

Figure 2. Schematic flow diagram of the experimental apparatus.

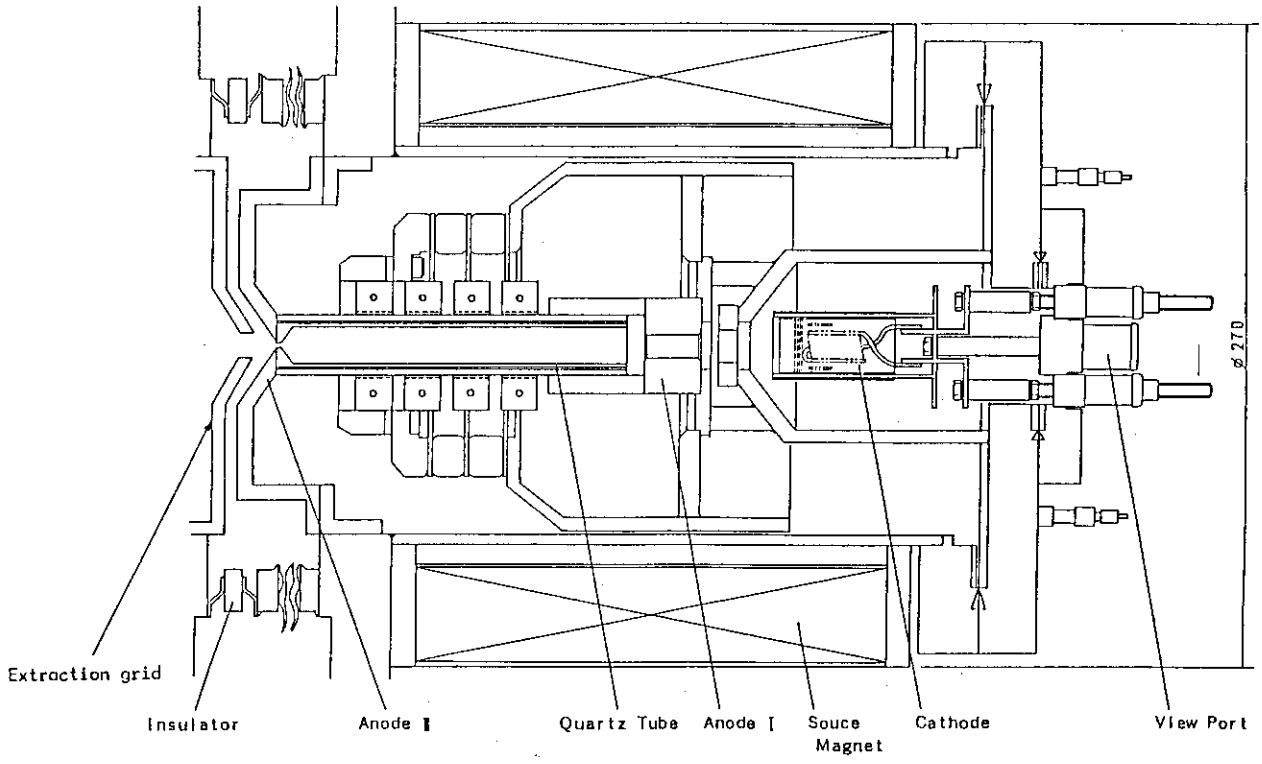

Figure 3. Conceptual drawing of the ion source.

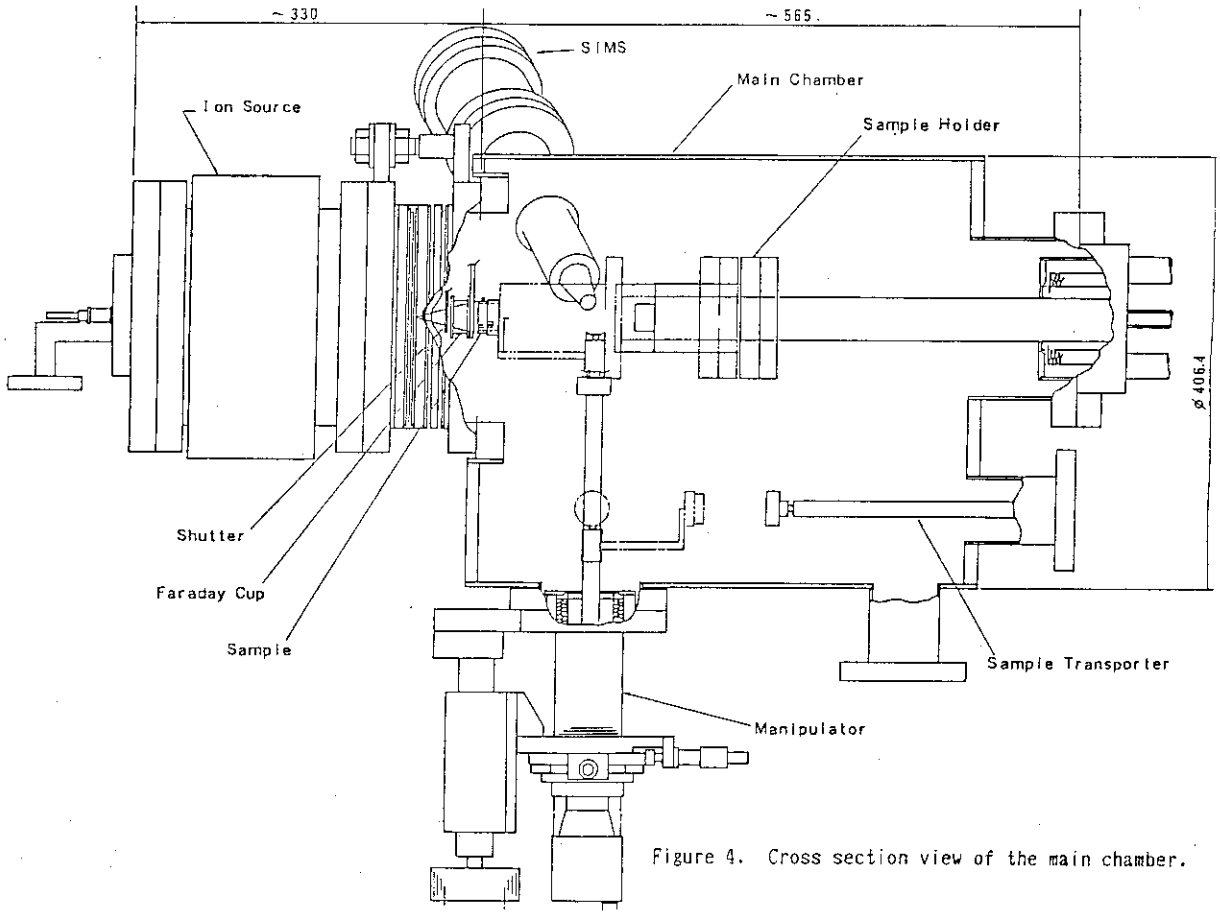

Figure 4. Cross section view of the main chamber.

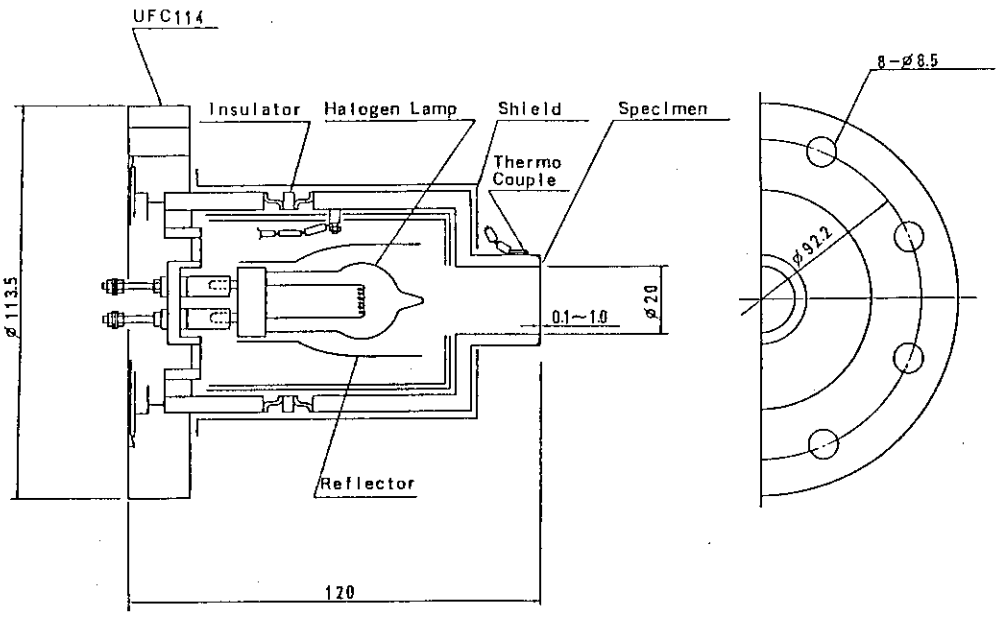

Figure 5. Schematic illustration of the sample holder.

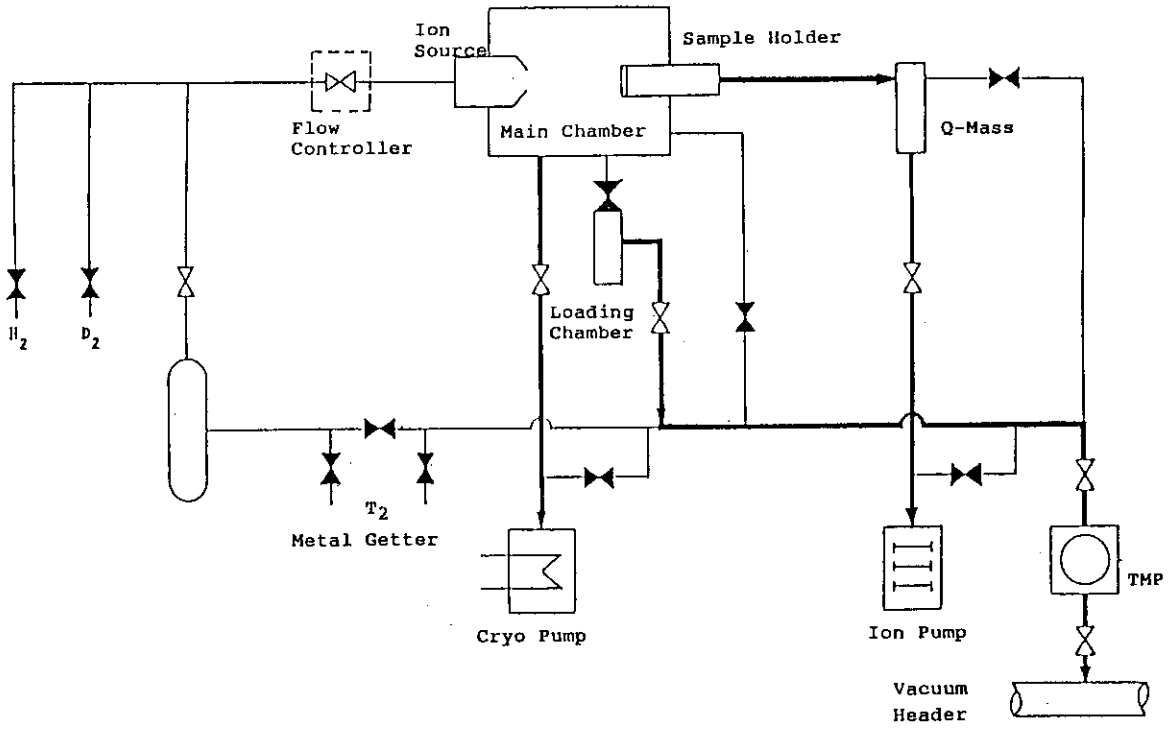

Figure 6. Schematic flow diagram (permeation experiment mode).

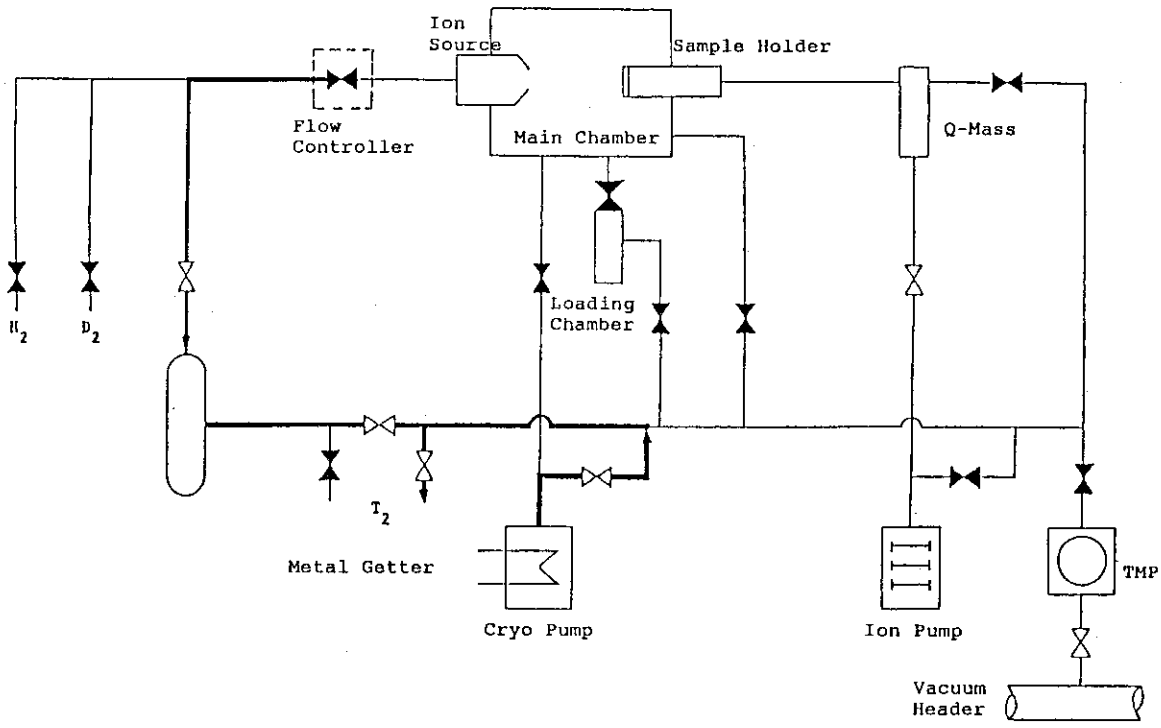

Figure 7. Schematic flow diagram (tritium recovery operation mode).

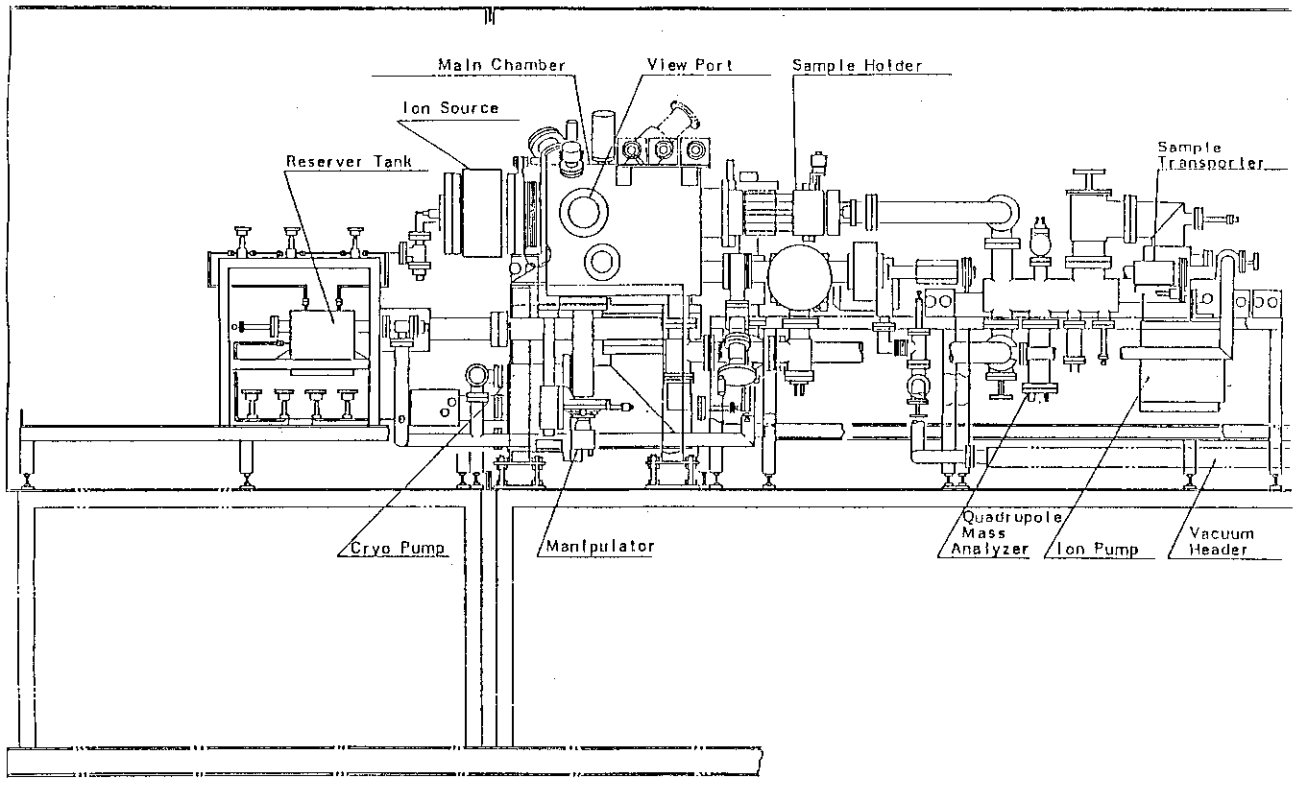

Figure 8. Layout plan of the apparatus in the glovebox.

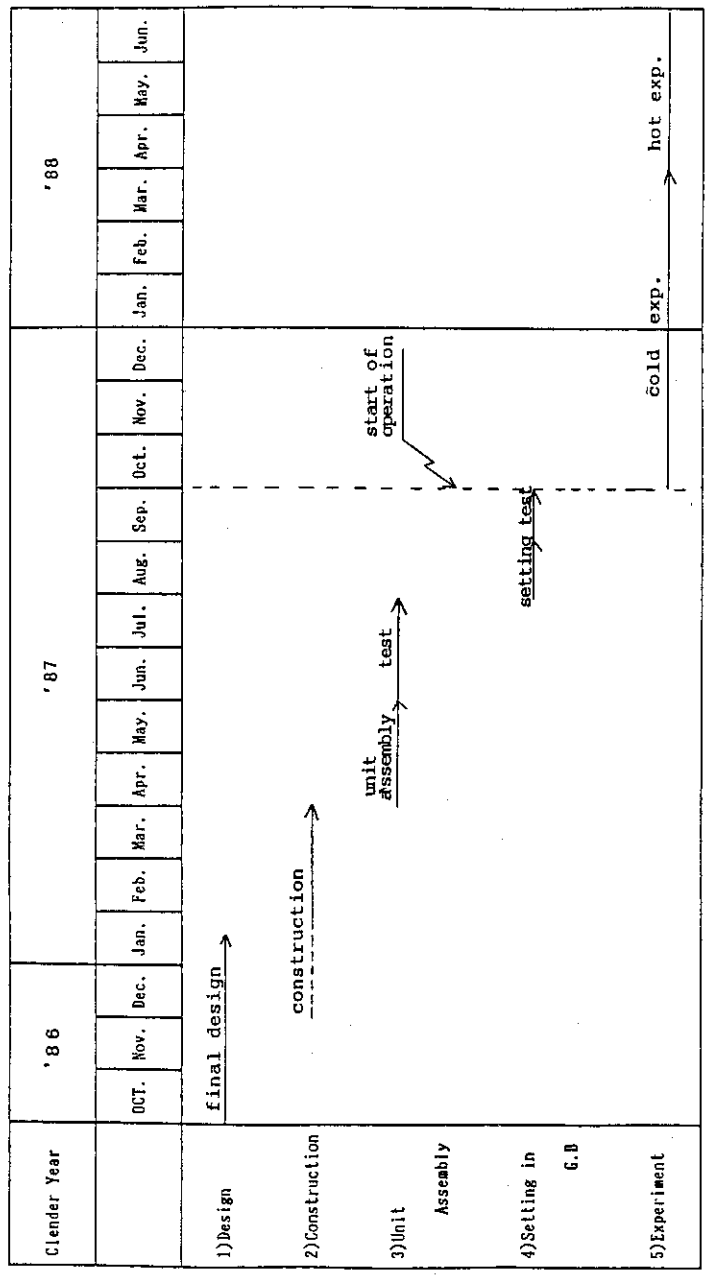

Figure 9. Time schedule.

CLOSING REMARK

by J. L. Anderson

We have seen much progress in T_2-handling since 1980 workshop.

TSTA - 50g T_2

TPL - Constructed, T_2 soon

TRIO

VOM

BEATRIX

University of Tokyo

Tokyo Institute of Technology

Permeation Studies

Tritium Plasma Experiment

T_2 Production at JAERI in 1000Ci Batches

Considerable work at Japan Universities

Tokyo Institute of Technology

University of Tokyo

Toyama

Osaka

Kyushu

Nagoya

Many now handling small quantities of T_2

We have made new friends and professional contacts which are profitable for both sides.

Exchanges and Cooperation agreements between U.S. and Japan have been important to both sides.

The future of T_2 work is very exciting:

1. Tritium Experiments at TPL will start soon.
2. TSTA will operate fully integrated fuel loop with 100g inventory.
3. International Blanket Experiments are underway.
4. Safety programs in both countries are working to assure reasonable approaches to tritium handling are followed.

A lot of exciting work is continuing in the Blanket Area. No clear cut choice for Breeder and Extraction System has emerged but there are many exciting experiments underway which will help to resolve this issue.

Additional Experiments must still be defined and started.

I see no reason to believe that tritium handling will be a barrier to fusion development. There are many unsolved and unresolved issues, but good scientists and engineers are making steady progress to solve these problems.

We appreciate the hard work of the organizing committee for this Workshop. It has been a very successful and valuable meeting.

The U.S. delegation is very appreciative of the warm and gracious welcome we have received from our Japanese friends and colleagues.

"ARIGATO GOZAIMASHITA."

Appendix : Agenda for Tritium Technology Workshop(P89)

Tritium Technology Workshop
P89 Japan-US Agreement on
Fusion Energy

Tokyo Headquaters, JAERI

Wednesday, October 22

9:00	Registration	
	Chairman K. Kawamura Tokyo Institute of Technology	
9:30	Welcome	M. Tanaka STA
9:40	Overview of the JAERI Tritium Research Program	Y. Naruse JAERI
10:10	Overview of the U.S. Magnetic Fusion Triitum Research Program	G.R. Nardella DOE (J.L. Anderson, LANL)
	10:40 BREAK	
	Chairman H. Yoshida JAERI	
10:50	Fusion Fuel Research Activities at Universities in Japan	M. Okamoto Tokyo Institute of Technology
11:20	Tritium Fueling for ICF Pellet Target	T. Norimatsu Osaka University
11:50	Overview of Tritium Processing Technology Development at TSTA	J.L. Anderson LANL
12:20	Tritium Scavenging from Gas Stream under Various Conditions	M. Nishikawa Kyushu University
	12:50 LUNCH	
	Chairman M. Nishikawa Kyushu University	
14:00	Test Production of Tritium in 1000Ci Level from ^{6}Li-Al Alloy Target	M. Tanase JAERI
14:30	An Assessment of Tritium Issues and Data Requirements for Liquid Breeders	Dai-Kai Sze ANL
	15:00 BREAK	
	Chairman Dai-Kai Sze ANL	
15:10	Studies on Steps Affecting Tritium Residence Time in Solid Blanket	S. Tanaka University of Tokyo
15:40	Overview of the In-Situ Tritium Release Experiments of the Solid Breeder Materials	H. Watanabe JAERI
16:10	LiF-PbF_2 Blanket System	K. Kawamura Tokyo Institute of Technology
16:40	Closing Discussions	

Thursday, October 23

	Chairman M. Okamoto Tokyo Institute of Technology	
9:00	Design Concept of Down Stream in Fusion Fuel Cycle	H. Amano Nagoya University
9:30	Comparison of Solid Breeder Materials for Tritium Production in Fusion Blankets	G. Hollenberg HEDL
10:00	Accumulation and Desorption of Hydrogen Isotopes Bomberded on Ti-Coated Surface of Metals	K. Higashi Kyoto University
	10:30 BREAK	
	Chairman K. Higashi	
10:40	Implications of Recent Implantation-Driven Permeation Experiments for Fusion Reactor Safety	G.R. Longhurst INEL, Idaho Falls
11:10	Transport of Deuterium Implanted into Metals	T. Nagasaki JAERI
11:40	Tritium Diffusion in Metals under Thermal Gradient	M. Sugisaki Kyushu University
12:10	The Retention of Tritium in Graphite	R.A. Causey SNL, Livermore
	12:40 LUNCH	

Chairman G.R. Longhurst
INEL, Idaho Falls

13:40	Conversion of Tritium Gas to Tritiated Water	H. Noguchi, JAERI
14:10	Analysis and Measurement of Tritium by Mass-Spectrometer, Ionization Gauge and Secondary Electron Multiplier	M. Matsuyama, Toyama University
14:40	Hydrogen Isotope(Tritium) Separation by Infrared Laser Multiple-Photon Dissociation	A. Yokoyama, JAERI

15:10 BREAK

Chairman J.L. Anderson

15:20	Program of Tritium Experiments at the TPL in JAERI	H. Yoshida, JAERI
15:30	Brief Description of Experimental Apparatus for Fuel Cleanup Process	S. Konishi, JAERI
16:00	Brief Description of Experimental Apparatus for Hydrogen Isotope Separation by Cryogenic Distillation	T. Yamanishi, JAERI
16:30	Brief Description of Experimental Apparatus for Tritium Permeation Studies	K. Okuno, JAERI
17:00	Closing Discussions	
17:30	Closing Speech	J.L. Anderson, LANL

JAERI – M 86 – 189